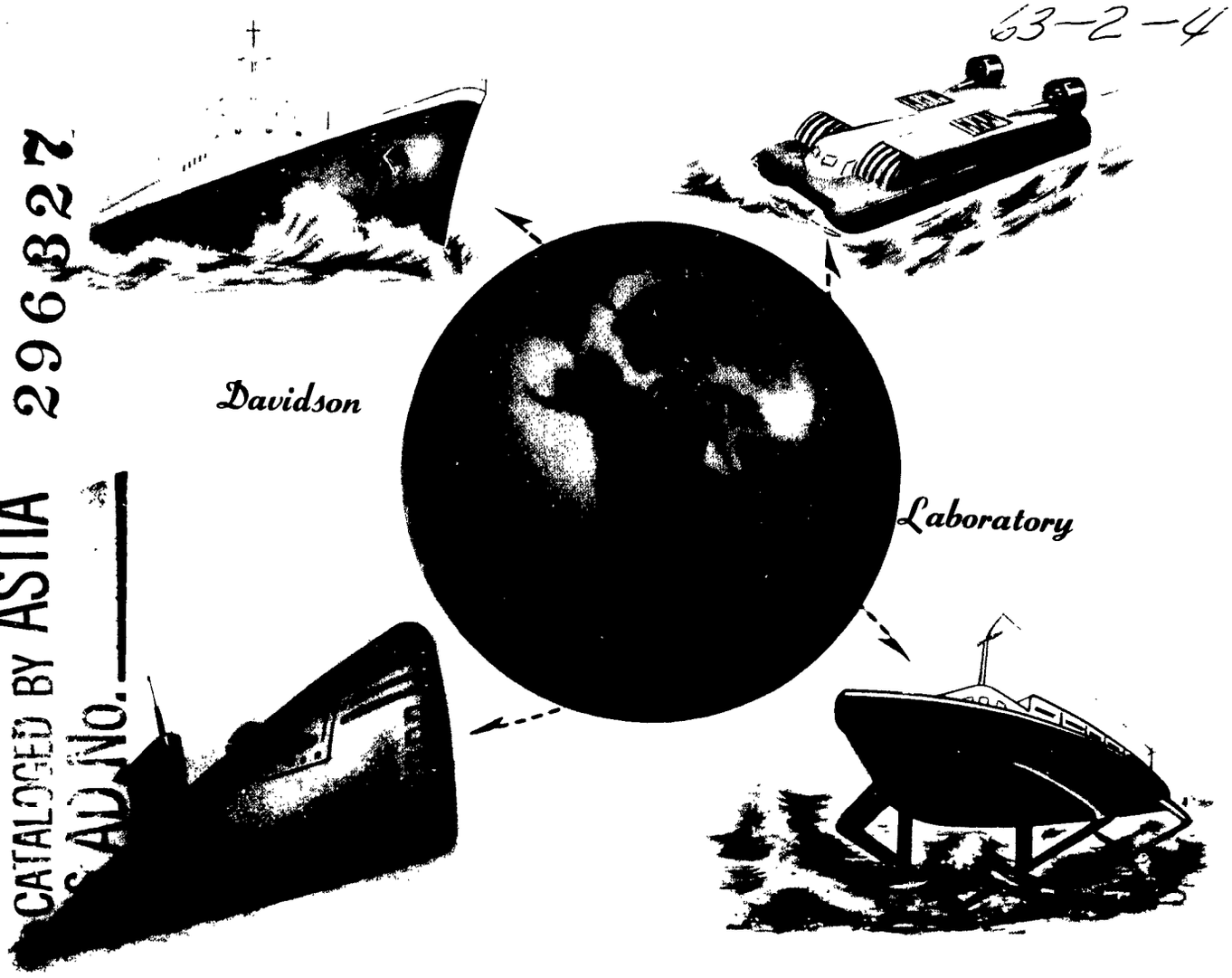

STEVENS INSTITUTE OF TECHNOLOGY

SHIP BEHAVIOR at SEA

NOTES
OF
4th BI-ANNUAL SEMINAR
SHIP BEHAVIOR AT SEA

TM-136

January 1963

DAVIDSON LABORATORY
Stevens Institute of Technology
Hoboken, New Jersey

CONTENTS

THEORY OF SHIP MOTIONS IN REGULAR HEAD SEAS

B. V. Korvin-Kroukovsky
Professor Emeritus - Consultant
Stevens Institute of Technology

This paper and a following one are concerned with the quantitative prediction of a ship's behavior at sea in the drawing board stage of ship design. This problem is too broad and complicated to be solved in its entirety and it is necessary to subdivide it into a number of smaller and simpler problems, which can be solved one by one. The first and major subdivision is into the ship motions in regular (uniform) waves and the motions in realistic sea waves, which are always irregular. The first problem, that of motions in regular long-crested waves, is solved by the methods available in the dynamics of rigid bodies and in hydrodynamics. The effects of a ship's form and weight distribution on ship motions are established in this solution. The second problem, that of motions in irregular waves, is solved purely mathematically, by statistical operations on the solutions of the first problem, together with the statistical description of sea waves. The exposition of these methods will be given by Prof. E. V. Lewis in the following paper.

However, even after the foregoing division of the general problem, the first problem, that of motions in regular waves, is still too complicated and has to be further subdivided. Following the general methods of rigid mechanics, a complex ship motion is considered as composed of six components-- three translational ones: surging, side-sway and heaving along x, y, and z axes; and three rotational ones: rolling, pitching and yawing about x, y, and z axes. The general problem can be simplified by considering first the case of a ship in head seas, in which case it surges, heaves and pitches, but the side-sway, rolling and yawing can be assumed to be absent. From now on we will focus our attention on this limited and idealized case of ship motions in regular, long-crested, head-on or following seas.

Numerous preliminary studies have indicated that surging motions have negligible effect on heaving and pitching, so that attention can be concentrated on these two motions, which occur simultaneously in waves and affect each other. The

analysis of a body's motion must invariably start with Newton's second law:

$$\left.\begin{aligned} m\ddot{z} &= Z \quad \text{for heaving} \\ \text{and} \\ J\ddot{\theta} &= M \quad \text{for pitching} \end{aligned}\right\} \qquad (1)$$

where: m is a ship's mass,

J is a ship's moment of inertia about lateral or y axis,

$\ddot{z}$ is the acceleration along vertical or z axis,

$\ddot{\theta}$ is the angular acceleration in pitching, i.e. about y axis,

Z is the total water-caused force along z axis, i.e. heaving force,

M is the total water-caused moment about y axis, i.e. pitching moment.

In the present study we are concerned with oscillation of ships, and only forces and moments causing and resulting from oscillations, will be considered. Steady, constantly acting forces, such as gravity, buoyancy, and a uniform suction force resulting from the forward ship motion will be excluded.

Various more or less complicated methods are available for evaluating the water-caused force Z and moment M, but they all lead to the solution in the form of polynomials, in which various terms are proportional to the displacement from equilibrium, z and θ body velocities, $\dot{z}$ and $\dot{\theta}$, and body accelerations, $\ddot{z}$ and $\ddot{\theta}$, and likewise the water surface elevation in waves, η, vertical surface velocity $\dot{\eta}$, and acceleration $\ddot{\eta}$. When these polynomials are inserted in eqs.1, the terms connected with body motions are transferred to the left-hand side, and those connected with waves to the right-hand side. Then eqs. 1 take the expanded form:

$$\left.\begin{aligned} a\ddot{z} + b\dot{z} + cz + d\ddot{\theta} + e\dot{\theta} + g\theta &= \bar{F}e^{i\omega t} \\ A\ddot{\theta} + B\dot{\theta} + C\theta + D\ddot{z} + E\dot{z} + Gz &= \bar{M}e^{i\omega t} \end{aligned}\right\} \qquad (2)$$

The wave-caused forces on the right-hand sides of these equations could have been written in the same form as the left-hand side, i.e. in terms or $\ddot{\eta}$, $\dot{\eta}$, and η, but the relationship among these three functions of wave elevation η is uniquely

defined in the classical theory of waves; their effect on a ship can be combined, therefore, in one compact expression.

The symbols $\bar{F}$ and $\bar{M}$ in eqs. 2 are "complex amplitudes" of oscillatory wave-caused force and moment, i.e., the quantitaties defining both the magnitudes and phase lags of these quantities with respect to the wave causing them. In writing eqs. 2 it was understood that real parts of the right-hand sides are to be taken, so that these can be re-written as

$$\left.\begin{aligned} \text{Re } \bar{F}e^{i\omega t} &= \text{Re}(F_o e^{i\sigma})\ e^{i\omega t} = F_o \cos(\omega t + \sigma) \\ \text{Re } \bar{M}e^{i\omega t} &= \text{Re}(M_o e^{i\tau})\ e^{i\omega t} = M_o \cos(\omega t + \tau) \end{aligned}\right\} \qquad (3)$$

The use of the complex forms for the right-hand sides of eqs. 2 simplifies the solution of these equations. The solution is a simple matter and is found in ref. 13. In this paper, therefore, attention will be concentrated on the physical nature of various coefficients of eqs. 2.

The coefficient a is evidently a mass, and the first term of eqs. 2 can be rewritten as $m\ddot{z} + m'\ddot{z}$, where m is the mass of a ship. The term $m'\ddot{z}$ is the force caused by acceleration of water particles. These particles move in many directions and at different accelerations, but it was found that the resultant vertical force acting on a ship can be expressed in terms of a fictitions water mass m', which is known as "added mass" or "hydrodynamic mass." Porter defined the added mass in a more rigorous form: "The added mass is the ratio of the hydrodynamic force in phase with acceleration to the acceleration."[21] The total effective mass, m + m', is known as "virtual mass." Likewise the coefficient A is expanded as J + J', where J is the ship's moment of inertia, and J' is the added or hydrodynamic moment of inertia.

If the masses of a ship are distributed in proportion to the sectional area curve, the first term of eqs. 2 can be written as $m(1 + k_2)$, where k_2 (equal to the ratio m'/m) is known as the "coefficient of accession to inertia."

The magnitude of m' and k_2 can be evaluated for three dimensional bodies only in special cases of mathematical forms, for instance, for ellipsoids. For an arbitrary ship form it is necessary to consider a ship as composed of a number of short sections of cylindrical bodies, and to replace a direct three-dimensional solution by the summation of a number of two-dimensional ones. The original evaluation of k_2 for cylindrical bodies, closely resembling practical ship sections, was made

by F. M. Lewis.[17] Probably the most convenient presentation of these data will be found in the paper by Landweber and Macagno.[14]

The values given by Lewis, Landweber, and Macagno neglect the effect of the surface wave formation and are derived on the assumption that water flow at sections of a surface ship is identical with the flow at a submerged double body. This assumption is valid for high frequency of oscillation and typical for ship vibration, which was the primary interest of Lewis. At a lower frequency, typical for ship heaving and pitching, a correction for the effect of surface waves must be applied, and the coefficient of accession to inertia is expressed as k_2k_4. Ursell[24] derived the values of k_4 as a function of frequency for a circular cylinder, and Korvin-Kroukovsky and Jacobs[13] assumed these values to apply to all ship forms. Later Tasai[22] derived k_4 values for ship sections which were used in F. M. Lewis' original derivation of k_2. Tasai's theoretical derivations were confirmed by independent theoretical work of Porter,[21] and theoretical work was verified by experiments of Porter[21] and of Pauling and Richardson.[20]

Coefficients b and B are known as "damping coefficients." They indicate the rate of dissipation of kinetic energy from an oscillating ship. In the case of a ship oscillating freely in smooth water, this dissipation causes gradual decrease of the oscillation amplitude. In the case of sustained oscillation in regular waves, the dissipated energy is replenished by the work of exciting forces, which appear on the right-hand sides of eqs. 2. The damping may be caused by friction, eddy-making, and wave-making resulting from a ship's oscillation. However, the comparison of the measured and calculated motions of ship models indicates that wave-making strongly predominates over other causes of damping, and appears to be the only one to consider in practical applications. The waves observed at, let us say, heaving ship appear to be complicated, but theoretical investigation shows them to be composed of two systems: a complicated standing wave system in close proximity to a ship, and a train of simple harmonic progressive waves which propagate away from a ship without change of form. The former is associated with the added mass (bringing about the k_4 factor), and the latter carries the energy away from a ship, i.e., provides the damping. It was found convenient to evaluate the damping coefficient in two steps: first, to evaluate the ratio (designated $\bar{A}$) of the oscillation-caused wave height η at a large distance from a ship to the ship's oscillation amplitude. The second step was to express the damping coefficient in terms of $\bar{A}$. The first step was originally accomplished by Holstein[9] and Havelock[7] in the form

$$\bar{A} = 2e^{-k_o f} \sin(k_o y) \qquad (4)$$

where $k_o = \omega^2/g$, y is the half beam, and f = (sectional area)/(beam) is the mean draft of a ship section. Equation 4 was derived on the basis of a simple but incomplete theory; nevertheless, it is valuable in clearly demonstrating the strong influence of the mean draft, f, on damping. More complete theories, derived later by Ursell,[24;25;26] Grim,[6] and Tasai,[22] require extensive numerical calculations to bring out results, which therefore are more difficult to appraise. Tasai[23] also verified his theory by experiments and at the present time can be considered as the most reliable as well as convenient source of information on added masses and damping. Tasai confirmed the results of Ursell and Grim, except for the sections of low section coefficient, for which Grim gives exaggerated values.

In the foregoing references to Grim, Tasai and Porter, the work is based on Lewis' type ship sections, i.e., those derived by transformation from a circle. These sections have the property of being tangent to a vertical at waterline, and to horizontal at the keel. Many ship sections, however, have inclined sides at LWL and it was first thought that this feature may be responsible for the lack of agreement among calculated and observed ship model motions in some cases. In order to investigate this, Kaplan and Jacobs[10] developed a theory applicable to ship sections sharp at the keel and composed of parabolic arcs, such as were used in theory of ship motions by Haskind.[8] These included straight-sided V-forms, and also concave sides inclined at LWL. Tasai[23] studied experimentally damping of Lewis' cusped forms of the low section coefficient, as well as wedges. These studies indicated that inclination of sides only slightly reduces damping, and that discrepancies were caused primarily by exaggeration of damping for low section coefficients in Grim's data which were used in Korvin-Kroukovsky and Jacobs'[13] investigation. Tasai introduced the term "wedge effect" for the ratio of experimentally measured damping of sections with inclined sides to theoretical damping of Lewis' type sections of comparable draft and section coefficients.

Once $\bar{A}$ is evaluated, the damping coefficient is expressed as

$$N(\xi) = \rho g^2 \bar{A}^2/\omega^3 \qquad (5)$$

The symbol $N(\xi)$ is habitually used for the damping of a ship section at a distance ξ from a ship's center of gravity. The damping coefficients b and B are obtained by integrating $N(\xi)$

values over the ship's length, as this is shown by eqs. 42 in ref. 13 (Korvin-Kroukovsky and Jacobs).

The foregoing discussion of the added mass and damping was essentially confined to two-dimensional evaluation for cylindrical bodies, assumed to be valid for a strip $\Delta\xi$ of a ship's length. The question now arises: how reasonable is the integration of sectional data over a ship's length neglecting the interaction of adjacent strips, i.e., how important is three-dimensional effect? Korvin-Kroukovsky[12] computed by strip theory the inertial forces acting on a submerged spheroid moving under waves and found a satisfactory agreement with more rigorous theory available for spheroids. Gerritsma[2,3,4] made experiments with surface ship models and found strip theory computations of added mass, made on the basis of the k_2k_4 factor, to be accurate within about 10%. On the other hand, these experiments indicated large uncertainty of damping evaluation. Tasai, Porter, and Pauling and Richardson's experiments confirmed the theoretical evaluation of two-dimensional damping. The inevitable conclusion is that uncertainty is caused by three-dimensional effects. Havelock[28] and Vossers[27] evaluated correction factors for three-dimensional effect on the basis of a linear theory, but the use of these factors appears only to aggravate disagreements among calculated and test data. It seems to me that the linear theory, i.e., infinitely small motions, is inadequate in this case, and that it is necessary to consider finite amplitudes of pitching.

Additional comments are needed on the damping coefficients b and B as they occur in coupled eqs. 2. Were the two equations uncoupled, i.e., d=e=g=D=E=G=0, the coefficients b and B would simply indicate the dissipation of energy. In a coupled system, however, each of these coefficients is composed of two terms: one indicating dissipation of energy, as in an uncoupled system, and the other indicating transfer of energy from one mode of motion to another. This transfer usually causes a certain reduction of pitching and increase of heaving motion, as compared to an uncoupled system.

Coefficients c and C of eqs. 2 are computed simply as changes of displacement with changes of section drafts and do not require further discussion.

The "cross-coupling" coefficients, d, e, g, D, E, and G, govern the forces acting on a mode of motion but caused by another "coupled" one, i.e., heaving forces caused by pitching motion, and pitching moments caused by heaving motion. They arise because of the lack of symmetry of forebody and afterbody. The coefficients g and G, determined by calculating

the displacement, evidently depend only on geometric unsymmetry of the waterplane. Other coefficients, however, depend on the lack of symmetry in hydrodynamic properties and usually will have a certain value even in the case of a geometrically symmetric hull. For instance, in the case of a symmetric ship moving at a certain speed, different forces will be generated at identical sections located at a distance ξ forward and aft of midship, i.e., in regions of diverging and converging flow.

Ship motions computed on the basis of coupled heaving and pitching eqs. 2 differ from the motions which would result if the heaving and pitching were considered independently without accounting for their mutual interaction. Nevertheless, the general character of the forced harmonic oscillation remains, as far as the amplitude and phase lag relationships to the exciting functions are concerned. For any given amplitude of the wave exciting force or moment, the amplitudes of heaving and pitching rapidly increase with the frequency of wave encounter, reach their maxima at the frequency approximately equal to a ship's natural frequency of oscillation in calm water, and then gradually diminish with further increase of the exciting frequency. The phase lag starts from zero at a very low frequency of wave encounter, is approximately 90 degrees at synchronous frequency, and asymptotically approaches 180 degrees at a high wave-encounter frequency. To this extent the significance of the coefficients a, A, b, B, c, and C is easily understood. The natural frequency of a ship's oscillation, ω_n, for instance in heaving, is defined by the relationship

$$\omega_n = \sqrt{c/a} \tag{6}$$

The higher the restoring moment per unit of the mass, c/a, the higher is the natural period. In any given wave length, therefore, the speed will be higher where synchronism will occur. E. V. Lewis[15] used this fact to show that slender ships of lower displacement/length ratio can maintain a higher speed in adverse weather than ships of larger displacement/length ratio.

Greater damping, indicated by higher values of the ratios of coefficients b/a and B/A, immediately leads to lower amplitudes of motions, and, therefore, is always desirable. For instance, Kempf[11] and E. V. Lewis obtained large improvement in ship model motions in waves by changing from a U-form to pronounced V-form (Meyer form). In this case, favorable effects of increased damping and restoring moment in pitching strongly predominated over the adverse effect of increased added mass.

The nature of the variation of phase lag with frequency explains the fact, well known to mariners, that a ship's behavior in adverse weather always can be improved by reduction of speed. At low ship speeds the frequency of encounter of large waves is small, and, therefore, the phase lag is small: a ship rises and falls with the wave. While the amplitude of pitching may be large, the ship moves with the wave, the relative motion of the ship's bow with respect to adjacent water is small, and the ship remains dry and relatively comfortable. Contrary to this, at a higher speed, a large phase lag makes the falling bow impinge on the rising surface of the oncoming wave flank, the relative ship to wave velocity is large, and this causes severe impacts (slamming), the subsequent bow immersion, and shipping of water.

Contrary to the evident effects of the coefficients a, A, b, B, c, and C, outlined in the foregoing, little is known regarding the effect of cross-coupling coefficients, d, D, e, E, g, and G, on ship motions. It is clear, however, that they affect phase lags, and in particular manifest themselves in modifying the lag of heaving after pitching. In uncoupled simple harmonic oscillations, the maximum amplitude of heaving occurs 90 degrees after that of pitching, regardless of the frequency of wave encounter. Towing tank tests of ship models in waves showed that in coupled heave-pitch oscillations this angle is usually reduced, and that the reduction is particularly large at synchronous frequency. In experiments of Akita and Ochi,[1] the angle as small as 20 degrees was recorded. In practice, the significance of this angle is manifested in the location of the "apparent pitching axis," i.e., a point on the length of a ship (usually aft of midships) at which the combined vertical motion due to heaving and pitching is smallest. Decrease of the phase angle of heaving after pitching indicates a movement of this point towards stern.

Outside of the foregoing qualitative discussion, the significance of the cross-coupling coefficients in seakeeping qualities of ships is not known. Their effects cannot be evaluated at a glance, as in the case of the primary coefficients a, A, b, B, c, and C, and it appears to be too involved to be brought out in closed formulae. It can be brought out numerically by a series of systematic computations, but these have not yet been made. The whole subject of analytically predicting ship motions in waves is new, and almost the entire effort to date was directed toward the development of methods and verifying them by comparison with model tests. While computations appear to be reasonably reliable, little practical application appears to have been made. An interesting example of such an application is found in the work of E. V. Lewis[18]

in which the effect of reducing the displacement/length ratio of a ship on the cost of transportation was investigated.

The exciting forces on the right-hand sides of eqs. 2 are evaluated by procedures similar to those discussed in the foregoing, but here we consider the water flow in waves around a stationary ship instead of a ship moving through still water. In fact, both motions are considered simultaneously in analytical derivation and two groups of forces are separated at the conclusion simply by a suitable re-grouping of several terms in a common solution. A complete three-dimensional solution is possible only for special mathematically defined ship forms composed of parabolic arcs by the use of advanced mathematical techniques and extensive computations. For ships of arbitrary form and in engineering application, it is necessary to resort to the strip theory, and an example of this procedure will be found in Korvin-Kroukovsky and Jacobs.[13] As in the case of F. M. Lewis' work,[17] an assumption is made that water flow at sections of a surface ship is identical with the one at a submerged double body, and the solution yields the displacement forces and inertia forces in terms of the coefficient of accession to inertia, k_2. In order to correct for the surface wave formation, induced by interaction of oncoming waves with the ship, an additional factor k_4 is introduced in the same manner, as this was heretofore discussed in connection with ship motions. The use of the k_4 factor accounts for the standing wave system, while the progressive wave part of the induced wave system (i.e., damping) is not accounted for. Therefore, it becomes necessary to introduce damping forces separately on the basis of the vertical water velocity in waves and the coefficients $\bar{A}$ and $N(\xi)$. Korvin-Kroukovsky and Jacobs[13] omitted this step in the final conclusions of their paper because preliminary calculations showed that sectional wave-caused damping forces yielded a negligibly small total force upon integration along the length of a ship. However, these forces cannot be neglected when the distribution of forces along a ship must be determined, as in the calculations of bending moments acting on ship hulls.

In the classical wave theory, all characteristics of a wave are uniquely connected, and any one can be chosen as a reference parameter in force evaluation. Thus Korvin-Kroukovsky and Jacobs defined wave-caused sectional heaving forces in terms of the wave amplitude. In later analyses of ship bending moments, it became desirable to separate the effects of water acceleration, velocity, and displacement. These were usually referred to as conditions at the water surface, $\ddot{\eta}$, $\dot{\eta}$, and η, and correction factors had to be developed to account for the attenuation of these quantities with depth. The subject is particularly well discussed by Motora.[18,19]

REFERENCES

1. Akita, Yoshio and Ochi, Kazuo: "Model Experiment on the Strength of Ships Moving in Waves," SNAME, Vol.63, 1955. pp. 202-236.

2. Gerritsma, J.: "Some Notes on the Calculation of Pitching and Heaving in Longitudinal Waves," Intl. Shipbuilding Progress, Vol.3, No.21, May 1956. pp. 225-264.

3. Gerritsma, J.: "Experimental Determination of Damping, Added Mass and Added Mass Moment of Inertia of a Ship Model," Intl. Shipbuilding Progress, Vol.4, No.38, October 1957. pp. 508-519.

4. Gerritsma, J.: "An Experimental Analysis of Ship Motions in Longitudinal Regular Waves," Intl. Shipbuilding Progress, Vol.5, No.52, December 1958. pp. 533-542.

5. Gerritsma, J.: "Ship Motions in Longitudinal Waves," Intl. Shipbuilding Progress, Vol.7, No.66, February 1960, pp. 49-76.

6. Grim, Otto: "Berechnung der durch Schwingungen eines Schiffskörpers erzengten hydrodynamischen Kräfte," JSTG, Band 47, 1953, pp. 277-299.

7. Havelock, Sir Thomas H.: "The Damping of the Heaving and Pitching Motion of a Ship," Phil. Mag., 33, pp.666-73, 1942.

8. Haskind, M. D.: a) "The Hydrodynamic Theory of the Oscillation of a Ship in Waves," (in Russian), Prikladnaya Matematika i Hakhanika, Vol. 10, No. 1, 1946. pp. 33-66.
b) "Oscillation of a Ship on a Calm Sea, (in Russian), Bulletin of the Academy of Sciences, USSR, Dept. of Technical Sciences, 1946, No. 1, pp. 23-24. English translation: "Two Papers on the Hydrodynamic Theory of Heaving and Pitching of a Ship," SNAME Technical and Research Bulletin No. 1-12, April 1953.

9. Holstein, Horst: "Untersuchungen an einem Tauchschwingungen ausführended Quader," WRH, December 1, 1936, pp. 385-389.

10. Kaplan, Paul and Jacobs, Winnifred R.: "1. Two-Dimensional Damping Coefficients from Thin-Ship Theory; 2. Theoretical Motions of Two Yacht Models in Regular Head Seas on the Basis of Damping Coefficients Derived for Wide V-Forms," DL Note 568, April 1960.

11. Kempf, Günther: "A Study of Ship Performance in Smooth and Rough Water," SNAME, Vol.44, 1936, pp. 195-227.

12. Korvin-Kroukovsky, B. V.: "Force Acting on a Submerged Body of Revolution Moving Under Waves," Proceedings of the Fourth Midwest Conference on Fluid Mechanics, Purdue University, 1955.

13. Korvin-Kroukovsky, B. V. and Jacobs, Winnifred R.: "Pitching and Heaving Motions of a Ship in Regular Waves," SNAME, Vol.65, 1957. pp. 590-632.

14. Landweber, L. and Macagno, M. C. de: "Added Mass of Two-Dimensional Forms Oscillating in a Free Surface," Journal of Ship Research, Vol.1, No.3, November 1957. pp. 20-30.

15. Lewis, Edward V.: "Ship Speeds in Irregular Seas," SNAME, Vol.63, 1955. pp. 134-202.

16. Lewis, Edward V.: "The Sea Speed of Cargo Ships in Rough Weather Services," Intl. Shipbuilding Progress, Vol.3, No.22, June 1956.

17. Lewis, Frank M.: "The Inertia of the Water Surrounding a Vibrating Ship," SNAME, Vol.37, 1929. pp. 1-20.

18. Motora, Seizo: "Drifting Force Caused by Beam Seas," Davidson Laboratory Note 653, 27 March 1962.

19. Motora, Seizo: "Stripwise Calculation of Hydrodynamic Forces due to Beam Seas," Davidson Laboratory Note 656, 4 April 1962.

20. Pauling, J. R. and Richardson, Robert K.: "Measurement of Pressures, Forces and Radiating Waves for Cylinders Oscillating in a Free Surface," Univ. of California, Inst. of Engr. Research, Series 82, Issue No.23, June 1962.

21. Porter, William R.: "Pressure Distribution, Added-Mass, and Damping Coefficients for Cylinders Oscillating in a Free Surface," Univ. of Calif., Inst. of Engr. Research, Series 82, Issue No. 16, July 1960.

22. Tasai, Fukuzō: "On the Damping Forces and Added Mass of Ships Heaving and Pitching," JZK, Vol. 105, July 1959, pp. 47-56, English Translation by Wen-Chin Lin, Univ. of Calif., Inst. of Engr. Res., Series 82, Issue No. 15, July 1960 .

23. Tasai, Fukuzō: "Measurement of the Wave Height Produced by the Forced Heaving of the Cylinders," Reports of Research Institute for Applied Mechanics, Kyushu University, Vol. VIII, No. 29, 1960.

24. Ursell, F.: "On the Heaving Motions of a Circular Cylinder on the Surface of a Fluid," Quart. J. of Mechanics and Applied Mathematics, Vol. 2, June 1949, pp. 218-231.

25. Ursell, F.: "Short Surface Waves due to an Oscillating Immersed Body," Proc. R. Soc. A., Vol. 220, 1953, pp. 90-103.

26. Ursell, F.: "Water Waves Generated by Oscillating Bodies," Quart. J. of Mechanics and Applied Mathematics, Vol. 7, 1954, pp. 427-437.

27. Vossers, G.: Discussion of Havelock's 1956 paper; INA, Vol. 98, No. 4, October 1956, pp. 467-468.

28. Havelock, Sir Thomas H.: "The Damping of Heave and Pitch: a comparison of Two-Dimensional and Three-Dimensional Calculations Trans. INA, 1956, pp. 464-9.

ABSTRACT
of

Basic Theory of Ship Behavior in Irregular Seas

by

Edward V. Lewis

In his Symposium talk, Professor Lewis reviewed the important features of the well-known theory for treating ship behavior in irregular seas, first presented by St. Denis and Pierson,[1] and covered by him at previous Summer Seminars.[2]

He explained how modern developments in oceanography permit an irregular ocean wave pattern to be described in terms of a "spectrum," which defines the amplitudes of all the component waves into which the irregular pattern can be broken down. He then showed how the behavior of a ship in such a sea pattern can be described on the basis of the assumption that the response is the sum of the ship's responses to all of the wave components present. Thus a spectrum can be obtained for any response such as pitch amplitude, heave amplitude, acceleration, wave bending stress, etc., and from it the statistical characteristics can be derived.

Some general conclusions regarding means of improving the seagoing qualities of ships were given. The lecture drew heavily on ref. 3, which may be used as a convenient reference.

REFERENCES

1. "On the Motions of Ships in Confused Seas," by M. St. Denis and W. J. Pierson, Jr. Trans. SNAME, 1953.

2. E. V. Lewis Lecture in Notes of the First "Ship Behavior at Sea" Seminar, DL Report 619, Sept. 1956.

3. "Ship Speeds in Irregular Seas," by E. V. Lewis Trans. SNAME, 1955.

Introduction of Theoretical, Experimental and Observational Work on Ship Motions at Sea

B. V. Korvin-Kroukovsky
Professor Emeritus - Consultant
Stevens Institute ot Technology

In my previous paper, I presented the introduction to the theory of ship motions in regular head waves, and Prof. Lewis gave the generalization of it for the irregular seas. While these theories are only a few years old, they already provide in many cases means of predicting seakindliness of ships from design data. The available techniques are, however, not complete and further research and development is needed to cover many aspects of a ship's behavior at sea not sufficiently clarified at present. Until recently this development was handicapped by the fact that available information was widely scattered in many publications and there was no collected source of information. Recently such sources became available in four books listed in the Appendix. Of these, the book by Kent is valuable primarily because of Kent's interpretation of his own observations on ships at sea as well as model tests. However, it is largely limited to old style ships and is very weak in theoretical interpretations. Korvin-Kroukovsky and Vossers give the most up-to-date available collection of material, but differ in the method of presentation: Vossers, as well as Blagoveshchensky, presents the gradual development of the theory through various stages, and Vossers includes the empirical trends based on model tests. Korvin-Kroukovsky omits the gradual development, presents in concise form only the latest workable methods and stresses functional relationships among sea properties and ship motions as well as loads imposed on a ship's hull by waves.

Further research and development in the ability to predict seakindliness of ships from design data must proceed along three parallel and interconnecting lines (as it has indeed been done in the past).

a. Observations on ships at sea

b. Towing tank tests on ship models

c. Theoretical methods.

It would appear at the first sight that observations on ships at sea is the most direct method of learning about seakindliness of ships. In fact, however, the irregular sea waves and ship motions in them are much too complicated to permit reliable interpretation, and supplementary model tests and theoretical analyses are necessary for the interpretation. Model tests in waves in towing tanks offer better possibilities of analysis and interpretation because the waves and model conditions can be simplified and controlled, and tests under any desired condition can be repeated as

many times as desired. But even model motions are too complicated to be understood at a glance, and the help of a theory is sought for reliable interpretation. Furthermore, experience has shown that model tests may be incorrect and misleading unless continuously compared with and checked against theoretical expectations.

A theory, on the other hand, is merely a logical development which starts with a number of postulated facts. If these initial facts are not correctly stated or if some important ones are overlooked, a correctly developed theory will yield erroneous results. The relevent initial factors and conditions generally have to be formed on the basis of ship and model observations. Furthermore, there is always a certain danger of error in choosing the relevant facts and in converting them into mathematical techniques. Achievements of the theory, therefore, must be checked against model tests and sea observations.

Model tests and theoretical methods used together will provide reliable quantitative data, for instance, such as the angle of a ship's pitching in certain waves. These data, while numerically correct, may still be misleading in regards to ships at sea, because the ambient conditions are too much under the control of an experimenter and may not correspond to reality. Model tests and theoretical analyses must be continually checked, therefore, against what has actually been observed on ships at sea.

There is also an important problem of interpretation of model test and theoretical data in terms of the seakindliness of ships as appraised by mariners at sea. It has not been established as yet which quantitative ship behavior data will be reflected, for instance, in a ship master's decision to reduce engine RPM in stormy seas or to change the course. This interpretation of quantitative data in terms of mariner's mental attitudes represents one of the most important, yet most neglected branches of research.

As far as this can be judged at present, a captain's decision to reduce RPM in a stormy bow sea is brought about primarily by excessive shipping of water and by slamming. The first usually will be the case with a fully loaded ship and the second with a ship in ballast. A ship making smooth, nearly sinusoidal, oscillations (easy motions) will be considered more seakindly than one executing jerky motions. That is, it appears that the rate of change of acceleration is a factor to consider when the well being of personnel is involved.

Professor E. V. Lewis and I previously presented in our papers an introduction to ship motion theory which has reached sufficient development to be used as a design tool in many cases. Although it is but a few years old, it essentially became "classical." This word, however, has a dangerous connotation: it tends to build excessive confidence in hitherto successful methods, and so to retard further development. Dr. Cummins will point to certain drawbacks of the classical method in the following paper, and will indicate another possible direction of theoretical development.

REFERENCES

1. Blagoveshchensky, S. N.: "Theory of Ship Motions," in two volumes, Dover Publications, Inc., New York, 1962, (translation of the original Russian book "Kachka Korablia" of 1954.)

2. Kent, J. L.: "Ships in Rough Water," Thomas Nelson and Sons Ltd., London, 1958.

3. Korvin-Kroukovsky, B. V.: "Theory of Seakeeping," The Society of Naval Architects and Marine Engineers, New York, dated 1961 (actually available in 1962).

4. Vossers, G.: "Fundamentals of the Behavior of Ships in Waves." appearing in a long series of installments in the "International Shipbuilding Progress," beginning with Vol. 6, November 1959.

THE IMPULSE RESPONSE FUNCTION AND SHIP MOTIONS

W. E. Cummins
Head, Seaworthiness and Fluid Dynamics Division
David Taylor Model Basin
Washington, D. C.

I. INTRODUCTION

The subject of this paper is a new formulation of the equations of motion for an oscillating ship. The paper will review some results previously presented at the Symposium on Ship Theory in Hamburg during January of this year. Here, we will concentrate on the significance of the results, and for brevity, some of the mathematical development will be omitted. For the complete development, see references 1 and 2.*

To provide a background for this new formulation, a brief discussion of the conventional formulation is desirable. This will be presented in the form of a sort of imaginary history of the way the formulation might have developed. We may be dignifying the process of development by making it seem more rational than it actually was.

The basic solution to the linearized (infinitesimal) gravity wave problem is of the following form:

$$\eta = a \cos \frac{2\pi}{\lambda}(\zeta - ct) \qquad [1]$$

where

η = wave elevation
a = wave amplitude
λ = wave length
ζ = horizontal distance
c = wave celerity
t = time

This is a progressive wave of permanent form. Wave systems of infinite variety can be obtained by adding up these elemental solutions. It is known that the linear theory provides an excellent approximation to nature, even when the amplitude of the waves becomes significant.

*References are listed on page 14.

Now suppose a ship to be placed in such a train of regular progressive waves. For the moment, we will concern ourselves with only one mode of motion, say heave. There will be an oscillating heaving force exerted on the ship by the wave train, and if the ship-wave system can also be treated as linear, the heave force will be of the form,

$$f(t) = F \cos \omega t \qquad [2]$$

where ω is the frequency of encounter. The response of the ship to this force will be

$$x(t) = X \cos(\omega t + \epsilon), \qquad [3]$$

a harmonic response to a harmonic excitation.

Up to this point, there can be no quarrel with the reasoning. But next, a bold assumption is made, though it is not recognized as such. Most harmonic oscillators satisfy second order differential equations, and it seems reasonable to assume that this one does too:

$$a\ddot{x} + b\dot{x} + cx = f(t) \qquad [4]$$

Determining the coefficients does not raise any difficulty. The cx term is the restoring force, and can readily be found from static measurements. Then, if we impose an excitation, F cos ωt, we easily obtain the equations,

$$\begin{aligned} (c - a\omega^2) \cos \epsilon - b\omega \sin \epsilon &= F/X \\ (c - a\omega^2) \sin \epsilon + b\omega \cos \epsilon &= 0 \end{aligned} \qquad [5]$$

With c known, these equations yield values for a and b.

Everything seems quite satisfactory. But when the experiment is actually carried out, there is one unpleasant difficulty. If the ship is forced to oscillate at different frequencies, different values are obtained for a and b. This implies that something is wrong with the assumed form for the relationship, equation [4].

But, the investigators were so attracted by the differential equation formulation, with terms which appear identifiable as inertial and damping effects, that they were reluctant to pass it up. Therefore, since most model work was done in regular seas, the artifice was adopted of considering a and b to be functions of ω.

This formulation is, of course, seriously limited, as it is not valid for arbitrary excitation, f(t). If f(t) is representable by Fourier series or Fourier integral, the principle of linear superposition can be used to generate a solution. Even here, we need an infinity (denumerable or non-denumerable) of equations, all of the form of [4]. But in the most general case, the deterministic response to an arbitrary excitation cannot be exhibited.

The first satisfactory treatment of motions in irregular waves was that of Pierson and St. Denis[3], when they introduced statistical techniques and spectral theory. In this analysis, each ω is treated separately, and the above formulation is no serious handicap. However, this theory yields statistical results only, not deterministic.

The present paper is directed toward a solution of this problem. Two new representations will be given, one based on the impulse response and one which may be considered an extension of equation [4]. In both cases, the development is based upon sound principles, rather than intuition. The only significant assumption is the one of linearity of the wave-ship system.

II. THE IMPULSE RESPONSE FUNCTION

When a force $f(t)$ is applied to a ship, there will be a response (in heave, say), $x(t)$. We assume that the ship response is linear. This means that if the responses $x_1(t)$ and $x_2(t)$ correspond to the excitation $f_1(t)$ and $f_2(t)$, the response $a_1 x_1(t) + a_2 x_2(t)$ corresponds to the excitation $a_1 f_1(t) + a_2 f_2(t)$.

Now suppose we have an arbitrary force $f(t)$. Select a sequence of

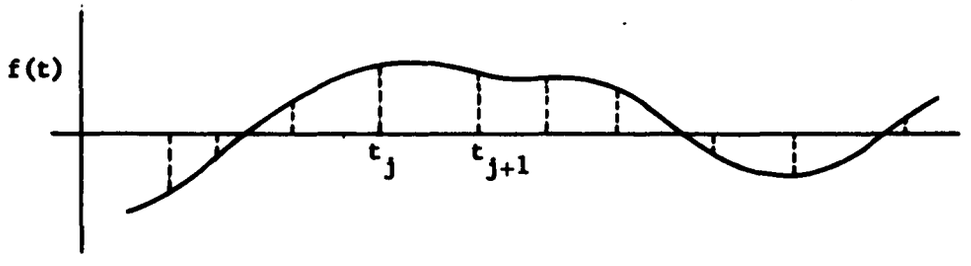

instants on the t axis which break the axis into intervals. Now let us define a function $f_j(t)$ such that

$$\begin{aligned} f_j(t) &= 0 && t < t_j \\ &= f(t) && t_j \le t < t_{j+1} \\ &= 0 && t_j \le t \end{aligned} \qquad [6]$$

It will have the appearance

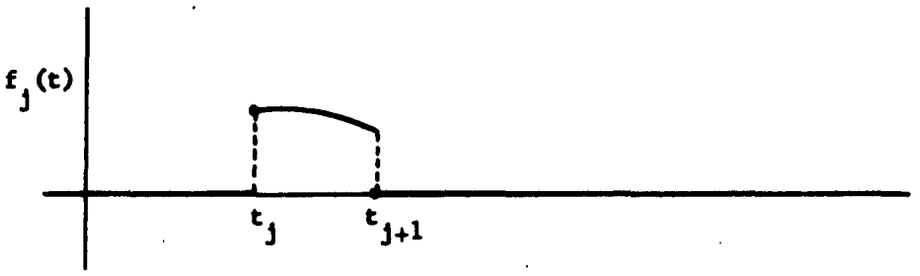

Then

$$f(t) = \Sigma\, f_j(t) \qquad [7]$$

To any $f_j(t)$, there corresponds an $x_j(t)$,

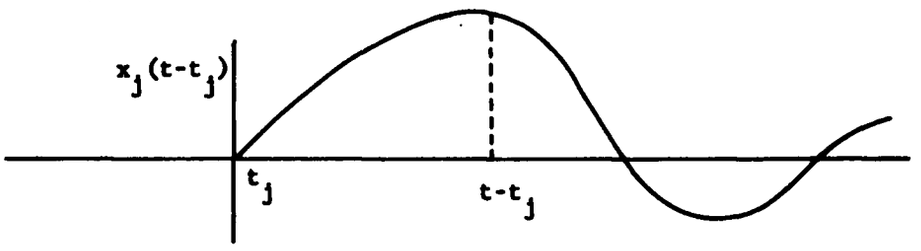

Since, in general, this response is zero until t exceeds t_j, it is convenient to shift the origin of the time axis to t_j. As a consequence of [7],

$$x(t) = \Sigma\, x_j(t-t_j) \qquad [8]$$

Let us define the ratio

$$\frac{x_j(t-t_j)}{f(t_j)\ \Delta_j t} = R_j(t-t_j) \qquad [9]$$

where

$$\Delta_j t = t_{j+1} - t_j$$

Now let the interval $\Delta_j t$ approach zero, holding t_j fixed. If f(t) is continuous to the right at t_j, the function $R_j(t-t_j)$ will approach some limit. This limiting function will be the same for any t_j which is a non-zero continuity point of f(t).

$$\lim \frac{x_j(t-t_j')}{f(t_j)\ \Delta_j t} = R(t-t_j) \qquad [10]$$

For a stable mode, it will ordinarily be of the form shown. R(t) is known as the impulse response function.

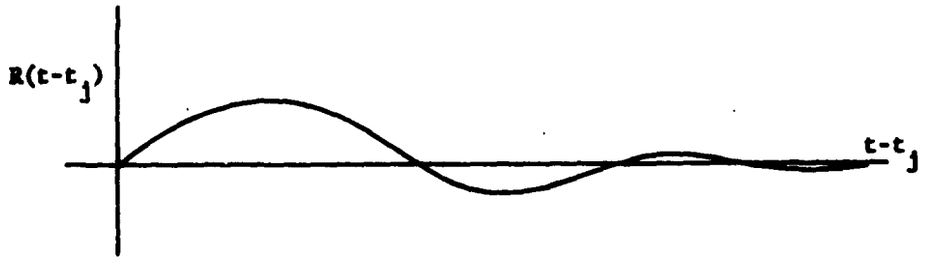

The excitation, given by equation [8], can be written

$$x(t) = \Sigma\ f(t_j)\ R_j(t-t_j)\ \Delta_j t$$

and in the limit,

$$x(t) = \int_{-\infty}^{t} f(\tau)\ R(t-\tau)\ d\tau \qquad [11]$$

By a simple transformation,

$$x(t) = \int_{o}^{\infty} R(\tau)\ f(t-\tau)\ d\tau \qquad [12]$$

Now let us consider the oscillation of a ship in more detail. There are six modes, and we shall designate oscillatory displacements by the following convention

x_1 ... surge	x_4 ... roll
x_2 ... sway	x_5 ... pitch
x_3 ... heave	x_6 ... yaw

Excitations in each of these modes will be designated by $f_i(t)$. If we impose an arbitrary set of excitations, acting in any or all modes, the response in the j^{th} mode can be written

$$x_j(t) = \sum_{i=1}^{6} \int_{o}^{\infty} R_{ij}(\tau)\ f_i(t-\tau)\ d\tau \qquad [13]$$

where, following equation [10], $R_{ij}(\tau)$ is the impulse response function in j^{th} mode for excitation in the i^{th} mode.

This representation is quite general, and holds for any set of $f_i(t)$, just so the response remains linear. The excitation can be continuous or discontinuous, irregular or periodic. Thus, once the functions $R_{ij}(\tau)$ are known, we have a general representation which is free from the restrictions of equation [4].

Now consider the particular case in which

$$f_i(t) = F_i \cos \omega t \qquad [14]$$

Then

$$x_j(t) = F_i \int_o^\infty R_{ij}(\tau) \cos \omega(t-\tau)\, d\tau$$

$$= F_i \left[\cos \omega t \int_o^\infty R_{ij}(\tau) \cos \omega\tau\, d\tau + \sin \omega t \int_o^\infty R_{ij}(\tau) \sin \omega\tau\, d\tau\right]$$

or

$$x_j(t) = F_i \left[R_{ij}{}^c(\omega) \cos \omega t + R_{ij}{}^s(\omega) \sin \omega t\right] \qquad [15]$$

where

$$R_{ij}{}^c(\omega) = \int_o^\infty R_{ij}(\tau) \cos \omega\tau\, d\tau$$

$$R_{ij}{}^s(\omega) = \int_o^\infty R_{ij}(\tau) \sin \omega\tau\, d\tau$$

are the Fourier cosine and sine transforms of $R_{ij}(\tau)$.

We can also write

$$x_j(t) = \left[(R_{ij}{}^c)^2 + (R_{ij}{}^s)^2\right]^{\frac{1}{2}} \cos (\omega t - \epsilon_j) \qquad [16]$$

where

$$\tan \epsilon_j = R_{ij}{}^s / R_{ij}{}^c$$

The functions, $R_{ij}{}^c(\omega)$ and $R_{ij}{}^s(\omega)$, can be considered a mapping in the frequency domain of the impulse response functions in the time

domain, $R_{ij}(\tau)$. They are, specifically, the amplitudes of the in-phase and out-of-phase components of the response, respectively, due to a unit sinusoidal excitation. They provide all the information derivable from equation [4], with its frequency dependent coefficients.

The following identities, which follow directly from the Fourier inversion theorem, are also important:

$$R_{ij}(t) = \frac{2}{\pi} \int_0^\infty R_{ij}^{c} \cos \omega t \, d\omega$$

$$= \frac{2}{\pi} \int_0^\infty R_{ij}^{s} \sin \omega t \, d\omega \qquad [17]$$

A convolution integral representation is not precisely new in the ship motion problem. Fuchs[4] made use of it in studying the motion of a barge in waves. More recently, Dalzell has used it very effectively in some yet unpublished work. Because of its flexibility, it deserves more consideration than it has generally received.

In spite of its advantages, however, it suffers from certain faults. The functions $R_{ij}(t)$ define the response of the ship, but they do not make it easy to analyze the system. For instance, the inertial effect of the water upon the motion is unclear. And if we wish to change the response in a certain way, it is not evident which is the best way to proceed. The usual representation, [4], appears to permit analysis, but the analysis is erroneous. For instance, effects are lumped into the so-called added mass coefficients which are not inertial in their nature, as we shall shortly show. Thus, there remains the need for a formulation which permits one to discuss the hydrodynamic aspects of the response.

III. EQUATIONS OF MOTION

In this section, we shall present a solution to this problem. Only the case for zero speed will be given in detail. For the case with forward speed, see reference 1 or 2.

Suppose a ship to be floating at rest. Let the coordinates of a point in space be $(\zeta_1, \zeta_2, \zeta_3)$, referred to a system of axes with the origin fixed in the free surface above the center of gravity of the ship.

Let the ship be subjected to an impulse which raises the velocity to V_j in the j^{th} mode. During the impulse, all finite velocities and forces may be neglected. The velocity potential of the fluid immediately after the impulse will be $V_j \psi_j(\zeta_1, \zeta_2, \zeta_3)$ where ψ_j satisfies the boundary conditions:

$$\psi_j = 0 \qquad \text{on } \zeta_3 = 0 \qquad [18a]$$

$$\frac{\partial \psi_j}{\partial n} = -s_j \qquad \text{on S (the wetted surface of the ship)} \qquad [18b]$$

where

$$s_j = \vec{n} \cdot \vec{i}_j \qquad j = 1,2,3$$

$$= \vec{r} \times \vec{n} \cdot \vec{i}_{j-3} \qquad j = 4,5,6$$

$\vec{n}$ = outwardly directed unit normal vector

$\vec{r}$ = position vector with respect to the center of gravity

The potential function, ψ_j, is the solution to the Neumann problem obtained by reflecting S in the plane $\zeta_3 = 0$ and assigning

$$\frac{\partial \psi_j}{\partial n} = s_j \qquad \text{on reflection of S} \qquad [19]$$

For all ordinary surfaces, S, this solution exists.

After a short time, Δt, we impose a negative impulse to the ship, reducing its velocity to zero. To first order in Δt, this negative impulse will also bring all fluid motion to a halt. The net effect after these two impulses will be a displacement of the ship by

$$\Delta x_j = V_j \Delta t \qquad [20a]$$

and an elevation of the free surface by

$$\Delta\eta_j = -V_j \frac{\partial \psi_j}{\partial \zeta_3} \Delta t = -\frac{\partial \psi_j}{\partial \zeta_3} \Delta x_j \qquad [20b]$$

Now suppose the ship to be held fixed. The surface elevation will dissipate in a radiating disturbance of the free surface. This wave motion will have a velocity potential, $\varphi_j \Delta x_j$ which satisfies the initial conditions:

$$\varphi_j(\zeta_1, \zeta_2, \zeta_3, 0) = 0 \qquad \text{everywhere} \qquad [21a]$$

and

$$\Delta x_j \frac{\partial \varphi_j}{\partial t} = g\ \Delta\eta_j = -g \frac{\partial \psi_j}{\partial \zeta_3} \Delta x_j$$

or

$$\frac{\partial \varphi_j}{\partial t} = -g \frac{\partial \psi_j}{\partial \zeta_3} \qquad \text{on } \zeta_3 = 0 \qquad [21b]$$

Afterward, we have the conditions

$$\frac{\partial^2 \varphi_j}{\partial t^2} + g \frac{\partial \varphi_j}{\partial \zeta_3} = 0 \qquad \text{on } \zeta_3 = 0 \qquad [22a]$$

$$\frac{\partial \varphi_j}{\partial n} = 0 \qquad \text{on } S \qquad [22b]$$

We assume that φ_j exists.

Now suppose the ship to be undergoing small oscillations, $x_j(t)$, in the j^{th} mode. The velocity potential for the fluid motion generated by this oscillation will be

$$\Theta = \dot{x}_j \psi_j + \int_{-\infty}^{t} \varphi_j(t-\tau)\ \dot{x}_j(\tau)\ d\tau \qquad [23]$$

That this is so is easily seen by verifying that Θ satisfies all the required conditions. It is evident that the boundary condition on S is satisfied. The first term provides the required normal velocity. And since $\frac{\partial \varphi_j}{\partial t} = 0$ (to first order in x_j) on S, the second term does not contribute to the normal velocity. The remaining requirement is the free surface condition.

First note that

$$\frac{\partial^2 \Theta}{\partial t^2} = \frac{d^2 x_j}{dt^2} \psi_j + \varphi_j(0) \frac{d\dot{x}_j}{dt} + \frac{\partial \varphi_j(0)}{dt} \dot{x}_j$$

$$+ \int_{-\infty}^{t} \frac{\partial^2 \varphi_j(t-\tau)}{\partial t^2} \dot{x}_j(\tau)\, d\tau$$

$$= \frac{d\varphi_j(0)}{dt} \dot{x}_j + \int_{-\infty}^{t} \frac{\partial^2 \varphi_j(t-\tau)}{\partial t^2} \dot{x}_j(\tau)\, d\tau$$

by [18a] and [21a]. Also

$$\frac{\partial \Theta}{\partial \zeta_a} = \dot{x}_j \frac{\partial \psi_j}{\partial \zeta_a} + \int_{-\infty}^{t} \frac{\partial \varphi_j(t-\tau)}{\partial \zeta_a} \dot{x}_j(\tau)\, d\tau$$

Therefore,

$$\frac{\partial^2 \Theta}{\partial t^2} + g \frac{\partial \Theta}{\partial \zeta_a} = \dot{x}_j \left[\frac{\partial \varphi_j(0)}{\partial t} + g \frac{\partial \psi_j}{\partial \zeta_a} \right]$$

$$+ \int_{-\infty}^{t} \left[\frac{\partial^2 \varphi_j}{\partial t^2} + g \frac{\partial \varphi_j}{\partial \zeta_a} \right] \dot{x}_j(\tau)\, d\tau$$

$$= 0$$

by [21b] and [22a]. Therefore, Θ is the stated velocity potential.

Equation [23] can be considered to be a sort of hydrodynamic analog of equation [11], with φ_j acting as an impulse response velocity potential and $\dot{x}_j(t)$ acting as the excitation. It is quite as general as [11], as the restriction here is also that the oscillations be sufficiently small for the hydrodynamic response to be linear.

The computation of the function ψ_j is well within the capability of modern high-speed computing machines[5], and it may be useful to compute it in practice. The determination of φ_j is orders of magnitude more difficult, and except for "thin ships" and other idealized surfaces, it cannot be found at the present time. However, as we are concerned here only with the form of the velocity potential, these difficulties do not concern us.

By integrating the pressure over S, we can obtain the hydrodynamic force acting on the ship, and thus set up equations of motion. This can be done without difficulty, and we obtain

$$\sum_{j=1}^{6}\left[(m_j\delta_{jk} + m_{jk})\,\ddot{x}_j + c_{jk}x_j + \int_{-\infty}^{t} K_{jk}(t-\tau)\dot{x}_j(\tau)\,d\tau\right] = f_k(t) \qquad [24]$$

where

$$m_{jk} = \rho\int_S \Psi_j\, s_k\, d\sigma$$

$$K_{jk}(\tau) = \rho\int_S \frac{\partial\varphi_j(\tau)}{\partial t}\, s_k\, d\sigma$$

m_j = inertia of ship in the j^{th} mode

c_{jk} = hydrostatic restoring force coefficient

δ_{jk} = 1 for j=k (the Kronecker delta)
= 0 for $j\neq k$

The above equations give the responses in all six modes to simultaneous excitations in all modes. This immediate extension is permissible because of the linearity of the problem.

The case for the ship having forward speed may be carried out by a similar procedure, though the extension is non-trivial. The equations of motion will resemble those above, except that there will be additional terms on the left, $b_{jk}\dot{x}_j$, the kernels, $K_{jk}(\tau)$ will be more complex, and the c_{jk} will include hydrodynamic restoring force effects. It is to be noted that the hydrodynamic "added mass" coefficients are not functions of velocity. It is also interesting to note that these coefficients are symmetric. That is

$$m_{jk} = m_{kj} \qquad [25]$$

These equations of motion are as generally valid as the assumption of linearity. The excitation can be periodic or non-periodic, continuous or discontinuous, or even impulsive. Comparison with the conventional representation (equation [4]) reveals several important facts. First of all, the inertial effects of the fluid are imbedded in the products, $m_{jk}\ddot{x}_j$, and the m_{jk} are both frequency independent and velocity independent, and are also independent of the past history of the motion. If the excitation is sinusoidal, there will be a component coming from the convolution integral which is in phase with $m_{jk}\ddot{x}_j$, but since it arises from the past history of the motion, and would exist even if $\ddot{x}_j$ were suddenly made zero, it is not inertial in any sense. This is the component which leads to the so-called frequency dependent added mass. The m_{jk}, on the other hand, are true added mass coefficients.

A somewhat similar situation develops with respect to the damping forces. It is usual to lump these in the term $b\dot{x}$. But note that when the forward speed is zero, there is no $b\dot{x}$ term, although there is certainly damping. For sinusoidal oscillation, there will be a component from the convolution integral which is in phase with $\dot{x}$, but since it also arises from the past history of the motion, it would exist even if the velocity, $\dot{x}$, were suddenly reduced to zero. Imbedding this force improperly into a $b\dot{x}$ term leads to the frequency dependent damping coefficient.

We now have two formulations for the response of a ship to an excitation, the convolution integral form based on the impulse response function, and the equations of motion, also involving convolution integrals. As both formulations hold for small oscillatory motions, there are relations between them. It is not difficult to derive the following system of integro-differential equations:

$$\sum_{j=1}^{6} \int_0^t K_{jk}(\tau)\, \dot{R}_{ij}(t-\tau)\, d\tau = \qquad [26]$$

$$-\sum_{j=1}^{6}\left[(m_j\delta_{jk} + m_{jk})\, \ddot{R}_{ij}(t) + b_{jk}\dot{R}_{ij}(t) + c_{jk}R_{ij}(t)\right]$$

A more useful set of algebraic relations may be obtained by means of Fourier transforms:

$$\sum_{j=1}^{6} \left\{ \left[(m_j \delta_{jk} + m_{jk})\, \omega^2 - c_{jk} - \omega K_{jk}^{\,s} \right] R_{ij}^{\,c} - (b_{jk} + K_{jk}^{\,c})\, \omega R_{ij}^{\,s} \right\} = -\delta_{ik}$$

$$\sum_{j=1}^{6} \left\{ (b_{jk} + K_{jk}^{\,c})\, \omega R_{ij}^{\,c} + \left[(m_j \delta_{jk} + m_{jk})\, \omega^2 - c_{jk} - \omega K_{jk}^{\,s} \right] R_{ij}^{\,s} \right\} = 0 \qquad [27]$$

where the superscripts c and s indicate the Fourier cosine and sign transforms.

These latter equations are particularly revealing. If the $K_{jk}^{\,c}$ and $K_{jk}^{\,s}$ were arbitrarily set to zero, these are the relations one would obtain between the frequency response functions, $R_{ij}^{\,c}$ and $R_{ij}^{\,s}$, and the usual frequency dependent coefficients.

It is clear that the frequency dependency of $K_{jk}^{\,c}$ and $K_{jk}^{\,s}$ is forced onto these coefficients in the conventional representation.

CONCLUSIONS

The impulse response functions, (or their transforms), provide a better tool for computing the response to a given excitation. The equations of motion are better for explaining why a ship behaves as it does, and how its behavior will change if certain parameters change. For instance, in model studies, the impulse response function in any mode will change if particular total restraints are imposed in any coupled mode. Or, the ship response will change if the gyradius is altered by changes in loading. But, both of these effects are easily included in modification to the coefficients in the equations of motion.

W. E. Cummins

Thus, these two systems complement each other. If it is possible to pass easily from one system to the other, as we hope, there are several important consequences:

(a) Model experiments can be designed for maximum accuracy rather than for maximum realism. Hydrodynamic effects could be emphasized by testing at small gyradius, and the test results corrected for any desired gyradius.

(b) Restraints may be imposed in any way desired, just so the force imposed on the model is fully known.

(c) Unstable modes would be no problem, as restraints could be used to ensure stability of the whole system. These effects could be removed by calculation, to obtain impulse response functions which are free of restraint.

REFERENCES

1. Cummins, W. E., "The Impulse Response Function and Ship Motions," Schiffstechnik, H.47 B.9, June 1962.

2. Cummins, W. E., "The Impulse Response Function and Ship Motions," David Taylor Model Basin Report 1661, October 1962.

3. St. Denis, M., and Pierson, W. J. Jr., "On the Motion of Ships in Confused Seas," Transactions, Society of Naval Architects and Marine Engineers, V. 62, 1953.

4. Fuchs, R. A., "A Linear Theory of Ship Motions in Irregular Waves," Proceedings, First Conference on Ships and Waves, Hoboken, N.J. 1953.

5. Hess, John L., and Smith, A. M. O., "Calculation of Non-Lifting Potential Flow about Arbitrary Three-Dimensional Bodies," Douglas Aircraft Company, Inc., Report ES 40622, 15 March 1962.

W. E. Cummins

SHIP MOTION RESEARCH IN THE UNITED KINGDOM

G. J. Goodrich
Principal Scientific Officer
Ship Division, National Physical Laboratory
Feltham, England

INTRODUCTION

It is not necessary, in a lecture such as this, to trace the development of the methods now used in the analysis of ship motion records, but it is worth outlining the organizational background to the ship motion research in the UK. Four years ago a number of organizations agreed to co-operate in working on this problem; they were the Ship Division of the National Physical Laboratory, the British Shipbuilding Research Association, the National Institute of Oceanography, and the Admiralty. Each organization had something to contribute to the research, and by virtue of this co-operation a powerful effort to open up this field of work in Great Britain was possible.

Ship Division, NPL, with access to the NPL Mathematics Division computer, was able to undertake the analysis of all the motion records obtained at sea. Model test programmes associated with this work were also undertaken in the Division as well as the theoretical calculations.

The British Shipbuilding Research Association, now the British Ship Research Association (BSRA), with its vast knowledge and 'know-how' of conducting full-scale trials, was responsible for the arrangement of the ship trials. It also undertook the provision of the recording equipment and the installation of such equipment in the ship.

The National Institute of Oceanography (NIO) were able to provide the knowledge for the analysis of sea states, both from the records obtained from a shipborne wave recorder[1] and from a stationary buoy.[2]

The Admiralty Experiment Works (AEW), although not taking an active part in the full-scale trials, provided some of the instrumentation for the ships and a great deal of knowledge on the solution of the problems associated with the analysis of the trials results.

The ship types tested in this co-operative research project are all merchant ships. The Admiralty carry out their own ship motion trials on warship types, and it is reasonable to say that in their case major emphasis is placed upon the motion side. For most merchant ship types more emphasis must be placed upon the prediction of power in irregular waves, although in passenger ships, motions and power predictions are probably of equal importance.

The initial object of the research was to collect data on ship motions and to investigate the possible existence of scale effect. It has always been assumed that scale effect on ship motions will be small, but this has never been firmly established. While valuable full-scale data have been collected, the complexity of the full-scale ship motions is such that accurate model-ship correlation is impossible. During the trials of a number of ships of different types, records were taken of the sea state, the ship motions of pitch, heave and roll, hull strains of propulsive performance. Following the full-scale trials, model experiments will be carried out, in both regular and irregular waves, to obtain a comparison between the model and ship results.

When the original programme was drawn up, the theory of linear superposition was not well established but the whole of the analysis procedure adopted was dependent upon it. The degree of success achieved would in fact throw light on the validity of this basic assumption.

Although a number of ships have been tested, the results of only one series of trials have so far been published.[3] This lecture deals with the results obtained during the trials on the OWS 'Weather Reporter'. The details of the ship dimensions are given in Table I.

TABLE I

Length between perpendiculars	225 ft
Breadth moulded	36 ft 6 in
Mean draught	14 ft 7¼ in
Displacement extreme	1810 tons
Block coefficient	0.528

The machinery is a triple expansion steam engine developing about 2650 ihp at 180 rpm.

THE SHIP TRIALS

The various organisations participating in the trials were represented on a Co-ordinating Committee. This Committee laid down the basic objectives of the research, and thereafter allocated various tasks to two Sub-Committees. The first Sub-Committee to be set up dealt with the problems of instrumentation, the second with the analysis and presentation of results, and both Sub-Committees had some members common to each.

It was decided that the ship motion and wave records obtained on the ship should be recorded both in digital and analogue form. Recorded digitally, the data could be fed directly into the computer for processing. The analogue records proved to be valuable in monitoring the results as taken, and were also useful in editing the digital data where necessary.

The ship was fitted with a shipborne wave recorder, an essential feature, since phase relationships were to be obtained between the waves encountered by the ship and the resulting motions. Such an instrument has to be calibrated as there is an attenuation of the wave height due to the 'Smith' effect and also due to the influence of the ship itself on the wave. The shipborne instrument gave no indication of the direction of the waves encountered, and hence a free buoy had to be used both to calibrate the shipborne recorder and provide data on the directional properties of the waves.[5]

Whilst the final objective in ship motion research must be the measurement and analysis of motions obtained in short-crested seas, it was decided that for the first trials the sea conditions should be as long-crested as possible, i.e. the conditions should if possible be uni-directional. This ideal was never achieved, but even so, analysis of some of the trials was possible. A study of ocean wave conditions was undertaken by NIO to determine the areas giving the biggest probability of long-crested sea conditions. The results of this study showed that the months of March and September were most promising, and that the best sea areas were south of latitude 20°N in the North Atlantic.

Consideration was given to the choice of the first vessel to be used in the research, and a suitable choice was thought to be an ocean weather ship. These ships are run by the Meteorological Office of the Air Ministry, and they were agreeable to the 'Weather Reporter' being used for such trials. The advantage in using such a ship was that the ship was available for trials at any time between her normal duties of weather observing, carried out at six-hour intervals. This particular ship was fitted with the NIO type shipborne wave recorder. The weather ships normally change station about every month; the most suitable weather station for the purpose of the sea trials was station Kilo

(45° N 16° W), and fortunately 'Weather Reporter' was due for a period at Kilo in September/October 1959; this period was therefore chosen for the trials.

The Analysis Sub-Committee considered the existing information on ship motions in an irregular sea and the statistical analysis of random signals such as those obtained at sea. It was anticipated that difficulty would be experienced in analysing the motions in quartering and following seas due to an "Overlap" of frequencies of encounter over a small range of frequencies. It is possible for certain different length waves to meet the ship at the same frequency of encounter and identification becomes impossible. Even so, it was thought to be worthwhile to collect data on the ship motions in quartering and following seas, and the manoeuvre adopted is shown in Fig.1.

In order to obtain data on the variation of ship speed with heading, the ship's engines were run at constant speed for each manoeuvre. Thirteen such trials were carried out in all, in various weather conditions and at a number of different speeds.

Details of the instrumentation used during the ship trials are given by Refs. 3 and 4. The following measurements were taken:

On the Ship

Analogue and digital:
- Shipborne wave height research
- Pitching motions
- Rolling motion
- Heave accelerations

Propeller thrust
Propeller torque
Propeller rpm
Speed (Pitometer log)
Ship heading
Relative wind speed
Relative wind direction

On the Buoy

Heave accelerations
Pitch angle
Roll
Direction of axis of roll observed from the ship.

Since the motions are being dealt with here, no consideration will be given to the power measurements.

G. J. Goodrich

THE RESULTS

The theoretical background to this work has been adequately covered by previous lectures and it is unnecessary to cover the ground again.

The primary result obtained is the two-dimensional wave spectrum. This is obtained from the buoy by methods described in Refs. 2 and 5. Without going into too much mathematical detail, it is worthwhile considering in broad terms the methods used in the development of the directional energy spectrum.

The buoy used is shown in Fig. 2. It was self-contained, carrying its own batteries for supplying the transducers and recording gear. It was equipped to measure vertical heave accelerations, and angular motions about two axes at right angles.

The determination of the axes of the two motions was not very accurate, since a sight had to be made of a red arrow on the shell of the buoy. A refinement to the instrumentation would be to have a gyro sensing the direction continuously.

A spectral analysis was carried out of the so-called roll and pitch records. For the heave accelerations the Fourier analysis was employed. Basically this was because the spectral analysis had too wide a band width and, since the heave displacement is obtained from the accelerations by dividing by $(2\pi f)^4$, accuracy was improved.

Initially the spread of energy is assumed to be of the form

$$E(f\phi) = E(f)\ G\ (S)\ [\mathrm{Cos}^{\frac{1}{2}}(\phi - \bar{\phi})]^{2S}$$

Neumann assumes, incidentally, that $S = 1$ for all frequencies, but the work done shows that S is not constant with frequency. It can be in fact as high as 15.

Cross-correlation of the vertical heave and the pitch and roll angles yields a series of five parameters, and from these parameters the spectrum of $E(f\phi)$ can be determined.

It is now necessary to make a conversion from the two-dimensional energy spectrum of zero speed for the buoy to a one-dimensional spectrum for the ship moving at a given speed in a given direction. For the given speed and direction, lines of constant fe can be drawn. By integrating the energy along these lines of constant fe, the total energy $E(fe)_B$ can be determined. This value of $E(fe)_B$ is plotted to the base of $\bar{f}$, where $\bar{f}$ is a mean frequency, approximately equal to the wave frequency assuming uni-directional waves. Comparisons between the mean frequency $\bar{f}$ and f (uni-directional) to base of fe show this to be justified.

It is now possible to compare directly the energy measured from the buoy $E(fe)_B$ and the energy measured on the shipborne wave recorder $E(fe)_S$. Fig. 3 shows the results for SK 12. The ratios are plotted on a log scale to a base of f^2, since they should be approximately of the form $0.69\, e^{(8\pi^2 f^2/g)d}$ where d is a depth comparable with the mean depth of the pressure transducer of the shipborne recorder. A good deal of scatter exists due to the statistical nature of the analysis. However, a straight line is a reasonable fit to the data and was calculated by least squares. It is interesting to consider the values of d obtained by the trials:

	d	d/d_r	$d_r = 7.1$ ft where d_r is the actual depth of the pressure transducer.
SK 11	18.7	2.63	
SK 12	16.8	2.37	
SK 13	16.2	2.28	

With the ship stationary, the mean value of the ratio for the three trials was 2.30.

The directional spectrum obtained from SK 12 is represented as a polar diagram, and is shown in Fig. 4. Only wave frequencies up to 0.15 cps are shown, but values up to 0.30 cps were included in the analysis. It can be seen that the dominant energy is of low frequency and was in fact the result of a low frequency swell. The high frequency waves were wind-generated and hence the spread of energy was fairly large. The spectrum is not symmetrical about the head sea direction but is skewed at the high frequencies.

Also contained in Fig. 4 are curves of coherency, obtained from the analysis, for wave to pitch, wave to heave and wave to roll. It can be seen that coherency is generally high for pitch and heave in head seas and low for roll; it is low for pitch but high for heave in beam seas and is highest for roll in beam seas.

The effect of sea direction on the ship motions is shown, together with the phases between the motions and the waves. The largest effect of direction is produced on the roll response, and the effect is rather small on the other motions. It is interesting to note the sharpness of the roll response. The peak is well defined at 0.1 cps, and the phase between wave and roll is zero at this frequency.

COMPARISON OF MODEL AND SHIP RESPONSES

Model experiments have been carried out on a 10 ft long model of the "Weather Reporter." The model was dynamically similar to the ship during the trials. The experiments have so far only been conducted in head seas and the motions of pitch and heave were recorded; roll and yaw were restrained.

A comparison of the model and ship results is shown in Fig. 5. The ship pitch response is less than the model response for $f_e < 0.2$ cps. At the high frequencies the slope of the responses are similar. The ship heave response and the model self-propelled heave response agree fairly well.

Also shown in these diagrams are the calculated responses. The calculations were based upon the work of Korvin-Kroukowsky,[6] although the damping characteristics have been determined using Grim's 1959 data.[7] The calculated pitch response agrees well with the ship results, but it must be remembered that the ship results may not be comparable with the calculated results owing to the directional spread of energy in the wave system encountered by the ship.

A great deal more work has to be carried out on the model to determine the effect of wave direction on the responses. From such results, it should be possible to build up the complex response of the model to a previously determined two-dimensional wave spectrum measured at sea. In this way a more direct comparison will be obtained between the model and the ship.

While the calculated results agree reasonably well with the model and ship, experiments will be carried out to determine the damping and entrained water characteristics of the model over a range of frequencies and forward speeds. These will be obtained from forced motion experiments in calm water.

FUTURE WORK

Further full-scale work will be carried out and plans are being made to test an 18,000 ton DW tanker next year. This work will be carried out in a similar way to the trials already done on other ships, though it may differ in points of detail. New digital equipment will be used, enabling more channels to be digitized.

The problem of the accurate determination of the directional energy spectrum is not yet solved, and the National Institute of Oceanography plan further work in this field.

The collection of sea data in a statistical form is under way, particularly in the fishing areas frequented by British trawlers. The White Fish Authority and Ship Division, NPL, are co-operating in this work. Twelve selected trawler skippers are to make regular reports on sea state data, and NPL have undertaken to analyse them.

Ship stresses are collected by the BSRA in a statistical form and this work should produce valuable data.

Although the Series 60 forms have been extensively tested in waves, these forms are not representative of modern European ship-building practice, and it is therefore important to obtain information on the effects of variations in form on the motions and propulsive performance. If the theoretical calculations can be proved to be accurate, it may not be necessary to carry out a full systematic series of tests. A major part of the data could be obtained using a computer, though this will depend upon whether or not non-linear effects can be dealt with accurately.

BIBLIOGRAPHY

1. Tucker, J.J. — A Shipborne Wave Recorder. Trans. INA, 1956.

2. Longuet-Higgins, M.S., Cartwright, D.E. and Smith, N.D. — Observations of the Directional Spectrum of Sea Waves using the Motions of a Floating Buoy. Conference on Ocean Wave Spectra, Easton, National Academy of Sciences, Washington, USA, 1961.

3. Canham, H.J.S., Cartwright, D.E., Goodrich, G.J. and Hogben, N. — Seakeeping Trials on OWS 'Weather Reporter'.

4. Canham, H.J.S. — Ship Trials. NPL Seminar on Seagoing Qualities of Ships. October, 1961.

5. Cartwright, D.E. — The Use of Directional Spectra in studying the Output of a Wave Recorder on a Moving Ship. Conference on Ocean Wave Spectra, Easton. National Academy of Sciences, Washington, USA, 1961.

6. Korvin-Kroukowsky, B.V. and Jacobs, Winnifred R. — Pitching and Heaving Motions of a Ship in Regular Waves. SNAME, 1957.

7. Grim, O. — Die Schwingungen von Schwimmenden, Zwei Dimensionale Körpen. Berechnung der Hydrodynamische Kräfte. HSVA Report 1171, 1959.

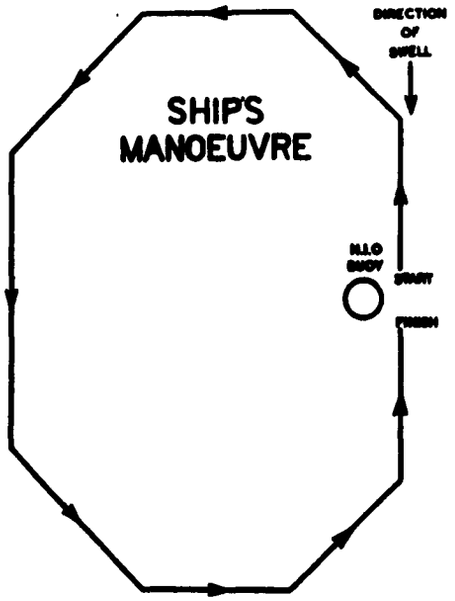

Fig.1 Ship's Manoeuvre

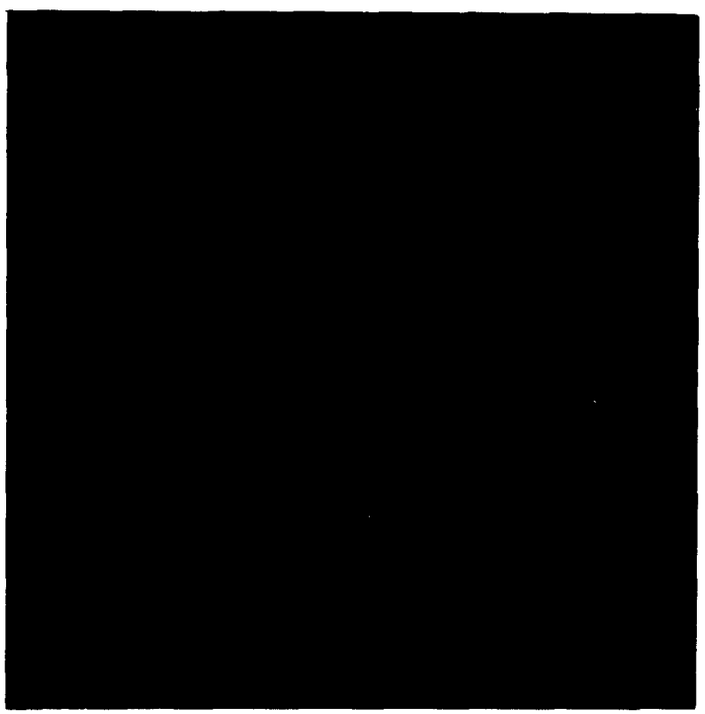

Fig.2 Wave Buoy

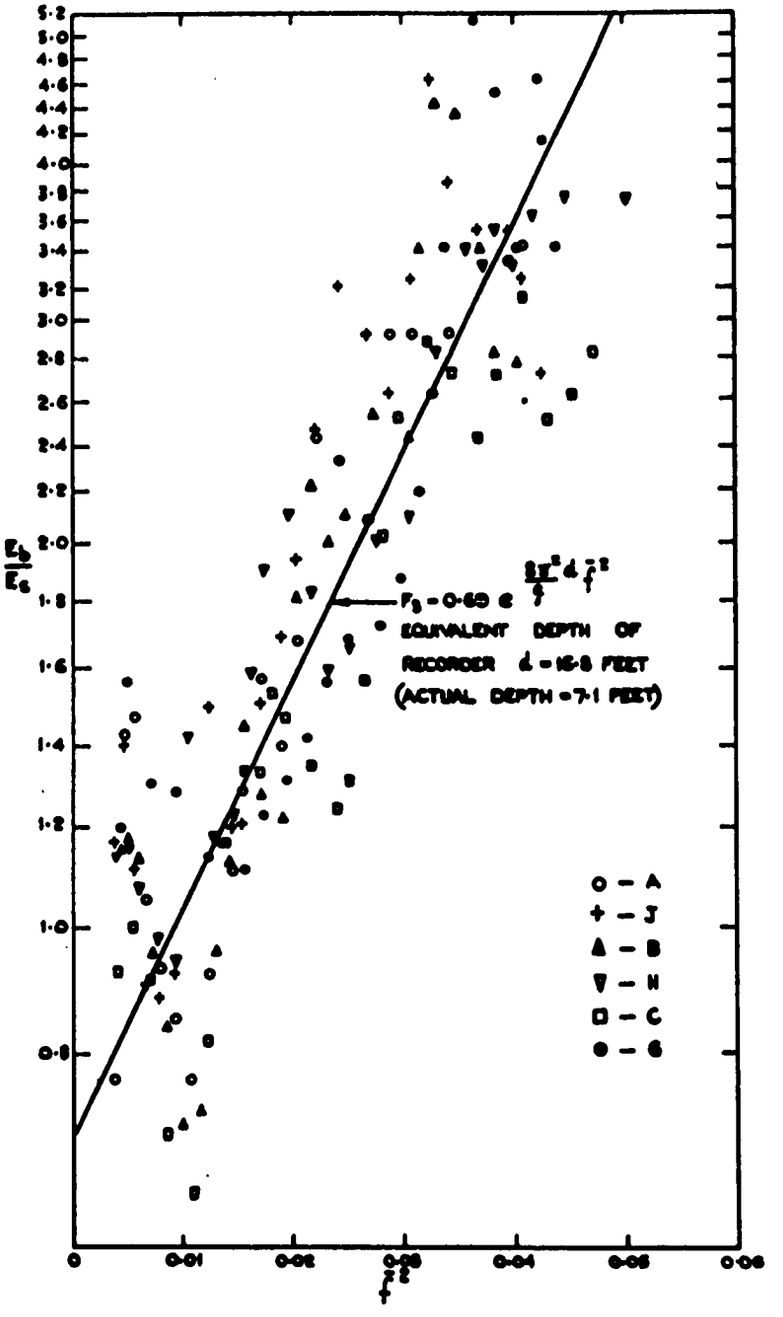

Fig.3 Ship and Buoy Correlation
(Log Plotting of E_B/E_S against $\bar{f}^2$)

G.J. Goodrich

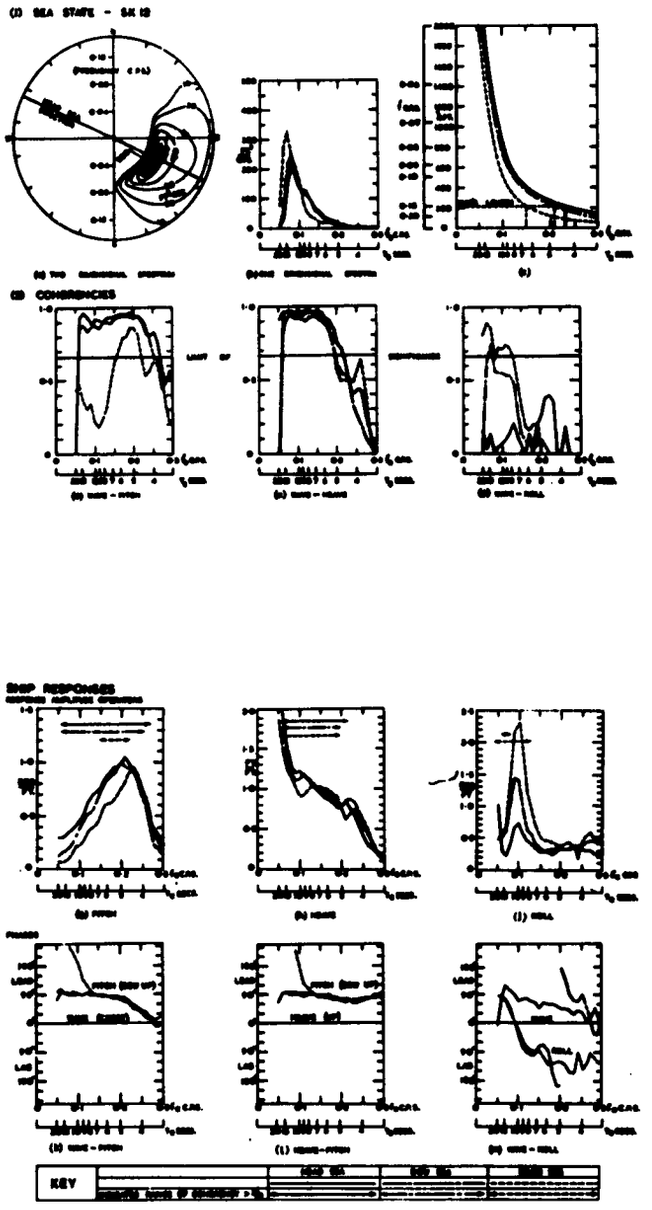

Fig.4 Results of Seakeeping Trial SK12

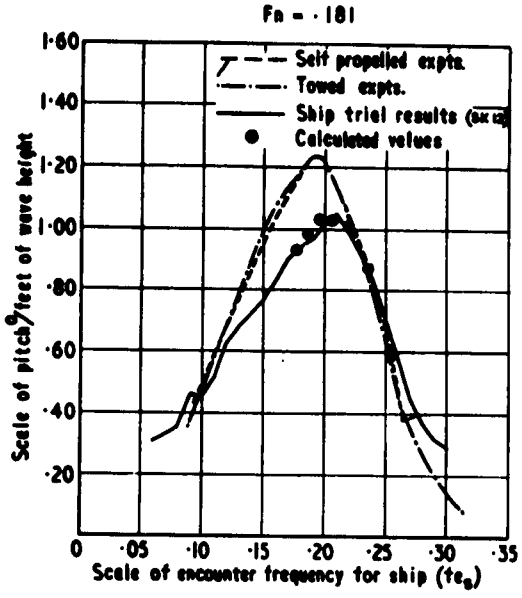

Fig. 5A Comparison of Ship and Model Pitch Response

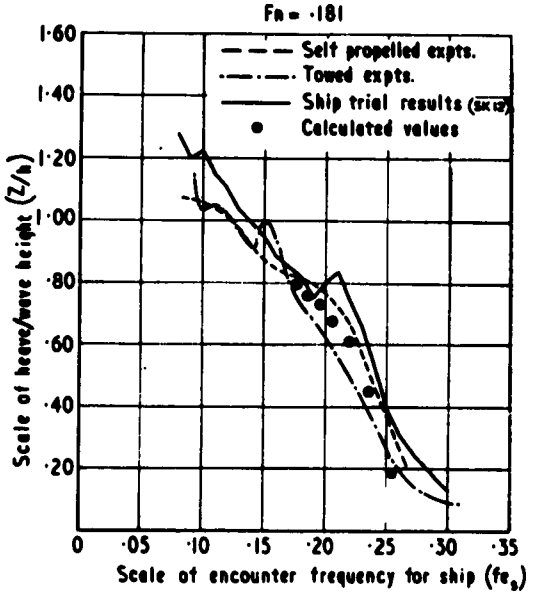

Fig. 5B Comparison of Ship and Model Heave Response

PROGRESS IN TANK STABILIZERS

A. J. Giddings
Naval Architect
Bureau of Ships
Navy Department
Washington, D.C.

I. INTRODUCTION

Tank stabilizers using the U-tube analogy have been designed for a variety of naval ships. None of these have been combatant ships, but they have been ships which meet one or more of the criteria for passive tank stabilization as expressed in reference (1). Repeating these criteria:

a. Low speed operations are a major characteristic.

b. Hull penetrations for retractable fins are not practicable and retraction is required or desired.

c. Only "some" rather than "a lot of" stabilization is needed.

d. Cost is more important than the degree of stabilization.

e. Space and weight are available with little penalty to the mission.

Ship types which have met the requirements are icebreakers, missile range ships, oceanographic research and survey ships, and other special purpose ships. More than 17 designs have been completed.

The very virtues of the free-surface type passive stabilizer tank that make it attractive in application, work against a large investment of time and effort in the scientific analysis of their performance. The tanks are cheap to install, and perform well without a great deal of design effort. As little as 3 man hours have been spent (by an experienced designer) on the geometric design of some tanks. More time, of course, is involved in structural design and performance prediction. A design data sheet will be issued in the near future (it is awaiting printing) which will simplify the geometric design process still further.

In spite of the foregoing de-emphasizing factors, certain results are available and a limited amount of analysis of them has been made.

References (2) and (5) are some of the published model test results while references (6) and (7) report full scale results. Through the cooperation of Military Sea Transportation Service the trials of reference (7) were especially complete in that a number of measured sea states were obtained and variations in tank water level, heading and speed were all obtained. References (8) and (9) are computer predictions of stabilizer performance.

II. FULL SCALE

Analysis of the full scale reports compared with predictions has been limited by a lack of suitable full scale trials. For example, references (2), (6) and (9) should be directly comparable, but the trials of reference (6) do not provide sufficient data. The trials of USNS ELTANIN, reference (7), were conducted in December 1961, and the report issued very recently. For this reason, little can be said in detail about the quality of the predictions. However, since the ELTANIN trials were so complete, it is expected that considerable analysis and comparison will be forthcoming.

The method of analysis of full scale motions which is being used as a design tool is a highly linearized and de-coupled approach to the equations of motion. The full-scale runs selected for analysis of roll performance are low speed beam-sea runs. The measured sea state spectrum is used as an input in the analysis, so such measurements are necessary.

The unstabilized ship is considered as a single degree of freedom harmonic oscillator, and the amplitude response curves for several damping coefficients are plotted. The sea spectrum is converted to a wave slope spectrum by:

$$\frac{\psi^2(\omega)}{\Delta\omega} = \left(\frac{\omega^4}{2g}\right)^2 \frac{H^2(\omega)}{\Delta\omega}$$

The "effective" wave slope on the ship is considered to be a function of the depth of the center of buoyancy and the ratio of ship beam to wave length.

The effect of center of buoyancy on the spectrum is

$$e^{-\frac{4\pi z}{\lambda}} = e^{-\frac{2\omega^2}{g} z}$$

where: "z" is the depth of the center of buoyancy.

The effect of ship beam is obtained by integrating the static moment generated by a sinusoidal wave and relating this to the moment obtained from a wave of infinite length and slope ψ_e, or:

$$\frac{\psi_e}{\psi} = \frac{3\left[\sin\frac{\pi B_e}{\lambda} + \frac{\pi B_e}{\lambda}\cos\frac{\pi B_e}{\lambda}\right]}{\left(\frac{\pi B_e}{\lambda}\right)^3}$$

where: ψ_e = effective wave slope

B_e = effective beam (actual beam times the prismatic coefficient)

λ = wave length

This may be sufficiently approximated by

$$\frac{\psi_e}{\psi} \approx e^{-\left(\frac{B_e}{\lambda}\right)^2} = e^{-\frac{B_e^2\omega^2}{(2\pi g)^2}}$$

The "effective" wave slope spectrum is then:

$$\frac{\psi_e^2(\omega)}{\Delta\omega} = \frac{H^2(\omega)}{\Delta\omega}\frac{\omega^4}{(2g)^2}e^{-2\left[\frac{\omega^2 z}{g^2} + \frac{B_e^2}{4\pi^2}\frac{\omega^4}{g^2}\right]}$$

This spectrum is multiplied by the square of amplitude response to obtain a roll spectrum. The average values of "predicted" roll and measured roll are compared to obtain a value of "full scale" linear ship roll damping.

A similar approach is used in analyzing the stabilized runs, except that the amplitude response curves used are those for the stabilized ship and various values of velocity-squared tank damping coefficient are investigated.

The same approach has been used to analyze other ship motions. The details of the shape of the predicted ship motion spectra do not agree with the measured spectra, but the approach is useful for comparison of various designs.

A. J. Giddings

III. MODEL

The larger number of model test reports has permitted the completion of some analysis. This analysis has been aimed at verifying the design process, which is aimed at selecting a tank geometry which will provide the desired frequency. Figure 3 summarizes the approach used in design at the Bureau of Ships. The contribution of the nozzles to the calculated frequency is usually very small so that the "basic" frequency can often be used alone.

Table 1 shows a comparison of the design frequency versus the measured frequency for 7 designs at different water depths. The measured frequency was determined from phase measurement of tank water transfer or moment as compared to roll angle. The moment and water transfer phase angles are usually close to each other. The tank models were oscillated in each case in "pure roll," in that the roll axis of the model tank was located to scale, and no sway of that point was permitted.

Table 2 is a similar comparison of the design approach with "exact" theory as taken from water wave theory in a rectangular tank.

Figure 1 is a graph of the values of tables 1 and 2 versus the parameter $1-\gamma^2$. It can be seen that both the model results and the exact theory bear the same relation to the design approach using the U-tube analogy. Even those model tanks having narrow cross-over ducts fall in line. (Ships 2, 3, 4, 6 and 7). Figure 2 is a plot of the same data arranged to investigate the dependence on water depth. This is not a strong dependence except for large values of γ. Practical considerations of U-tube "moment" terms will lead the design to values of γ between .4 and .7, so that this effect as shown by "exact" theory is not important.

It is recommended that the curve of figure 1 be used to correct the U-tube frequency in the design process.

NOTE: The opinions expressed in this paper are those of the author and do not necessarily represent those of the Navy Department.

A. J. Giddings

REFERENCES

(1) Roll Stabilization by Means of Passive Tanks - Vasta, et al - SNAME Annual Meeting, November 1961

(2) Experimental Model Investigation of Heeling Tank Stabilizer for AK253 - Odenbrett and Yamanouchi, ETT Letter Report 725

(3) Experimental Study of a Passive Rolling Tank Stabilizer Installation for a Pacific Missile Range Recovery Ship AG(PMR) - Odenbrett, Davidson Laboratory Report 778

(4) Experimental Investigation of a Passive Rolling Tank Stabilizer Installation for an Oceanographic Research Ship (AGS) - Odenbrett, Davidson Laboratory Letter Report 799

(5) Model Test of a Passive Anti-Roll Tank for a Class III Survey Ship - Russ, DTMB Report 1618

(6) A Full Scale Evaluation of Passive Anti-Roll Tanks Aboard an AK-Type Ship - Golovato, DTMB Report 1414

(7) Preliminary Evaluation of Passive Roll Stabilization Tanks Installed Aboard the USNS ELTANIN (TAK 270) - Foster, DTMB Report 1632

(8) Analog Simulation of a Passive Anti-Rolling Tank System for an Oceanographic Survey Vessel - Oliver and Church, DTMB Report 1233

(9) Analog Simulation of a Passive Anti-Rolling Tank System for a Missile Range Ship - Church, DTMB Report 1322

A. J. Giddings

TABLE 1. COMPARISON OF MEASURED TANK FREQUENCY AND U-TUBE ANALOGY FREQUENCY

SHIP	ω_{DES}	ω_{MEAS}	γ	ℓ/R_2	AR	$1-\gamma^2$	$\frac{\omega_{MEAS}}{\omega_{DES}}$
1	.800	.695	.606	1.00	.053	.633	.869
	.902	.779	.606	1.00	.068	.633	.864
2	.511	.460	.51	.57	.068	.74	.900
3	.666	.675	.389	.50	.111	.849	1.014
4	.462	.470	.462	.50	.082	.838	1.017
	.504	.501	.462	.50	.098	.838	.994
	.542	.533	.462	.50	.114	.838	.983
5	.550	.452	.709	1.00	.042	.497	.822
	.632	.535	.709	1.00	.056	.497	.846
	.701	.603	.709	1.00	.070	.497	.860
6	.661	.671	.486	.396	.108	.764	1.015
	.775	.743	.486	.396	.149	.764	.959
	.867	.912	.486	.396	.189	.764	1.051
7	.570	.504	.51	.57	.085	.74	.884

TABLE 2. COMPARISON OF EXACT WAVE THEORY IN A RECTANGULAR TANK WITH U-TUBE ANALOGY

$$\omega_{exact} = \sqrt{\tfrac{g}{B}\pi \tanh \pi AR} \qquad \text{(Lamb; Art 251)}$$

$$\omega_{U\text{-}tube} = \sqrt{\frac{2g}{B}\frac{1}{AR + \frac{1-\gamma^2}{4R}}}$$

	$\omega_{exact}/\omega_{U\text{-}tube}$					
AR	γ 0	.4	.5	.6	.8	1.0
.04	1.112	1.020	.964	.892	.671	.086
.06	1.112	1.021	.966	.894	.676	.132
.08	1.114	1.023	.968	.897	.682	.176
.10	1.116	1.026	.972	.902	.692	.219
.15	1.121	1.035	.983	.917	.720	.322
.20	1.127	1.047	.998	.936	.761	.419
$1-\gamma^2$	1.0	.84	.75	.64	.36	.0

A. J. Giddings

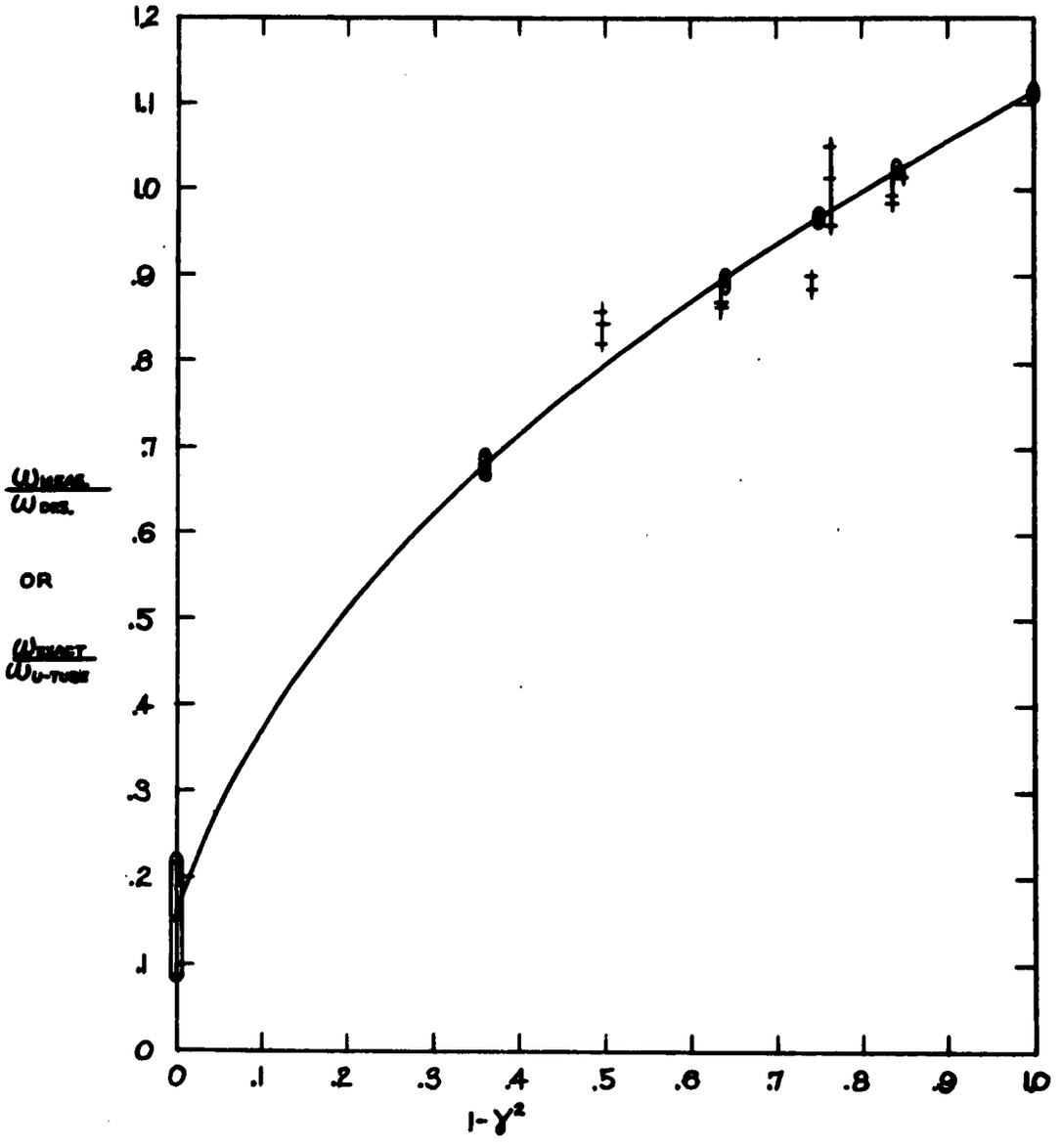

A COMPARISON OF DESIGN VALUES WITH MEASURED OR "EXACT" VALUES AS A FUNCTION OF $1-\gamma^2$.

‡ RANGE OF MEASURED VALUES.

▮ RANGE OF EXACT VALUES FOR $AR = .04$ TO $AR = .10$.

FIG. 1

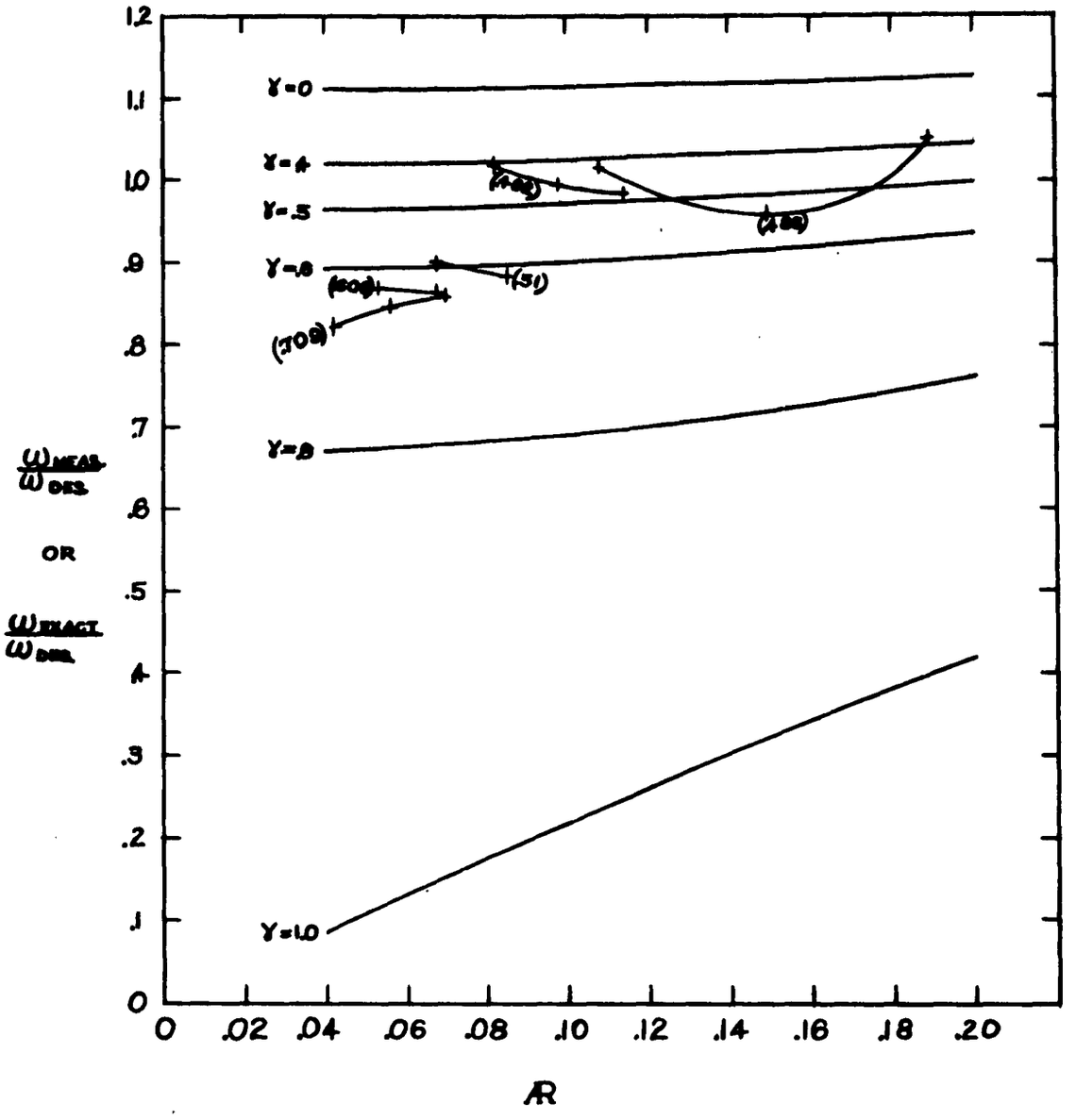

THE DEPENDENCE OF $\frac{\omega_{MEAS.}}{\omega_{DES.}}$ AND $\frac{\omega_{EXACT}}{\omega_{DES.}}$ ON AR AND Y.

NUMBERS IN PARENTHESES ARE Y VALUES FOR THE PARTICULAR TANK.

— : EXACT
+ : MEASURED

FIG. 2

TANK NATURAL FREQUENCY - U-TUBE ANALOGY

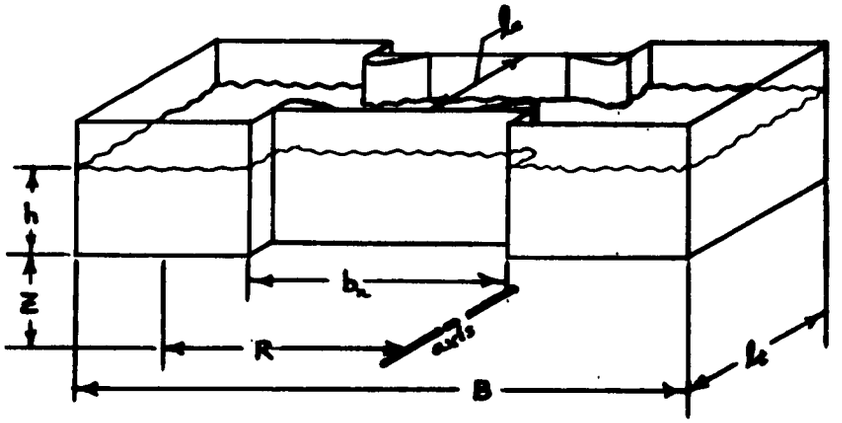

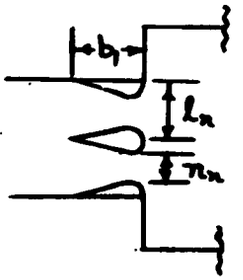

NOZZLE PLAN

$$\omega_t = \sqrt{\frac{2g}{S'}} \quad \text{, RAD/SEC.}$$

$$S' = \int_0^L \frac{A_o}{A_{(\ell)}}\, d\ell \qquad \tau_t^2 = \frac{S'}{B} = \frac{2g}{B\omega_t^2}$$

let $\tau_t^2 = \tau_b^2 + \tau_n^2$ ("BASIC" PLUS "NOZZLE")

$$\tau_b^2 = AR + \frac{M}{AR} \quad , \qquad M = \frac{(1-\gamma)^2 + 2(1-\gamma)\gamma\frac{\ell_s}{\ell_c}}{4}$$

$$\tau_n^2 = \frac{(1-\gamma)\,C_W}{AR}\,\frac{b_1}{\ell_c}\left[\frac{\ell_s}{N\eta_n}F - 1\right]$$

A_o = SURFACE AREA OF ONE "WING" TANK
$A_{(\ell)}$ = CROSS SECTION AREA AT "ℓ"
ℓ = DISTANCE ALONG "ℓ" OF EQUIVALENT U-TUBE.

$AR = \frac{h}{B}$ $\quad \gamma = \frac{b_n}{B}$ $\quad C_W = \frac{\ell_s}{B}$ $\quad$ N = NO. OF NOZZLE OPENINGS

"M" and "F" ARE GRAPHED IN THE DDS.

FIG. 3

A. J. Giddings

STABILITY AUGMENTATION FOR SURFACE PIERCING HYDROFOIL CRAFT

Henry R. Ask
Senior Analytical Engineer
Hamilton Standard Division UAC
Broad Brook, Connecticut

I INTRODUCTION

Early in 1960, the decision was made by Hamilton Standard to perform a feasibility study for Grumman Aircraft and the former Dynamic Developments, Inc. on providing stability augmentation for the craft now called Denison. A two part study [1,2] was made, the results of which form the main body of this paper. As a result of the Phase I study, Hamilton was awarded the contract to supply the stability augmentation system for the prototype craft. Since that time, Hamilton has performed many similar studies on both fully submerged and surface piercing foil equipped craft and currently is providing hardware for a number of development programs.

In those cases studied, involving several different craft configurations using surface piercing hydrofoils, the general conclusion was the same. Longitudinal stability augmentation of the craft configurations studied afforded a significant increase in the seakeeping capabilities. In fact, the term stability augmentation might well be dropped, in this case, in favor of "seakeeping augmentation". The craft investigated were, in most cases, quite stable inherently or could be modified for improved stability. However, studies showed that a significant increment in improved performance could always be obtained when operating in a seaway. The type of augmentation and the degree of complexity were variable, but the performance gains were apparent.

The study results that follow are typical of the theoretically predicted results of other investigations. Because of the current interest in Denison, it is believed that the Denison investigation would prove most interesting.

II DETAILED DISCUSSION

All the surface piercing craft studied were conventional in design, i.e., all were configured with the main supporting foils forward. In addition, the aft foils were fully submerged.

Figure I is a schematic side view of the Denison foil system plus the general terminology used for the analytical investigation. The aft foil assembly is fully submerged with the foil rotatable for incidence control. The forward foil is a swept double dihedral assembly with a portion of the lower foil section flapped.

The angular rotation of the aft foil with respect to its neutral position is designated (δa) and the forward flap angular rotation (δf). The basic motions investigated were the heaving motions of the craft (Z), the pitching motions (ψ), and their derivatives. The instantaneous forward and aft foil immersions were designated h_f and h_a respectively. The longitudinal response of the craft was studied, using the equations of motion presented to this seminar two years ago by Dr. Francis Ogilvie.

For a detailed study of the basic assumptions and equation development, Dr. Ogilvie's paper 3 is referenced. For this study, the unsteadiness effects were ignored and the equations were modified to include the non-linearities of the particular craft under study.

Figure 2 is a compilation of the longitudinal equations in general form. A brief review of the equation representation is given below:

The first equation is the summation of forces along the x axis and the second is the summation of torques about the horizontal longitudinal axis. The general lift equation is shown, where the area factor (s), the lift curve slop (C') and the angle of attack (α) are all variables for the surface piercing forward foil. For the controlled case, the term ($K\delta$) is summed with α. ($K\delta$ being flap or foil angle times flap effectiveness.)

The area term forward (S_f) is shown as $2A_f$ (h_f), where (h_f) is the instantaneous forward foil immersion defined as a function of the steady state calm water value (d'_f), the instantaneous craft heave (Z), the product of the pitching term (ψ) and the variable forward moment arm (l_f). When operating in a seaway representation, the area is also a function of the instantaneous sea amplitude shown as acos ($\nu t + kl_{fr}$). The term (ν) is the incidental wave frequency and (kl_{fr}) is the phase lead of the wave motion with respect to the craft cg position. For the aft foil which is fully submerged with no dihedral, the general lift equation is modified by making the area (S_a) constant or zero when h_a equals zero and sign changes on the terms l_a and K_{la}. The lift curve slopes are also functions of the instantaneous immersion and were treated accordingly, based on experimental data.

Basically, the angle of attack (α) of the foils can be expressed as a function of the craft pitching angle (ψ), the vertical component of the orbital water velocity (v_w) and the instantaneous foil vertical velocity (v). Specifically (v_w) is equal to the product of the wave amplitude (a), the wave frequency (ω) in radians, the depth exponential

$e^{-K\zeta}$ and the sine instead of cosine of the same terms described for the wave amplitude expression. The depth exponental is evaluated by an iterative process in computation using the mean values of foil immersion (ζ).

The foil vertical velocity (v) is simply the sum of the craft vertical velocity at the cg ($\dot{z}$) and the local vertical velocity component due to pitching. ($l_f\dot{\psi}$). Due to the swept back forward foil and hence longitudinal travel of the center of pressure, the forward moment arm was considered variable in the torque summation equation being a function of the instantaneous immersion. The aft moment arm was considered constant.

The actuator dynamics were assumed second order having an exponentially decaying simusoidal time response. The damping (ζ) was assumed near critical and cutoff frequency (f_o) was adjusted to not seriously degrade controller response. Other non-linear constraints (not shown), such as actuator velocity limiting and position limiting, were used if the initially computed values were found excessive.

The control dynamics were variable in the course of optimizing the craft performance.

The command input ($c_{a,f}$) to the actuators was made a function of basic craft motions and/or its derivatives modified by simulated internal controller dynamics.

This particular study used a sinusoidal sea representation. Although not necessarily a realistic disturbance input, the sinusoidal sea is nevertheless invaluable in determining trends in performance. Later studies on a similar craft using statistical seas showed that although performance might be predicted for a particular sea state, trends in performance were indeed difficult to assess for varying craft and controller dynamics.

The equations analyzed were not bounded by the hull. Whenever motions exceeded values which were indicative of substantial hull contact, the performance was considered unsatisfactory. The equations shown were mechanized on a high speed repetitive analog computer. All significant non-linearities were programmed from experimental or geometric data.

Figures 3, 4 and 5 are curves which describe the variation of the parameters S_f, l_f, C'_f and C'_a with immersion. In each case, the variables were programmed on the computer exactly as shown or by a number of straight segments. Figure 3 also shows a line drawing of the front view of a forward foil as well as the projected and planform areas as a function of immersion. Figure 4 shows that the forward moment arm due to sweep varies by approximately 15% or greater, depending on immersion.

III COMPUTER PERFORMANCE

Figure 6 shows the smooth water transient response of the craft uncontrolled. The transient response is also shown for the 40 and 50 knot cases with a typical controller implementation. It can be seen that the craft is fairly well behaved uncontrolled, requiring approximately 2 cycles to settle after an impulse disturbance. The damped natural frequency of the craft varied from .2 cps at 60 knots to .11 cps at 40 knots. It is interesting to note that when this craft is operating in a following sea with wave amplitudes roughly equal to the effective strut length, the incidental waves with $\frac{\lambda}{2a}$ ratios in the 20/1 to 40/1 band are arriving around .1 to .2 cycles per second. On the basic of this observation and the computed calm water stability as shown, one might tentatively conclude that the performance in a following sea with the above conditions would be marginal, since the uncontrolled craft damping in pitch and heave is less than critical. One must expect amplification of a wave forcing function when it occurs at the damped natural frequency of the vessel.

The seakeeping performance investigation of the craft was restricted to the following conditions:

head seas
following seas } $2a = 5$ ft, $\lambda/2a = 20/1,\ 40/1$

head seas
following seas } $2a = 8$ f5, $\lambda/2a = 20/1,\ 40/1$

These conditions are somewhat indicative of sea state 5 with a wind velocity of 20 knots where 5 feet is the average height and 8 feet the significant wave height. From the energy standpoint, however, even the sinusoidal 5 foot sea representation contains more energy than a true statistical sea in a 20 knot wind. In addition, all the energy is concentrated in a single frequency. If this single frequency occurs at or near the natural frequency of the craft, a more rigorous sea representative could hardly be chosen. As was pointed out earlier, however, this study was not to determine actual performance in a particular seaway but to determine trends in performance.

Regular wave trains were applied to the longitudinal craft representation as determined by the particular amplitude, wavelength, craft heading and velocity conditions. It was found that operation in head seas, where the impinging wave frequencies were high, yielded results similar to the short crested following sea case. From the standpoint of what is required to keep the craft foil borne, the following sea case is much more rigorous. Hence, all results shown are for following seas.

Figures 7, 8 and 9 are shown as typical computer response photos for the following sea condition. Figure 7 shows what is believed to be the three most important parameters used in assessing craft longitudinal performance. The top photo is the vertical accelerations at the cg. The top trace indicates the uncontrolled acceleration level and the lower trace the level with a control implementation considered near optimum for the conditions. The two lower photos show the forward and aft instantaneous foil immersions respectively. These parameters contain all the motions of interest with respect to the surface and hence are a direct indication of either foil broach (h = 0) or hull contact (h = effective strut length). The H = 0 level is the short solid trace to the left before the oscillations start. The point of hull contact is found by measuring off a distance equal to 8 feet from the zero immersion line.

The typical computer responses on Figures 8 and 9 are shown for three following sea conditions. Examination of the pitching and heaving motions will show that the control system is not as effective for the short crested case, based on the relative improvement. This is due primarily to the actuator response limitations. However, the short crested case can be negotiated successfully without augmentation.

One of the most important conclusions resulting from previous analytical and experimental investigations on surface piercing craft was the steady state downward shift in heave in a seaway. This shift, due to the non-linearities, was observed in the results computed for this study also. Further, the measured offset was found to be a direct function of the magnitude of the craft oscillations. With augmentation, the steady heave component was small and not easily measured. Uncontrolled, the steady heave for some cases exceeded 50 percent of the wave amplitude forcing function. Figure 10 shows the ($\Sigma dc/2a$) for four following sea conditions. Obviously this shift can contribute to the craft's inability to perform under certain sea conditions and could make the difference between success or failure.

Figure 11 is a normalized plot of pitching amplitude versus wave length. Again, for the short crested sea, the control system provides no apparent advantage. However, for longer wave lengths, the pitching motions were reduced 5 to 10 times that of the uncontrolled motions. The lowest points indicate that use of both fore and aft control of foils yields an additional significant reduction in pitching amplitudes. Figure 12 is a similar plot of normalized heave motions versus wave length. Figures 13 and 14 show the maximum instantaneous immersion versus wave length for the fore and aft foils. The points plotted significantly above the hull clearance line are, of course, unrealistic. As was pointed out earlier, the problem was not bounded by the hull.

The points plotted do illustrate that the chances for success are markedly improved when the optimum fore and aft augmentation control is used. Figure 15 shows the improvement in accelerations mea-

sured. For large amplitudes, the accelerations followed no set pattern because of non-linearities. However, for the controlled case where motion amplitudes are small, the acceleration levels are near those which may be predicted from linear theory.

IV TYPICAL SYSTEM IMPLEMENTATION

The actual implementation of a stability augmentation system to achieve the performance gains cited follows techniques presently used for airborne vehicles.

Figure 16 shows, in simplified schematic form, the system composition for longitudinal stability augmentation. To stabilize the craft in heave, an accelerometer is used to sense heave accelerations. The heave acceleration signal is processed in the electronics to remove undesirable inputs and integrated in approximate form. The processed signal is then fed to a servo valve in the port and starboard actuator servo loops. The actuator drives the flap until the sensed flap position signal feedback cancels the input.

The pitching motions of the craft are sensed with a vertical gyro. The electronics processes the signal to drive the servo valve in the aft foil position servo loop. The present Denison System utilizes heave rate as the basic feedback signal to the forward flaps and pitch rate to the aft foil. To take full advantage of the forward flap actuator implementation, the Denison System has been expanded to provide augmentation in roll also. This is done by actuating the flaps differentially, in response to processed roll error as sensed by the vertical gyro. In addition, yaw rate as sensed by a separate rate gyro is fed differentially to the forward flaps to cause the craft to bank into a turn for increased maneuverability.

The system described is quite sophisticated since it performs a number of functions. It is entirely possible, however, that for this craft or any other craft, only a single axis control would be used for simplicity and economy. The studies performed to date have shown that substantial longitudinal performance gains can be had with single axis foil or flapped foil control alone.

Experimental results will be forthcoming in the near future with the Denison System now in the early phases of flight testing. A manned-fifth scale model has been undergoing testing for some time with stability augmentation. Weight and size restrictions have minimized the on-board instrumentation, hence, performance to date has been assessed primarily on a qualitative basis. Some quantitative data has been taken on the one fifth scale manned model which is quite promising.

Figure 17 is a composite plot of impulse response of the craft in pitch as computed theoretically and as measured experimentally. The experimental data was recorded on the 1/5.5 Froude scale manned model and corrected to prototype time units by $\sqrt{5.5}$. The damping and the natural periods are in quite good agreement. Also shown is the impulse response measured experimentally for the same conditions using the stability augmentation system.

Figure 18 is data taken experimentally with the manned model running in a following sea. The waves were approximately 1 foot in height with a crest to crest distance extimated between 10 and 15 feet. Theoretical studies predicted that the stability augmentation system would not be very beneficial for such a short crested wave condition. However, the experimental data shows that a better than expected reduction in the craft oscillatory responses does occur for this relatively high wave encounter frequency. There is little doubt that a substantial improvement in seakeeping qualities does take place on the model and the fully instrumented prototype will soon provide the comprehensive quantitive data required.

The basic conclusion of this study and other studies on similar surface piercing foil equipped vessels is that stability augmentation can provide a significant improvement in seakeeping ability, even though the vessel may have good inherent stability characteristics.

Present thinking revolves about two basic hydrofoil craft types:

1. Surface Piercing
   Fixed Foil Hydrofoil Craft:
   Limited to inland waters or sheltered ocean areas.

2. Fully Submerged Hydrofoil Craft:
   Potentially capable of operation in the open sea better than 90% of the time.

From this and other similar studies performed to date, plus the experimental flight testing accomplished thus far, a third category of hydrofoil craft is suggested.

3. Surface Piercing Hybrid
   Hydrofoil Craft With Sea Keeping Augmentation:
   Capable of operation in moderate to heavy open sea conditions with augmentation and possessing the ability to perform without controls for less rigorous conditions.

It would seem reasonable that, just as aircraft designs are extremely variable for many uses, the "hybrid" hydrofoil craft will also find its place in the rapidly expanding field of hydrofoil craft application.

REFERENCES

1. "A Study of the Longitudinal Stability of the Marad Hydrofoil and Possible Automatic Control Applications" -- HSER 2209.

2. "A Continuation of the Study of the Longitudinal Stability of the Marad Hydrofoil Utilizing Forward and Aft Flap Control" -- HSER 2220.

3. "The Theoretical Prediction of the Longitudinal Motions of Hydrofoil Craft" -- T. F. Ogilvie (USN-DTMB Report - 1138.)

4. "Methods for Estimating the Longitudinal and Lateral Dynamic Stability of Hydrofoil Craft" -- Kaplan, Hu & Tsakonas (SIT Report No. 691).

5. "Observing and Forecasting Ocean Waves" -- N. O. Pub. No. 603, USN Hydrographic Office.

6. "Experimental and Theoretical Studies of Hydrofoil Configurations in Regular Waves" -- Leehey and Steele (USN-DTMB Report-1140).

7. "Experimental and Analytical Studies of the Longitudinal Motions of a Tandem Dihedral Hydrofoil Craft in Regular Waves" -- V. M. Wetzel, University of Minnesota, St. Anthony Falls Hyd. Lab Technical Paper No. 30, Series B.

8. "Theory of Wing Sections" -- Albott and VonDoenhoff.

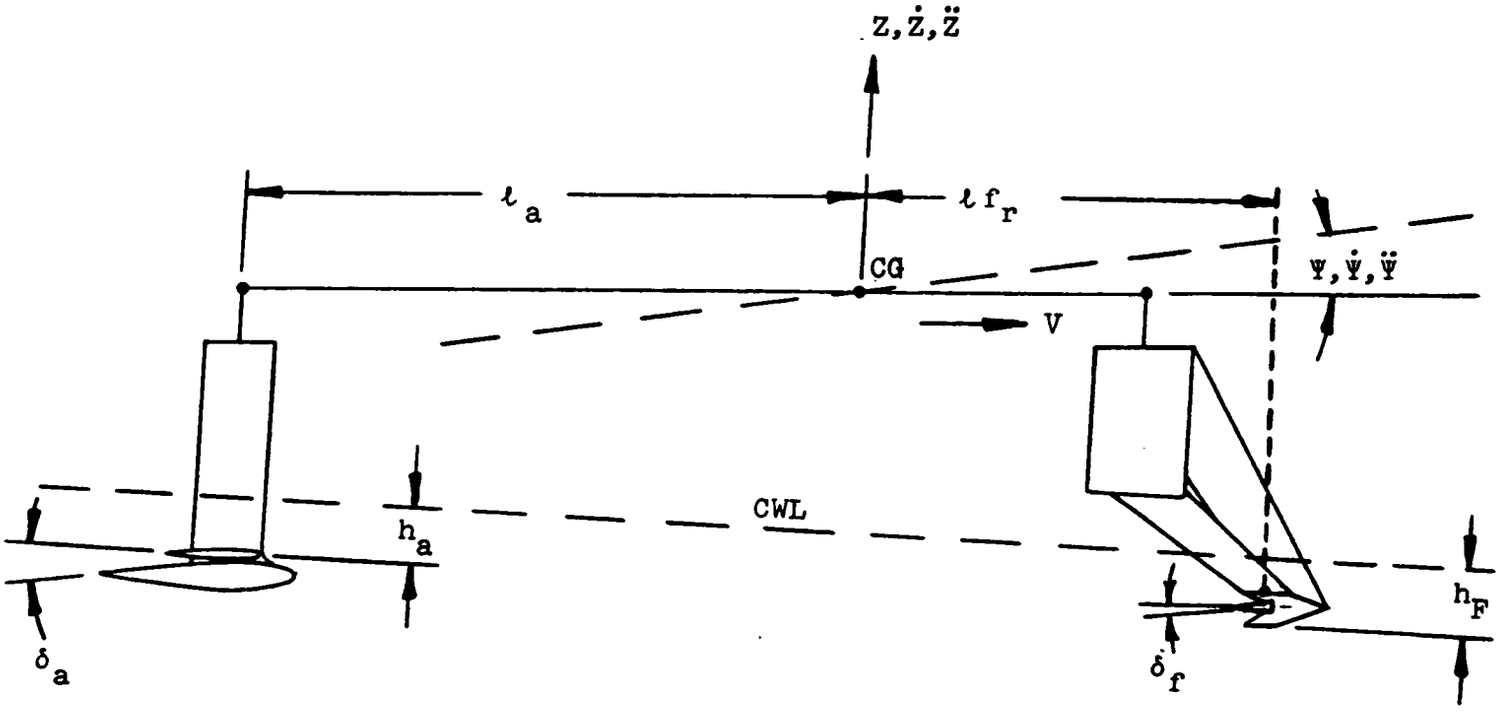

FIGURE I. GENERAL FOIL CONFIGURATION USED

CRAFT:

$$M\ddot{Z} = L_f + L_a - W$$

$$I\ddot{\Psi} = L_f l_f - L_a l_a$$

where:

$$L_{f,a} = \frac{\rho V^2}{2} S_{f,a} [C_0 + C' (\alpha + K_{f,a} \delta_{f,a})]$$

specifically:

$S_f = 2A_f(h_f)$. $\quad h_f = [d'_f - Z - l_f\Psi + a \cos(\nu t + Kl_{fr})]$

S_a = Constant or 0 when $h_a = 0$

$C'_{f,a} = f(h_{f,a})$. $\quad \alpha = \Psi + \frac{v_w - v}{V}$

where $v_w = \pm a\omega e^{-K\beta} \sin(\nu t + kl_f)$

$v = \dot{Z} + l_f\Psi'$

$l_f = f(h_f)$ l_a = Constant

Actuators:

$$\delta_{f,a} = c_{f,a} Ke^{-\beta t} \sin 2\pi f_0 t \quad \text{(Linearized)}$$

Control:

$c_{f,a} = f(\ddot{Z}, \dot{Z}, Z, \dot{\Psi}, \Psi)$ (Depending on Control Implementation)

Figure 2. GENERAL EQUATIONS OF MOTION

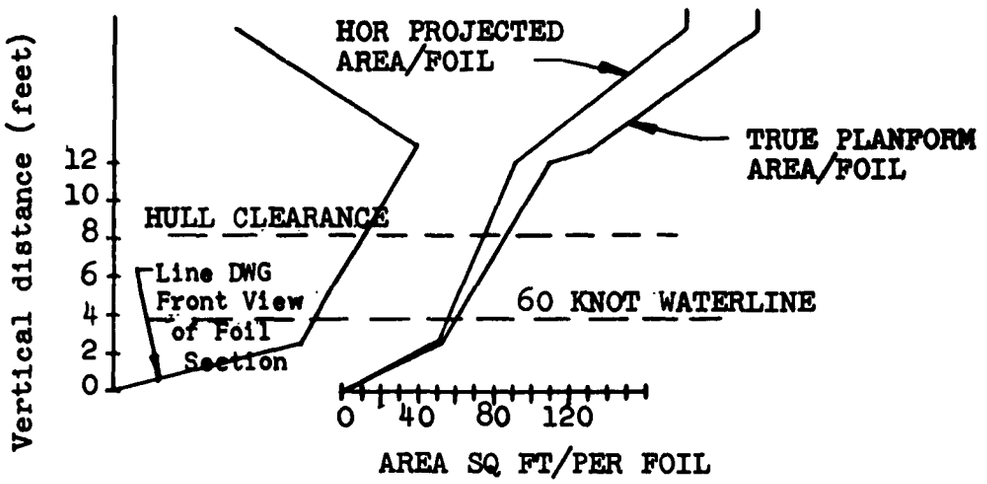

FIGURE 3. FORWARD FOIL AREA VS IMMERSION

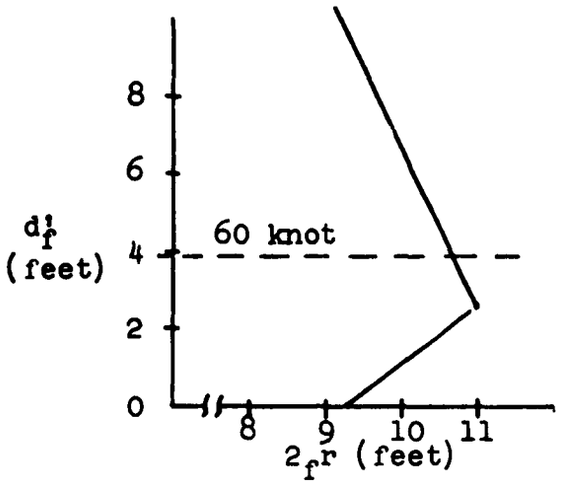

FIG.4. VARIATION IN FORWARD MOMENT ARM VS IMMERSION

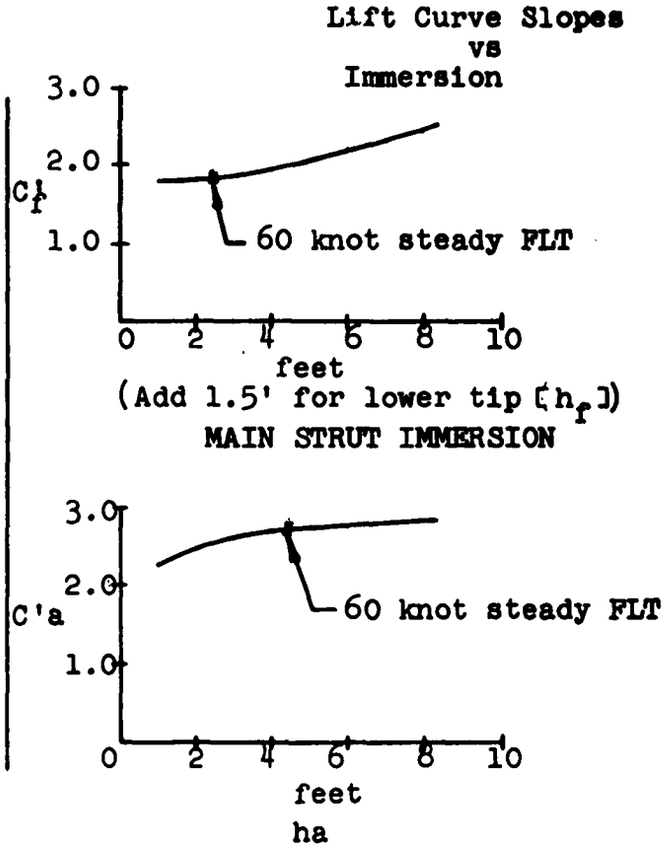

FIG.5. TAIL FOIL IMMERSION

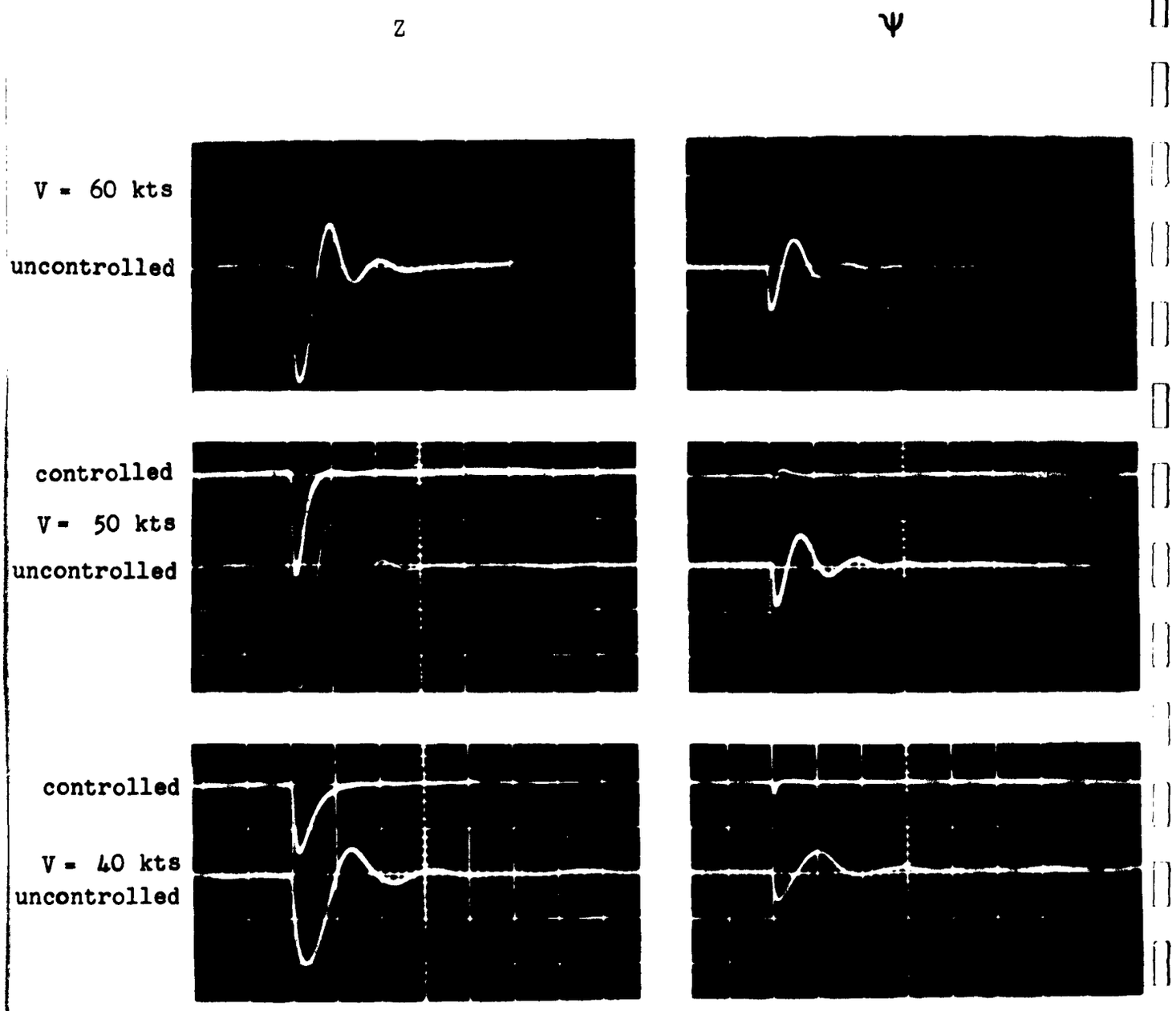

Z - Vertical Motion at the C.G.

Ψ - Pitching Motion at the C.G.

Time Scale - 5 sec/Major Division

FIGURE 6

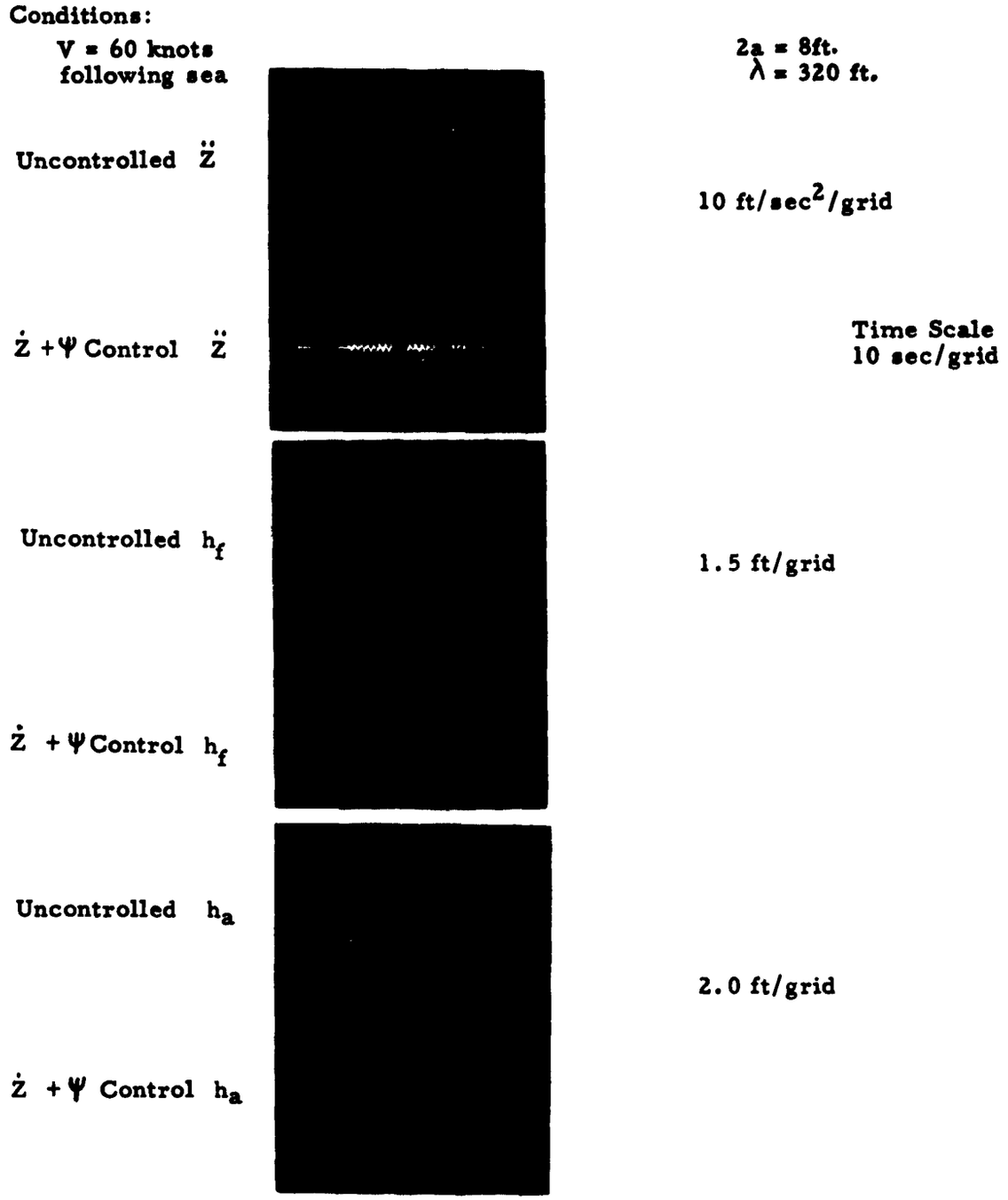

Figure 7. IMPORTANT PARAMETER RESPONSES IN A SEAWAY

General Conditions

V = 60 knots following sea

Time Scale
10 sec/grid

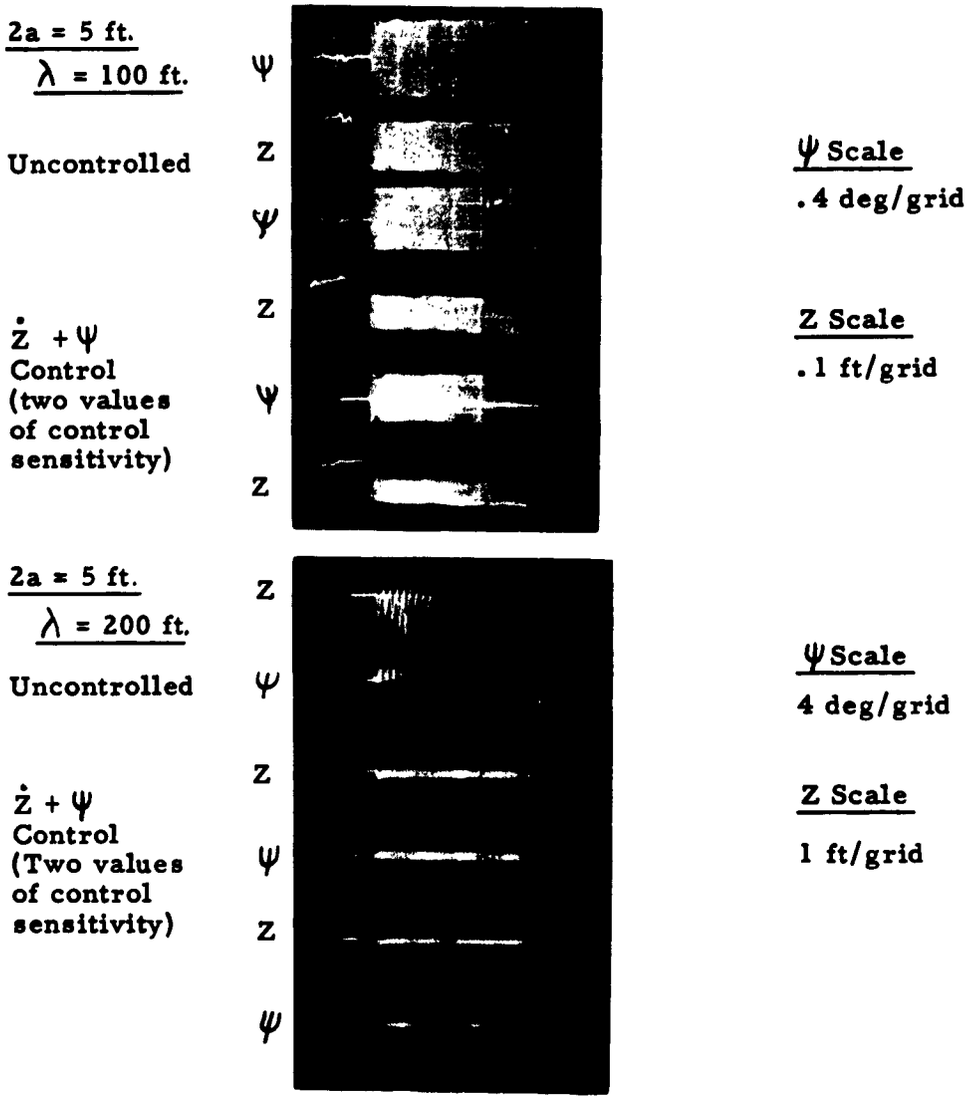

Figure 8. PARAMETER RESPONSES IN A SEAWAY

GENERAL CONDITIONS:

V = 60 knots following sea

Time Scale:
10 sec/grid

2a = 8 ft.
λ = 340 ft.

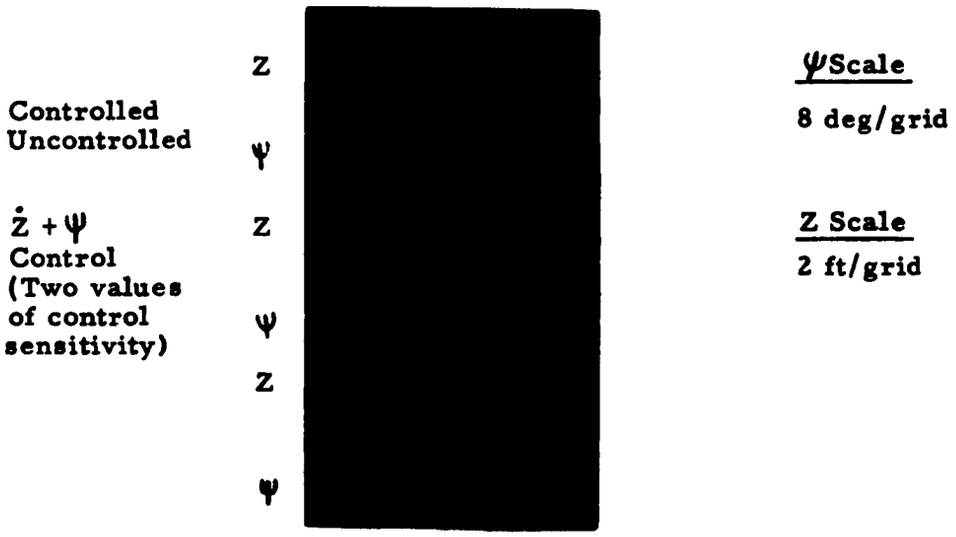

Figure 9. PARAMETER RESPONSES IN A SEAWAY

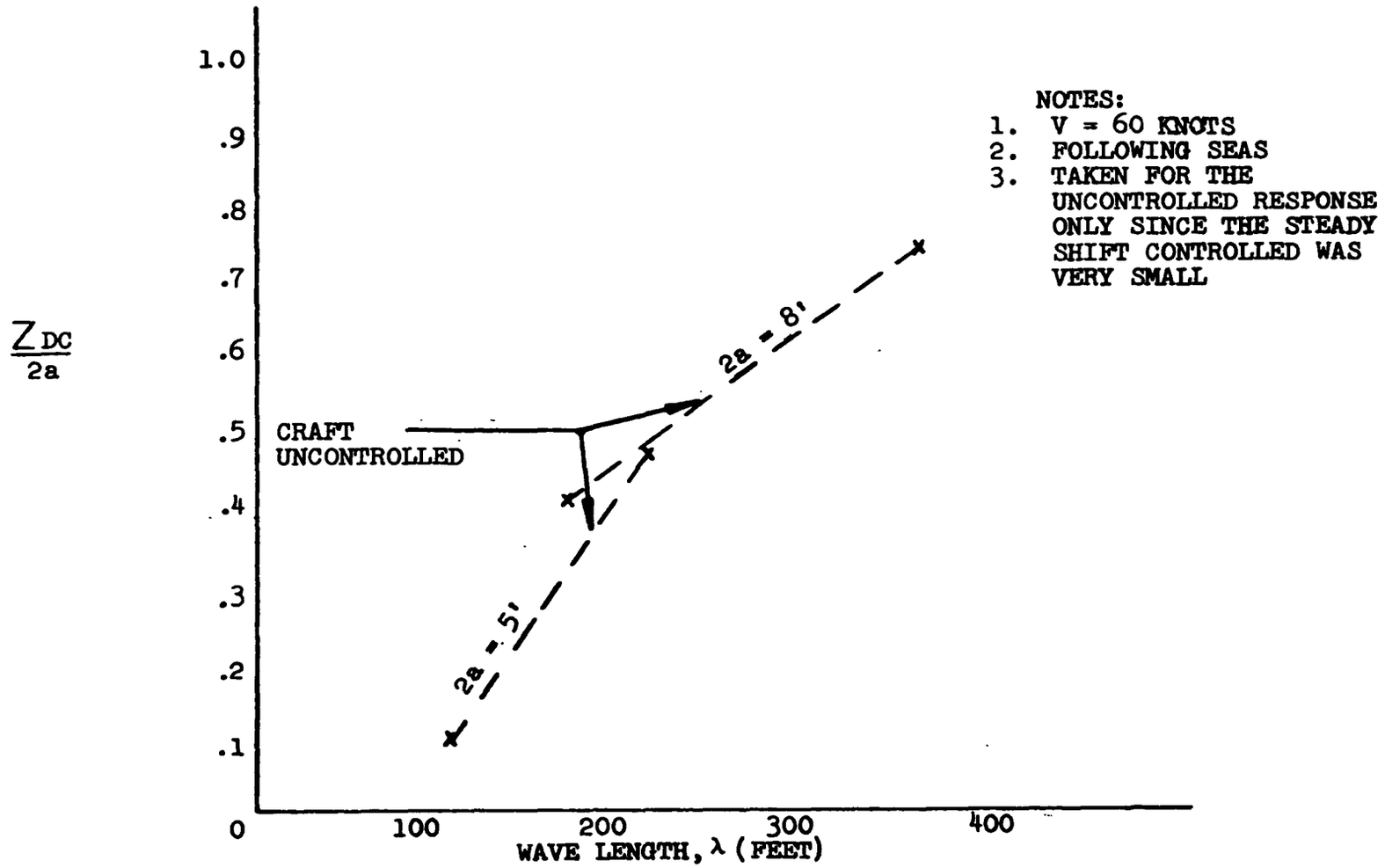

FIGURE 10. STEADY SHIFT IN HEAVE VS WAVE LENGTH

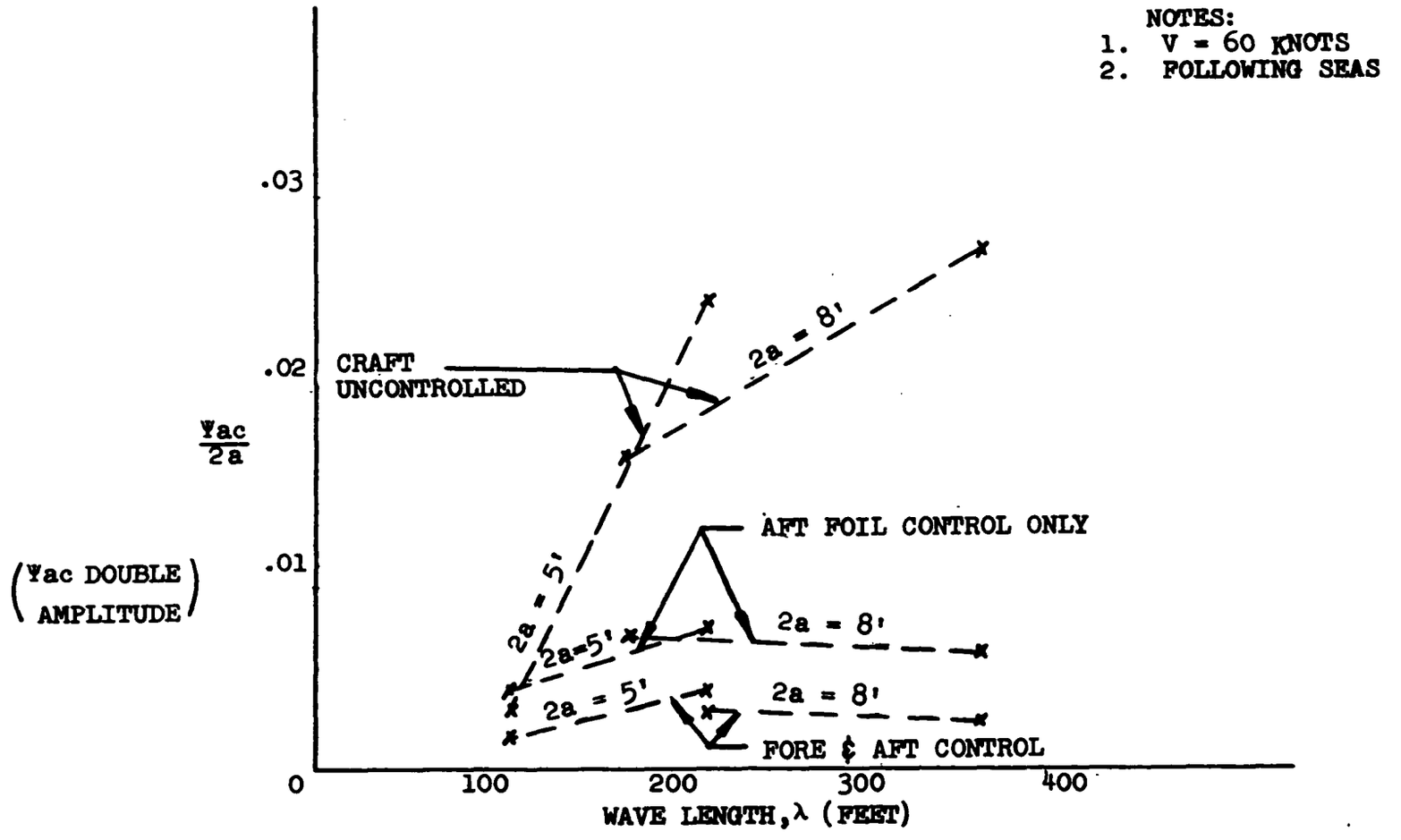

FIGURE 11. PITCH OSCILLATIONS VS WAVE LENGTH

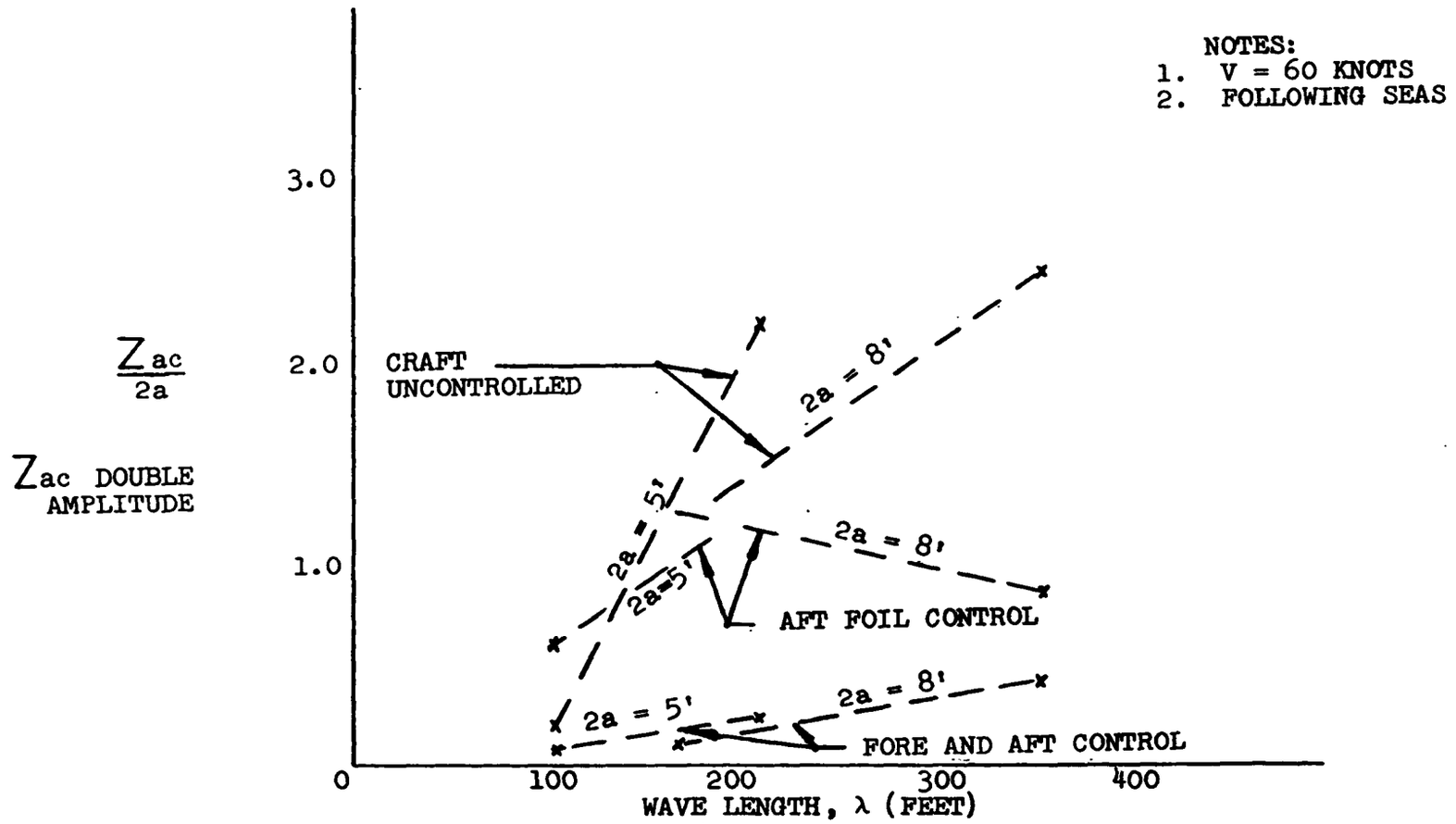

FIGURE 12. HEAVE OSCILLATIONS VS WAVE LENGTH

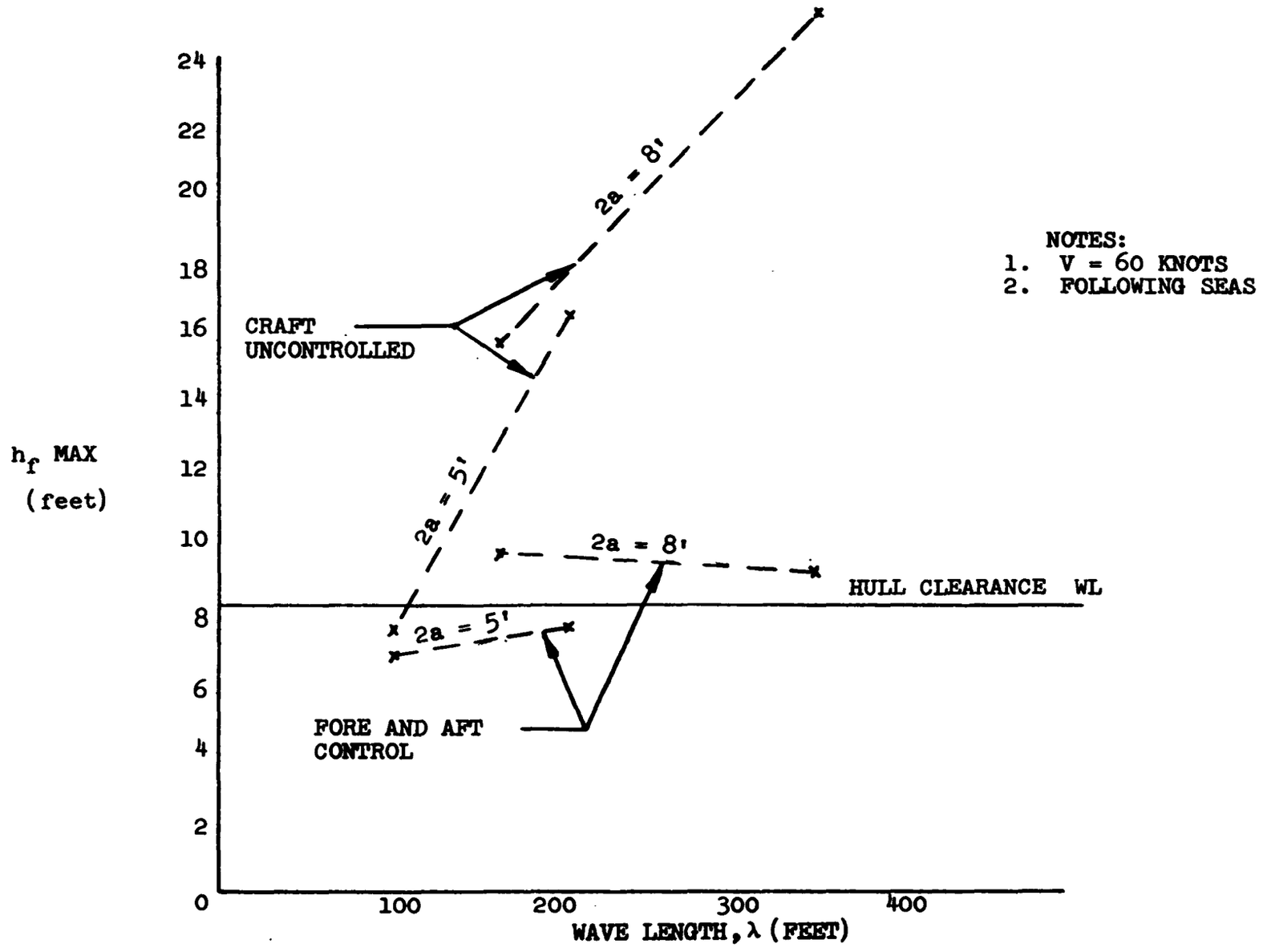

FIGURE 13. MAXIMUM INSTANTANEOUS FORWARD FOIL IMMERSION VS WAVE LENGTH

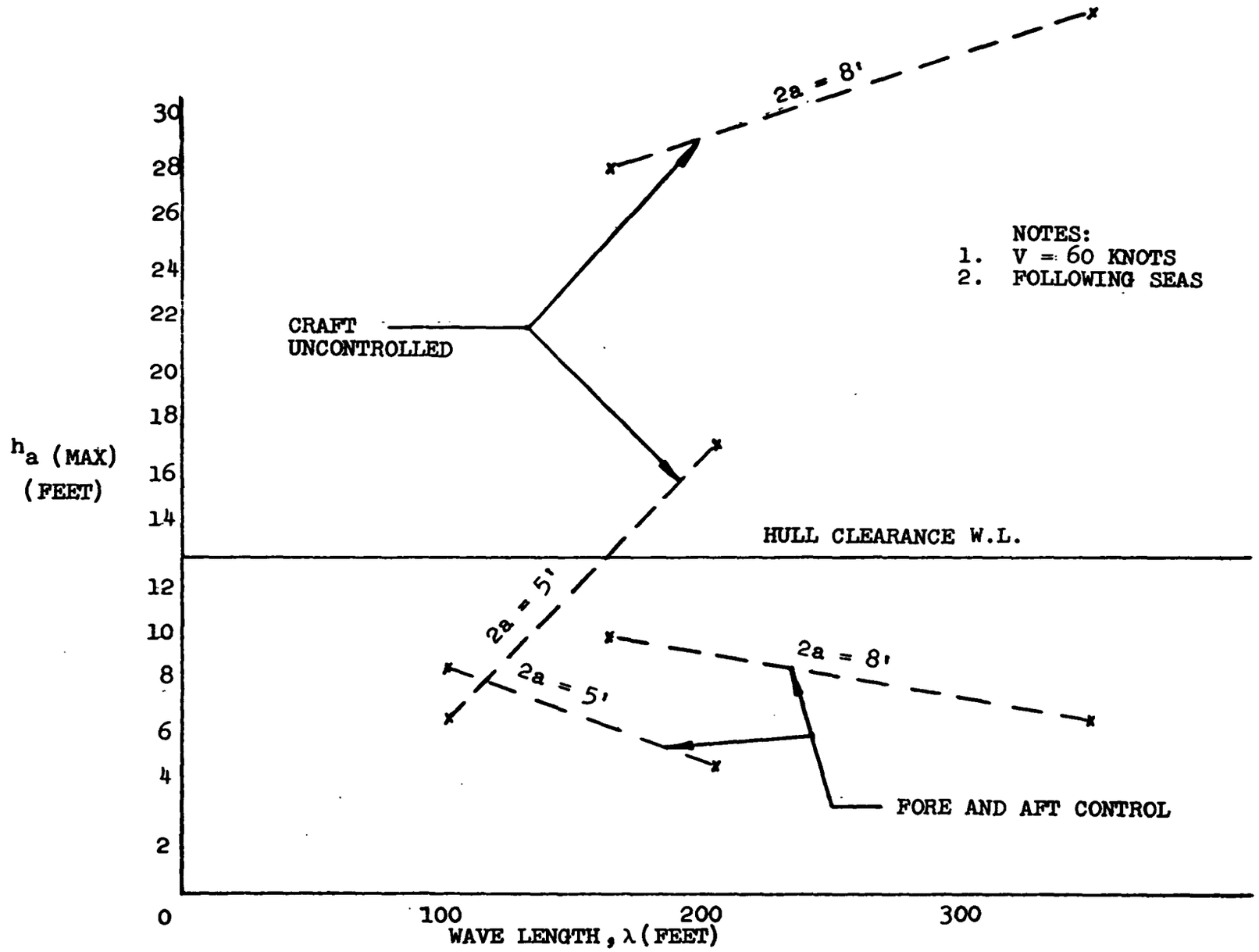

FIGURE 14. MAXIMUM INSTANTANEOUS REAR FOIL IMMERSION VS WAVE LENGTH

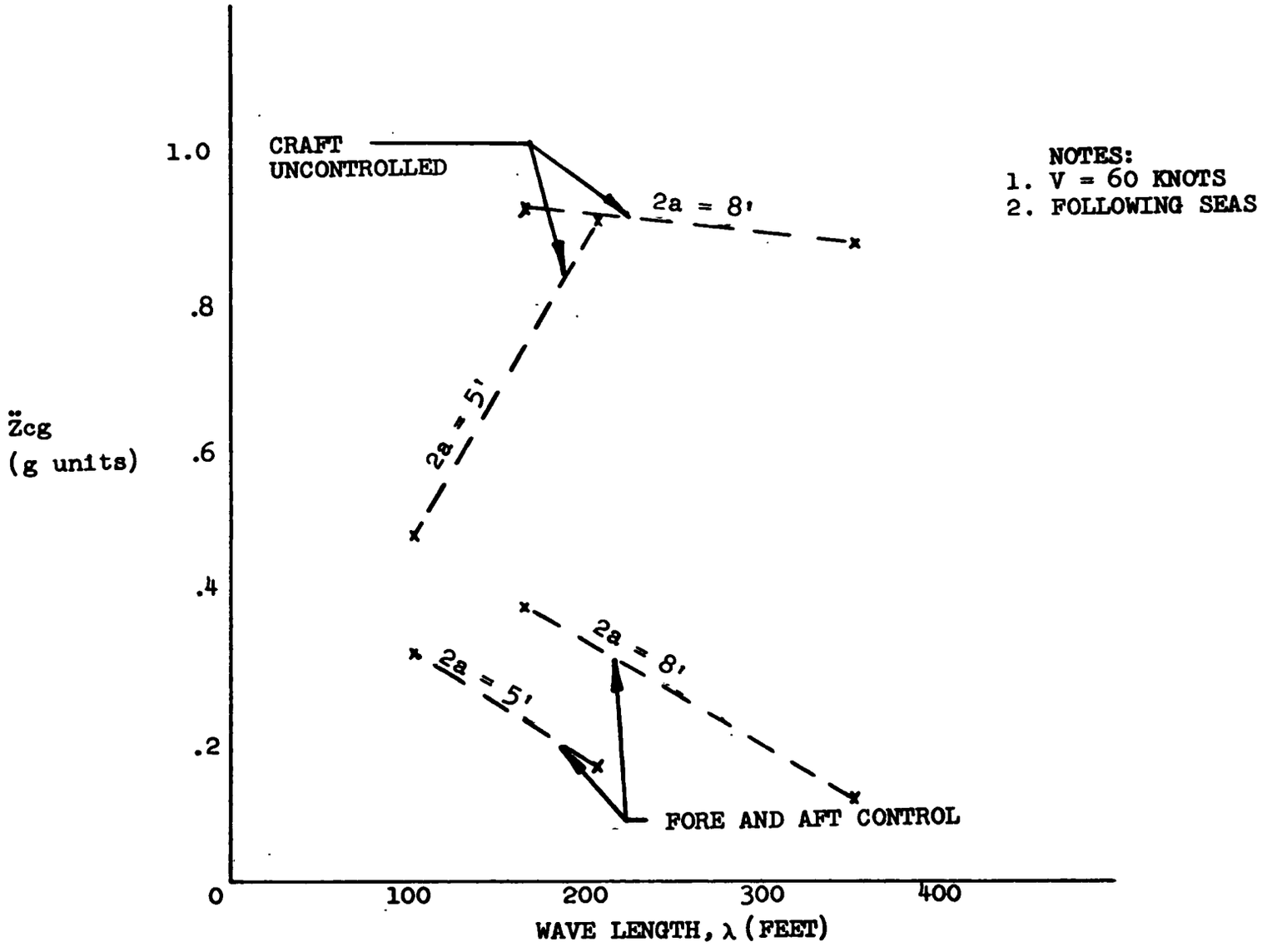

FIGURE 15. ACCELERATION AT C.G. VS WAVE LENGTH

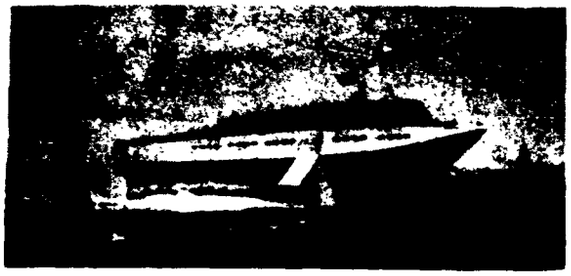

80-TON RESEARCH CRAFT, expected to be launched in June, will be 104 ft long and is designed for speed of 60 knots. Control system adjusts flaps similarly to ailerons, elevators or trim tabs of an airplane. Two V-shaped foils are used at bow and one flat section in rear.

FIGURE 16

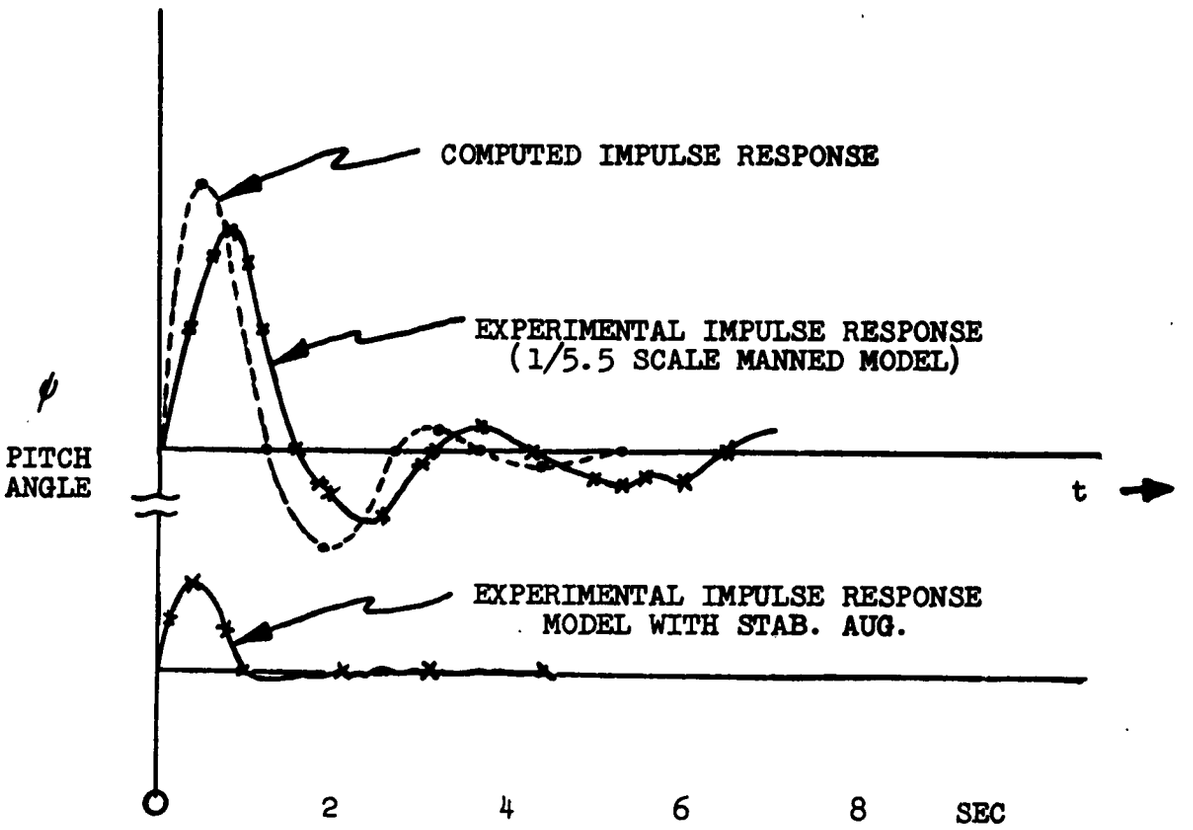

FIGURE 17

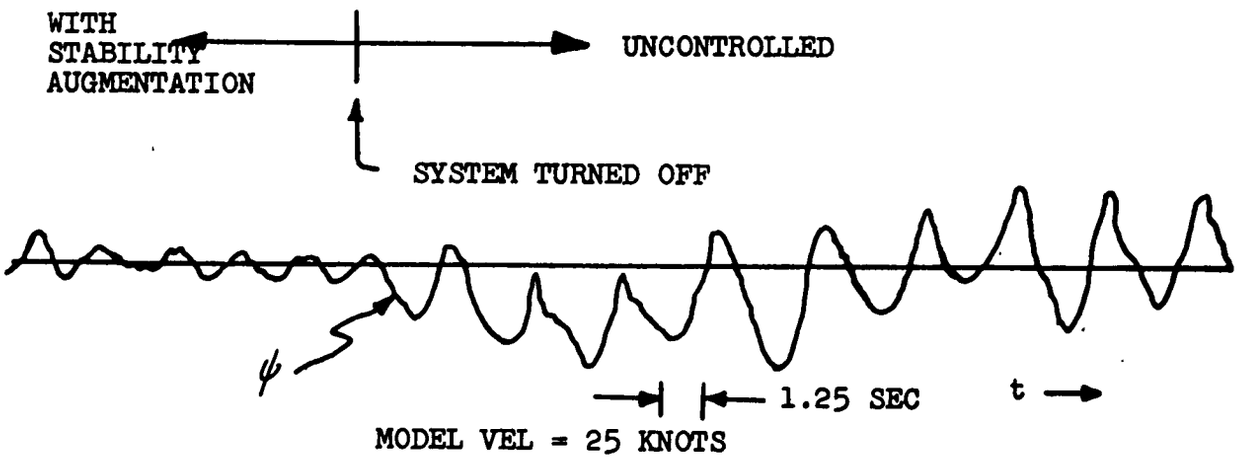

Waves - Approx 1 ft crest to trough,
10 to 15 ft crest to crest

FIGURE 18. MANNED MODEL PITCHING MOTIONS IN SEAWAY

HYDROFOIL MOTIONS IN IRREGULAR SEAS

Richard P. Bernicker
Associate Research Engineer
Davidson Laboratory

I. INTRODUCTION

The successful development of hydrofoil craft to a large extent depends upon their satisfactory operation in a seaway. This aspect of hydrofoil performance has been investigated, both analytically and experimentally, but for the most part has been restricted to seaways consisting of regular waves. Actual hydrofoil craft will operate in seas whose most obvious characteristic is their complete lack of regularity, and it therefore seems timely to develop techniques for predicting and optimizing the performance of hydrofoil craft in irregular seas.

Because of the random nature of the sea surface, statistical techniques should be applied to measure and characterize the sea surface. Consequently, similar statistical methods must be used to describe and analyze the motions of hydrofoil craft in irregular seas.

Suitable statistical techniques are developed herein and applied to the analysis and prediction of the motions of hydrofoil craft running in a seaway, and are verified experimentally. The techniques used are general but are restricted in this specific investigation to craft equipped with surface piercing, non-ventilated dihedral foils.

Method for Predicting Motions in Waves. The principle of linear superposition is the method used for predicting hydrofoil motions in irregular waves. In this theory, the complex random seaway is assumed to be composed of a number of component regular waves of varying frequency and amplitude, and the response of the craft to each component is obtained. The total motion of the craft is then obtained by superposition of the responses to the individual components of the wave. This technique may be rigorously applied to linear systems; its successful application to hydrofoil craft motions depends upon nonlinear effects being minor, and has to be demonstrated experimentally.

In predicting the motions of hydrofoil craft, the first step is a description of the random seaway. This is done by applying the theory of power spectrum analysis, as developed by Tukey,[1] Rice,[2] Tukey and Hamming[3] and others, to the random wave pattern and obtaining the energy spectrum of the seaway. Details of the treatment of such data and its use to represent an actual sea state can be found in ref. 14.

The next step is to determine the motion of the craft in regular seas of varying frequency. The response of the craft is essentially sinusoidal when running in a regular train of sinusoidal waves, and the

ratio of the amplitude of the heaving and pitching motions to the wave amplitude determines the modulus of the transfer function, or the square root of the response amplitude operator, at each encounter frequency. By varying the wave length and speed of advance, the response amplitude operator is determined as a function of the frequency of encounter for any one particular craft heading.

The response amplitude operator, as determined from regular sea analysis, is then used with the wave spectrum to construct the predicted energy spectrum of the craft motions. This is accomplished by multiplying the energy density in the wave spectrum at each frequency and continuing the calculation over the entire frequency range of the wave spectrum. The result of this procedure of linear superposition of the component responses then yields the predicted energy spectrum for the motion of the craft in the random sea. From this, statistical interpretation can be made as to the severity of the motions in a given seaway.

Experimental verification consists of carrying out the above investigations for a particular craft in regular seas to determine the response amplitude operators, then testing in irregular seas of varying severity at several speeds and headings, and comparing the predicted rough water behavior with that actually observed.

II. EXPERIMENT

To investigate the validity of linear superposition techniques applied to hydrofoil motions in irregular seas, an experiment was devised in which a tandem hydrofoil craft was constructed and tested in regular head and following seas, and at different speeds, to determine the transfer function modulus for the longitudinal motions. After these were determined, the model was tested in irregular seas to determine both the wave and motion spectra for each case. Predictions of motion spectra using linear superposition techniques then enabled a direct comparison with actually observed motion spectra to determine the validity of the technique.

The craft constructed for the experimental program employed tandem "V-foils." This configuration was chosen to simplify the program as much as possible, in that the area-stabilized system would eliminate complex control mechanisms. The craft is shown in Fig. 1. It consisted of two identical foils placed symmetrically with respect to the center of gravity. The foil section was a 12% thick NACA Series "16," with a 2-inch chord, 30° dihedral angle, and 20-inch span. The foils were attached to a box frame having rectangular dimensions of 8 inches by 48 inches. The foil spacing from mid-chord points was 44 inches. A ball bearing pivot box was attached to a center plate on the model frame to allow freedom in pitch, and the pivot box was attached to a vertical pole in the carriage apparatus which was free to heave. During the testing, the geometrical incidence of both foils was the same. Two vertical poles fore and aft of the center plate allowed weights to be attached

to ballast the model, so that at all times the model center of gravity was located at the axis of the pivot.

The experiments were carried out in Tank No. 3 of Davidson Laboratory. A main carriage, running on an overhead rail, was used to carry the model down the tank. This carriage incorporates a vertical pole running through bearing traces, to which the model was attached and was free to heave with certain pre-set limits (Fig. 1).

Measurements of heaving and pitch motions were obtained using calibrated differential transducers. The pitch transducer was of the rotary type and attached to the pivot box on the model. The heave measurement used a linear type Schaevitz attached to the vertical heave pole. Both signals from the transducers were brought from the model through overhead telemetry cables, which played out as the model traveled down the tank, and were fed into Sanborn carrier amplifiers. A record on oscillograph tape gave a time history of the longitudinal motions of the craft.

Two resistance-type wave wires were used to record the surface elevation of the waves into which the model traveled. One wave wire was mounted on the model 3 feet forward of the center of gravity, the other mounted in a fixed position about the 150-foot mark of the tank. Both signals were amplified in the Sanborns and displayed in analog form on the oscillograph strip charts.

In addition to the analog records of the motions and wave heights obtained on the strip charts, the irregular sea experiments employed a 14-channel magnetic tape recorder with a variable speed capacity. In these tests, the signals from the wave wire and transducers were fed into the magnetic tape recorder, and later replayed at a slower speed into the Davidson Laboratory's analog-to-digital converter.[4] This yielded a punched tape, which represented in octal code form all the analog data sampled at a real time interval of 0.10 seconds. With the required four information channels, the maximum digitizer sampling rate was 10 readings per second. Since this rate was inadequate for the tests at high speed, using the magnetic tape recorder and replaying the record at a slower speed increased the capacity of the analog-to-digital conversion process by simulating an increased sampling rate which could not otherwise be obtained due to mechanical limitations of the digitizing apparatus.

The punched tape in digital code was then converted to a set of IBM punched cards for use as input to the spectral analysis program, performed on an IBM 1620 at Stevens Institute.[13]

Test Program. The craft was tested in regular head seas at two speeds, 5 and 8 fps, and in regular following seas at 5 fps. Several wave heights were used as a check on the linearity of the response in heave and pitch with wave height. A range of wave lengths was used to cover the expected range of significant frequencies in the irregular waves. Long wave lengths were required to cover the lower range of frequencies.

In head seas, within the physical limits of the testing facility, this could be accomplished only for waves of small amplitudes. In the following sea case, low frequencies of encounter were unattainable since the model did not sustain even one complete oscillation over the length of tank available. Hence response data at all frequencies in the range of interest could not be obtained.

The hydrofoil craft was tested in various irregular seas of increasing severity to check on the linearity of the results. Tests were conducted at 5 and 8 fps in head seas and 5 fps in following seas. The irregular wave program in use at Davidson Laboratory involves a cycle of 100 frequency changes to the wave-making paddle, controlled by a stepping switch. The length of tank available at the test speeds did not permit a continuous run through the entire wave program; five shorter runs were taken each over a different part of the wave cycle. The results for the five shorter records were analyzed and then averaged to obtain the spectrum for the full cycle. The sea state was altered by changing the radius of the crank arm to the wave paddle. Three sea states were used for tests at 5 fps in head seas, and when preliminary results indicated no dependence on sea state severity within the range contemplated for these tests, the other tests were conducted omitting this check.

No experiments have been carried out to determine exactly what tolerances apply to the experimental measurements. However, from past experience in similar experiments in the towing tank, it is believed that the heave motion is accurate to within ±0.02 inches and the trim measurements to within 0.10 of a degree. Measurements of wave heights recorded are believed accurate to about 10%. The error involved in conversion to digital form of the analog data in the irregular sea tests is of the order of at most 1%.

III. RESULTS AND ANALYSIS

Regular Sea Response Operators. The craft was tested in head seas at speeds of 5 and 8 fps and in following seas at a speed of 5 fps. For each wave length, several wave heights were employed, and the resulting wave profiles and craft responses were recorded on calibrated strip charts. The amplitudes of the motions in heave and pitch were obtained directly from these charts, and division by the wave height then yielded the square root of the response operator in the heaving and pitching degrees of freedom. These response amplitude operators were then plotted against the frequency of encounter to obtain the response spectrum for the craft. Figures 2 to 4 show the results for heave and pitch responses as a function of encounter frequency. These data cover a variety of wave heights, ranging from 0.5 to 1.75 chords, indicating that the values of the response operator are independent of wave height.

The encounter frequency in a following sea is a triple-valued function of the wave frequency for a given speed of advance, and thus the results for following sea response operators are given as separate curves for each of two regions of wave frequencies of interest.

Irregular Sea Spectra. The power spectra for the static wave and longitudinal motions were obtained using the procedure outlined in ref. 9 and the results are shown in Figs. 8a to 8e. Figures 8a, 8b and 8c show spectra for heave and pitch in each of the three sea states tested at 5 fps; Fig. 8d indicates the results for the higher speed test, while Fig. 8e shows the results for following seas. In each of these spectra, the data point shown represents the value of the average energy density in a frequency band-width.

Figure 5 shows the wave spectra for the three sea states tested at the lower speed in head seas. It is seen that the major portion of wave energy lies in a range of frequencies from 2 to 10 rad/sec.

The severity of the sea state is indicated by the area under the spectrum which is given by the value of R for each case. The significant wave heights are then estimated by

$$h = 2.83\sqrt{R}$$

which, in terms of the chord of the foil, gives significant wave heights of 1.65, 1.45 and 1.05 chords respectively.

Based on the Tukey degrees of freedom, the 90% confidence limits on the computed spectra are about 25% for the number of data points used in the spectral analysis program. In all cases, in computing the spectra, 40 lags were used for the longitudinal motions, and 50 lags for the static wave wire analysis. The sampling interval was 0.10 seconds.

Analysis of Data. Application of the procedure outlined in ref. 14 converts the analog records of the wave wire and longitudinal motions into the power spectra. However, since the data for the longitudinal motions were obtained in a moving reference frame, the appropriate frequency is the encounter frequency, ω_e, which is related to the wave frequency by the following relation:

$$\omega_e = \omega\left(1 \pm \frac{\omega V}{g}\right) \qquad (1)$$

Here the positive sign is to be taken for head seas, and the negative sign for following seas. The motion spectra shown in Figs. 8a to 8e are plotted with ω_e as the frequency. However, the wave spectrum is obtained in the ω domain, independent of speed of advance. Before any comparison between the spectra can be drawn, the wave spectrum must be transformed into the encounter frequency domain.

1. Frequency Transformation for Head Seas. The transformation from the stationary frequency to the encounter frequency domain is accomplished using eq. 1 with the positive sign for head seas, and the requirement that the total energy in the wave remains unchanged. The total energy is essentially give by the area under the spectrum,

$$R = \int_0^\infty \left[r(\omega)\right]^2 d\omega \qquad (2)$$

where $r(\omega)^2$ is the energy density. Thus, in preserving the energy, we must take

$$R = \int_0^\infty \left[r(\omega_e)\right]^2 d\omega_e \tag{3}$$

hence

$$r(\omega)^2 \cdot d\omega/d\omega_e = r(\omega_e)^2 \tag{4}$$

where $d\omega/d\omega_e$ is the Jacobian of the transformation between the ω and ω_e domains. For head seas, the correspondence between these two frequencies is one-to-one, hence the Jacobian never vanishes.

From eq. 1:

$$J(\omega_e) = \frac{\partial\omega}{\partial\omega_e} = \left[1 + \frac{4V}{g}\,\omega_e\right]^{-1/2} \tag{5}$$

The moving wave spectrum (encounter frequency domain) is then obtained from the energy spectrum by multiplying the ordinate $r(\omega)^2$ by the Jacobian, $J(\omega_e)$, at each frequency, and plotting these at the corresponding encounter frequency. The resulting spectrum obtained in the ω_e domain then is that which would be obtained by an observer moving with the craft into the sea. Figure 6 illustrates the wave spectrum for head seas after transforming to the ω_e domain.

2. Frequency Transformation for Following Seas. In this case

$$\omega_e = \omega\left(1 - \frac{\omega V}{g}\right) \tag{6}$$

so that the encounter frequency is parabolic about the line $\omega V/g = 1/2$, and becomes negative for $\omega V/g > 1$. Clearly, the negative frequency has no meaning, and is equivalent to the corresponding positive frequency with a direction of wave travel opposite to that observed. In following seas, it is possible for three values of ω to yield the same encounter frequency. Figure 7 illustrates the relationship between ω_e and ω for this case. In transforming from the ω to the ω_e domain, there are three values of ω in regions 1, 2 and 3 which transform into a single value of ω_e. Hence, in the transformed region $0 < \omega_e < g/4V$, the three contributions from the three regions 1, 2 and 3 overlap and the spectrum for $\left[r(\omega_e)\right]^2$ is the sum of the three. For values of $\omega_e > g/4V$, the correspondence is again one-to-one, and only region 3 contributes to the encounter frequency spectrum. In obtaining the transformed spectrum, for $\omega_e < g/4V$, the Jacobian, $J(\omega_e)$, is computed at each value of ω corresponding to the single value of ω_e, and the energy computed from

$$r(\omega_e)^2 = J(\omega_e)\cdot\left[r(\omega)\right]^2$$

as was the case for head seas. The total energy spectrum then is the sum of the contributions from regions 1, 2 and 3. Denoting the contributions from the i^{th} region by a subscript i, there results:

for $\omega_e < g/4V$,

$$\left[r(\omega_e)\right]^2 = \sum_{i=i}^{3} \left\{ J(\omega_e)\cdot\left[r(\omega)\right]^2 \right\}_i \tag{7}$$

It is noticed that at $\omega V/g = 1/2$, $J(\omega_e)$ becomes infinite, so that a sharp spike arises in the energy spectrum for the ω_e domain; this occurs at $\omega_e = g/4V$. For $\omega_e > g/4V$,

$$\left[r(\omega_e)\right]^2 = \left\{ J(\omega_e) \left[r(\omega)\right]^2 \right\}_3 \tag{8}$$

as only region 3 contributes in this part of the ω_e domain.

3. Principle of Linear Superposition. In the paper of St. Denis and Pierson,[9] spectral methods were applied to motions of surface ships using the principle of linear superposition. The method consists of constructing the motion spectrum of the craft from a knowledge of the responses to individual frequency components. Thus, if $S(\omega_e)^2$ is the energy spectrum for the longitudinal motions,

$$S(\omega_e)^2 = r(\omega_e)^2 \cdot A(\omega_e) \tag{9}$$

where $A(\omega_e)$ is the response amplitude operator for regular seas. Hence the energy density of the sea state is multiplied by the response amplitude operator to obtain the energy density of the motion spectrum.

For head seas, where the correspondence between ω and ω_e is one-to-one, the method is straightforward. Alternately, the motion spectrum can be divided by the wave spectrum in the ω_e domain to obtain a response operator spectrum, which can then be compared to regular sea results. Comparison of either of the two methods will then indicate the validity of linear superposition.

For following seas, however, the methods are more complex, since there is now a three-to-one correspondence between ω and ω_e over a range of the spectrum. In this case, division of the response spectrum by the wave spectrum yields

$$\frac{\left[S(\omega_e)\right]^2}{\left[r(\omega_e)\right]^2} = \frac{\sum_{i=1}^{3} \left\{ J(\omega_e) \left[r(\omega)\right]^2 A(\omega_e) \right\}_i}{\sum_{i=1}^{3} \left\{ J(\omega_e) \left[r(\omega)\right]^2 \right\}_i} \tag{10}$$

hence, if significant energy is present in at least two of the three overlapping regions, no comparison with regular sea response operator data is possible in this manner. The linear superposition principle can only be validated by constructing the motion spectrum from the static wave spectrum and response operators obtained from regular sea results, and comparing these to the actual spectrum from the irregular sea tests. To this end, regular sea response data must be obtained over a wide range of wave frequencies to give the response operator spectrum in each of the three regions in a following sea. The motion spectrum is then estimated from

$$\left[S(\omega_e)\right]^2 = \sum_{i=1}^{3} \left\{ J(\omega_e) \cdot \left[r(\omega)\right]^2 \cdot A(\omega_e) \right\}_i \tag{11}$$

for $\omega_e < g/4V$, and

$$\left[S(\omega_e)\right]^2 = \left\{ J(\omega_e) \left[r(\omega)\right]^2 A(\omega_e) \right\}_3 \quad \text{for } \omega_e > g/4V \tag{12}$$

Comparison of Linear Superposition Theory with Experiment. Using Figs. 8a to 8c, the energy spectra for the longitudinal motions in head seas at 5 fps were divided by the corresponding transformed wave spectra (Fig. 6a) for each of the three sea states tested. The result was square-rooted at each frequency to obtain the derived modulus of the transfer function, which is shown in Fig. 9 for both heave and pitch motions. The regular sea data points are also shown superimposed on this spectrum for comparison. Figure 10 shows a similar result for the head sea tests at the higher speed of 8 fps. The 90% confidence limits based on the Tukey degrees of freedom are about +45% and -24% for the computed spectra; considering this, the comparison shows good agreement between the derived response operators and those obtained experimentally in regular head seas.

Predictions of the motion spectra from the transformed wave spectra and regular sea response data are also compared (see Figs. 11 and 12). The prediction again seems to validate the linear superposition hypothesis, at least to the degree attainable with power spectral methods.

Figure 13 indicates the comparison between the spectrum obtained in irregular following seas and that predicted by using regular sea data and the transformation of the wave spectrum. The energy content in the wave in region 1 was negligible; hence, the superposition was simplified. Response operators obtained in regular seas were used at the exact corresponding frequencies and the results for the two regions of interest added together to construct the estimate of the spectrum. The singularity in the following sea spectrum at $\omega_e = 1.6$ has not been displayed, since the sampling process, in reality, estimates the integral of the spectrum over $\Delta\omega_e$, and hence the exact shape of the spectrum is lost. The motion spectrum was predicted using regular sea data on either side of the singularity, and the curve faired through these points in the region $\omega_e = 1.6$. The results for the predicted heave spectrum exhibit the same shape as the experimental spectrum, and are at most 33% too low in the range of significant energies. Since the response operators used for the prediction were squared, any corresponding error in experimental determination of these quantities are squared; hence, the difference is exaggerated. The true measure of the deviation is perhaps best given by one-half that shown on the spectrum graphs. Within the limits of confidence of spectral analysis methods, and considering what has been done for surface ships in following seas, these results exhibit an excellent comparison between the experimental spectra and those predicted using regular sea data.

IV. DISCUSSION OF RESULTS

Figures 11 to 13 compare the computed spectra with those predicted using linear superposition techniques, and Figs. 9 and 10 compare derived and experimental response operators. In general, these figures indicate the validity of the linear superposition hypothesis, at least for the moderate irregular seas used in the experiment. The predicted spectra generally deviate no more than 20% from the experimental spectra in the range of significant energies for the head sea tests, and slightly more than this for the following sea case. Previous experiments by Lewis and Numata,[5] utilizing linear superposition techniques applied to surface vessels, yielded correspondence of the same order of magnitude. It appears that results using this technique applied to non-ventilated hydrofoil craft exhibit the same general agreement between prediction and experimental motion spectra.

With the technique established, it is then necessary to know only the regular sea behavior of the hydrofoil craft and apply the (presumed) known wave spectrum for the sea state to be considered to predict the irregular sea motions. To this end, experimental programs for model craft can be carried out as in the present investigation. Alternatively, one can attempt to predict the regular sea motions theoretically, and use the theoretically determined response operator spectrum to predict the motion spectra. Several such analytical procedures have been studied previously. Weinblum[6] first presented a linearized theory for predicting motion responses of hydrofoil craft in regular waves. Experiments of Leehey and Steele[7] found discrepancies between Weinblum's analytically predicted motions and those observed experimentally and later Ogilvie[8] modified Weinblum's theory to include nonlinear and non-steady effects. Ogilvie's theory compared favorably with the experimental data of Leehey and Steele and appears to yield the best results for prediction of longitudinal motions. Hence, it is possible to eliminate preliminary experimental programs to determine the regular sea response operators by use of these theories, which, in effect, would form the "building blocks" upon which the irregular sea motions could be constructed.

V. CONCLUSIONS

As a result of these experiments, it is concluded that linear superposition techniques applied to irregular sea motions of non-ventilated, dihedral hydrofoil craft are valid. The maximum speed tested was 8 fps, corresponding to a Froude number of about 3.5 based on foil chord, and the severest sea tested employed a significant wave height of 1.65 times the chord, which indicates that the results cover a practical, significant range of hydrofoil craft operation.

In light of the results from this experiment, it is suggested that future work along these lines should be extended to higher speeds and fully-ventilated and/or cavitated foils. Such an investigation would involve the same techniques as used herein, and validation of linear superposition techniques in this type of foil operation would be useful for future development of high speed craft in rough water operation.

VI. REFERENCES

1. Tukey, J. W.: "The Sampling Theory of Power Spectrum Estimates," Symposium on Applications of Auto Correlation Analysis to Physical Problems, Woods Hole Oceanographic Institute, Woods Hole, Mass., 1949, ONR, Washington, D.C.
2. Rice, S. O.: "Mathematical Analysis of Random Noise," Bell System Technical Journal, Vol. 23, 1944, Vol. 24, 1945.
3. Tukey, J. W. and Hamming R. W.: "Measuring Noise Color," Bell Telephone Laboratory Notes 1949.
4. Spens, P.: "A Digital Recording System for Model Tests in Irregular Waves," DL Note 550, presented at the 12th Meeting of ATTC, Berkeley, California, August 1959.
5. Lewis, E. V. and Numata, E.: "Ship Model Tests in Regular and Irregular Seas," ETT Report 567, September 1956.
6. Weinblum, G. P.: "An Approximate Theory of Heaving and Pitching of Hydrofoils in Regular Shallow Waves," DTMB Report C-479, October 1954.
7. Leehey, P. and Steele, J. M., Jr.: "Experimental and Theoretical Studies of Hydrofoil Configurations in Regular Waves," DTMB Report 1140, October 1957.
8. Ogilvie, F. T.: "The Theoretical Prediction of the Longitudinal Motions of Hydrofoil Craft," Journal of Ship Research, Vol. 3, No. 3, December 1959.
9. St. Denis, M. and Pierson, W. J., Jr.: "On the Motions of Ships in Confused Seas," Trans. SNAME 1953.
10. Pierson, W. J., Jr. and Markes, E.: "The Power Spectrum Analysis of Ocean Wave Records," Trans. American Geophysical Union, Vol. 33, No. 6, December 1952.
11. Dalzell, J. F. and Yamanouchi, Y.: "Analysis of Model Test Results in Irregular Head Seas to Determine Motion Amplitudes and Phase Relationships to Waves," Ship Behavior at Sea, Second Summer Seminar, S.I.T., June 1958.
12. Dalzell, J. F.: "Some Notes on the Design of Irregular Wave Experiments in the Towing Tank with respect to Spectral Analysis," DL Note 659, April 1962.
13. Clapp, R.: "1620 Spectrum Analysis; Spectral and Cross-spectral Analysis of Two-dimensional Stationary Gaussian Time Series," DL Technical Note 678 (to be published).
14. Bernicker, R. P.: "Hydrofoil Motions in Irregular Seas," DL Report 909, November 1962.

NOMENCLATURE

$A(\omega_e)$	general response amplitude operator for longitudinal motions
g	gravitational constant, ft/sec^2
h	significant wave height
J	Jacobian of transformation between wave and encounter frequencies
m	represents a lag
n	total number of sampled data points
R	area under spectrum
$[r(\omega)]^2$	energy density of wave spectrum
$[S(\omega_e)]^2$	energy density of longitudinal motion spectrum
Δt	sampling interval, seconds
V	speed of advance, ft/sec
$\varepsilon(\omega)$	random phase
$(\zeta_m)^2$	response amplitude operator for heave
$(\phi_m)^2$	response amplitude operator for pitch
ω	circular frequency, rad/sec
ω_e	circular frequency of encounter, rad/sec

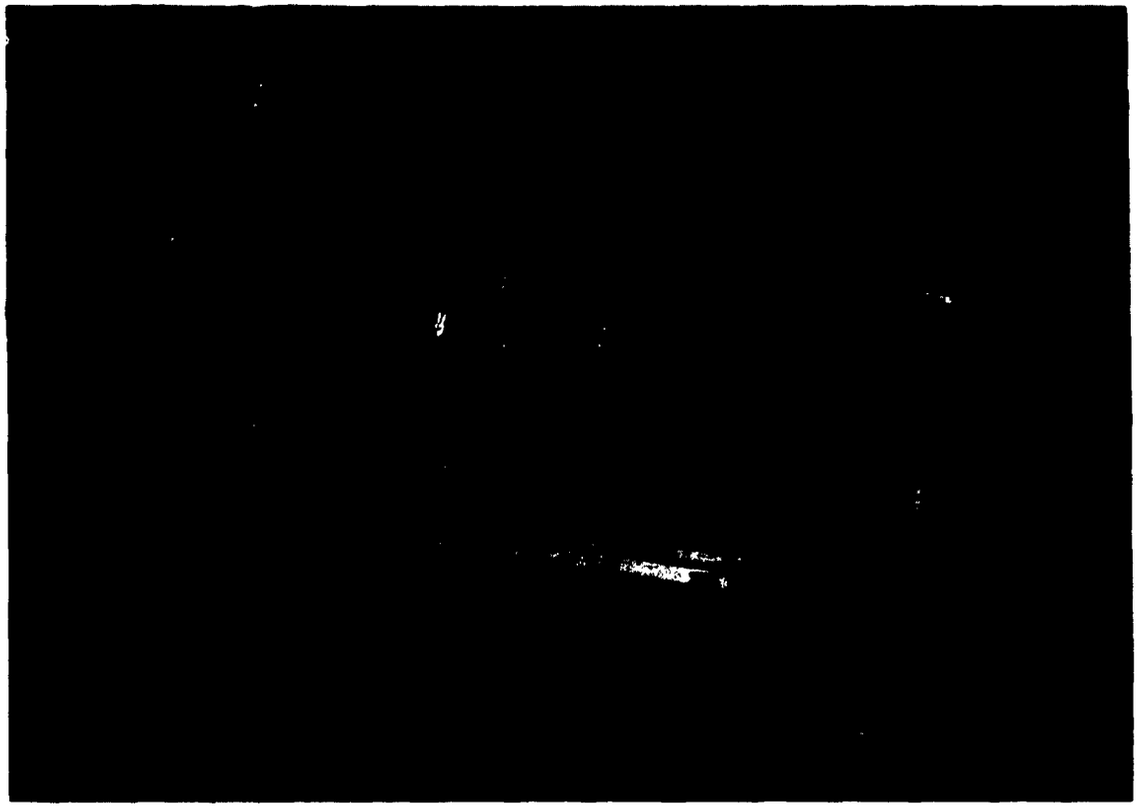

FIGURE 1 TEST SET-UP OF TANDEM HYDROFOIL MODEL

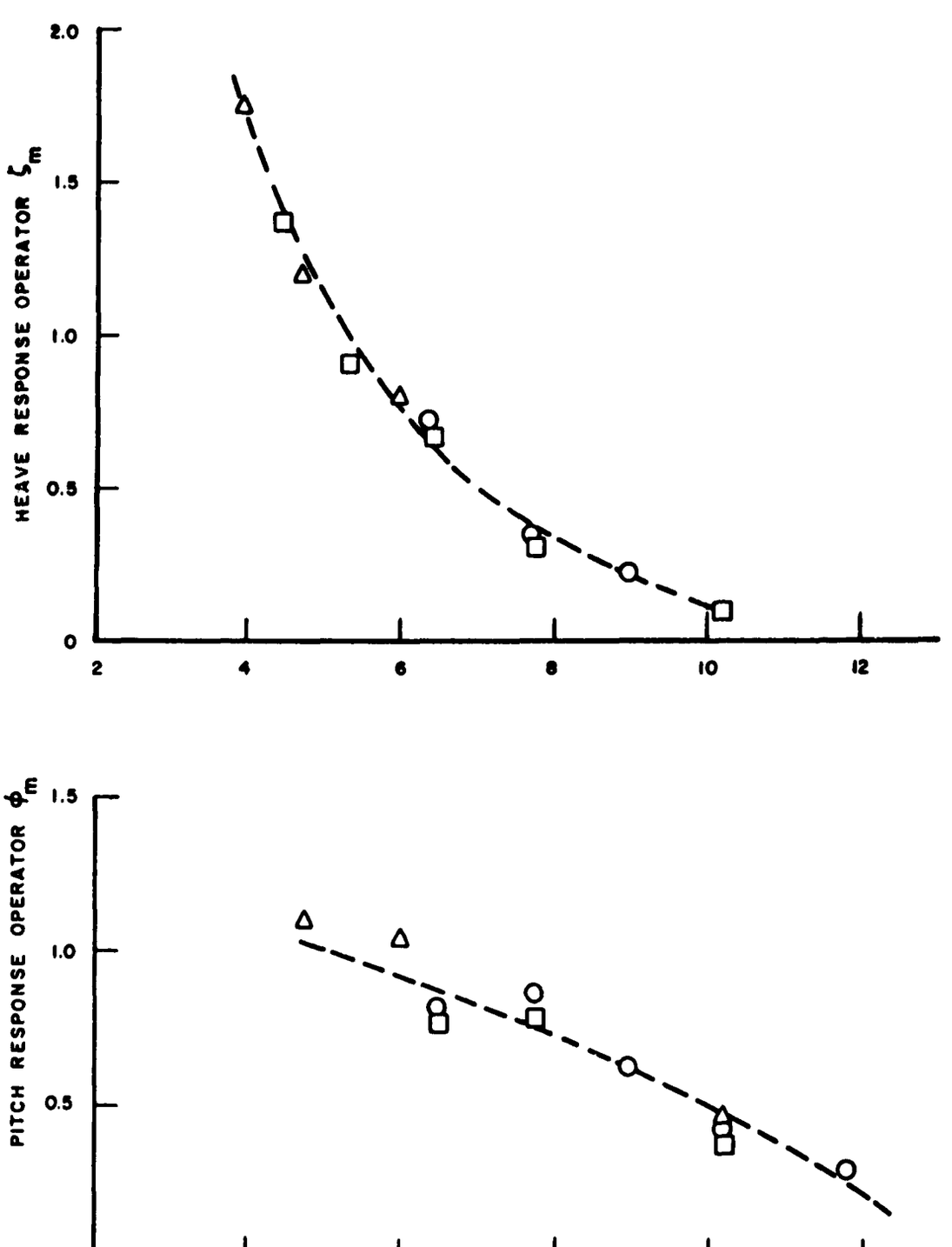

FIGURE 2. TRANSFER FUNCTIONS FOR REGULAR HEAD SEA EXPERIMENTS AT V=5 FEET/SECOND

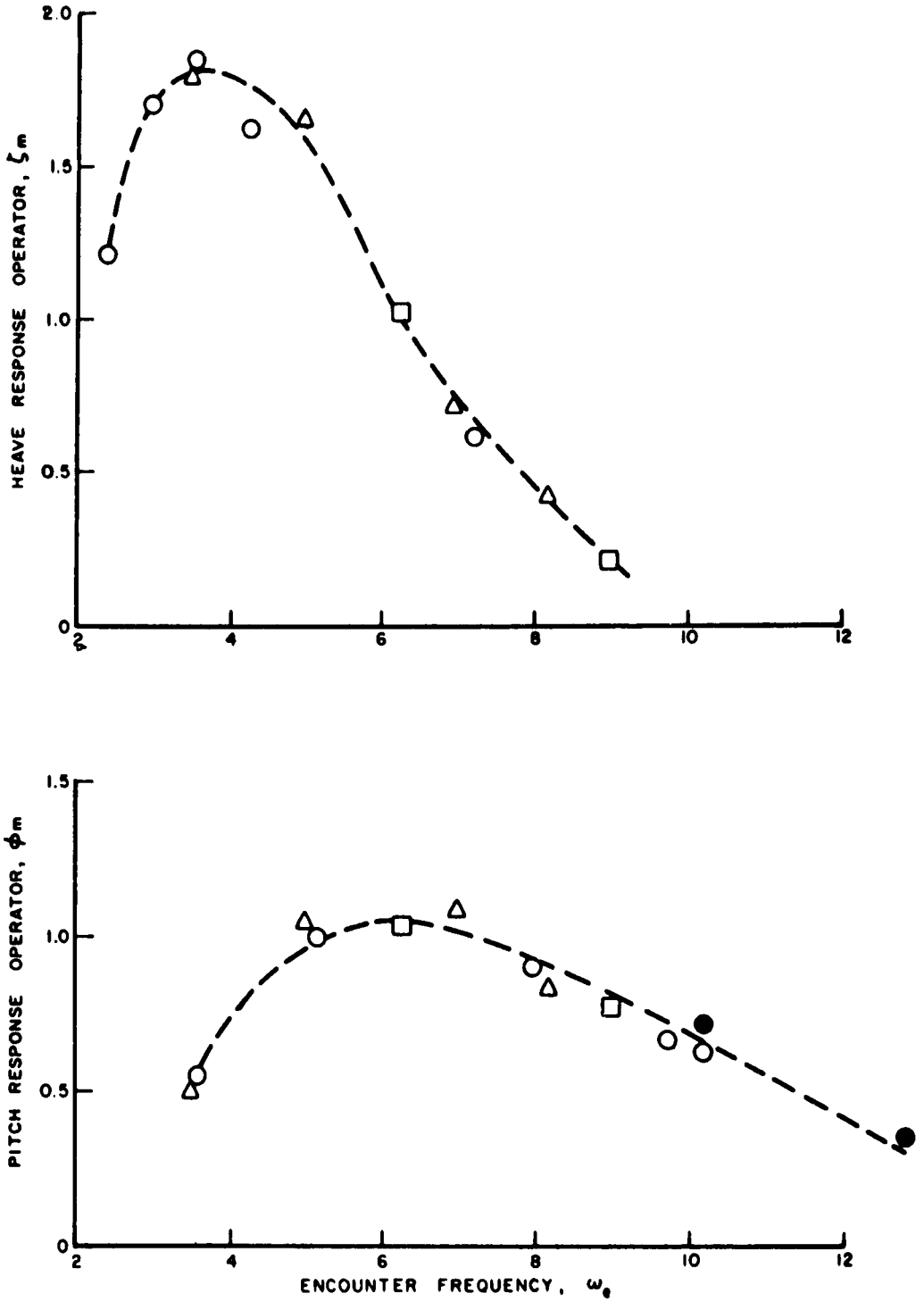

FIGURE 3. TRANSFER FUNCTIONS FOR REGULAR HEAD SEA EXPERIMENTS AT V = 8 FEET/SECOND.

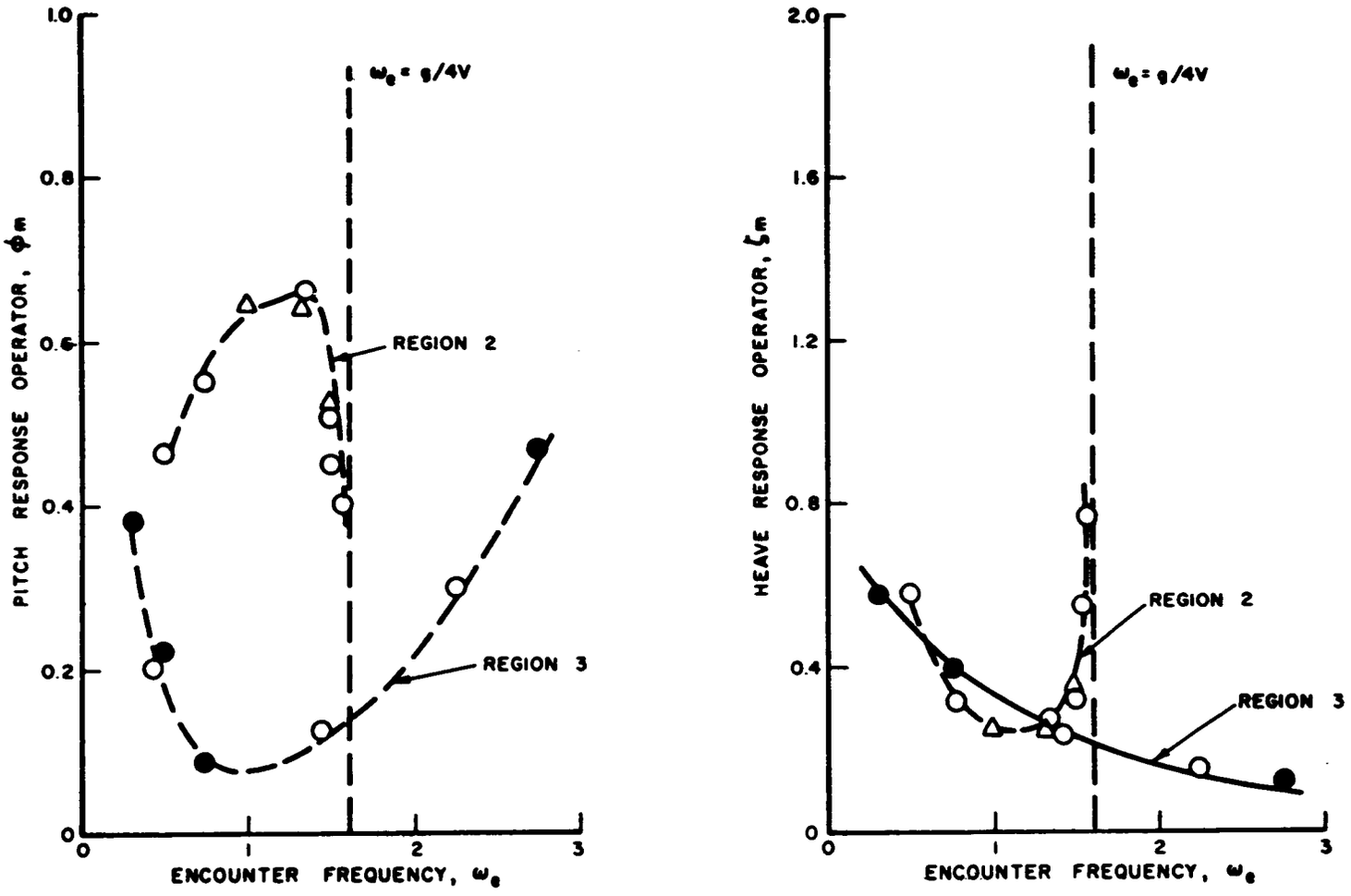

FIGURE 4. TRANSFER FUNCTION FOR REGULAR FOLLOWING SEA EXPERIMENTS AT V=5 FEET / SECOND.

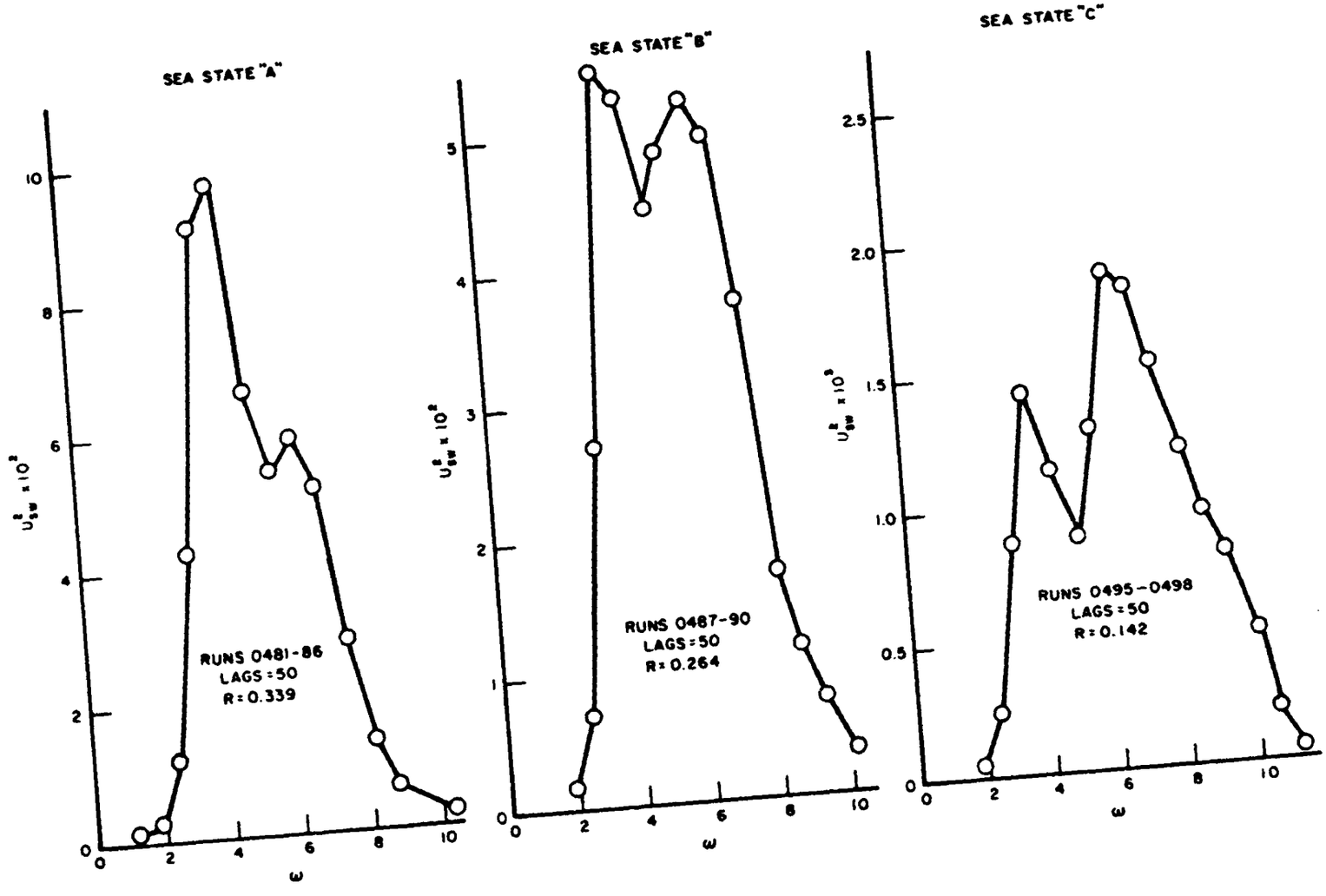

FIGURE 5. STATIC WAVE WIRE SPECTRA FOR THREE SEA STATES IN HEAD SEA TESTS AT 5 FEET/SECOND

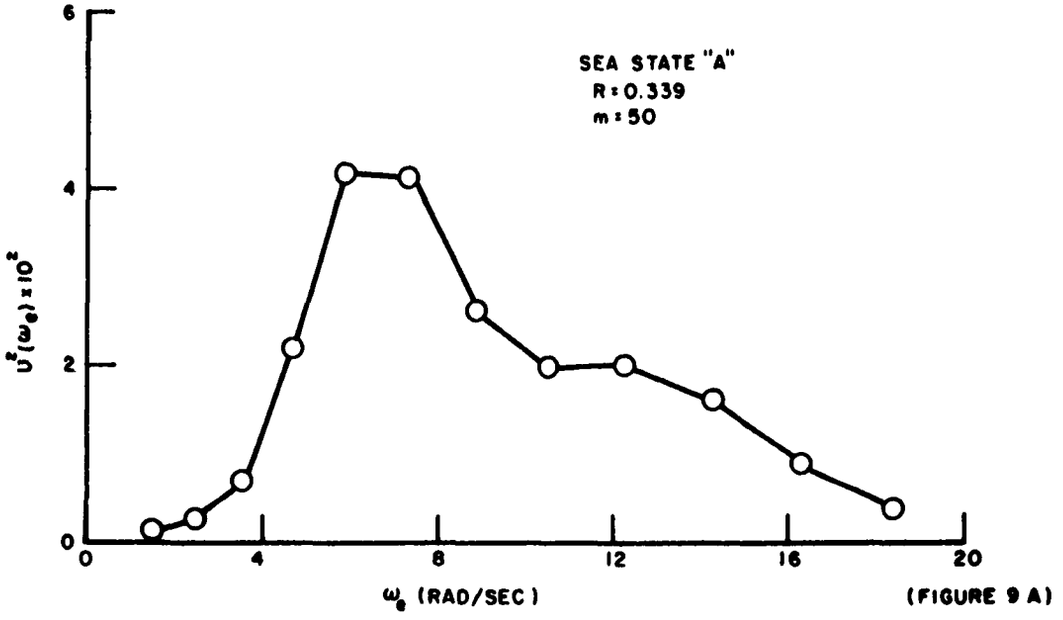

(FIGURE 9 A)

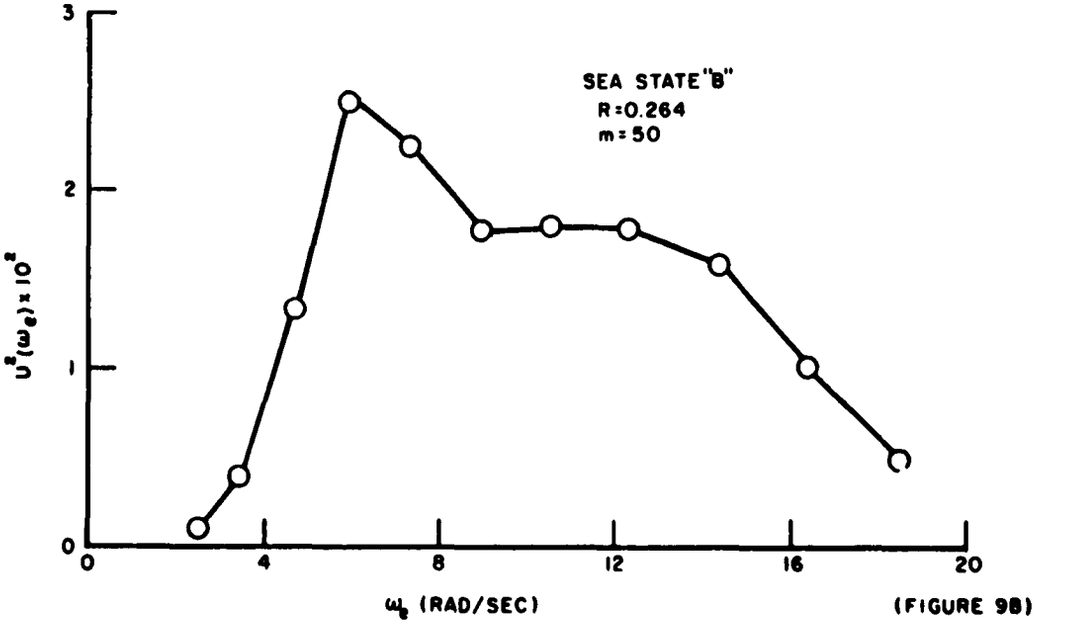

(FIGURE 9B)

FIGURE 6. WAVE SPECTRA AFTER TRANSFORMATION TO ENCOUNTER FREQUENCY DOMAIN. HEAD SEAS, V = 5 FEET/SECOND

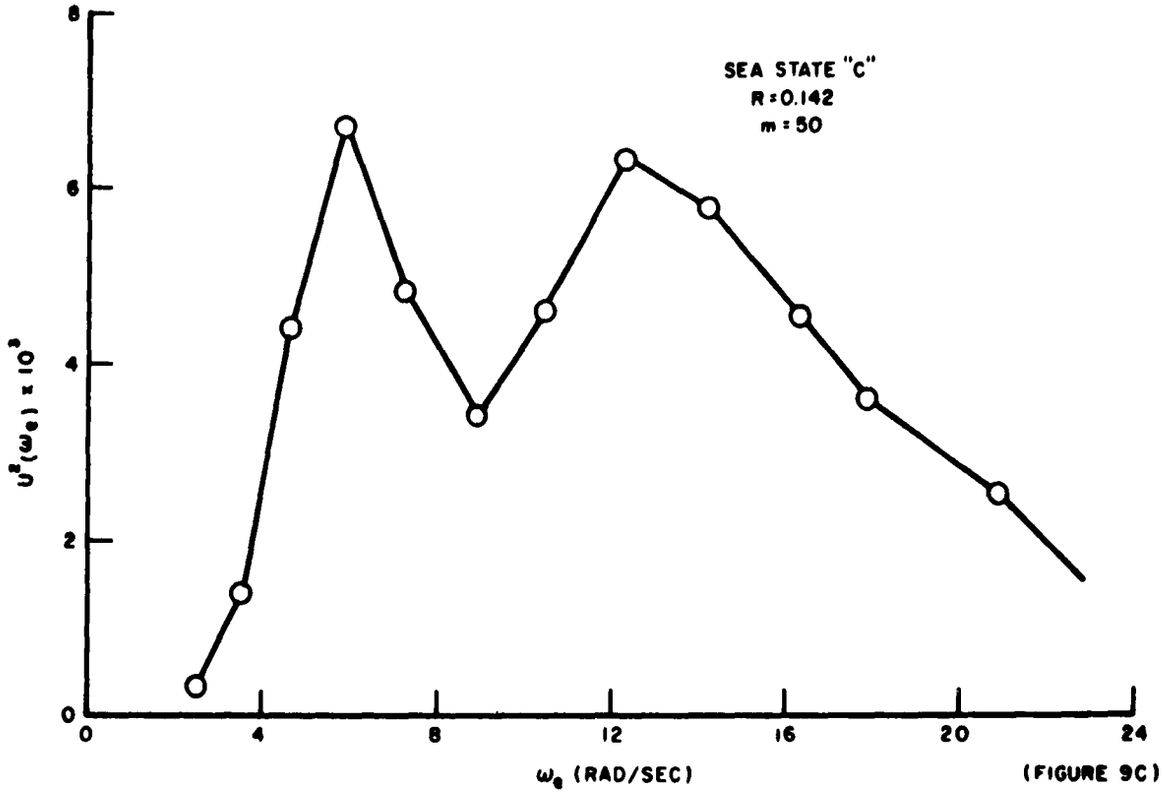

FIGURE 6. (CONCLUDED) WAVE SPECTRA AFTER TRANSFORMATION TO ENCOUNTER FREQUENCY DOMAIN. HEAD SEAS, V = 5 FEET/SECOND

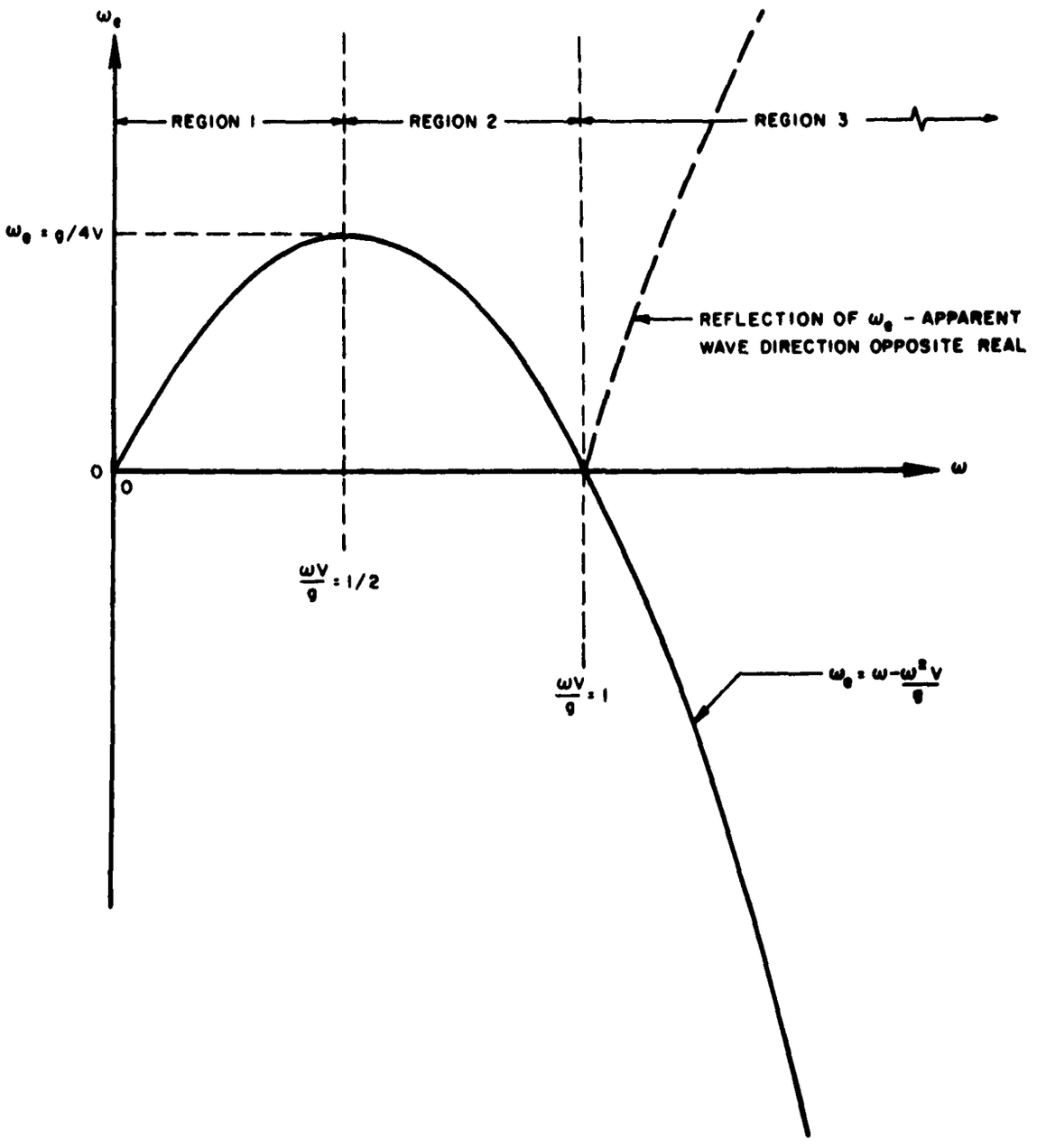

FIGURE 7. RELATIONSHIP BETWEEN ω AND ω_e FOR FOLLOWING SEAS

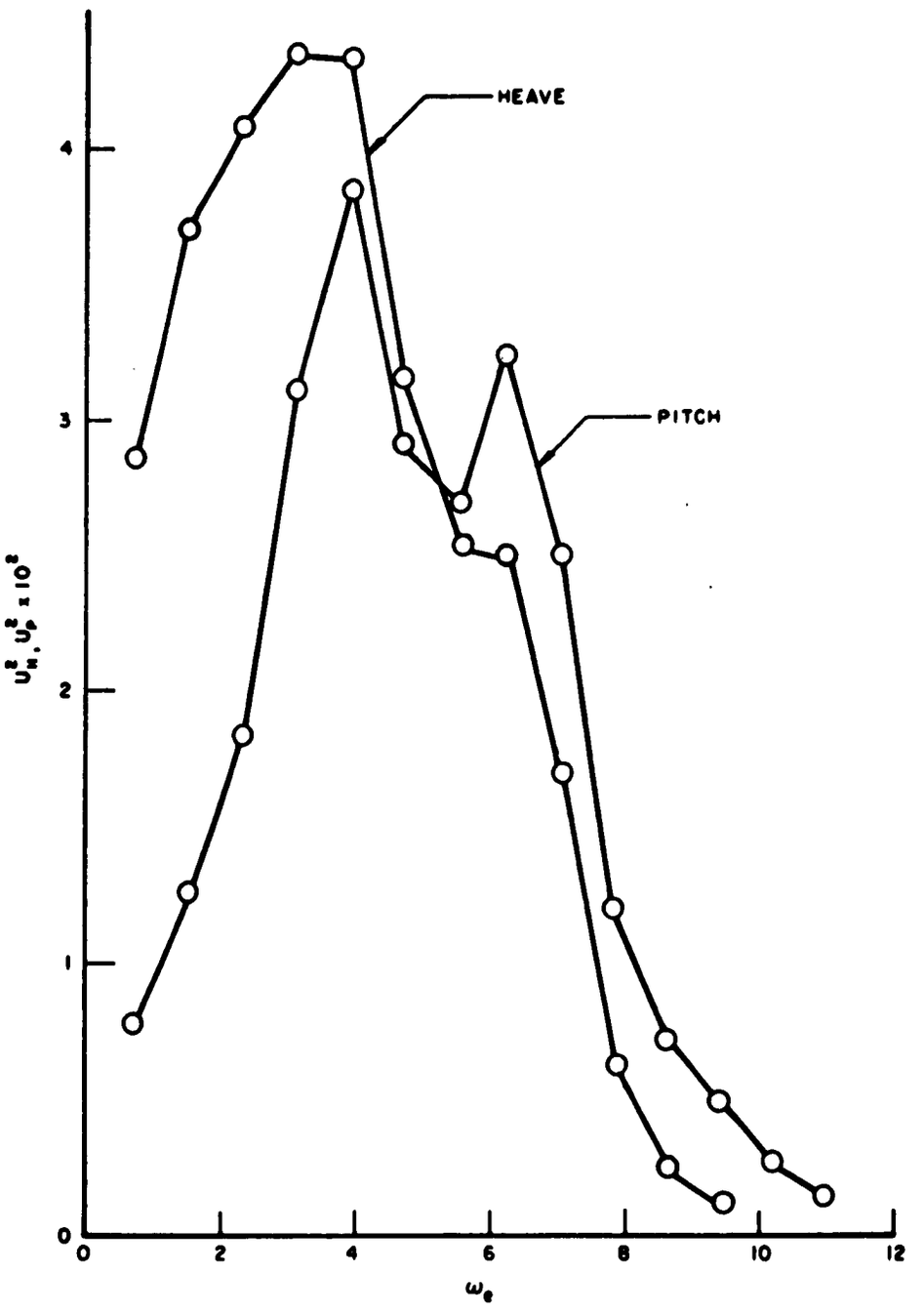

FIGURE 8a. LONGITUDINAL MOTIONS SPECTRA FOR RUNS 0481-0486. IRREGULAR HEAD SEAS, V = 5 FEET/SECOND R = 0.339, SEA STATE "A"

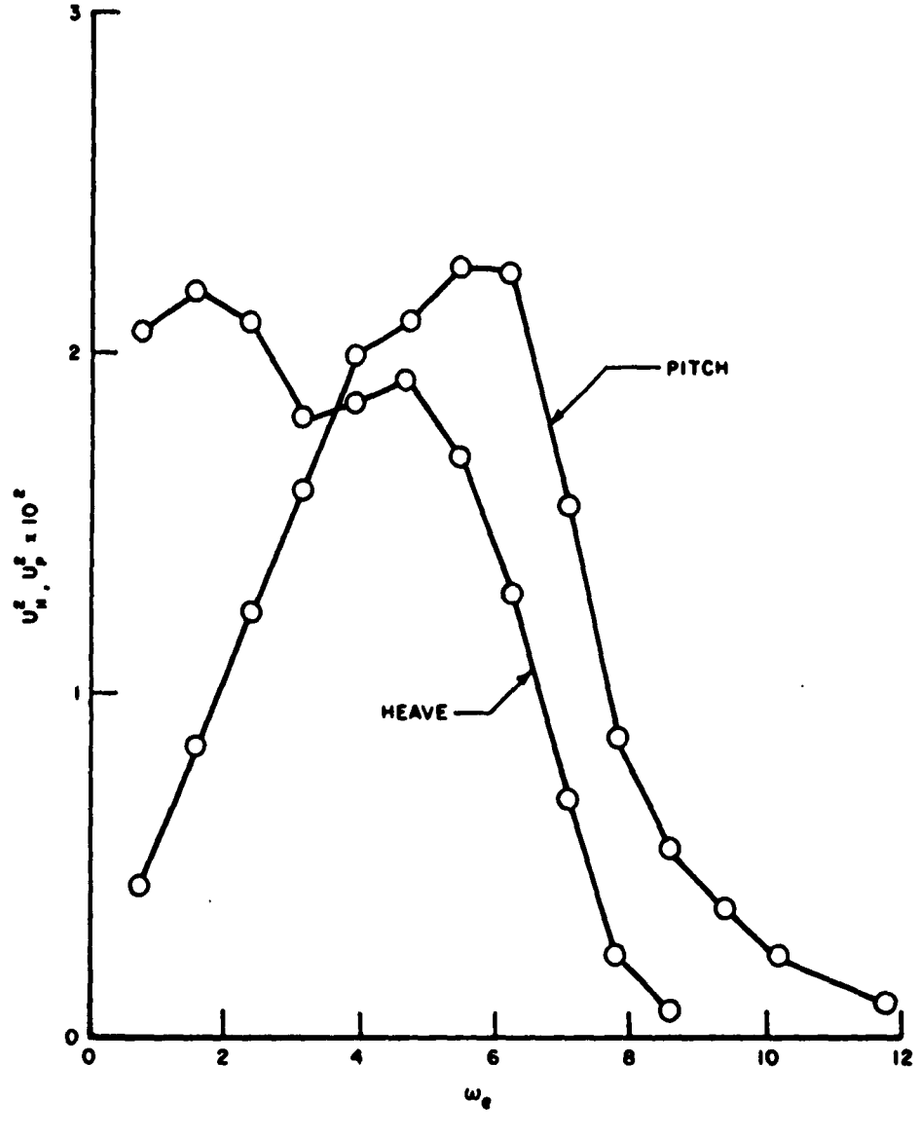

FIGURE 8b. LONGITUDINAL MOTIONS SPECTRA FOR RUNS 0487-0490 IRREGULAR HEAD SEAS, V = 5 FEET/SECOND, R = 0.264, SEA STATE "B".

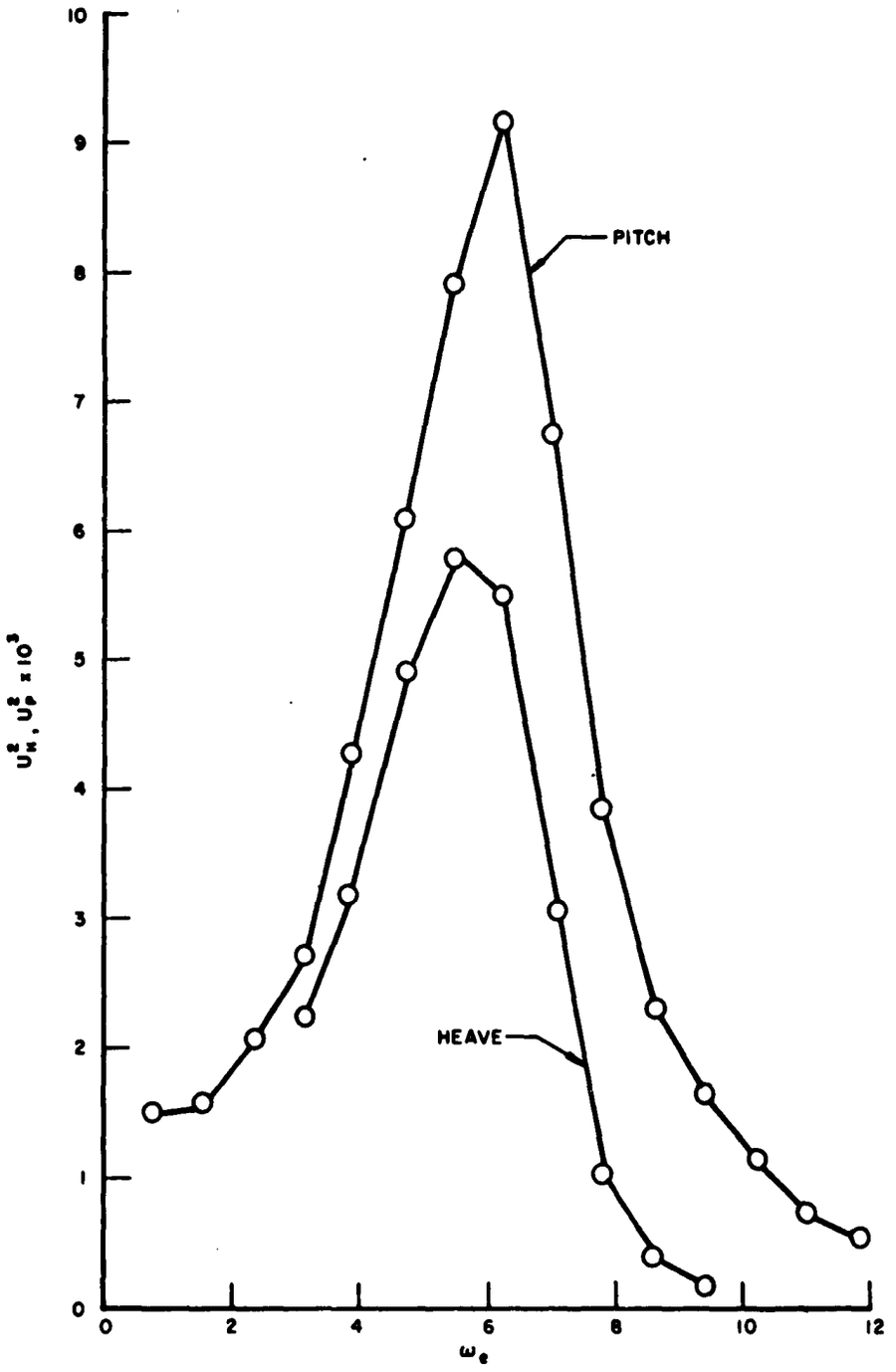

FIGURE 8c. LONGITUDINAL MOTIONS SPECTRA FOR RUNS 0 495 - 0 498. IRREGULAR HEAD SEAS, V = 5 FEET/SECOND R = 0.142, SEA STATE "C".

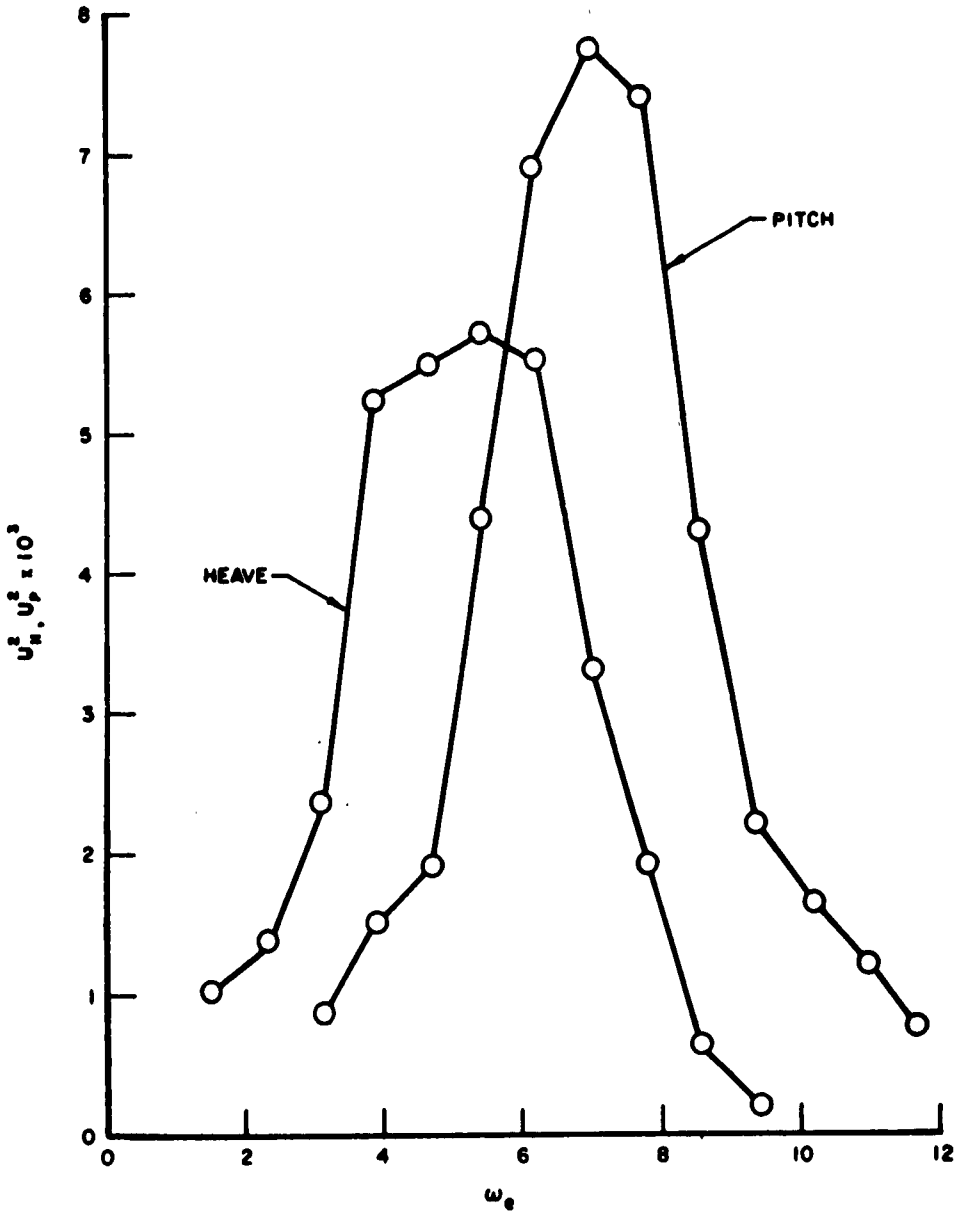

FIGURE 8d. LONGITUDINAL MOTIONS SPECTRA RUNS 0560-0564. IRREGULAR HEAD SEAS, V = 8 FEET/SECOND R = 0.110

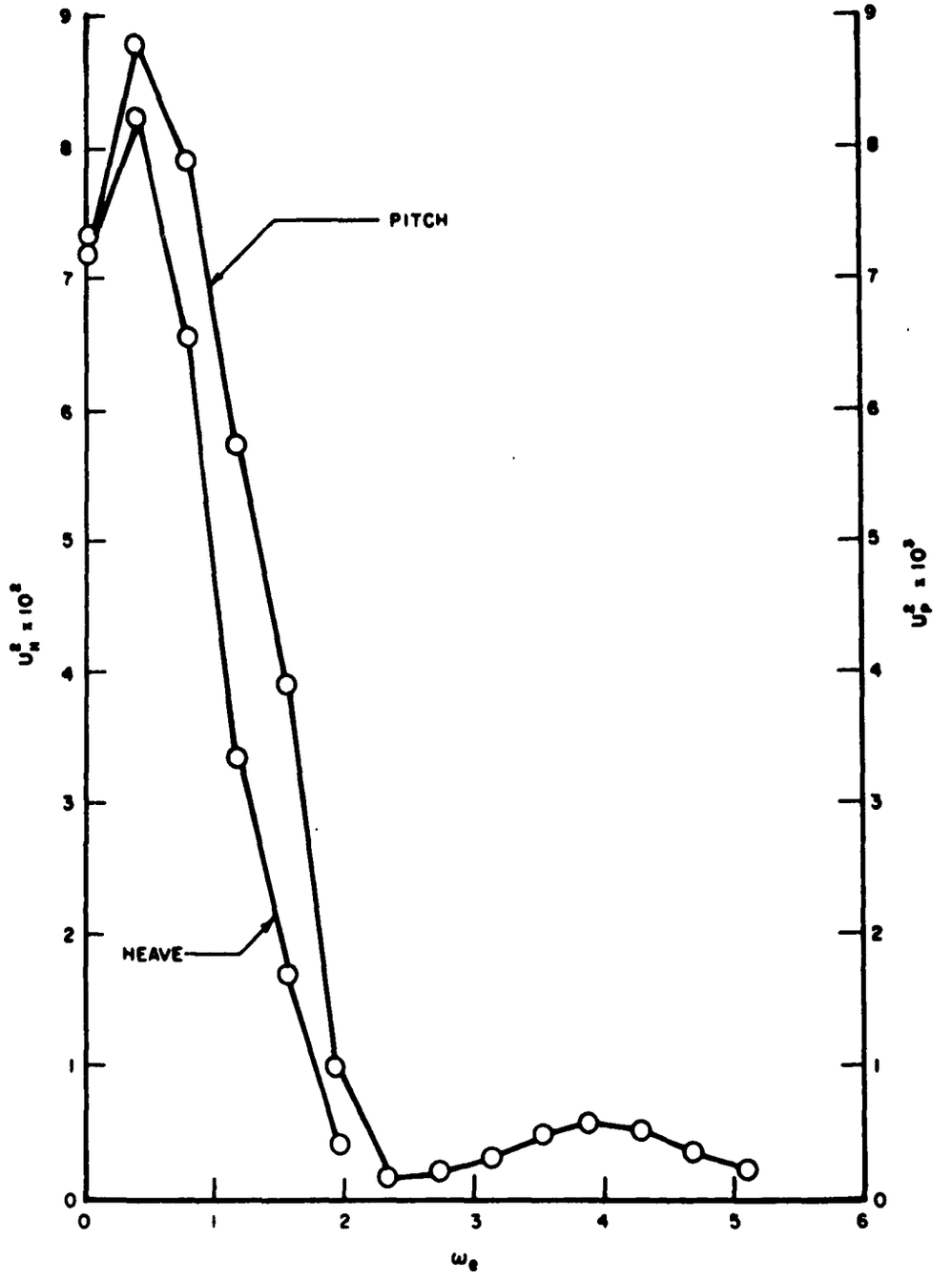

FIGURE 8e. LONGITUDINAL MOTIONS SPECTRA RUNS 0502 - 0505. IRREGULAR FOLLOWING SEA, V = 5 FEET/SECOND R = 0.128

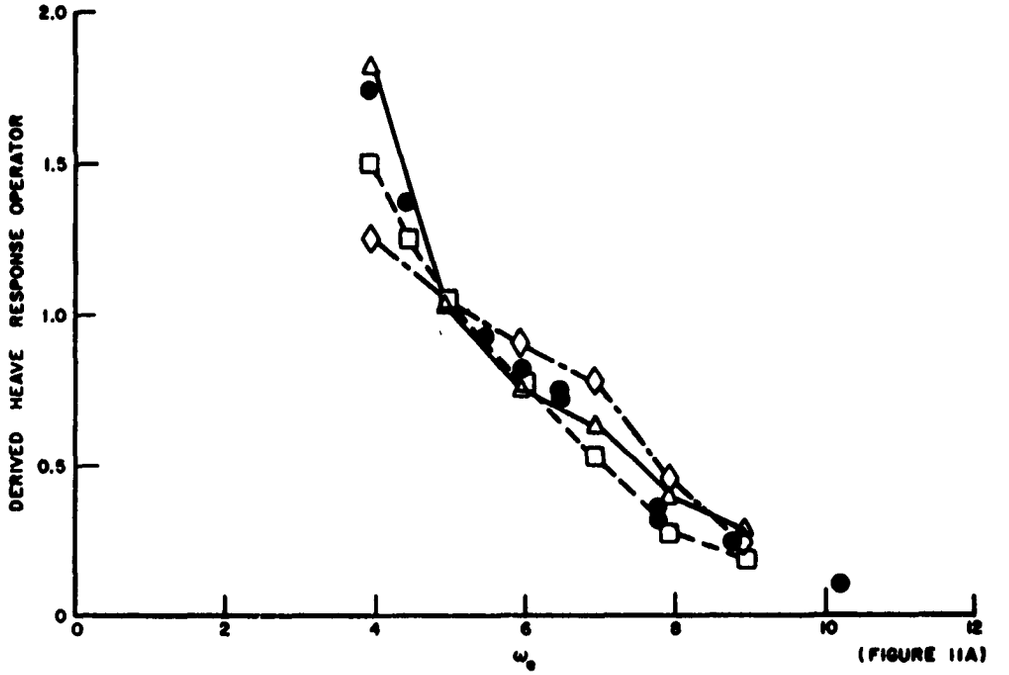

(FIGURE 11A)

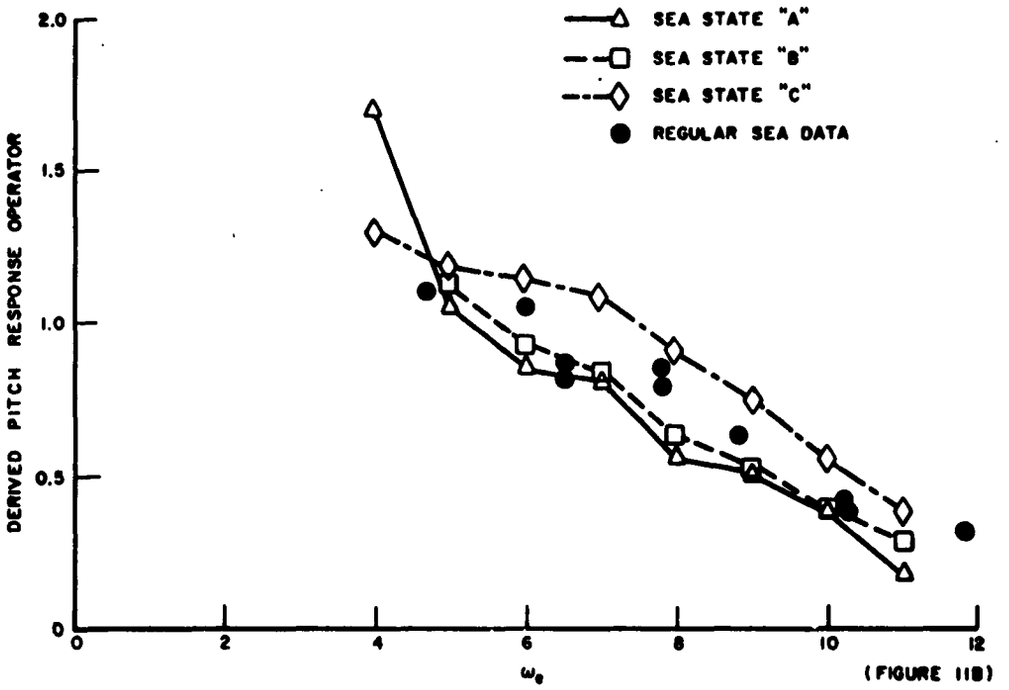

(FIGURE 11B)

FIGURE 9. COMPARISON OF DERIVED RESPONSE OPERATORS FOR TESTS AT V = 5 FEET/SECOND IN HEAD SEAS WITH REGULAR SEA RESULTS.

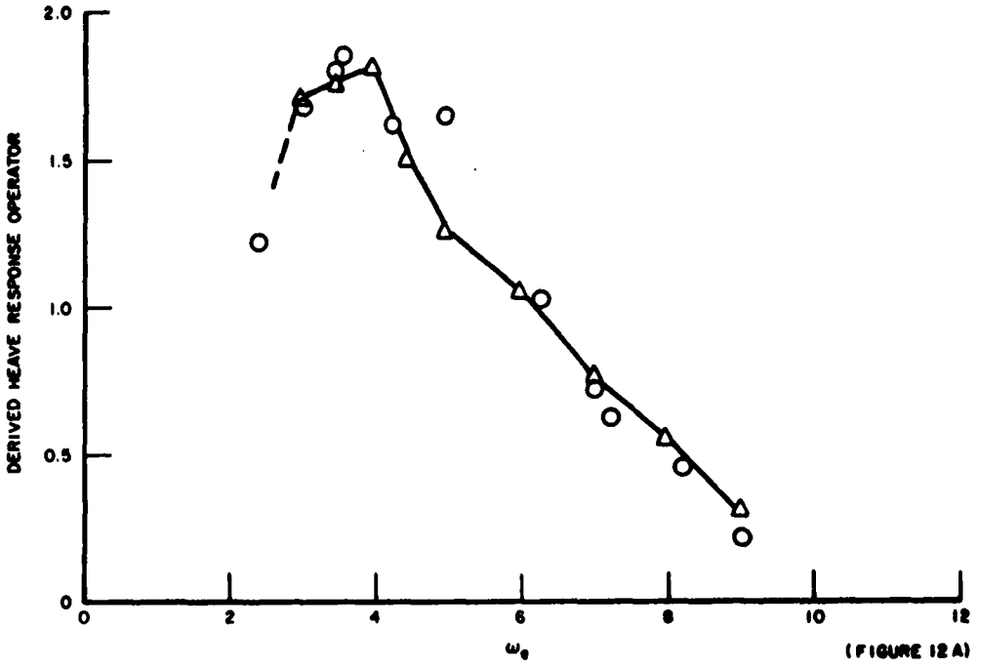

(FIGURE 12A)

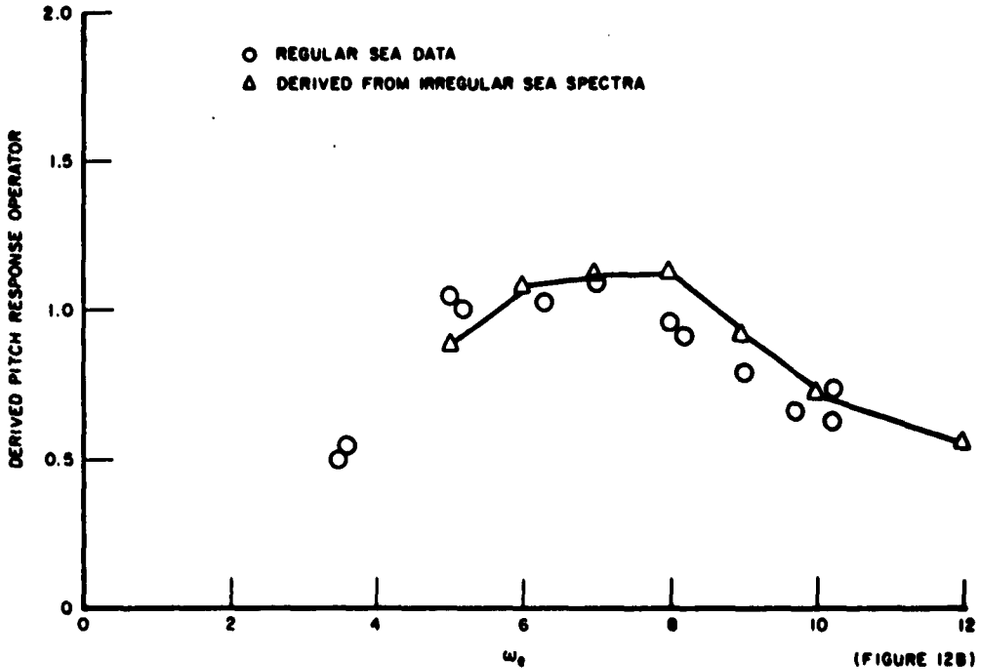

(FIGURE 12B)

FIGURE 10. COMPARISON OF DERIVED RESPONSE OPERATORS FOR HEAD SEAS AT V=8FEET/SECOND WITH REGULA SEA DATA

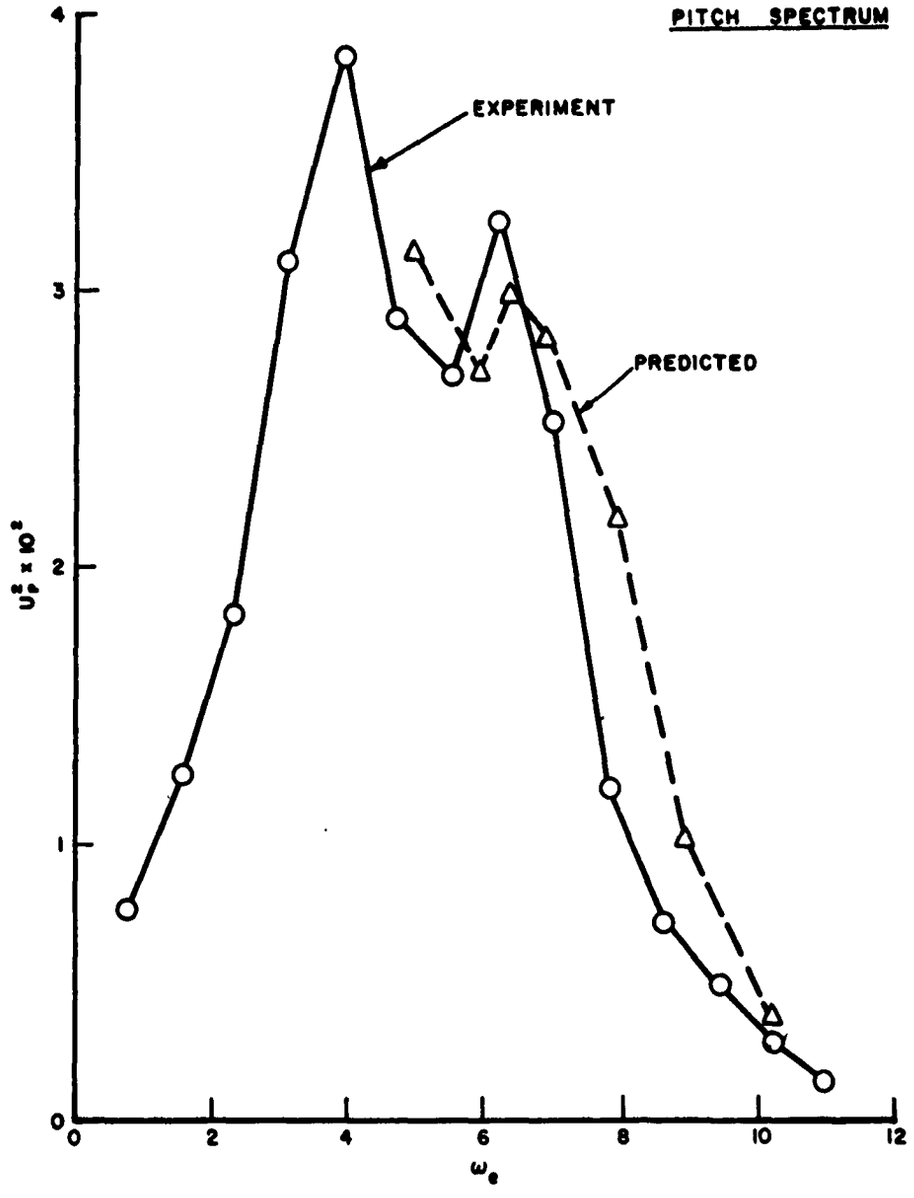

FIGURE 11a. COMPARISON OF EXPERIMENTAL SPECTRA WITH PREDICTED SPECTRA USING REGULAR SEA DATA. (a) V=5 FEET / SECOND, HEAD SEAS, SEA STATE "A". R =0.339.

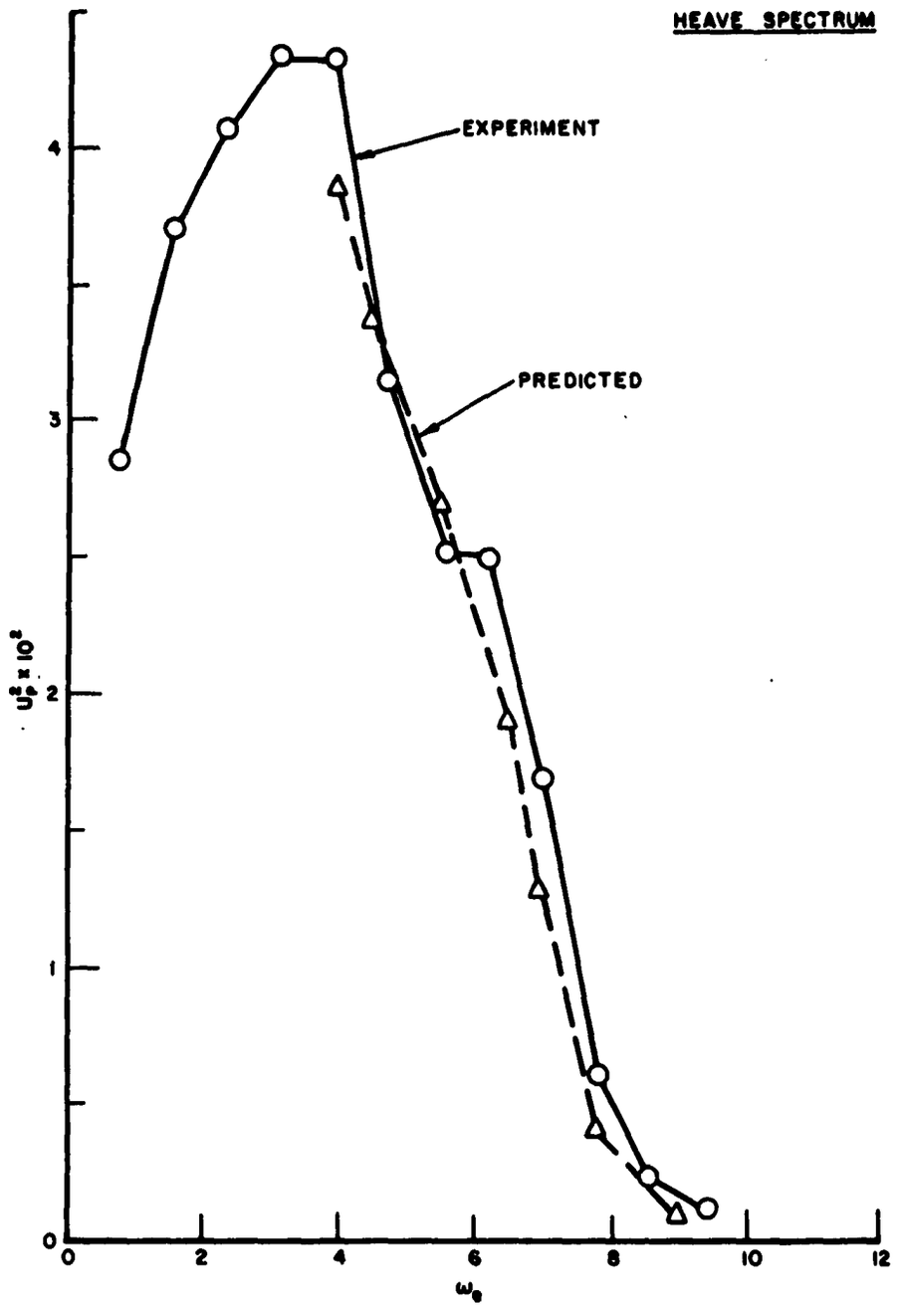

FIGURE 11b. V= 5 FEET / SECOND, HEAD SEAS, SEA STATE "A".

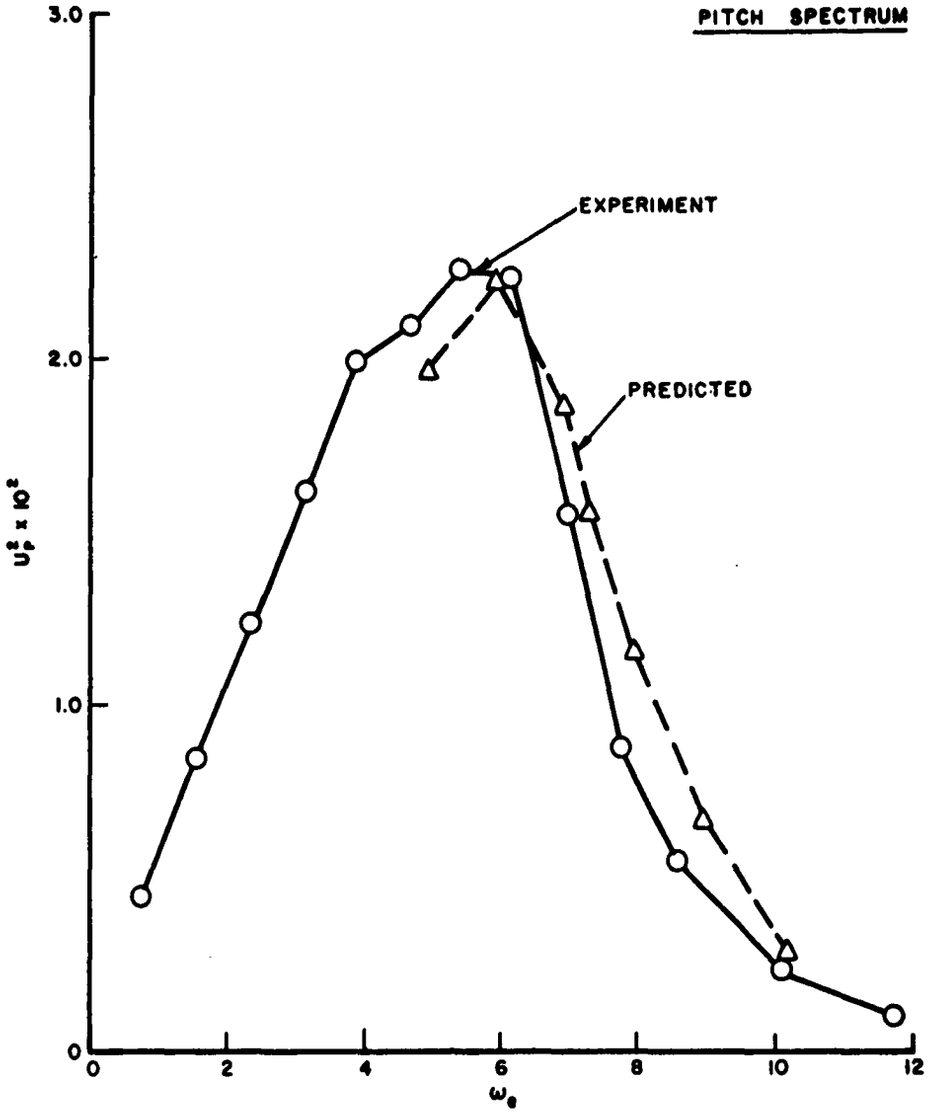

FIGURE 11c. V=5 FEET SECOND, HEAD SEAS, SEA STATE "B."

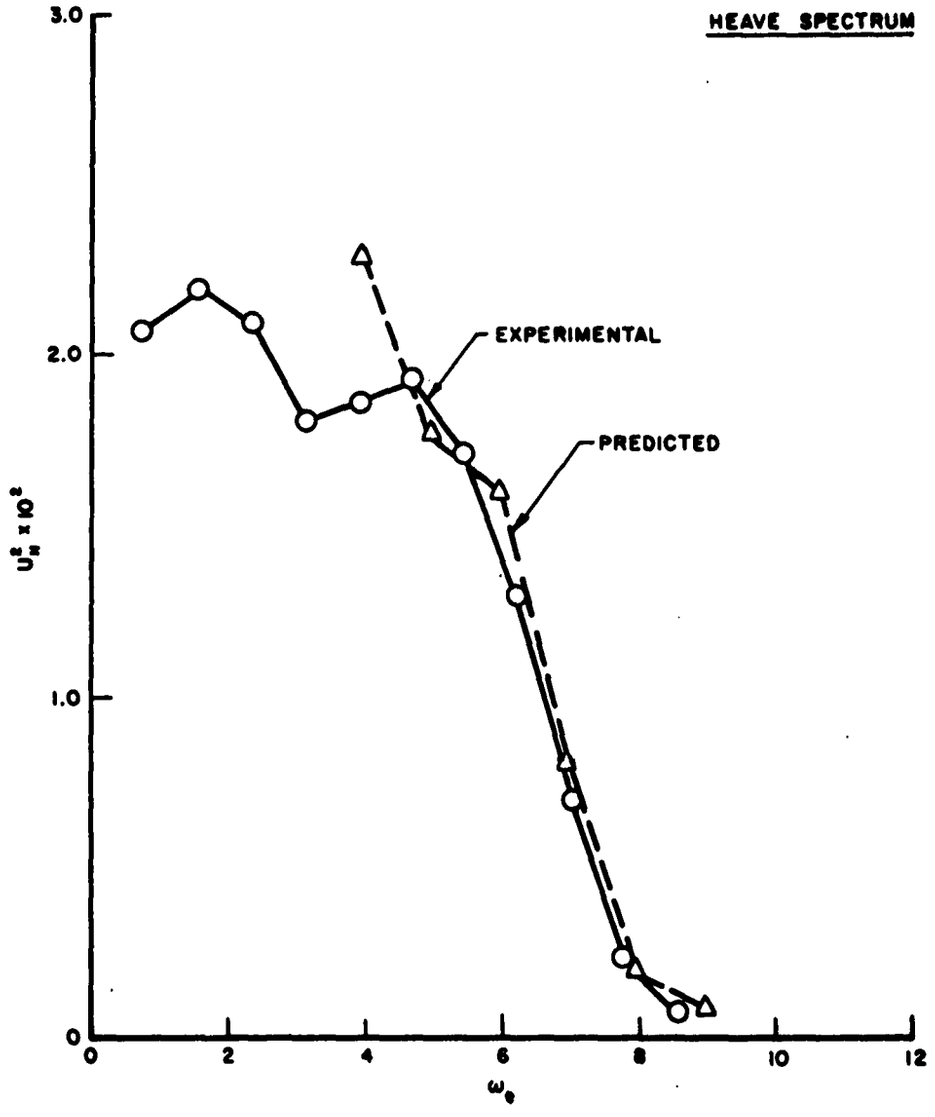

FIGURE 11d. V=5 FEET / SECOND, HEAD SEAS, SEA STATE "B."

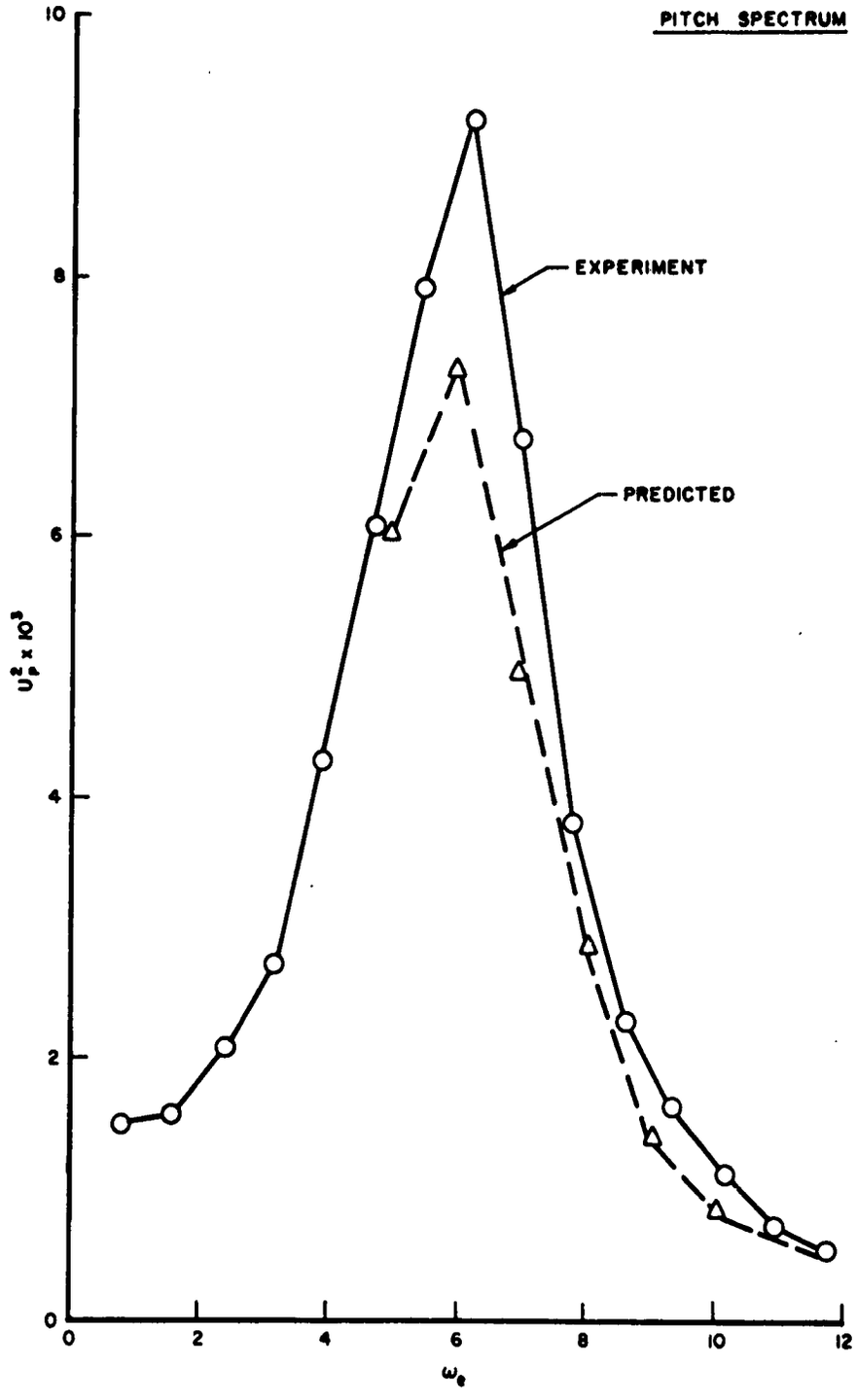

FIGURE 11e. V=5 FEET/SECOND HEAD SEAS, SEA STATE "C"

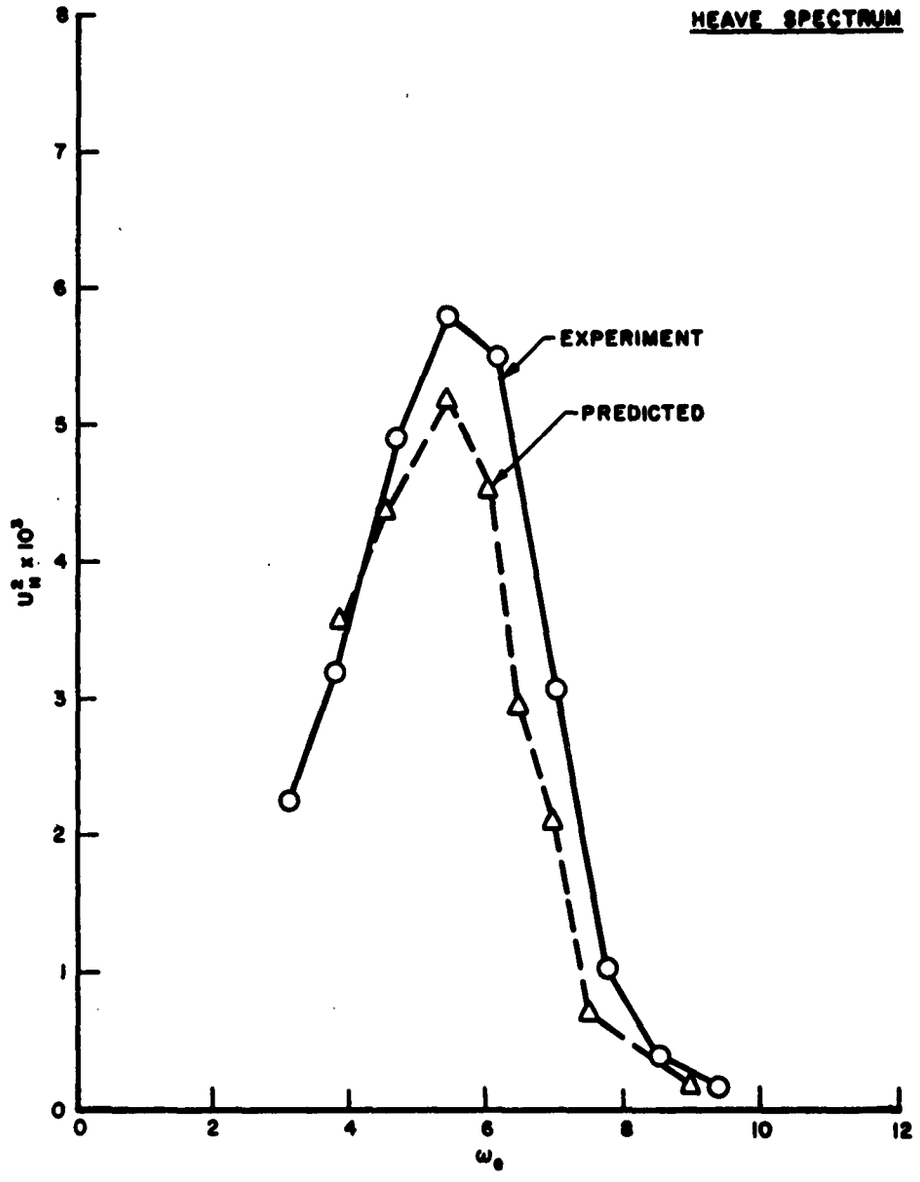

FIGURE 11f. V=5 FEET / SECOND HEAD SEAS, SEA STATE "C"

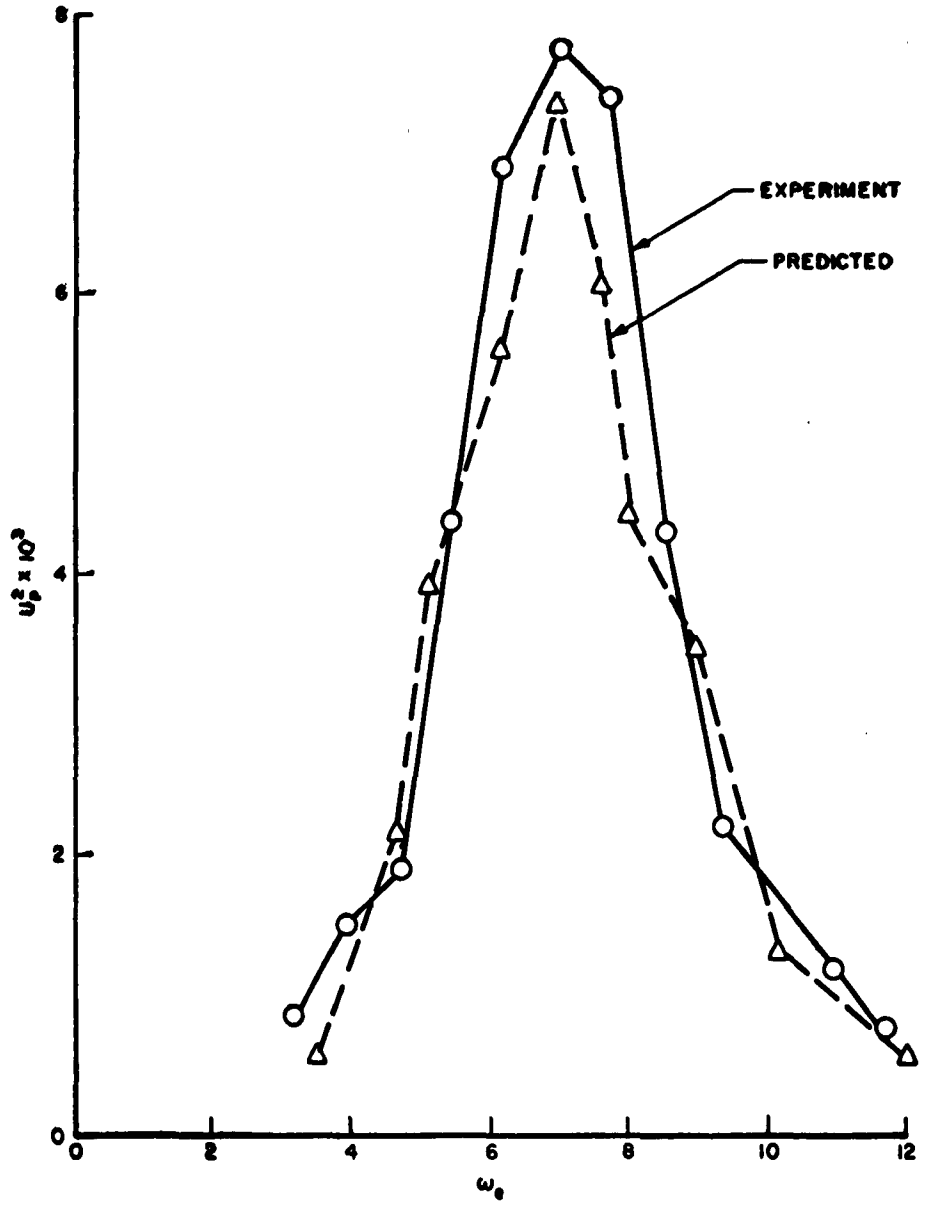

FIGURE 12a. COMPARISON OF EXPERIMENTAL SPECTRA WITH PREDICTION USING REGULAR SEA DATA, V=8 FEET/SECOND, HEAD SEAS. (a) PITCH SPECTRUM.

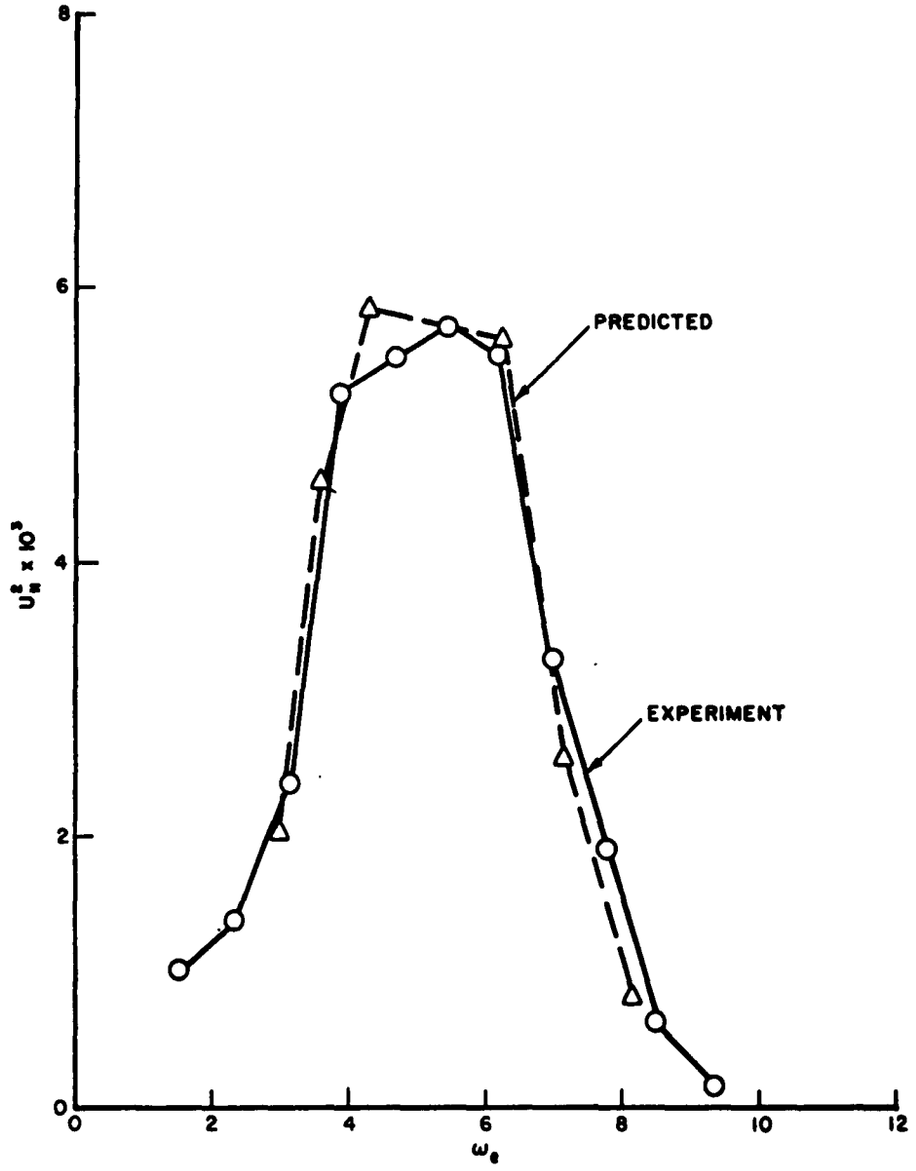

FIGURE 12b. HEAVE SPECTRUM

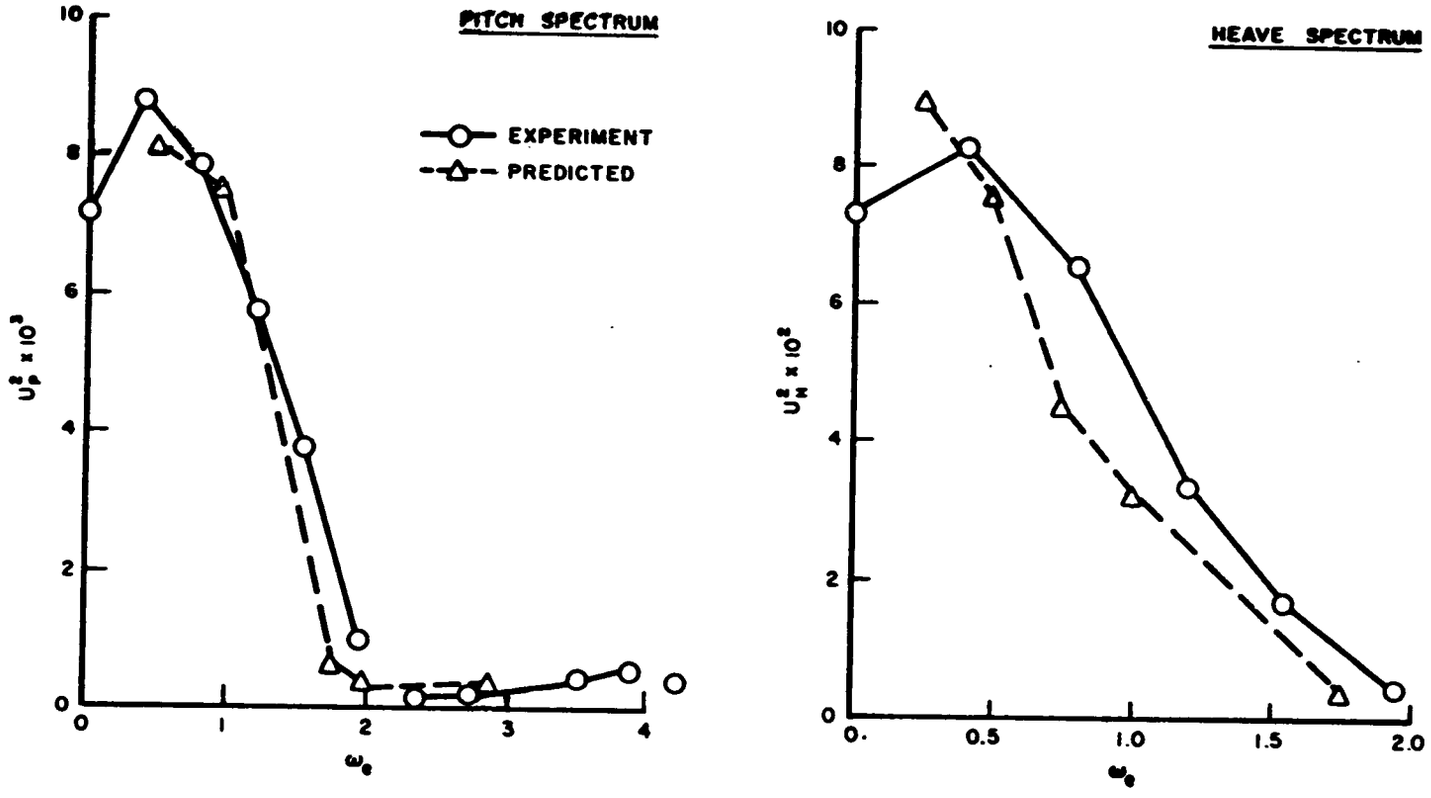

FIGURE 13. COMPARISON OF EXPERIMENTAL SPECTRA WITH PREDICTION USING REGULAR SEA DATA. V = 5 FEET/SECOND, FOLLOWING SEAS.

SOME EXPERIMENTS ON THE LONGITUDINAL SEAKEEPING CHARACTERISTICS OF A GROUND EFFECT MACHINE

by S. C. Y. Chen and T. Kowalski
Davidson Laboratory

I. INTRODUCTION

The experiments described in this paper were performed on a model of one of the BuShips "Hydroskimmer" Ground Effect Machines. The tests were of a developmental nature with the main effort directed toward obtaining longitudinal seakeeping characteristics in a State 3 sea. The characteristics measured were pitch, heave, accelerations at the bow and CG resulting from oscillatory response of the model to waves, as well as from direct wave impacts. The effect of introducing springs of varying stiffness in the pitch system of the model was studied. The springs simulated automatic restoring moments proportional to pitch amplitudes.

A second objective of the program was to study the applicability of superposition theory and spectral analysis techniques in the investigation of GEM motions. For this purpose, regular wave tests were performed and results compared with the results of spectral analysis of selected irregular wave runs.

II. MODEL AND INSTRUMENTATION

A 1/15 scale model was used in the experiments (Fig. 1). The design of this annular jet craft had a unique double tunnel base and a flared motor torpedo boat type bow. The side jets were of uniform thickness and parallel to the water surface. The end jets were of variable thickness, proportional to the height of the tunnel above the water surface. This design possesses a number of apparent advantages, viz:

a) Economy of lift power since side jets operate very close to the water surface.

b) Structural strength of an arched construction.

c) Roll stability when cushion borne, since the center rib acts as a partition of the air cushion in preventing cross-flow.

The full-scale characteristics of the craft were as follows:

Length overall	65 ft
Beam overall	22 ft
Height of craft	12 ft
Length of nozzles	
Side nozzles	48 ft
End nozzles	10 ft each
Jet angle with vertical	60° inward
Weight	45,000 lbs
Maximum speed	70 knots
Normal operating clearance:	
6" at the side jets over solid ground	

Figure 2 is a sketch of the genral arrrangement of model, air system, and test apparatus. Due to weight limitations of the model, an external air supply system was adopted causing complications with weight ballasting and moment of inertia adjustments. The air was supplied by an electric driven aircraft-type blower supported by the main towing carriage and piped into the model by a ducting system. The sections of the ducts were connected by light weight ball bearings with labyrinth seals to allow freedom of pitch, heave and surge motions. The ducting was statically counter-balanced to eliminate vertical and horizontal thrusts on the model. The overall effect of the ducting system was treated as an equivalent mass at the CG coupled with a moment of inertia about the CG. The model was towed on a servo motions apparatus which allowed freedom in heave, pitch and surge. At speeds in excess of 30 knots (full size), the surge was locked out. Servo apparatus permitted the drag of the model to be measured in calm water and in waves.

The test data were recorded on a light sensitive paper tape. Part of the irregular wave data were simultaneously recorded on magnetic tape for subsequent transcription onto IBM cards and analysis by the IBM 1620 Computer.

III. TEST PROGRAM

A. Static and Calibration Tests. The effective mass and moment of inertia of the fully instrumented model and the ducting without air flow were evaluated by free oscillation tests with calibrated springs. The natural frequencies of the model in heave and pitch when hovering over ground board or water could not be measured because of the small clearance height and the insufficient pitch stability. At that clearance, one end tended to touch the ground or water surface under the slightest disturbance.

The air tare resistance of the model, apparatus and air ducting was measured by running the model cushion-borne over a ground board moving down the tank with the model. In this and all subsequent tests, initial clearance heights were obtained by adjusting the fan power input with the model hovering over a ground board. After the board was removed, the model settled at an equilibrium height over the water and this position was used as a datum for heave measurements. Since momentum drag was not measured by this system, the calm water drag as measured by the towing force at a constant speed minus air tare represents the wave-making spray resistance of the model at that speed.

B. Regular Wave Tests. Regular wave tests were carried out with one pitch restoring spring of spring rate 2.87 in lbs/deg (12100 ft-lbs/deg full size) and also without spring. Initial clearance height settings were 0.5" and 1.0". The speed range was 0-13 fps (30 knots) with surge and to 20 fps (46 knots) without surge. The regular waves had the following sizes:

WAVE LENGTH	MODEL SCALE		FULL SIZE	
Vehicle Length	Wave Length Ins.	Wave Height Ins.	Wave Length Ft	Wave Height Ft
1.5	60	2	75	2.50
2.0	80	3	100	3.75
2.0	80	4	100	5.00
4.0	160	4	200	5.00
4.0	160	5	200	6.25

Shorter waves than 1.5L were not used because the wave-making machine was unable to generate high enough waves of short lengths to produce large motions.

C. Irregular Wave Tests

The following parametric variations were used:

Sea State	3
Clearance Height	0.4" (6" full size) 0.5" (7-1/2" full size) and 1.0" (15" full size)
Pitch Springs	4 springs from 2.87 in-lbs/deg to 12.20 in-lbs/deg (12100 ft-lbs/deg to 51500 ft-lbs/deg full size) and also no spring
Speeds	0-13 fps (30 knots full size) with surge 13-20 fps (46 knots full size) no surge
Sea State	2
Clearance Height	0.4" (6" full size)
Pitch Spring	Not used
Speeds	Same as for State 3 sea

IV. RESULTS AND DISCUSSION

A. Resistance. All resistance data are given for the full-size craft.

1. Regular wave drag, presented on Figs. 3 and 4 to the base of the frequencies of encounter, indicate the following trends:

a) Longer waves produce higher drag than shorter waves of the same height.

b) The drag curves have steep slopes at low frequencies but flatten out at higher frequencies. This reflects the effect of reduced heave and pitch at super-critical speeds and is a favorable aspect of GEM's which normally cruise above resonance speeds.

c) Generally lower drag values in waves can be obtained by increasing the clearance height.

2. Irregular Wave Drag. The rough water resistance (Figs. 5 and 6) is presented as a band covering the scatter of points obtained in tests using different pitch springs and with the model flying over different portions of the wave program. The calm water drag is also shown for comparison.

The curves display the general trend of a drag curve for a displacement ship within the speed range tested. It is believed that at higher speeds a decrease of drag dependence on the speed would be obtained similar to the trend found with regular waves.

B. Heave and Pitch. All heave and pitch data are presented in model scale.

1. Irregular Waves. Figures 7, 8, 9, and 10 are representative plots giving the average model response amplitudes in heave and pitch to irregular waves approximating a State 3 sea. Ground clearance and pitch spring stiffness are the parameters.

Figure 11 presents the average model heave and pitch responses to a scaled State 2 sea, with the corresponding model responses to State 3 sea shown in dotted lines. It is seen that the average response amplitudes increase with the sea state, the ratio of increase roughly in the order of magnitude of the average wave heights of the two sea states. No consistent dependence of the model response on spring rates and small variations of initial ground clearance heights could be detected.

2. Regular Waves. The regular wave heave and pitch responses of the model are given in Figures 12, 13, 14, and 15. These plots all exhibit pronounced magnification characteristics. In the absence of reliable measurements of the natural frequencies of the model in heave and pitch over water, only the following qualitative observations can be made:

a) The location of the peaks shifts to the left (lower ω_e) as the wave length increases. This indicates the effect of added mass of water, which varies with the size of the wave, on natural frequency and damping.

b) Pitch decreases and heave increases with increasing wave length.

c) No significant and consistent dependence on spring stiffness and initial ground clearance of pitch and heave responses is apparent.

C. Acceleration. Some typical curves of vertical up and down acceleration in regular and irregular seas, as measured by the accelerometers located at the bow and the CG, are presented in Figs. 16, 17, and 18. On the irregular wave acceleration plots (Fig. 18), the average of about 1/3 highest readings are shown by solid lines and maximum impact accelerations by dotted lines.

Figure 19 presents a comparison of irregular wave accelerations obtained with and without the pitch spring. A reduction of the upward bow impact accelerations seems to be possible with a suitable pitch restoring control. However, in view of the smallness of the samples taken, this result is far from being conclusive. The reduction of upward bow accelerations by decreasing the severity of waves is, however, quite apparent from Figure 20 which shows bow accelerations in State 3 and State 2 seas.

The most striking feature of the acceleration data is the severity of upward bow impact in both regular and random seas, even at the relatively low speeds tested. If the clearance heights of the curved end jets are averaged, it is seen that the wave height/clearance height ratios obtained for these tests are by no means excessive in GEM design practice. The actual clearance at the side jets, however, is only a small fraction of the average clearance and the wave height/clearance ratios based on side jet heights are much higher. This pinpoints the reason for the 10g impact accelerations. From this point of view, the configuration under study is unfavorable in that it has too much solid structure protruding close to the water surface. Possible direction of improvement would therefore be (1) the use of a flat bottom configuration, and (2) the use of flexible curtains on both sides of the jets. Both of these measures will allow a greater clearance under the solid bottom of the craft.

D. Spectral Analysis. Linear superposition theory and spectral analysis techniques have been shown to give good correlation between predicted and measured motions in the case of displacement ships in irregular head seas. In the case of air cushion vehicles, there is no direct displacement of water by the craft, however, and the motions are produced by the waves either via the air cushion or by direct impact. On the one hand, the air cushion acts like a filter producing attenuated and phased motions. On the other hand, direct

wave impacts produce more abrupt and discontinuous motions when compared to displacement ships. There was no prima facie reason to believe that this useful technique could be extended to air cushion vehicles. An experimental verification of the applicability of the superposition theory utilizing the available test data was therefore considered desirable.

Figures 21 and 22 are typical transfer function moduli obtained as a result of spectral analysis of the irregular wave experiments. The response amplitudes used are in model scale.

On the graphs of the transfer functions, data points from regular waves tests are shown in square boxed points. It was found that the correlation between the predicted motions (represented by the transfer function curves) and the observed motions in regular waves are reasonably good within the small range of speeds tested (0-10 fps). The few large discrepancies found (of the order of 20 percent or more) could be attributed to the following factors:

a) instabilities of the regular waves generated, making it difficult to obtain a representative wave height and frequency, also producing a scatter in the model response,

b) large statistical scatter of the irregular wave data due to insufficient sample size, and

c) intrinsic non-linearity of the system.

V. CONCLUSIONS

The following conclusions are made on the longitudinal seakeeping behavior.

1. No significant and consistent improvement in drag, pitch and heave motions, and accelerations are found by the use of pitch restoring moments simulated on the model by springs.

2. An apparent improvement in the magnitude of all the motions measured is observed when the irregular waves are lowered from those approximating State 3 sea to those approximating State 2 sea.

3. Pitch and heave responses in regular and random seas bear striking resemblence to displacement ships. Pitch

resonance occurs in a low speed region. At higher speeds at which GEMs are designed to cruise, pitch tends to flatten out and fall within acceptable magnitudes. This tendency is not observed in the case of heave motions. In comparison, in tests performed recently at Davidson Laboratory on two ship models, supercritical operation was attained for pitch motions but not for heave motions.

4. The vertical accelerations at the bow, caused by direct wave impacts of short duration, is quite unfavorable for this base configuration. From visual observations of the test runs as well as from the magnitudes of accelerations due to bow impacts, the motions of this craft resemble that of a planing boat rather than a true air cushion vehicle flying above the water.

Bow accelerations of the order of 7g have been reported for a V-bottom boat at 45 knots in heavy seas. Model tests of a planing boat conducted in the Davidson Laboratory has also yielded similar accelerations at similar speeds and sea state as the present hydroskimmer tests.

5. The spray characteristics of this vehicle appear quite favorable in model scale. The extended flared bow formed an effective spray deflector. In full size, the spray is expected to be higher since it is not a quantity which obeys Froude scaling used for constructing the model.

The following conclusions are made on the verification of the superposition theory.

The limited work done in verifying the applicability of linear superposition theory and spectral analysis techniques to air cushion vehicles has yielded some positive results. Further study is however required in this direction. The investigation should be extended to include accelerations and phases of motions and cover higher speeds. If reasonably affirmative results are obtained, one would have an effective technique for the experimental study of air cushion vehicles.

VI. ACKNOWLEDGEMENT

The experiments described in this paper have been sponsored by the Bureau of Ships, Department of the Navy, under Contract NObs 84330. The Bureau's permission to publish this paper is gratefully acknowledged.

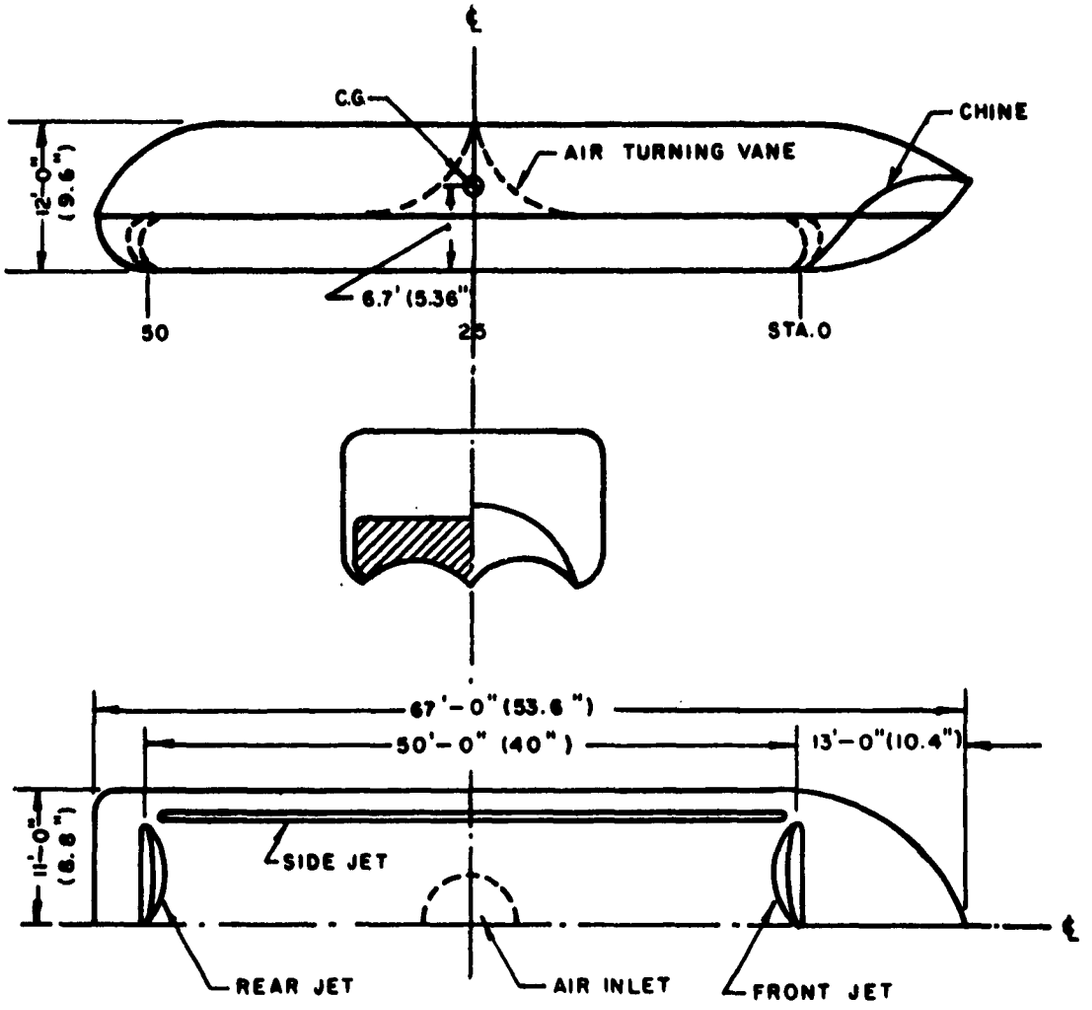

NOTE: NUMBERS IN PARENTHESIS INDICATE DIMENSIONS OF $\frac{1}{15}$ SCALE MODEL

FIGURE 1. MODEL DRAWING OF BUSHIPS HYDROSKIMMER

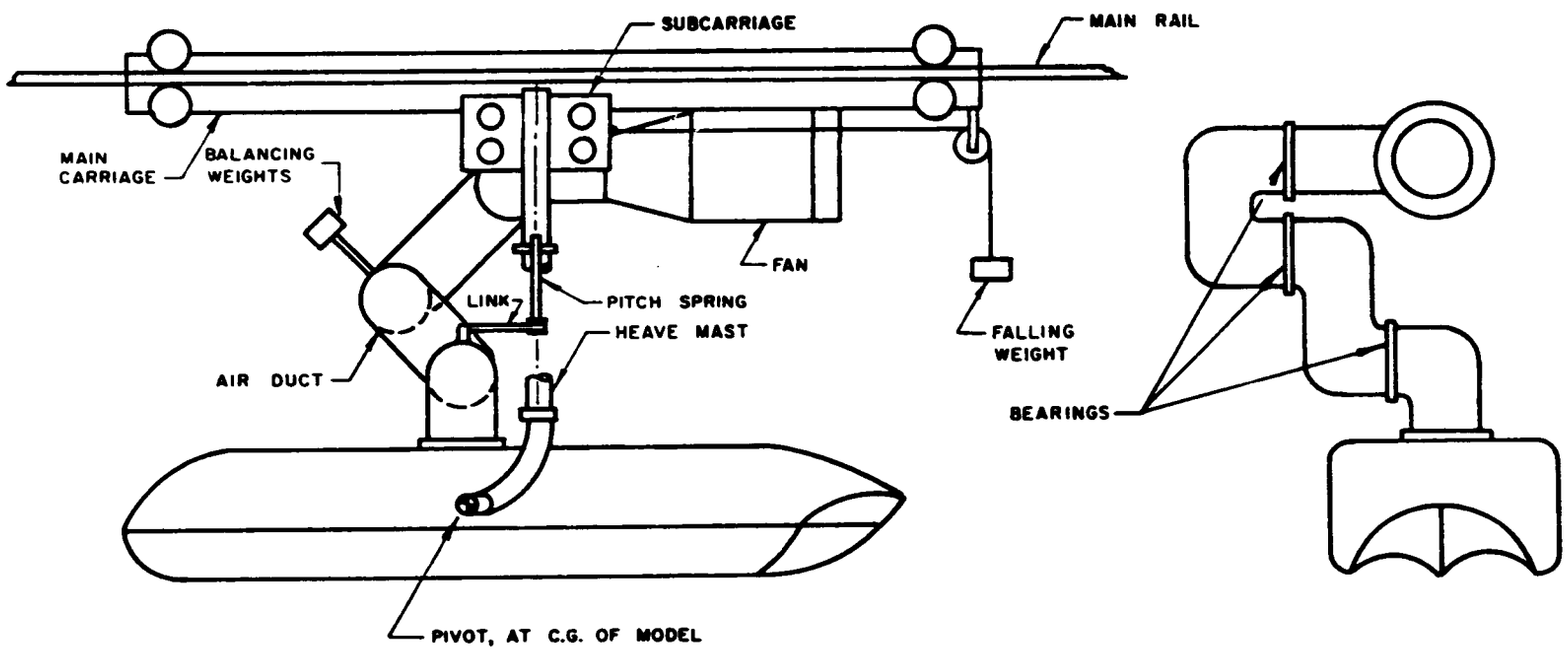

FIGURE 2. GENERAL ARRANGEMENT OF MODEL, AIR SYSTEM, AND TEST APPARATUS

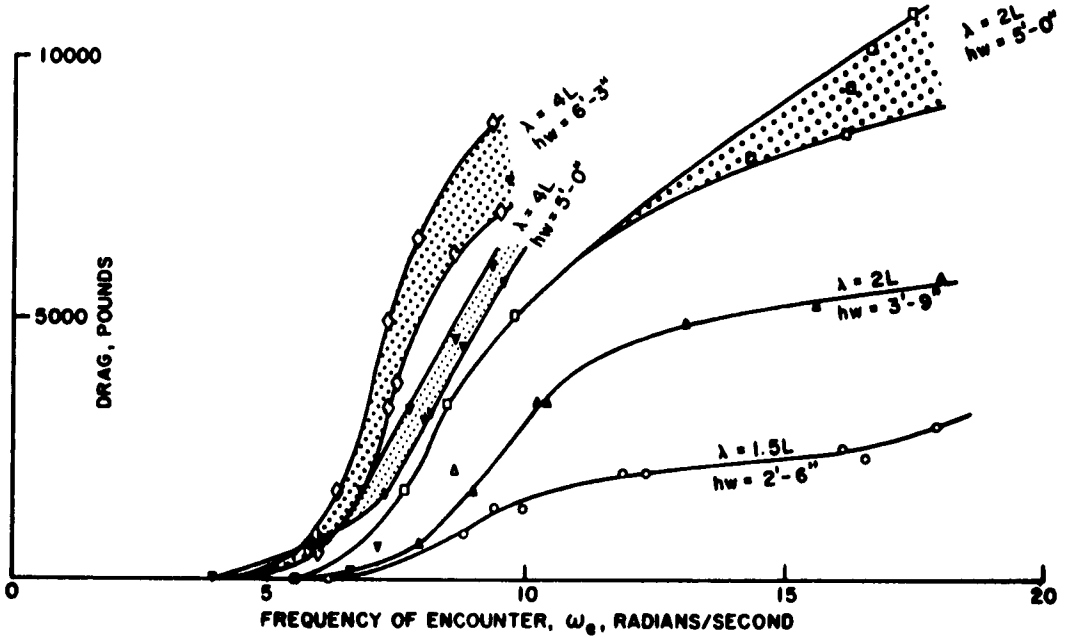

FIGURE 3. DRAG VERSUS FREQUENCY OF ENCOUNTER (REGULAR WAVES) h_e = 15"

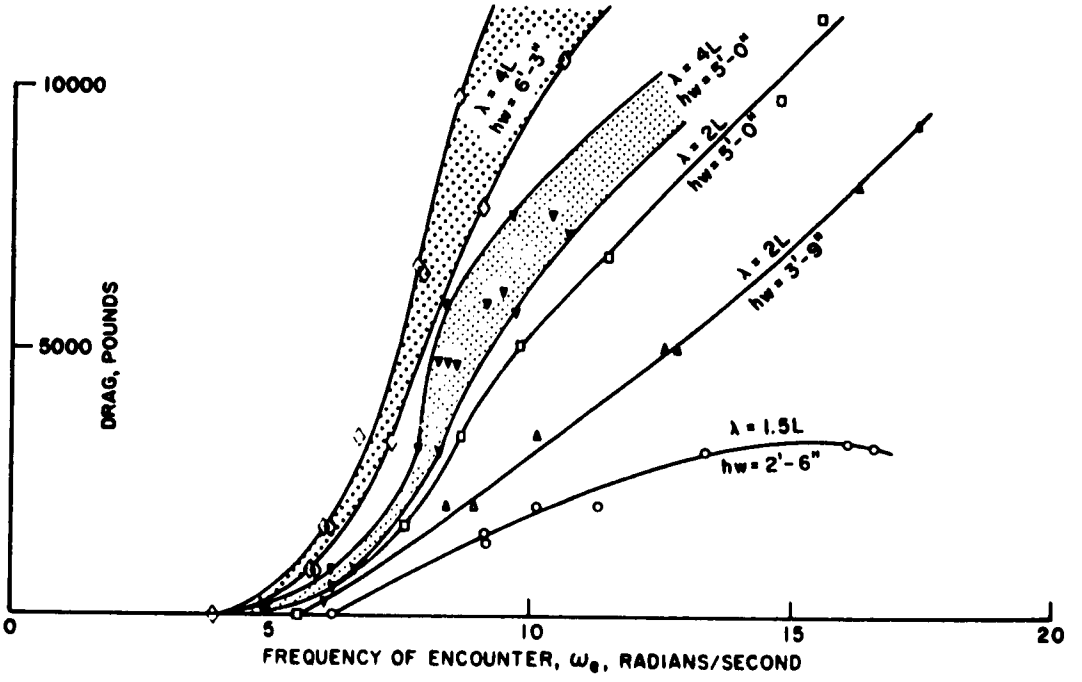

FIGURE 4. DRAG VERSUS FREQUENCY OF ENCOUNTER (REGULAR WAVES) h_e = 7-1/2"

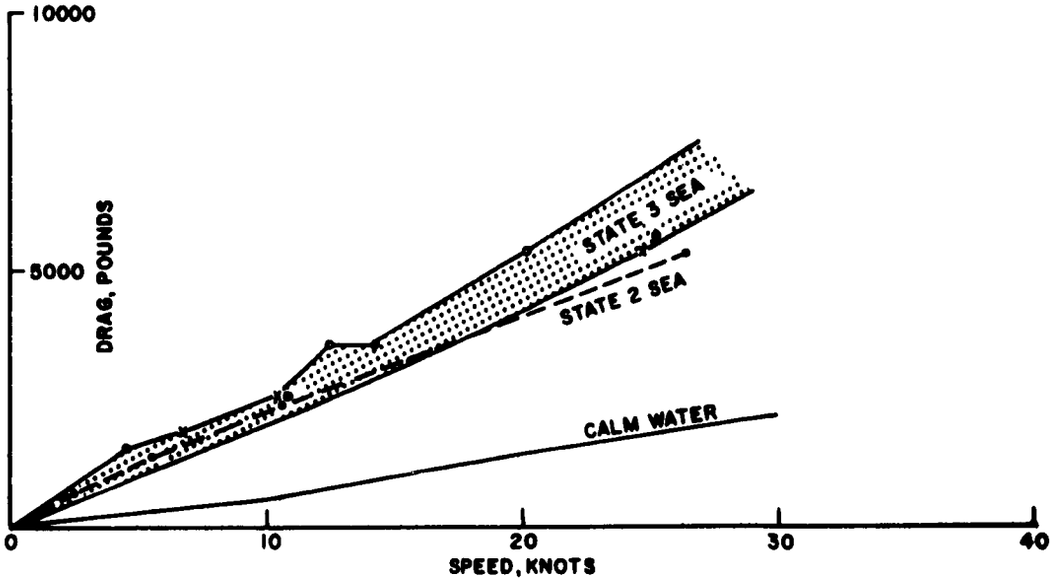

FIGURE 5. IRREGULAR WAVE DRAG (FULL SIZE) CLEARANCE HEIGHT h_e = 7-1/2"

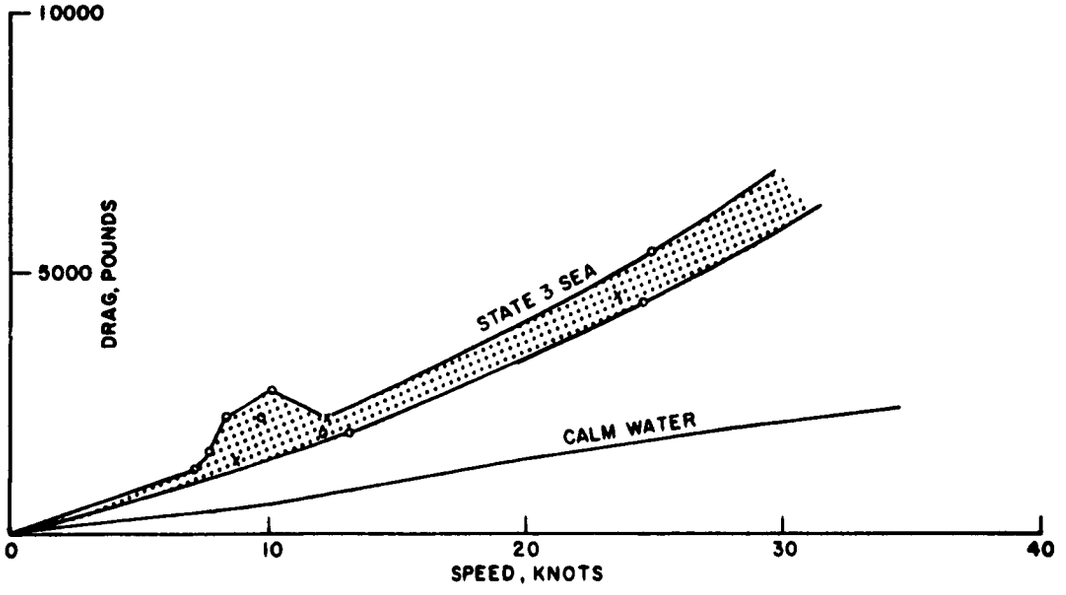

FIGURE 6. IRREGULAR WAVE DRAG (FULL SIZE) CLEARANCE HEIGHT h_e = 15"

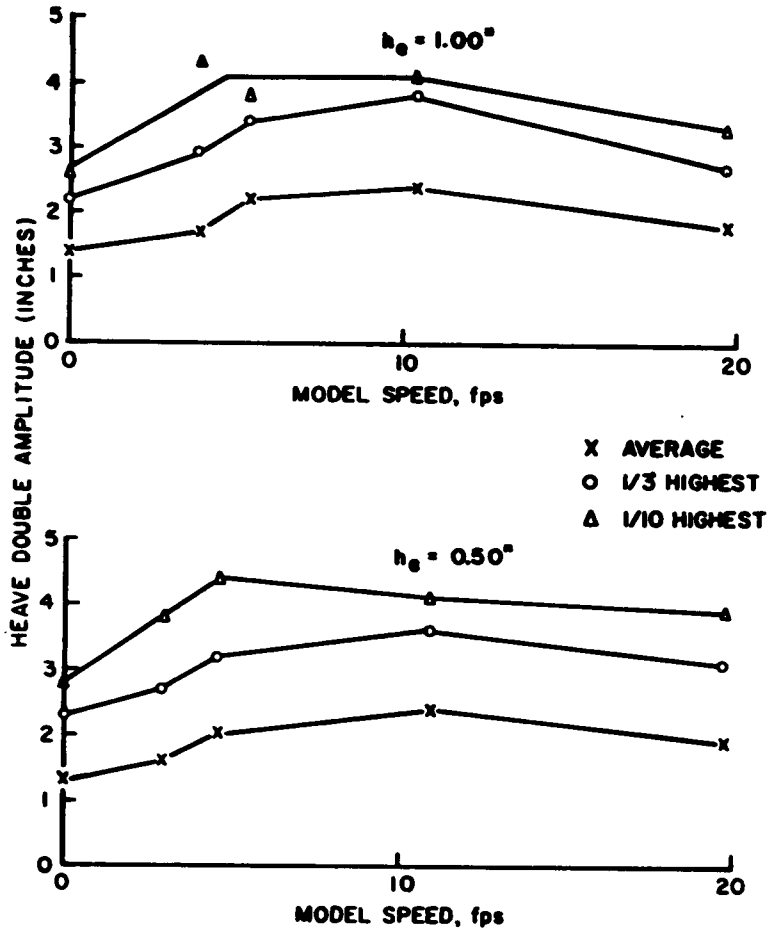

FIGURE 7. MODEL HEAVE RESPONSE, NO SPRING (STATE 3 SEA)

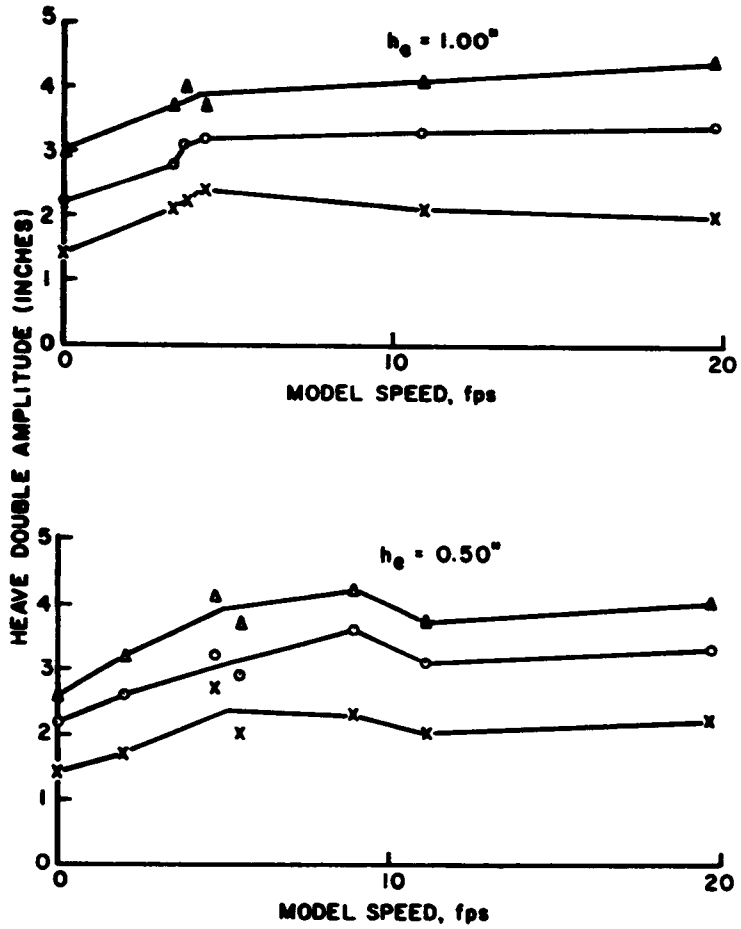

FIGURE 8. MODEL HEAVE RESPONSE, SPRING CONSTANT, 2.87 IN-POUND/DEGREE (STATE 3 SEA)

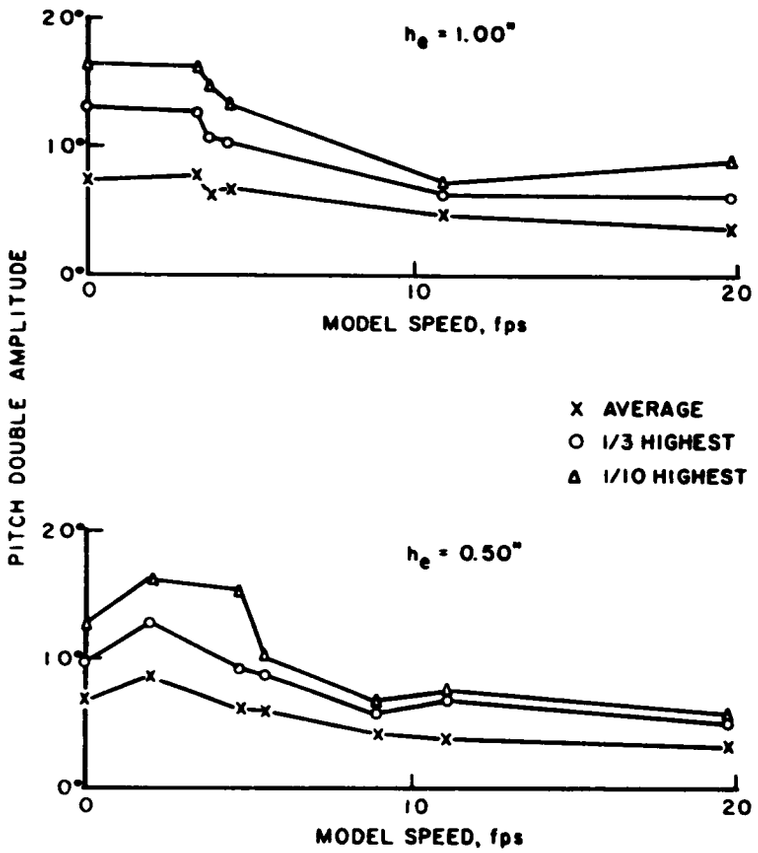

FIGURE 9. MODEL PITCH RESPONSE-SPRING USED SPRING CONSTANT- 2.87 IN-POUNDS/ DEGREE (STATE 3 SEA)

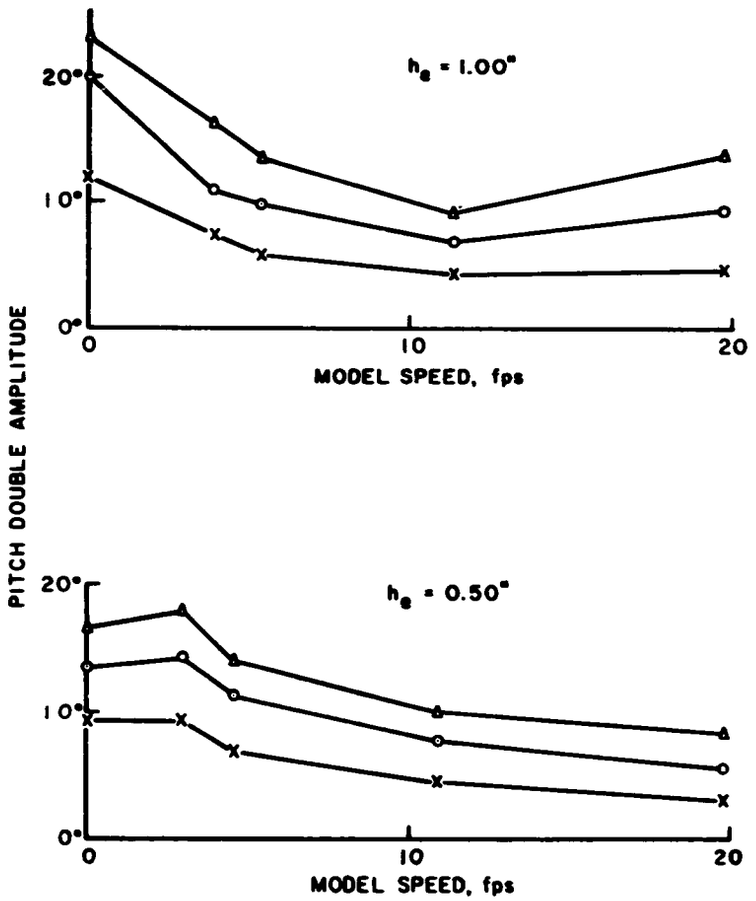

FIGURE 10. MODEL PITCH RESPONSE-NO SPRING (STATE 3 SEA)

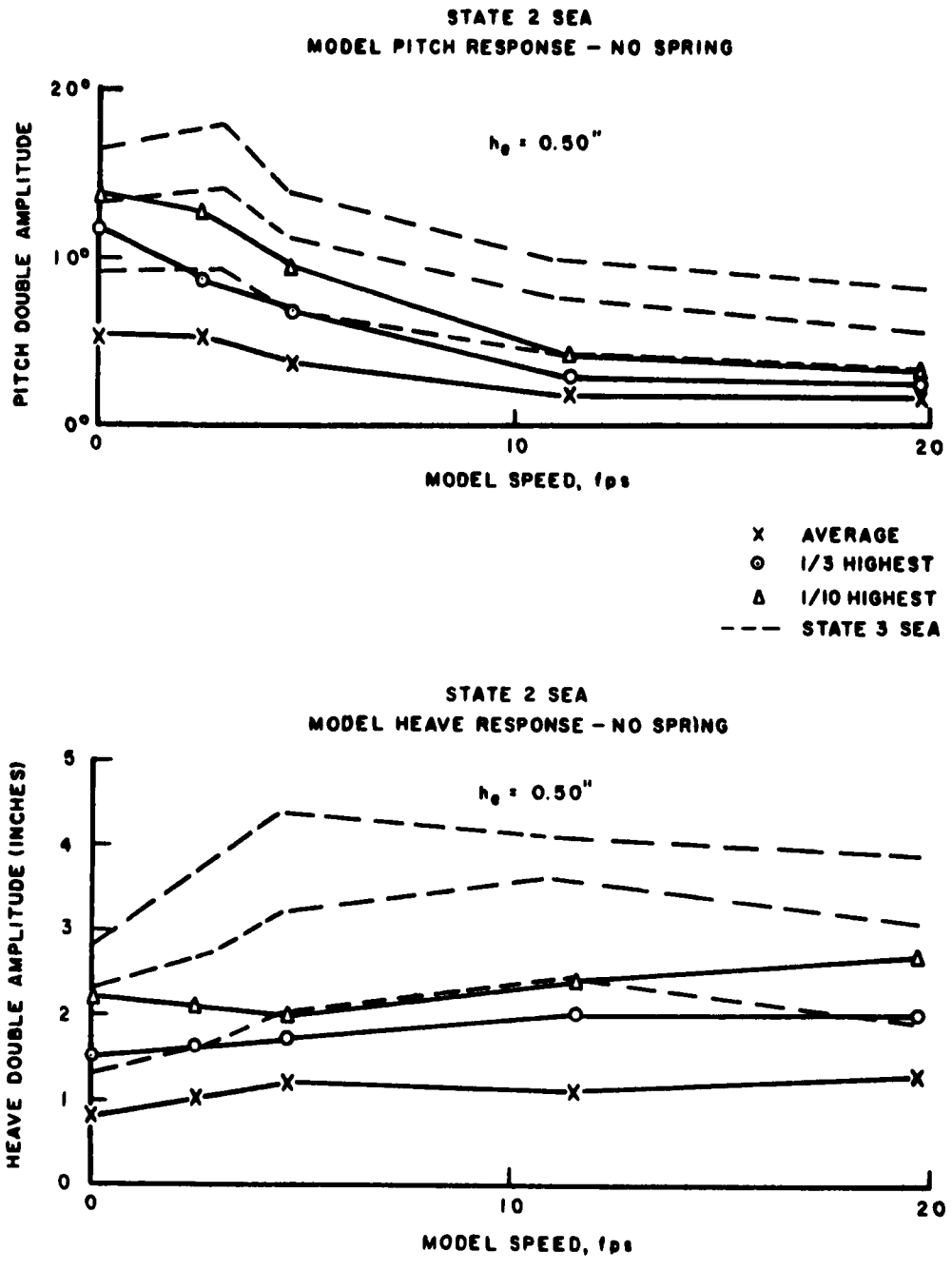

FIGURE 11. PITCH AND HEAVE RESPONSES

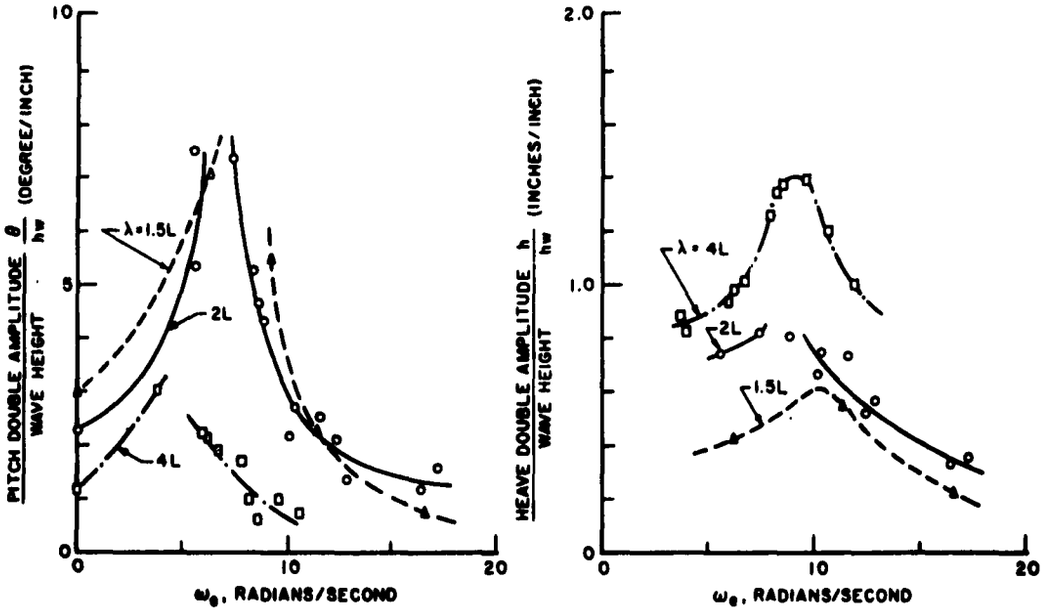

FIGURE 12. PITCH AND HEAVE RESPONSES IN REGULAR WAVES, h_e = 0.50", NO PITCH SPRING

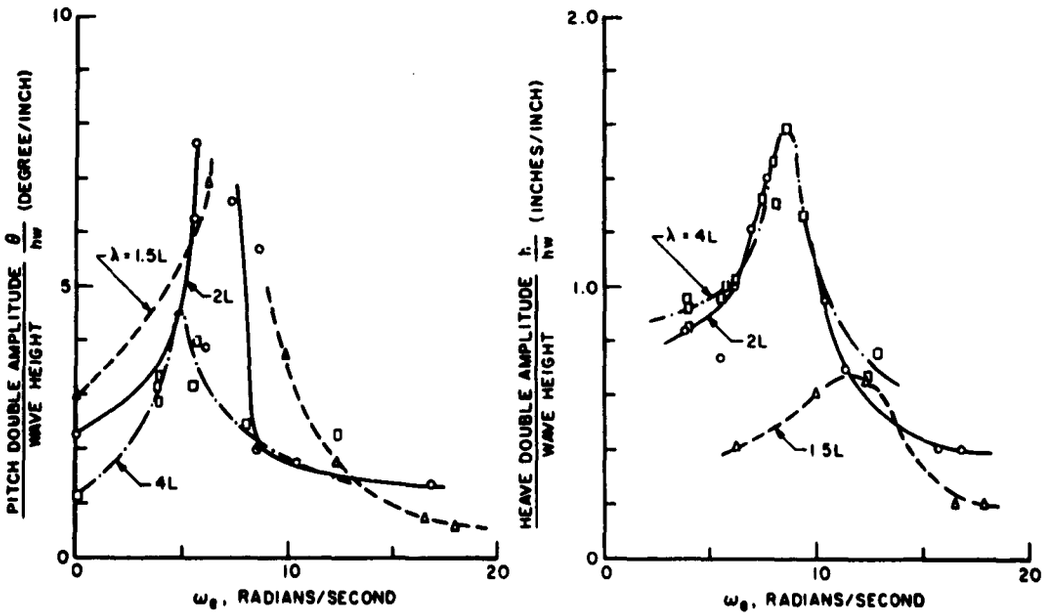

FIGURE 13. PITCH AND HEAVE RESPONSES IN REGULAR WAVES, h_e = 1.00", NO PITCH SPRING

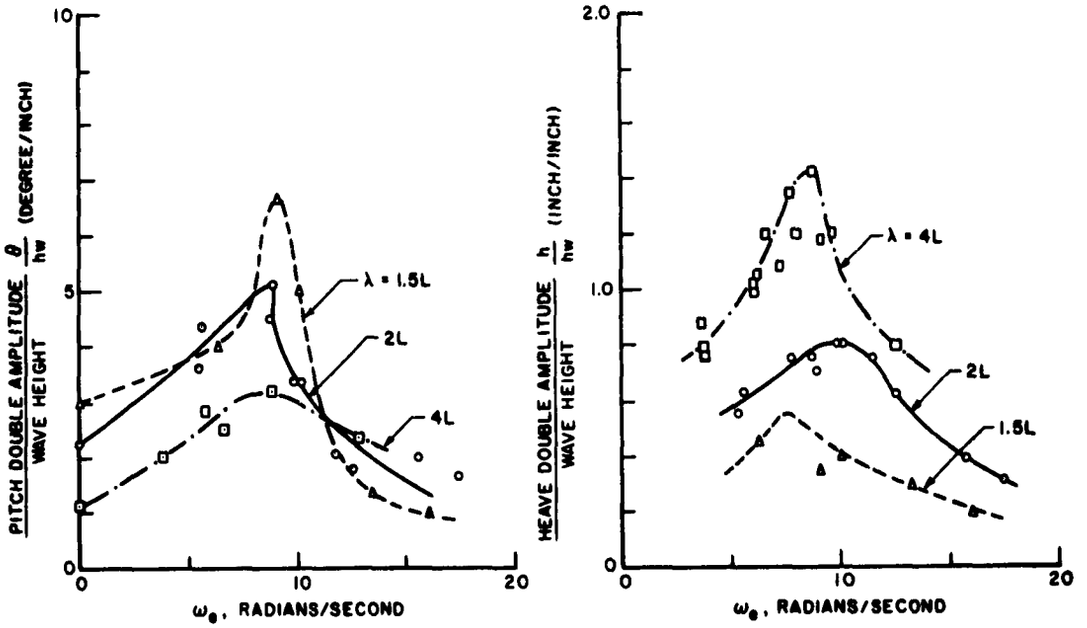

FIGURE 14. PITCH AND HEAVE RESPONSES IN REGULAR WAVES, $h_e = 0.50"$, SPRING RATE 2.87 IN-POUNDS/DEGREE

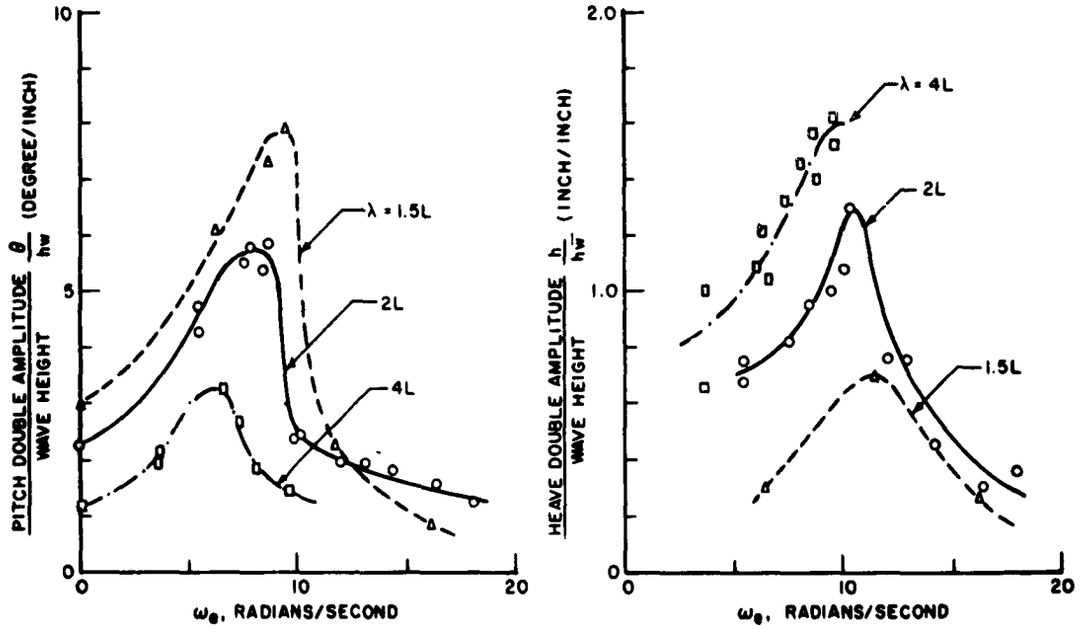

FIGURE 15. PITCH AND HEAVE RESPONSES IN REGULAR WAVES, $h_e = 1.00"$, SPRING RATE 2.87 IN-POUNDS/DEGREE

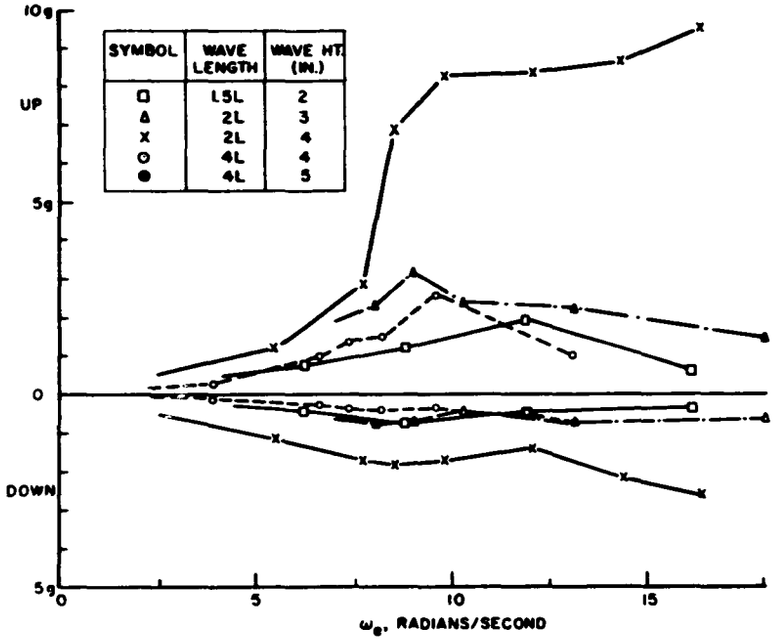

FIGURE 16. BOW ACCELERATION IN REGULAR WAVES, SPRING RATE 2.87 IN-POUNDS PER DEGREE, h_e = 1.00°

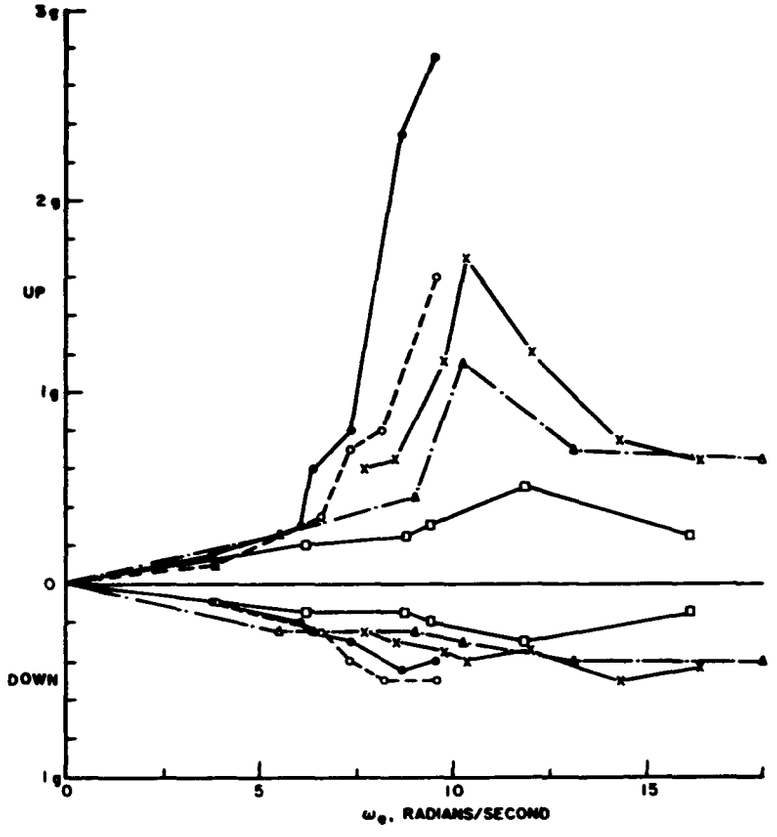

FIGURE 17. C.G. ACCELERATION IN REGULAR WAVES, h_e = 1.00° SPRING RATE 2.87 IN-POUNDS PER DEGREE

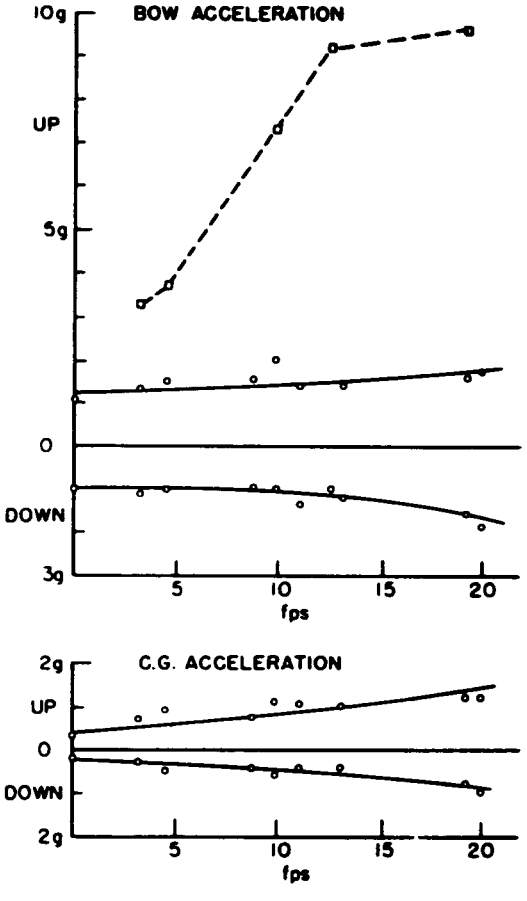

FIGURE 18. STATE 3 SEA, h_e = 0.40", SPRING RATE 5.03 IN.-POUNDS PER DEGREE

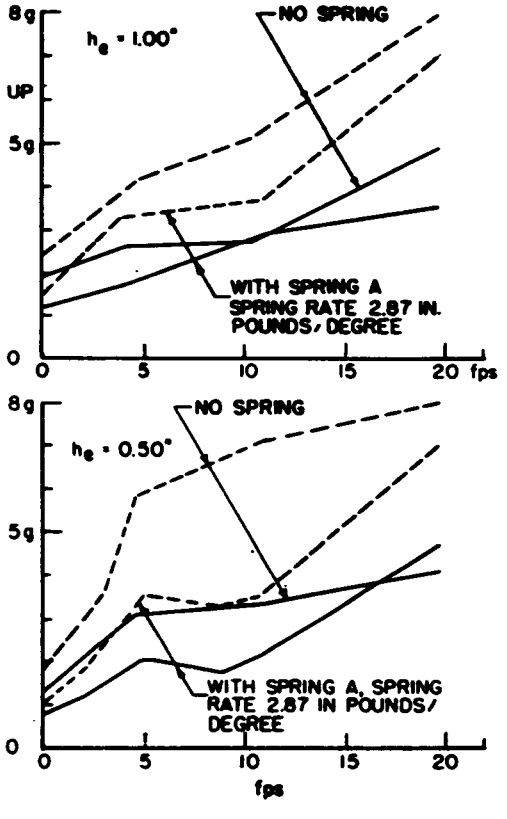

FIGURE 19. BOW ACCELERATION (UPWARD) WITH AND WITHOUT PITCH SPRING, h_e = 1.00" (STATE 3 SEA)

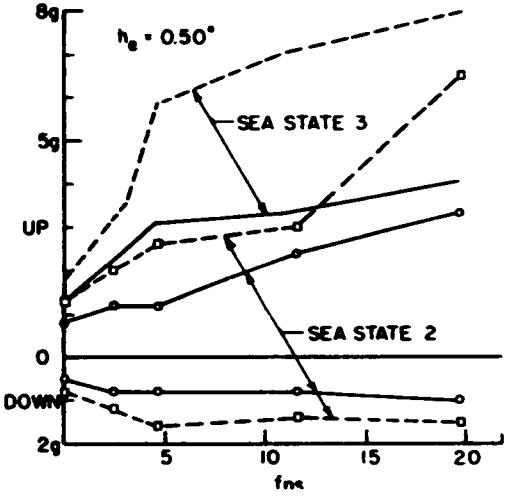

FIGURE 20. COMPARISON OF BOW ACCELERATION IN STATE 2 SEA AND STATE 3 SEA, NO SPRING

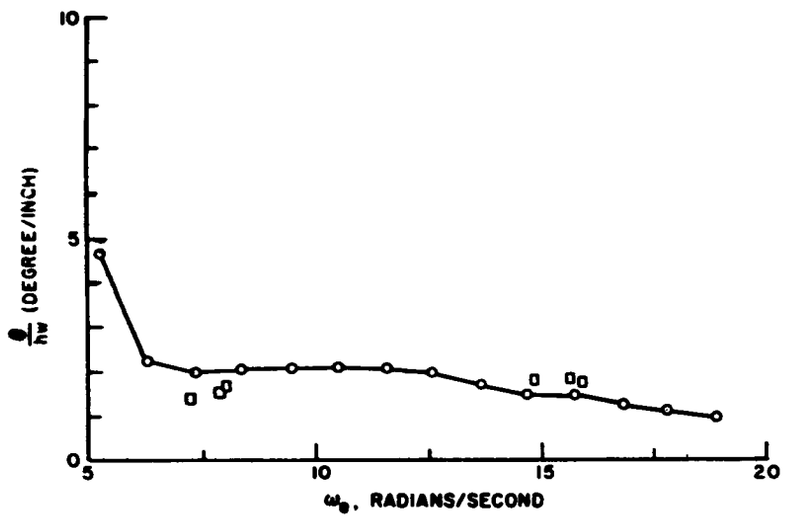

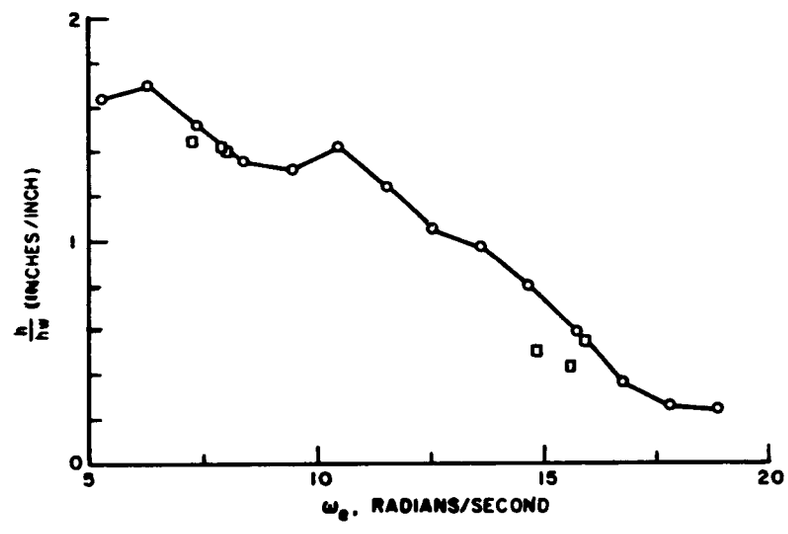

FIGURE 21. PITCH AND HEAVE TRANSFER FUNCTIONS, h_e = 0.50", SPRING RATE 2.87 IN-POUNDS/DEGREE V = 10.58 fps (SEA STATE 3

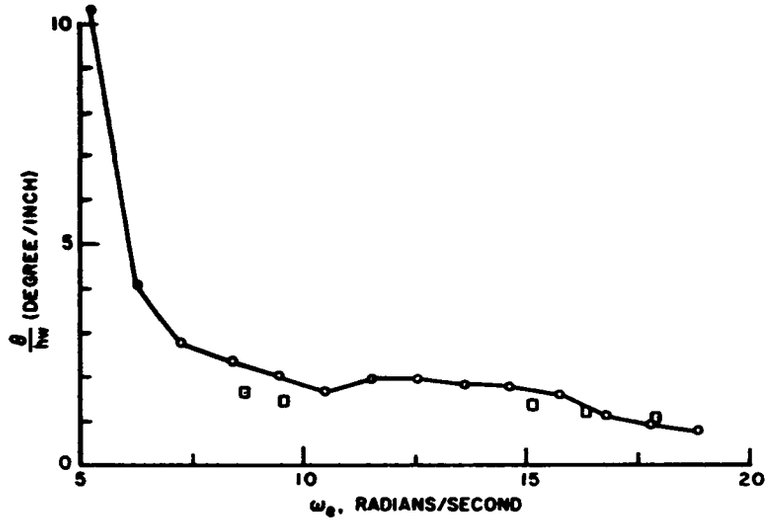

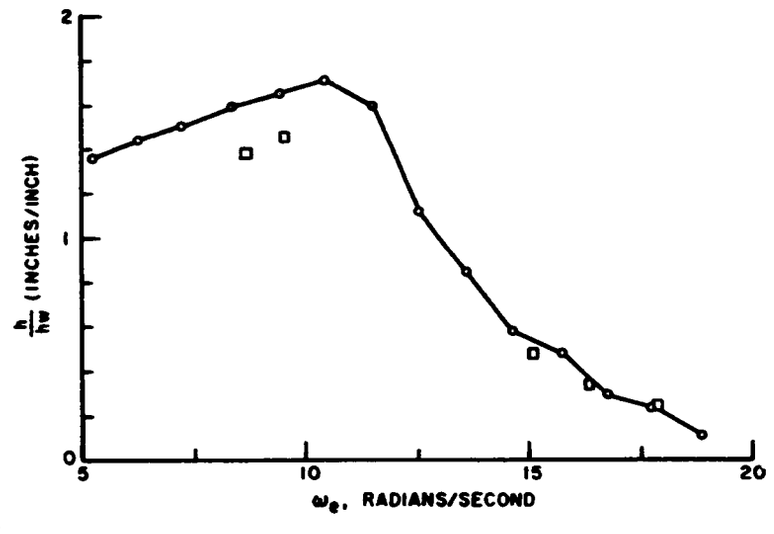

FIGURE 22. PITCH AND HEAVE TRANSFER FUNCTIONS, h_e = 0.50", NO SPRING, V= 10.81 fps (SEA STATE 3)

RESEARCH ON SHIP CONTROLLABILITY
(Steering Characteristics of a Cargo Ship)

Haruzo Eda
Visiting Research Engineer
and
C. Lincoln Crane
Associate Research Engineer
Davidson Laboratory

I. INTRODUCTION

An investigation of the steering characteristics of a high-speed cargo ship was performed as part of a broad study to improve merchant ship steering and maneuvering qualities.

The Series 60 was selected as a typical cargo ship model for this research. At David Taylor Model Basin, Davidson Laboratory and other model basins, this hull form was tested to determine such characteristics as resistance, propulsion, and motions in various seas, including oblique headings. These accumulated data would be quite useful for further tests of the model for research into the controllability of ships at sea.

The experiments consisted of rotating arm tests and free-turning tests of a five-foot model in Tank No. 2 of Davidson Laboratory.

An analysis, based on derivatives of hydrodynamic forces and moments acting on the model, was made to examine the steering characteristics of the ship in calm water. The predicted motions based on the rotating arm test results were compared with the free-turning test results to check the feasibility of using the linear equations of motion for further predictions of steering qualities. The comparisons indicate that the linear calculation would be quite useful in predicting lateral motions provided the rudder angle is not large. Based on these observations, techniques of frequency response and harmonic analysis were employed in the calculation of yaw response. Zig-zag maneuvers are predicted through applying these techniques and using the force and moment derivatives obtained in the rotating arm tests. Ship speed

reduction due to yaw and sway is also predicted from rotating arm test results and compared with free-turning test results.

This study was sponsored by the Maritime Administration, Department of Commerce, Contract No. MA 2701, T/O 1.

II. TEST PROCEDURE

A. Characteristics of the Model

TABLE I.
PRINCIPAL CHARACTERISTICS OF THE SERIES 60 MODEL

Length BP, L	5.00 ft
Breadth, B	0.667 ft
Draft, H	0.267 ft
L/B	7.5
B/H	2.5
L/H	18.8
Block Coefficient, C_b	0.60
Displacement (FW), Δ	33.27 lbs
LxH	1.335 ft^2
Lateral Area of Hull	1.320 ft^2
Lateral Area of Rudder	0.0210 ft^2
Aspect Ratio of Rudder	1.91
Mass of Model, M	1.03 slugs
CG aft of FP/L	0.515
Rudder Post aft of CG/L	0.485
Radius of Gyration in Air, kL	0.255L

The size and shape of the rudder were chosen to represent a typical design for a cargo ship. Rudder area expressed as a ratio to profile area is 1.6%, and has an aspect ratio of 1.91. The maximum thickness ratio of the rudder is 16.7% of the chord length, and it occurs at 35% of the chord aft of the leading edge.[1]

The diameter of the propeller is 0.187 ft and the pitch ratio is 0.945.

B. Rotating Arm Tests. The model was constrained in a given yaw attitude at radii between 12 and 32 ft under the rotating arm in Tank No. 2 of Davidson Laboratory (see ref. 2 for description of the test facilities). A flexure plate, permitting freedom in pitch and heave, was used to fix the model to a "balance beam" under the arm. The balance beam is a three-component dynamometer of the differential transformer type, which measures lateral forces at two points along length of the model, and the drag force. Outputs of the dynamometer were recorded on an oscillograph recorder located ashore. A two-component rudder dynamometer, also of the differential transformer type, was newly built and used for these tests.

During tests of the model with propeller, the propeller revolutions were adjusted to obtain a zero drag condition at a predetermined model speed. Figure 1 shows the model being tested under the rotating arm.

C. Free-Turning Tests. The model was propelled by a DC motor and was battery powered. A steering engine was programmed to lay the rudder to a predetermined angle after a certain number of propeller revolutions.

Test runs were made in semi-darkness, with the position of the model recorded by a camera fixed to a catwalk above the maneuvering area. The camera shutter was alternately opened and closed at half second intervals, providing a measure of time on the film. Miniature lights were fixed at the model's forward and after perpendiculars. A third light, located off the model's centerline, was extinguished to indicate the position of the model at the time when the rudder was laid.

Model path, speed, and drift angle were obtained by direct measurements of the light traces on the 14x11 in. photographic plate.

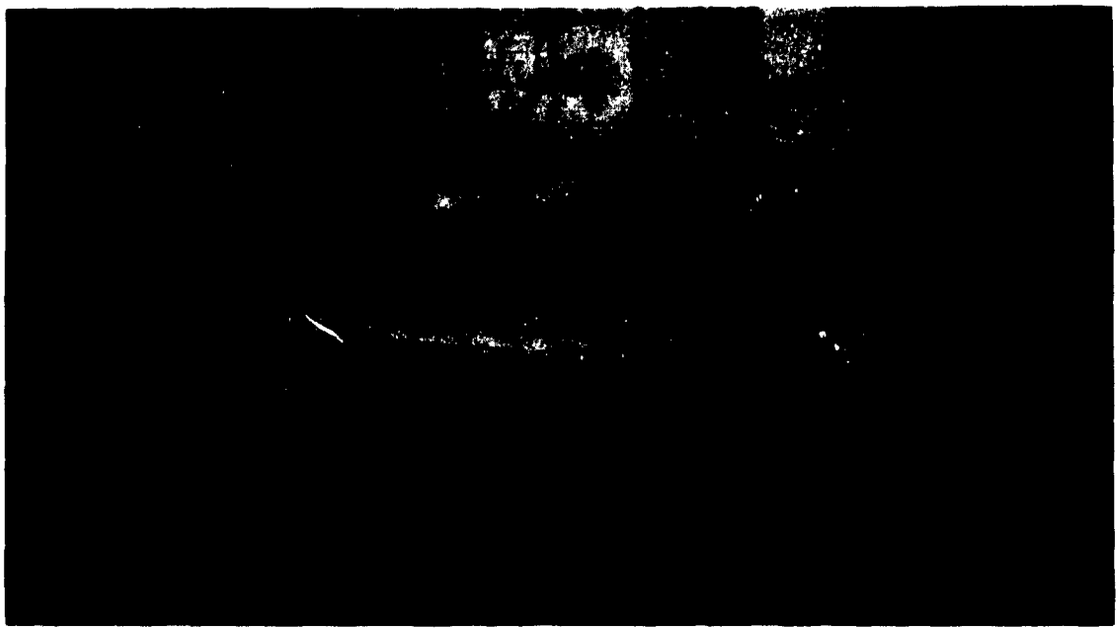

SERIES 60 (C_b = 0.60) MODEL BEING TESTED ON ROTATING ARM

FIGURE 1.

III. EXPERIMENTAL RESULTS

A total of approximately 250 runs in the rotating arm tests and about 60 runs in the free-turning tests were carried out, with various parameters changed. However, results described here will be limited to the most standard condition, i.e., the full load (even keel) condition, with propeller and rudder, at a speed of 2.5 ft/sec (Froude No. = 0.20).

Forces acting on the model were obtained by a three-component dynamometer at the rotating arm basin. Data were then corrected for inertia forces due to rotation.

Hydrodynamic force coefficients were derived from test data using the formulae in refs. 3 and 4 (see also Fig. 2).

$$Y' = \frac{Y_m}{1/2\rho LHV^2} + \frac{M(1+k_1)}{1/2\rho LH}\frac{\cos\beta}{R}$$

$$N' = \frac{N_m}{1/2\rho L^2HV^2}$$

where X_m, Y_m, N_m = measured forces (longitudinal and lateral) and yawing moment, respectively.

β = drift angle
M = mass of the ship
ρ = density of water
L = length of the ship
H = draft of the ship
V = speed of the ship
k_1 = longitudinal coefficient of accession of inertia
R = radius of turning path

Forces and moments on a hull proceeding on straight path, but having drift angle, were obtained by interpolation of the rotating arm test data.

Experimental results from rotating arm tests are presented in Figs. 2 through 7.

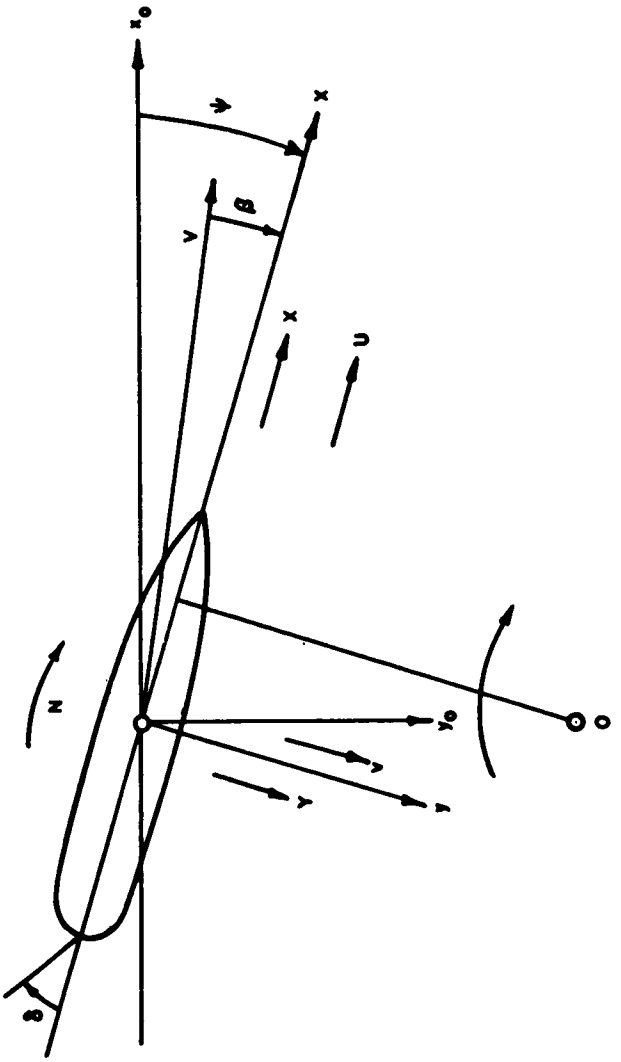

FIGURE 2. ORIENTATION OF MOMENTS AND FORCES IN THE HORIZONTAL PLANE WITH RESPECT TO FIXED BODY AXES

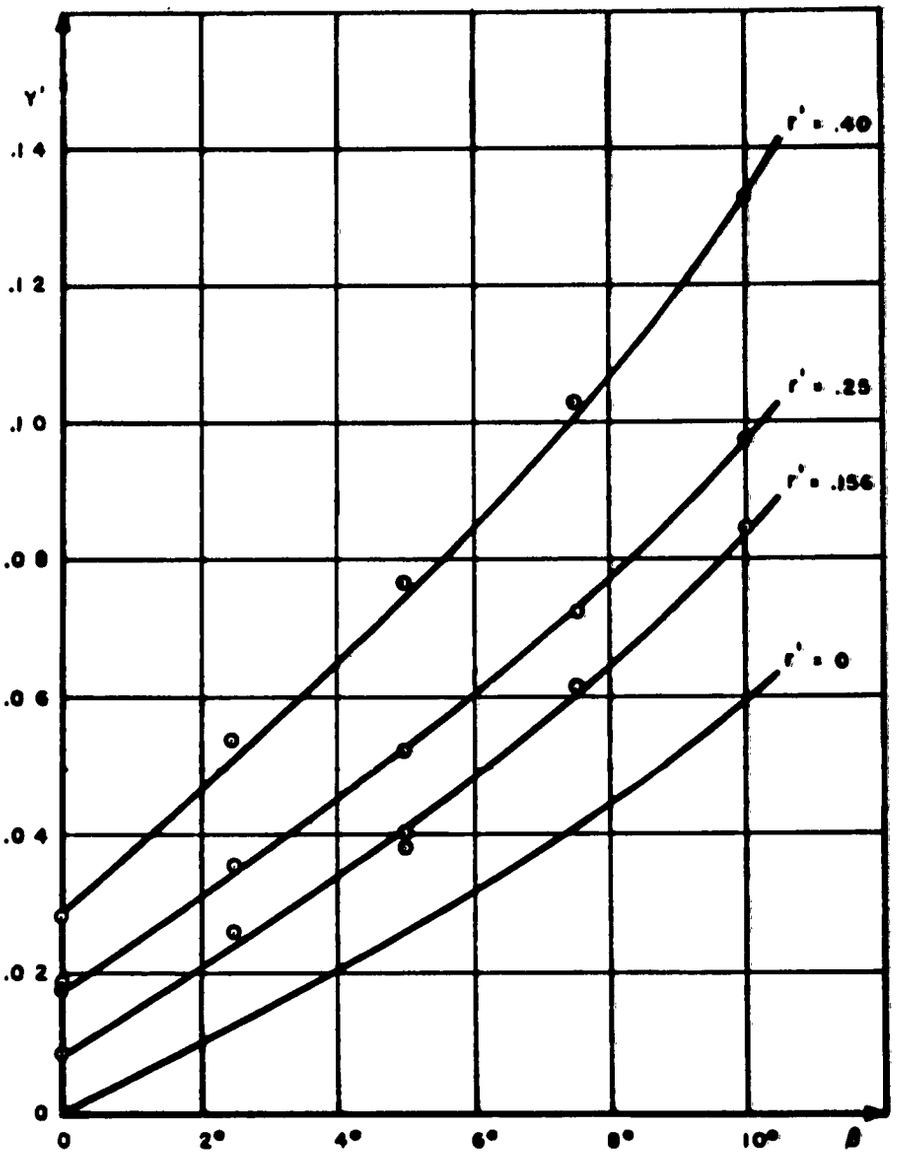

FIGURE 3. Y' VERSUS β (WITH PROPELLER AND RUDDER)

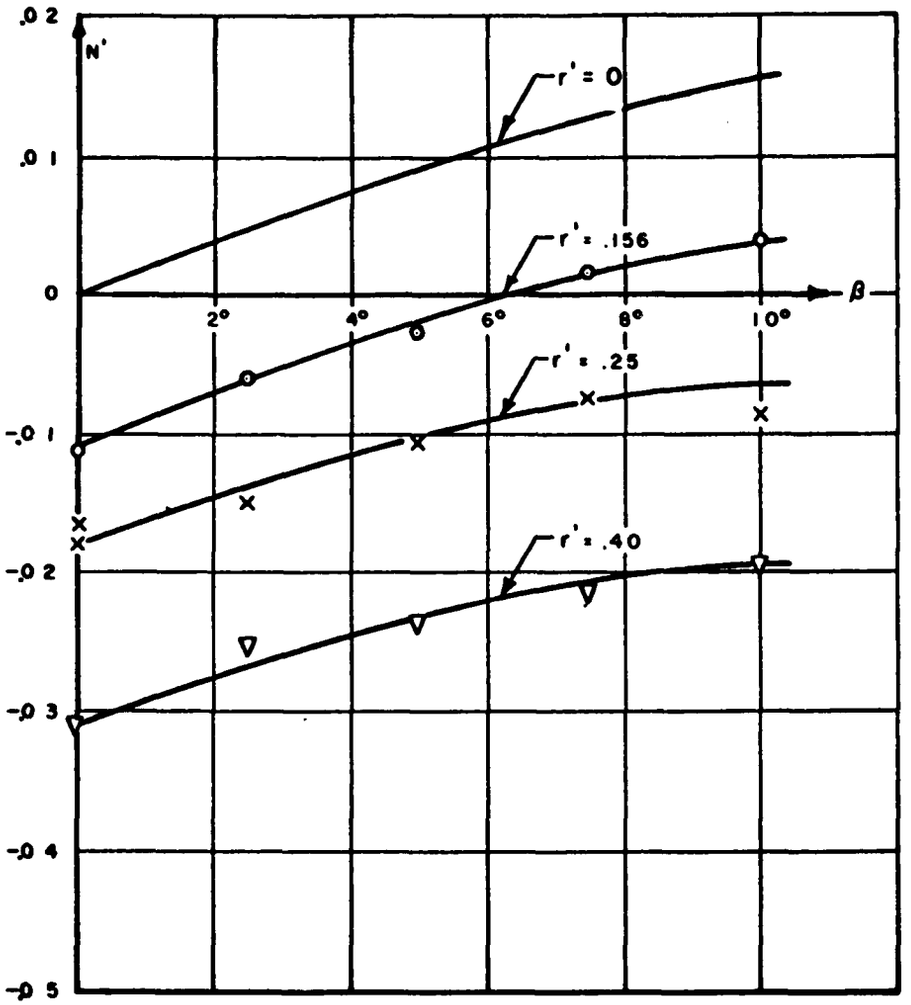

FIGURE 4. N' VERSUS β (WITH PROPELLER AND RUDDER)

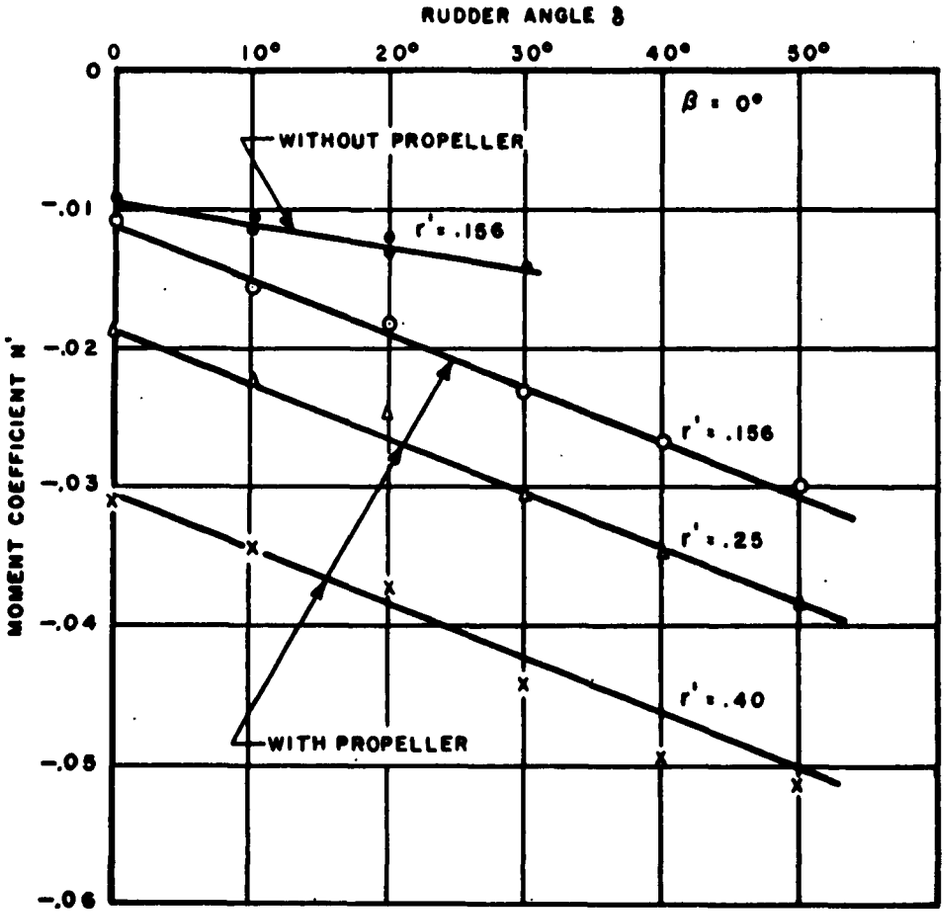

FIGURE 5. MOMENT COEFFICIENT VERSUS RUDDER ANGLE

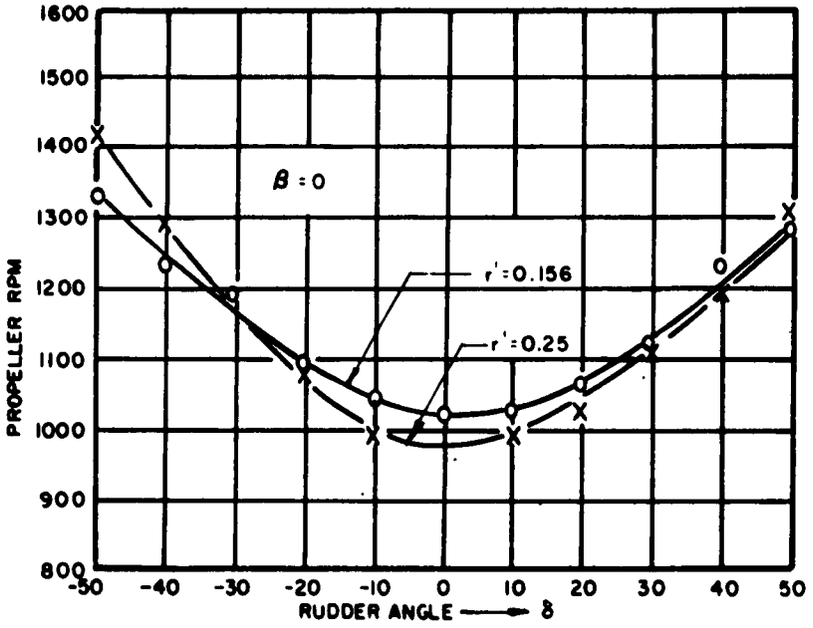

FIGURE 6 VARIATION OF PROPELLER RPM VERSUS RUDDER ANGLE

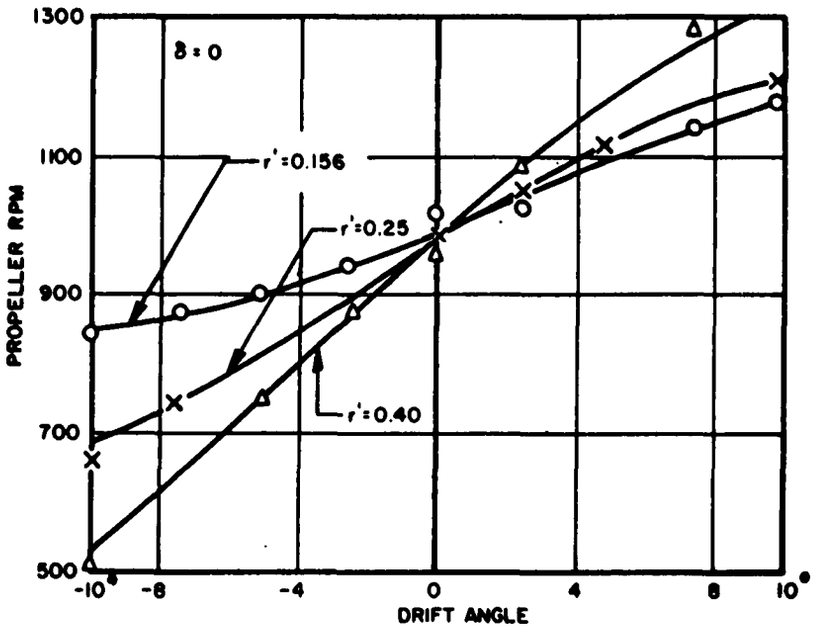

FIGURE 7. VARIATION OF PROPELLER RPM VERSUS DRIFT ANGLE

IV. EVALUATION OF STABILITY INDEX AND TURNING ABILITY

A. Equations of Lateral Motion. The linear equations of lateral motion (Fig. 2 and ref. 5) can be written as:

$$-m_y\dot{\beta} + (m_x - Y_r)\dot{\psi} - Y_\beta\beta = Y_\delta\delta \text{ (sway)} \quad (1)$$

$$n_z\ddot{\psi} - N_\beta\beta - N_r\dot{\psi} = N_\delta\delta \text{ (yaw)} \quad (2)$$

where ψ = yaw angle, β = drift angle

$\dot{\psi} = d\psi/ds$, $\dot{\beta} = \frac{d\beta}{ds}$, s = space time

$m_x = \frac{M + M_x}{1/2\rho L^2 H}$, M_x = added mass in longitudinal direction

$m_y = \frac{M + M_y}{1/2\rho L^2 H}$, M_y = added mass in lateral direction

$n_z = \frac{I_z + J_z}{1/2\rho L^4 H}$, I_z = moment inertia of the ship about z-axis

J_z = added moment of inertia of the ship about z-axis

Y_β = static derivative of lateral force = $\frac{\partial Y'}{\partial \beta}$

Y_r = rotary derivative of lateral force = $\frac{\partial Y'}{\partial r'}$

N_β = static derivative of moment = $\frac{\partial N'}{\partial \beta}$

N_r = rotary derivative of moment = $\frac{\partial N'}{\partial r'}$

Y_δ = rudder force derivative = $\frac{\partial Y'}{\partial \delta}$, δ = rudder angle

N_δ = rudder moment derivative = $\frac{\partial N'}{\partial \delta}$

Added mass in the lateral direction and added moment of inertia about the z-axis in the equations of motion were determined by a strip theory following the computations of Lewis and Prohaska. The results were then corrected for three-dimensional effect.

$$k_2 = \frac{M_y}{M} = \frac{\frac{1}{2}\int_{x_b}^{x_s} C_s(x)\pi H^2 dx}{\int_{x_b}^{x_s} A_s(x)\,dx} \times k_c$$

where k_2 = lateral coefficient of accession to inertia

$C_s(x)$ = two dimensional lateral added mass coefficient (sectional inertia coefficient). This was determined for ship-like sections by Lewis' method.[6]

$A_s(x)$ = sectional area

x_s, x_b = x-coordinate of stern and bow, respectively, from CG

k_c = three dimensional correction factor. This was determined from the three-dimensional correction for the prolated spheroid by comparing the added mass obtained from the exact calculation and the strip method.

This procedure leads to larger values of added inertia coefficient than is determined by analogy with the prolated spheroid. The larger values appear quite reasonable for the ship form in view of the following: 1) nearly constant draft in the longitudinal direction; 2) ratio of breadth to depth at both bow and stern much less than that at amidships.

The virtual mass coefficient in the longitudinal direction was considered equivalent to that of the prolate spheroid, which is given by Lamb as a function of the ratio of minor to major axes.

The inertia coefficients determined for the Series 60 model are as follows:

$m_x = 0.160$

$m_y = 0.326$

$n_z = 0.0215$

The values of the force and moment derivatives obtained from rotating arm test results for the full load condition

(even keel) with rudder and propeller are as follows:

$$Y'_\beta = \frac{\partial Y'}{\partial \beta} = 0.290$$

$$Y'_r = \frac{\partial Y'}{\partial r'} = 0.067$$

$$N'_\beta = \frac{\partial N'}{\partial \beta} = 0.100$$

$$N'_r = \frac{\partial N'}{\partial r'} = -0.074$$

$$Y'_\delta = \frac{\partial Y'}{\partial \delta} = 0.046$$

$$N'_\delta = \frac{\partial N'}{\partial \delta} = -0.022$$

Using these derivatives the dynamic stability on course and the turning ability of the Series 60 ($C_b = 0.60$) can be determined.

B. Dynamic Stability. Eliminating β from eqs. 1 and 2,

$$m_y n_z \dddot{\psi} + (Y_\beta n_z - N_r m_y)\ddot{\psi} + (-m N_\beta - N_r Y_\beta)\dot{\psi} = m_y N_\delta \dot{\delta} + (Y_\beta N_\delta - N_\beta Y_\delta)\delta \qquad (3)$$

If we take $\delta = o$ in discussing the dynamic stability of a ship, eq. 3 becomes the homogeneous differential equation. The solution for this homogeneous differential equation is:

$$\dot{\psi} = \dot{\psi}_1 e^{\sigma_1 s} + \dot{\psi}_2 e^{\sigma_2 s} \qquad (4)$$

where $\dot{\psi}_1$, $\dot{\psi}_2$ are constants.

When σ_1, $\sigma_2 < 0$, the ship is dynamically stable. $\sigma_{1,2}$ can be obtained as follows:

$$\sigma_{1,2} = \frac{-(n_z Y_\beta - m_y N_r) \pm \sqrt{(n_z Y_\beta - m_y N_r)^2 + 4 m_y n_z (Y_\beta N_r + m N_\beta)}}{2 n_z m_y} \qquad (5)$$

For the Series 60 ($C_b = 0.60$) model, σ_1 and σ_2 were evaluated from rotating arm test data as follows:

$$\sigma_{1,2} = -.447, -3.88$$

C. Turning Rate. The turning rate in steady turning for a certain magnitude of rudder angle can be obtained from eq. 3, with $\ddot{\psi} = \dot{\psi} = \dot{\delta} = 0$

$$\frac{\dot{\psi}}{\delta} = \frac{Y_\delta N_\beta - N_\delta Y_\beta}{Y_\beta N_r + m N_\beta} \tag{6}$$

Substituting the values of derivatives experimentally obtained, we get

$$\dot{\psi}/\delta = -0.90$$

Data are available for comparing turning and course keeping qualities.[7,8,9,10] An example is shown in Fig. 8. The above values of σ_1 and $\frac{\dot{\psi}}{\delta}$ lead to the conclusion that the series 60 ($C_b = 0.60$), with a rudder of typical size (relative rudder area ratio to the underwater profile = 1.62%), possesses sufficient dynamic stability, but somewhat less than average turning ability.

D. Comparison of Rotating Arm and Free-Turning Tests. The relationship existing between turning rate and rudder angle was evaluated from rotating arm test data and compared with data of the free-running model tests. The straight dashed line in Fig. 9 shows the linear prediction based on rotating arm test data (eq. 6). Good agreement is seen to exist for rudder angles less than 10 degrees. It is also apparent that a nonlinear term should be taken into account when the rudder angle is greater than 10 degrees. This can be done without difficulty by using a graphical method[7] or a computer.

The linear prediction was made to compare trimmed condition data obtained by free-turning tests. The derivatives for the trimmed condition (1.8% trim by stern) were interpolated from trimmed condition data obtained at rotating arm tests.

Predicted turning rate is obtained from eq. 6:

$$\frac{\dot{\psi}}{\delta} = -0.58$$

Figure 10 shows the free-turning test data for 1.8% trim by the stern. The fair curve of the data coincides almost exactly with the linear prediction. One curve, therefore, represents both experimental data and prediction. It can be said that the more dynamically stable the ship, the better is the linear prediction. In the same figure the data of the

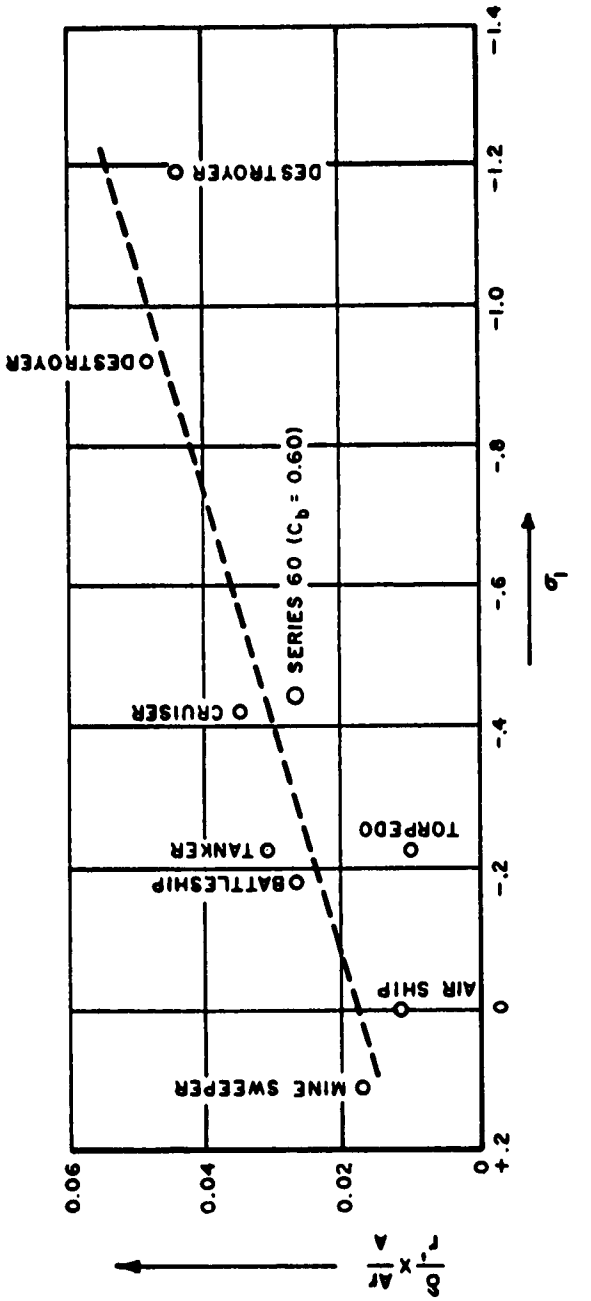

FIGURE 8. COMPARISON OF STABILITY AND TURNING ABILITY AMONG VARIOUS SHIPS

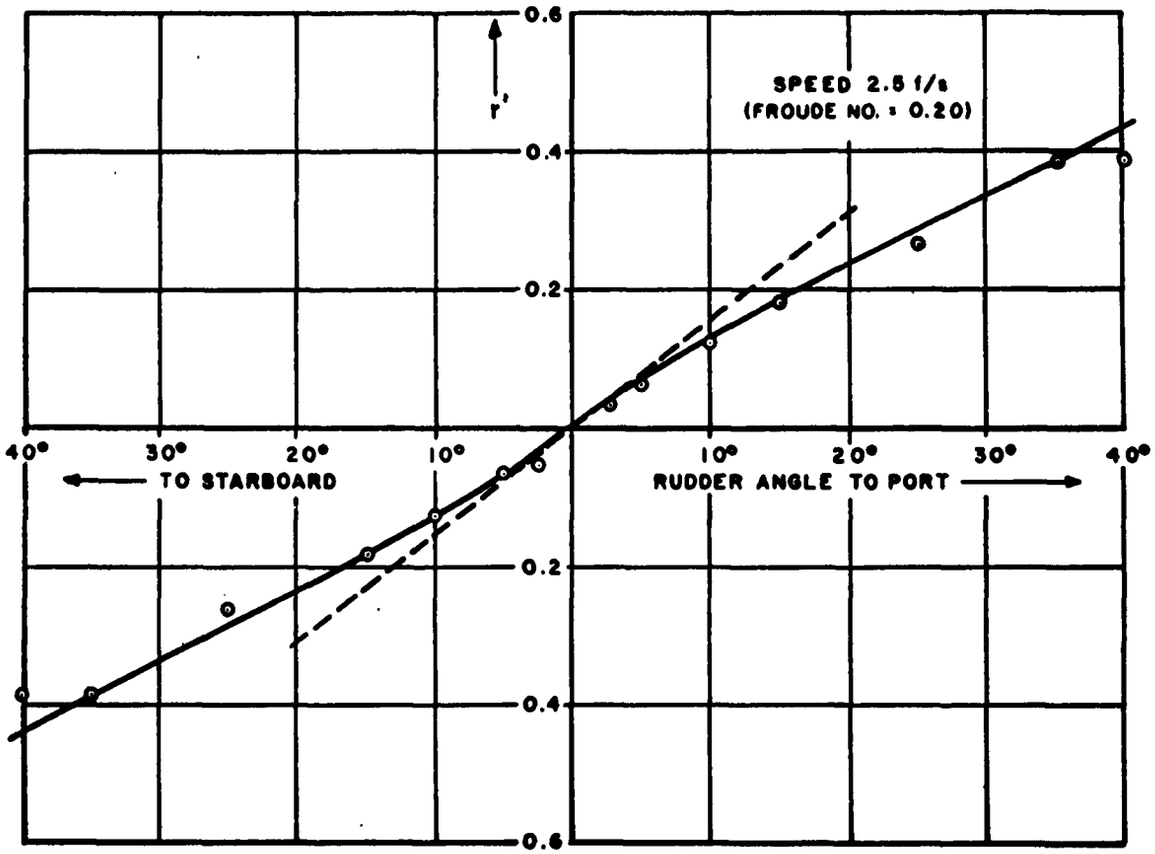

FIGURE 9. TURNING RATE VERSUS RUDDER ANGLE

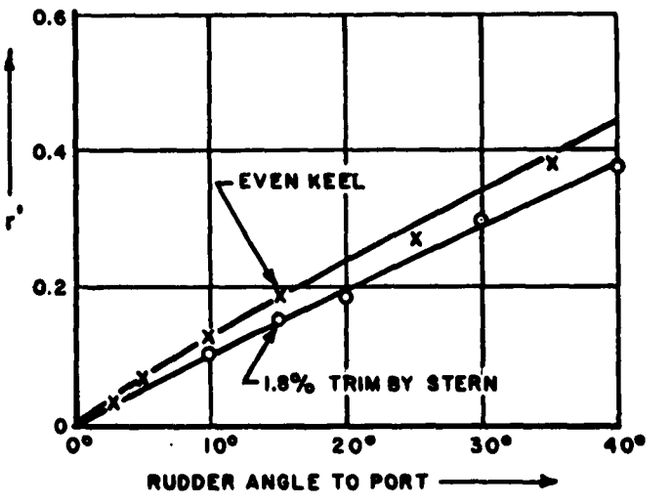

FIGUR E 10. EFFECT OF TRIM ON TURNING

even keel condition are shown for comparison with the trimmed condition. It is seen in the figure that a small trim by the stern induces a large change in the steering quality.

The characteristics of calculated drift angle are quite similar to those of turning rate, and the comparison made between linear prediction and free-turning tests shows the same tendency in Fig. 11.

These comparisons indicate that the linear calculation would be quite useful for the evaluation of lateral motion due to rudder activity provided that the rudder angle is not large. Based on this observation the lateral motion behavior of the Series 60 is computed and discussed in a later section.

V. SHIP RESPONSE DUE TO RUDDER ACTIVITY

It has been shown in the previous section that linear calculations can predict lateral motions adequately when rudder angles are not large. Based on this observation it is possible to evaluate the lateral motions resulting from arbitrary rudder motions by employing the eight coefficients obtained in previous sections in the linear equations of yaw and sway.

The response of a system to an arbitrary input can be determined by a technique based on harmonic analysis or the convolution integral.

Frequency response of the yaw motion of the Series 60 model, the dynamically stable ship, was calculated from available data on the forces and moments acting on the hull and on the rudder. This was done to provide a clear basis for discussing steering characteristics in terms of ship performance.

Rudder motion is specified by

$$\delta(s) = \delta \sin \omega_s \qquad (7)$$

where ω = circular frequency of rudder motion

s = space time

Substituting eq. 7 into the equation of yaw (eq. 3), we obtain

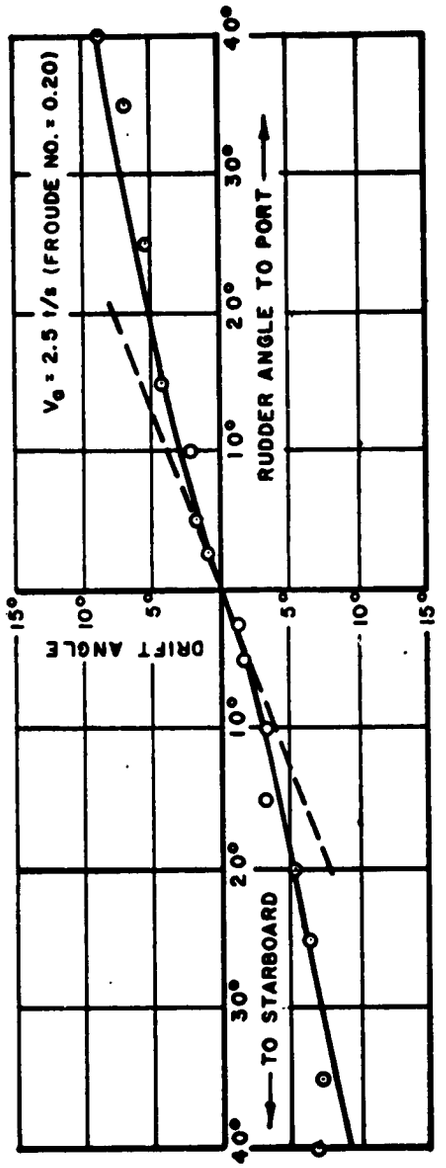

FIGURE 11. DRIFT ANGLE VERSUS RUDDER ANGLE

$$m_y n_z \dddot{\psi} + (Y_\beta n_z - N_r m_y)\ddot{\psi} + (-mN_\beta - N_r Y_\beta)\dot{\psi} \tag{8}$$

$$= \delta\sqrt{(Y_\beta N_\delta - N_\beta Y_\delta)^2 + (m_y N_\delta \omega)^2}\ \sin(\omega_s + \alpha_1)$$

where $\alpha_1 = \tan^{-1} \dfrac{m_y N_\delta \omega}{Y_\beta N_\delta - N_\beta Y_\delta}$

The solution of eq. 8 can be written in the following familiar form:

$$\dot{\psi} = d_s\ \mu\ \sin(\omega_s - \alpha) \tag{9}$$

where

d_s = static deflection = $\dfrac{d_m}{-mN_\beta - N_r Y_\beta}$

μ = magnification factor = $\dfrac{1}{\sqrt{\left[1-(\frac{\omega}{\omega_n})^2\right]^2 + \left[2(\frac{\omega}{\omega_n})(\frac{c}{c_c})\right]^2}}$

ω_n = natural frequency (undamped) = $\sqrt{\dfrac{-mN_\beta - N_r Y_\beta}{m_y n_z}}$

c = damping = $Y_\beta n_z - N_r m_y$

c_c = critical damping = $2\sqrt{m_y n_z(-mN_\beta - N_r Y_\beta)}$

α = phase lag = $\alpha_2 - \alpha_1$, $\quad \alpha_2 = \tan^{-1} \dfrac{2(\frac{c}{c_n})(\frac{\omega}{\omega_n})}{1 - (\frac{\omega}{\omega_n})^2}$

The yaw angle response is obtained from eq. 9

$$\psi = \frac{d_s}{\omega} \sin\left[\ \omega_s - (\alpha + 90^\circ)\ \right] \tag{10}$$

The responses of yaw for each of three different trim conditions, including even keel, are shown in the vector locus diagram (Fig. 11).

The vector locus diagram shows the relationship between the input (rudder angle) and the output (yaw response) on a frequency base.

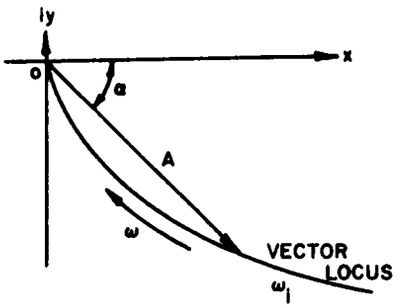

In the figure, Vector A represents the response at frequency = ω_1.

A = amplitude ratio of response to input (ψ/δ or ψ/δ)

α = phase lag

Yaw response due to an arbitrary motion of the rudder can be obtained by combining the techniques of harmonic analysis and frequency response.

The rudder motion $\delta(s)$, with a period of T (in space time), can be represented as follows:

$$\delta(s) = \frac{1}{2}A_o + \sum_{n=1}^{\infty} A_n \cos\frac{2\pi n}{T}s + \sum_{n=1}^{\infty} B_n \sin\frac{2\pi n}{T}s \qquad (11)$$

where

$$A_o = \frac{2}{T}\int_o^T \delta(s)ds$$

$$A_n = \frac{2}{T}\int_o^T \delta(s)\cos\frac{2\pi n}{T}sds$$

$$B_n = \frac{2}{T}\int_o^T \delta(s)\sin\frac{2\pi n}{T}sds$$

The computations of the harmonic analysis were carried out by the IBM 1620 digital computer of Stevens Institute of Technology.

In the analysis of zig-zag tests, the iterative method was employed to determine the value of period T (in space time), whereas T is determined automatically in the process of the full-size zig-zag maneuvers.

A_n and B_n for yaw responses (ψ and $\dot{\psi}$) due to the Nth component of rudder motion were determined directly from frequency response results.

Results are presented in the form of a vector locus diagram for all three trim conditions in Fig. 12. The response at any particular frequency value is represented by the vector connecting the origin with the point associated with that frequency on the vector locus. The middle curve of Fig. 12 represents the even keel condition, the inside curve the condition of 3% trim by stern, and the outside curve the condition of 2% trim by the bow. It should be noted that a 2 or 3% change in trim induces a large difference in response. This tendency agrees with results obtained during free-turning tests, as are shown in Fig. 9.

During full-size ship trials a zig-zag test is often carried out to determine the steering characteristics of the ship. In this way a considerable amount of full-size test data[8] has become available for examination. It is therefore desirable to correlate the rotating arm tests with the zig-zag test data.

Predicted response of the Series 60 ($C_b = 0.60$) to the zig-zag rudder sequence was calculated using a harmonic analysis. In Fig. 13 the zig-zag movement of the rudder and the calculated yaw response (yaw angle and yaw rate) of the ship are shown. The dashed lines represent the fundamental components of the response. It is seen that the fundamental components of yaw angle response represent the behavior fairly well except for some differences in the regions where the rudder is shifted to the opposite side. Accordingly, the fundamental component is not considered sufficient for evaluation of the zig-zag response, although it gives the general tendency.

In order to make clear the effect of trim, the response of the ship was calculated for three different trim conditions. In Fig. 14 one cycle of the steady response of the zig-zag test is shown. Trim by the stern, which is consistent with greater dynamic stability, has the smallest response amplitude. Trim by the bow, on the other hand, results in greater tendency to overshoot because of reduced dynamic stability.

Yaw response induced by rudder motion has been described above. Exactly the same technique can be applied in a treatment of yawing motion due to waves, although certain problems such as the evaluation of the coupling terms, damping terms, and wave excitation in the equations of motion should be further investigated first.

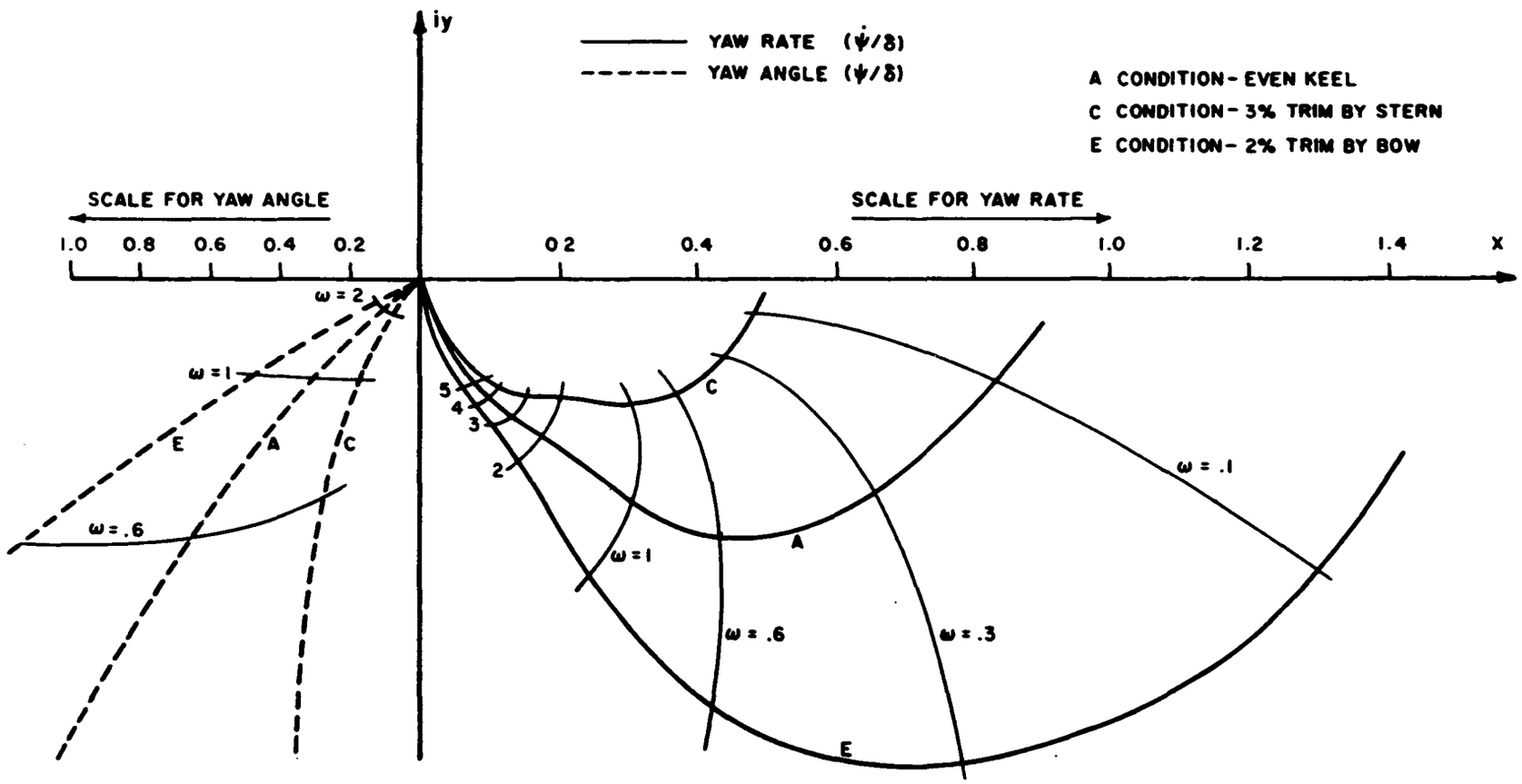

FIGURE 12. VECTOR LOCUS DIAGRAM OF YAW RESPONSE

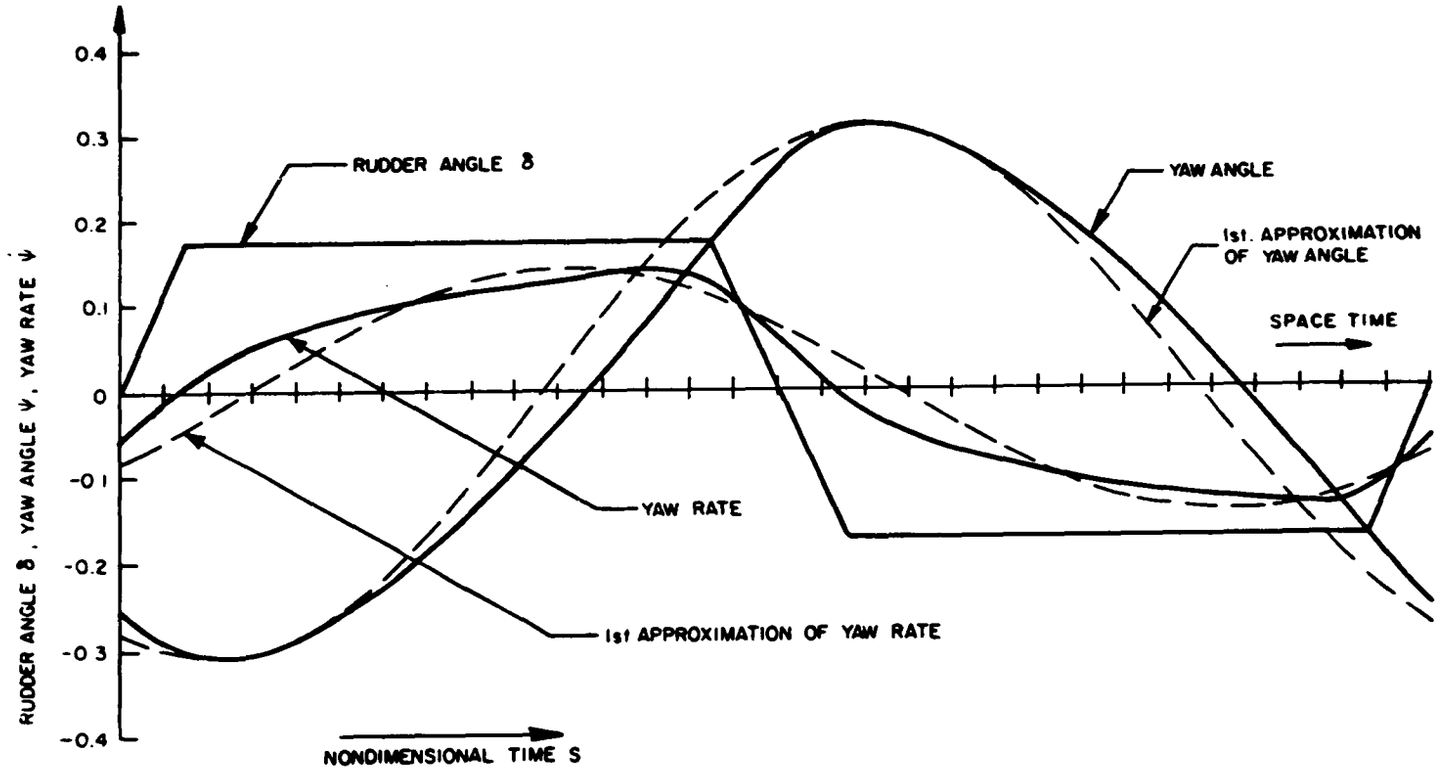

FIGURE 13. RESPONSE OF ZIG-ZAG TEST (CALCULATED)

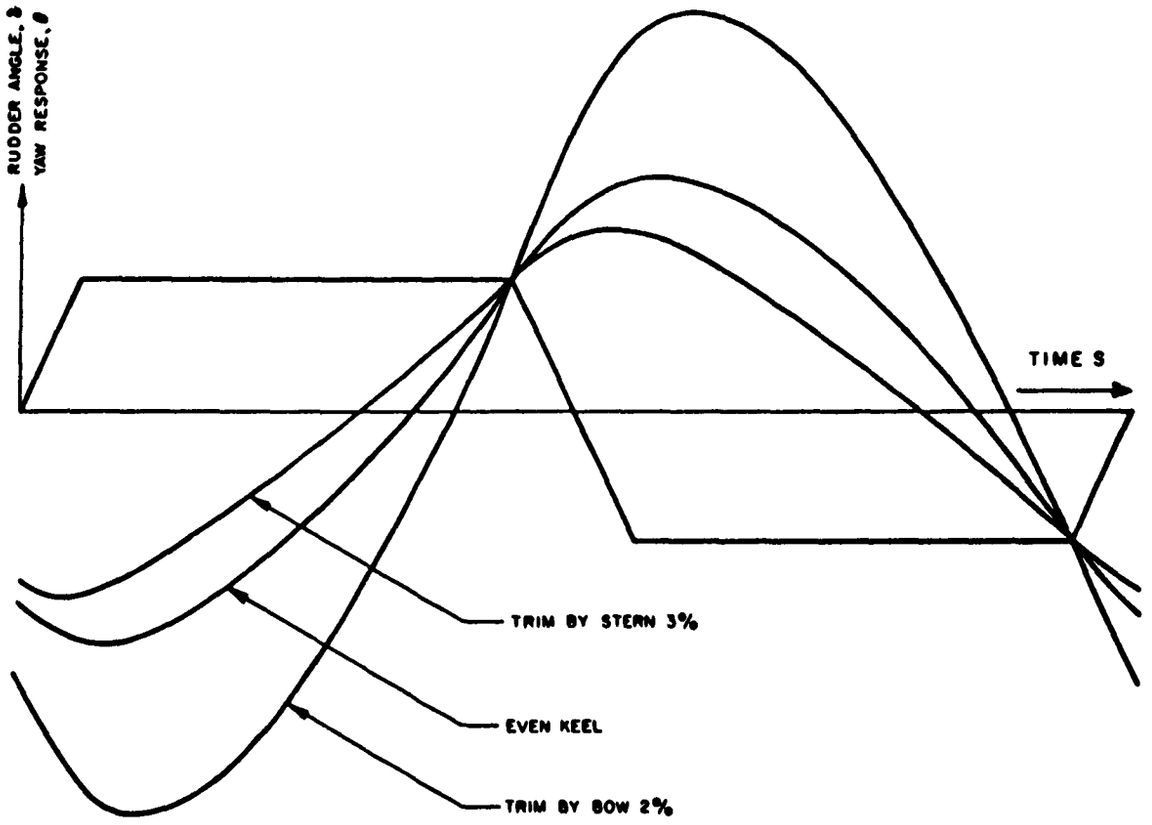

FIGURE 14. EFFECT OF TRIM ON THE RESPONSE OF ZIG-ZAG TEST (ONE CYCLE OF STEADY STATE)

VI. SPEED REDUCTION DUE TO YAW AND SWAY

Reduction of speed due to yaw and sway was found to be of significant magnitude in the free-turning tests.

In the procedure of the rotating arm tests made with propeller, propeller revolutions in each case were adjusted to achieve the zero drag condition.

Since thrust coefficient is quite linear for a wide range of advance constants, the increased resistance could be evaluated from the data on propeller revolutions which were obtained.

One of the dominant factors of speed reduction is that due to rudder angle. Variation of propeller revolutions is plotted against rudder angle for three rotating arm radii in Fig. 6. From these data the ratio of increased resistance to the total resistance was obtained. Figure 15 shows the ratio of increased resistance plotted against rudder angle.

Drift angle is another important factor of speed reduction. Variations of propeller revolutions versus drift angle are shown in three curves for different turning rates in Fig. 7. If increased resistance in turning is plotted with relation to the product $r\beta$, the data from the three curves of Fig. 7 will define a single straight line as shown in Fig. 16. This establishes a relation, i.e., that increased resistance in the longitudinal direction due to yaw and sway, is approximately proportional to the product $r\beta$. This relation can be interpreted as the longitudinal component of the total centrifugal force due to turning.

For the range of speeds of the present tests, the total resistance of the model can be considered proportional to the square of the advance speed.[11]

Assuming the thrust given to the ship is constant, we obtain the following simple relationship for speed reduction (provided the reduction in speed is not large):

$$\frac{R_o - \left[\Delta R_\delta(\delta) + \Delta R_{r\beta}(r,\beta)\right]}{R_o} = \left(\frac{V}{V_o}\right)^2 \qquad (12)$$

where V_o = initial speed

V = reduced speed

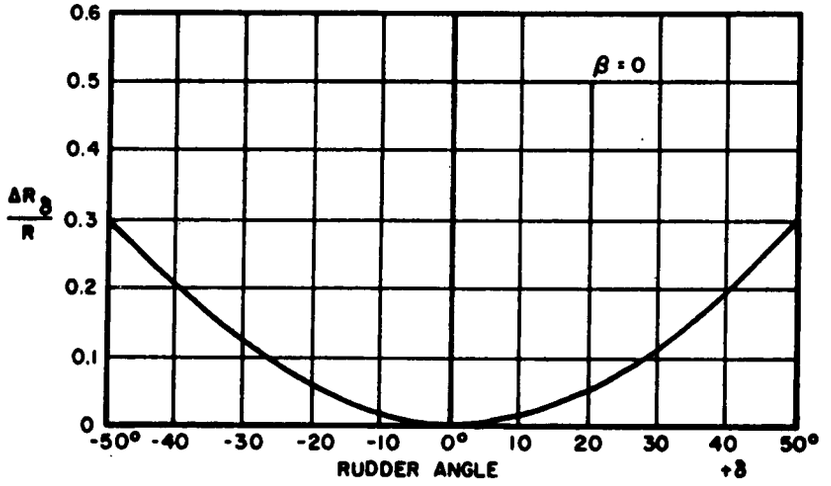

FIGURE 15. INCREASED RESISTANCE DUE TO RUDDER ANGLE

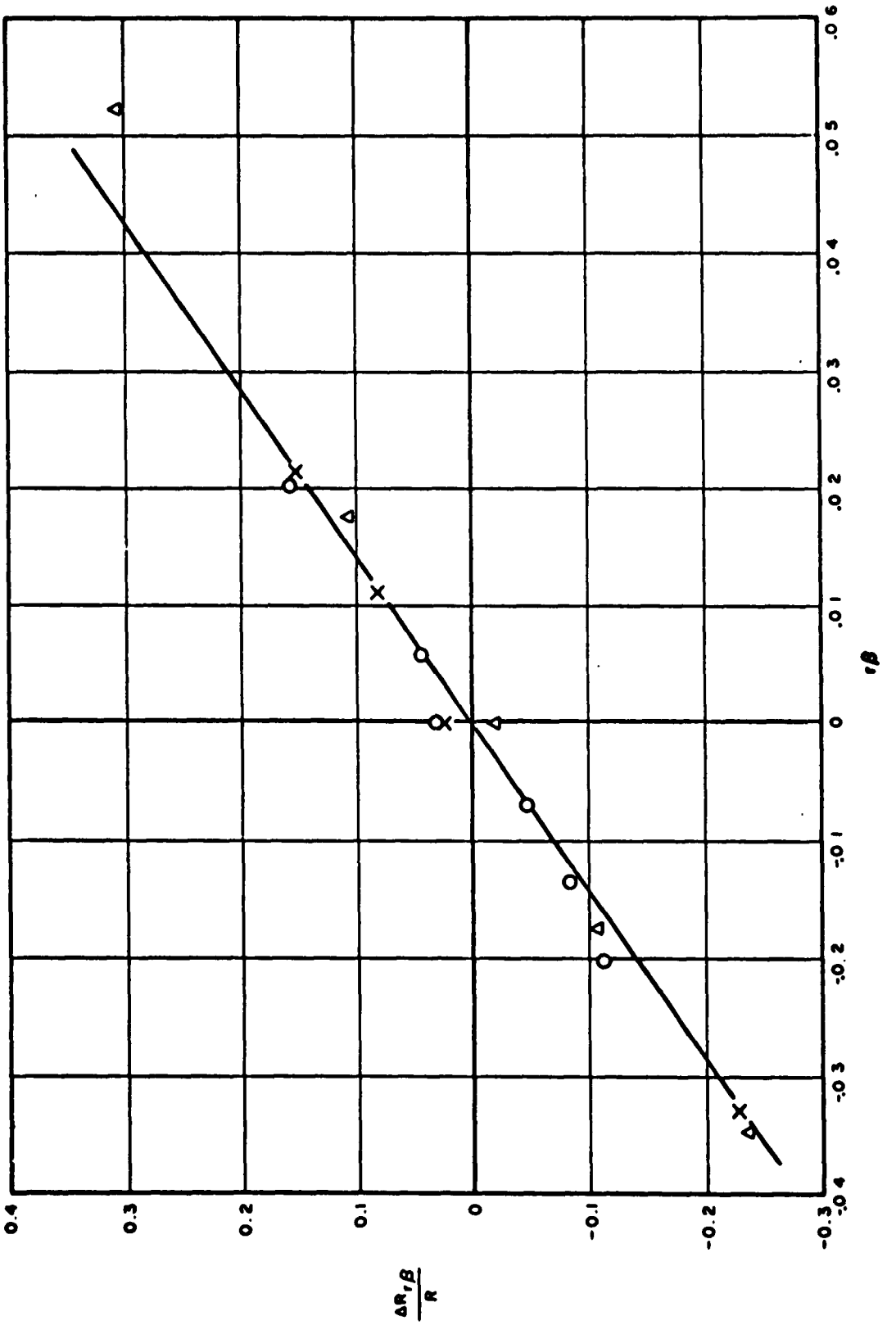

FIGURE 16 INCREASED RESISTANCE DUE TO OBJECT ANGLE AND TURNING RATE

R_o = initial resistance

$\Delta R_\delta(\delta)$ = increased resistance due to rudder angle (Fig. 15)

$\Delta R_{r\beta}(r,\beta)$ = increased resistance due to yaw and sway (Fig. 16)

Based on these relations speed reduction for the free-turning tests was evaluated and compared with actual test results. Fairly good agreement is apparent in Fig. 17. Slight differences appear at large turning rates. This accounts for the existence of other factors causing speed reduction. The comparison in Fig. 17 shows, however, that other factors present are small enough to be neglected except at large turning rates. The above-mentioned relationships bearing on speed reduction are believed to form a reasonable basis for evaluating the speed loss of a ship due to steering action for course keeping in waves. It is expected that further research will determine some relationship between speed loss in waves and steering characteristics such as the dynamic stability index of ships.

VII. CONCLUSIONS

1. Predictions of lateral motion using linear theory indicate satisfactory agreement with experimental results for rudder angles less than approximately 10^o. Yaw and sway within this range can be satisfactorily treated as linear motions. From these observations it is concluded that linear treatments of lateral motions will give reasonable predictions in further analyses of steering qualities.

2. Calculation of frequency response and harmonic analysis, based on the rotating arm test data, show that the dependence of yaw amplitude on trim is very strong. Yaw amplitude increases substantially with trim by the bow and decreases with trim by the stern. This tendency was also observed in the free-turning tests. In other words, trim by the stern induces an increase of dynamic stability and a decrease of turning ability, and trim by the bow induces a decrease of dynamic stability and an increase of turning ability.

3. An attempt to use rotating arm test results to predict the response to a zig-zag maneuver was made. This kind of technique will be developed in conjunction with experimental work during further research on ship controllability.

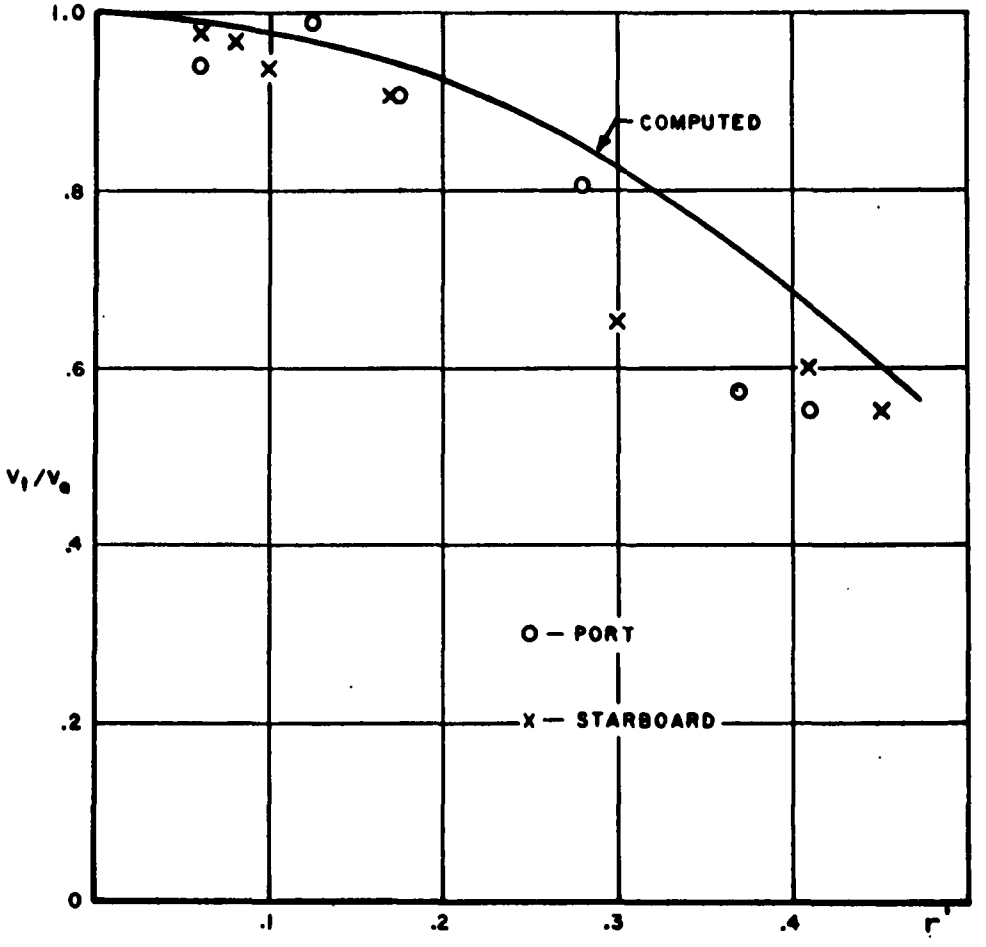

FIGURE 17. SPEED REDUCTION DUE TO LATERAL MOTIONS

4. Speed reduction due to yaw and sway was predicted from rotating arm test results. Comparisons between predictions and free-turning results showed good agreement. This technique will also be developed in further research on the steering problems of ships at sea.

5. The effect of placing a ship's rudder directly in the propeller race is known to improve steering qualities to a large extent. Measurement of lateral rudder force of the Series 60 model showed this to be more than two times as great with the rudder behind the propeller as with the propeller removed. The tendency mentioned here can be generalized for ordinary type cargo ships, having single screw and single rudder.

6. The Series 60 model (C_b = 0.60), with a rudder of typical size for this kind of ship, possesses sufficient dynamic stability, but somewhat less than average turning ability.

VIII. REFERENCES

1. Hadler, J. B., Stuntz, G. R. and Pien, P. C.: "Propulsion Experiments on Single-Screw Merchant Ship Forms - Series 60," SNAME, Vol. 62, 1954.

2. Eda, H. and Crane, C. L., Jr.: "Research on Ship Controllability, Part I, Survey and Long Range Program," DL Report 922, 1962.

3. Martin, M.: "Analysis of Lateral Force and Moment Caused by Yaw During Ship Turning," DL Report 792, 1961.

4. Tsakonas, S.: "Effect of Appendage and Hull Form on Hydrodynamic Coefficients of Surface Ships," DL Report 740, 1959.

5. Eda, H. and Crane, C. L., Jr.: "Research on Ship Controllability, Part II, Steering Characteristics of the Series 60 (C_b = 0.60)," DL Report 923, 1962.

6. Lewis, F. M.: "The Inertia of the Water Surrounding a Vibrating Ship," SNAME, Vol. 34, 1922.

7. Motora, S. and Couch, R. B.: "Maneuverability of Full-Bodied Ships in Restricted Waters," Prepared for the Great Lakes Section SNAME, 1961.

8. "The First Symposium on Ship Maneuverability, Washington, D. C." DTMB Report 1461, 1960.

9. Shiba, Mizuno, Tomita, Eda: "Turning Experiments on Optimum Rudder Area of Ships," JSNA, Vol. 105, 1959.

10. Davidson, K. S. M. and Schiff, L.: "Turning and Course Keeping Qualities of Ships," SNAME Vol. 54, 1946.

11. Todd, F. H., Stuntz, G. R., and Pien, P. C.: "Series 60 - The Effect Upon Resistance and Power of Variation in Ship Proportions," SNAME, Vol. 65, 1957.

12. Rydill, L. J.: "A Linear Theory for the Steered Motion of Ships in Waves," TINA, Vol. 101, 1959.

DESIGN TRENDS IN SHIP STEERING CONTROL

J. Bentkowsky
Engineering Section Head - Controls
Sperry Piedmont Company
Division of Sperry Rand Corporation

The purpose of this paper is to discuss the art of ship control from the point of view of the control engineer, rather than that of the ship designer. The basic consideration of this approach is that the ship itself is a fixed object to be controlled. It's hydrodynamic characteristics are given and it is the function of the control engineer to build a set of controls which will enable the ship to attain the type of performance inherent in the ship.

Automatic ship steering controls have been in existence for many years, and today virtually every ocean going merchant ship is equipped with automatic controls. In the past few years there has been an increasing concern about the performance of these ships, particularly in extremely heavy weather. Until recently this had not been a matter of great concern, inasmuch as all ships have a helmsman on station who can be called upon to substitute for the automatic pilot in extremely heavy weather. Since the probability of such weather is small, no great hardship resulted. On the other hand, there is today considerable interest in reducing the size of crew aboard ship. To do this successfully requires complete elimination of the helmsman. The automatic pilot must now have 100 percent utilization in all kinds of weather.

Virtually without exception, all automatic controls to date have been designed for maneuvering in calm water rather than for course keeping. Sensitivities have been adjusted to make smooth, well-damped turns rather than to keep course optimally in seas. While this has been done primarily as a matter of expedience, experience has shown that it works satisfactorily for course keeping in moderate seas.

The time has come, however, when we must start designing specifically for course keeping, particularly for heavy weather.

My talk today, therefore, is divided into two parts. First, I would like to describe the state of the art of automatic steering and secondly, I will describe the approaches to designing for course keeping.

A block diagram of an automatic control system is shown in Figure 1. The automatic control receives as inputs a command signal of ordered course, and a signal of own ship's course from a gyro-compass. The difference between these two signals is measured and fed into the control computer which is the "brains" of the system. Here it is amplified and differentiated, filtered, integrated, or otherwise operated upon. The output of the computer is an ordered rudder angle signal which may be either in electrical or mechanical form. This signal is then used to position the rudder through a hydraulic servo actuator which provides the "muscles" of the control system.

As we continue around the steering loop, we see that the rudder applies both a force and a moment to the ship. The ship is also subjected to sea and wind disturbances which, in the methods of control system analysis, are shown summed with the rudder force and moment in their effects on the ship. The gyro-compass on the ship provides the signal to close the steering control loop.

All automatic pilots are designed with both a fully automatic mode, as shown, and a manual or hand-electric mode. In the hand-electric mode the rudder is positioned directly from orders inserted into the rudder actuator from the helm. Inasmuch as the same servo mechanism is used for both manual and automatic control, the separation of the autopilot into computer and actuator subsystems is a convenient one.

Intuitively, it is apparent that the faster the rudder can move the greater the performance potential of the system. However, on a practical basis there are very severe limitations. The actuator is by far the most costly portion of the system. Since rudder power is directly proportional to rudder speed, additional size and power dissipation accompanying increased rudder rate are serious economic limitations which must be weighed against potential performance improvements. While increasing the maximum available rate never deteriorates the performance, it does not, beyond a point, necessarily improve performance. The forces available from the rudder are also limited and after a while this force limitation overrides the rate limitation. Selection of a maximum rudder rate thus represents one of the major design decisions.

One effect of limiting the maximum rudder rate can be seen in Figure 2. Coast Guard regulations require, for merchant ships,

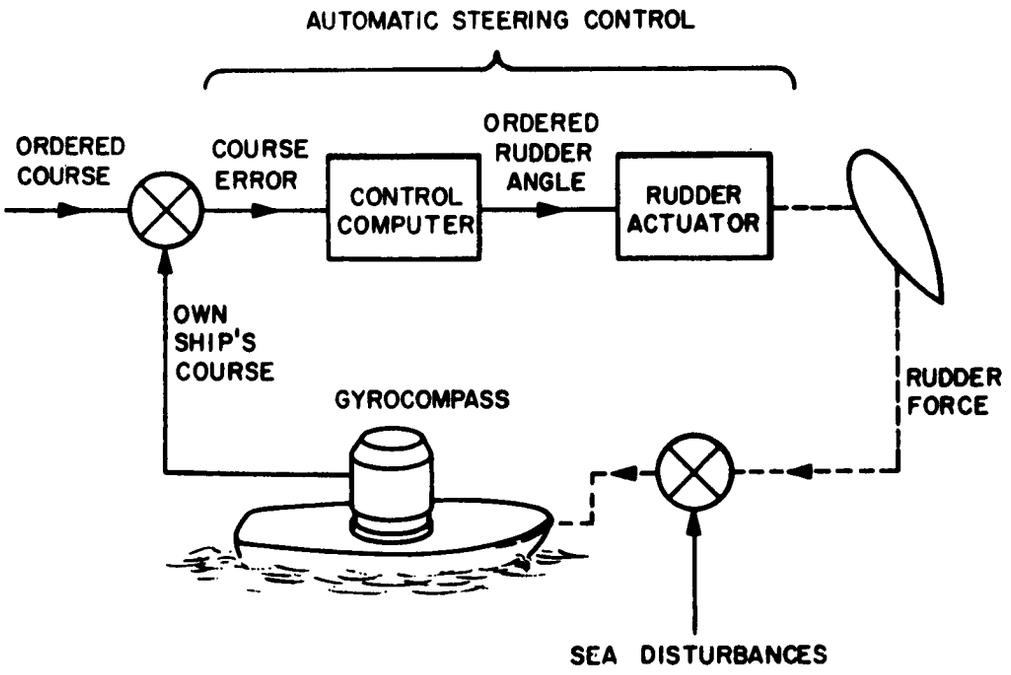

BLOCK DIAGRAM OF AUTOMATIC STEERING CONTROL SYSTEM

Figure 1

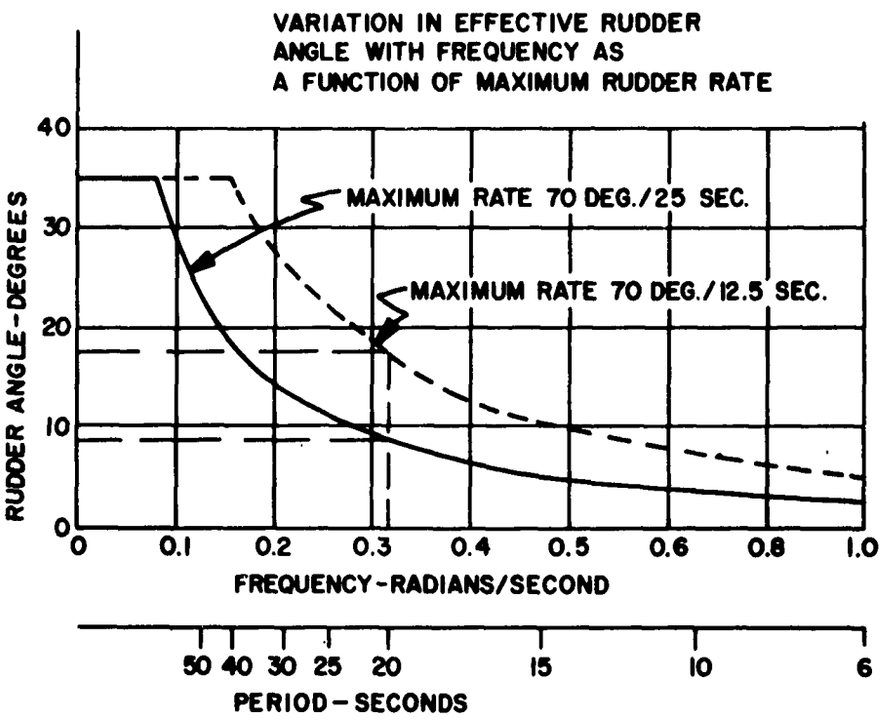
VARIATION IN EFFECTIVE RUDDER
ANGLE WITH FREQUENCY AS
A FUNCTION OF MAXIMUM RUDDER RATE
RUDDER ANGLE-DEGREES
40
30
20
10
0
MAXIMUM RATE 70 DEG./25 SEC.
MAXIMUM RATE 70 DEG./12.5 SEC.
0
0.1
0.2
0.3
0.4
0.5
0.6
0.8
1.0
FREQUENCY-RADIANS/SECOND
50 40 30 25 20 15 10 6
PERIOD-SECONDS

Figure 2

a minimum rudder rate capability of hardover to hardover (70 deg) in 25 seconds. It is seen that, with this rate, the maximum frequency at which the rudder can be oscillated sinusoidally between limits is 0.08 radians per second. This corresponds to a period of approximately 80 seconds. At a 20 second period the maximum effective rudder angle is only nine degrees. This can be increased to 18 degrees by doubling the maximum rudder rate.

The frequency response characteristics of the actuator system could be a limiting factor. However, in general, actuator bandwidths in the order of 0.25 to 0.5 radians per second are sufficient and are relatively simple to attain. The actuator, including the linkage to the rudder, should have a minimum of dead zone or back lash so that the rudder can respond to small signal orders. With reasonably designed systems a total dead band of approximately one-quarter degree is not difficult to attain and does not inhibit the performance.

Let us examine briefly several configurations of hydraulic servo actuators in current use.

Figure 3 illustrates the most commonly used steering system actuator. A servo valve is actuated from a servo amplifier and is used to position a hydraulic cylinder. The cylinder, operating through a mechanical differential strokes a variable delivery pump which ports oil to the hydraulic ram which, in turn, moves the rudder. A linkage operating off the rudder operates through the differential to take the pump off stroke. An electrical transducer, usually a potentiometer, is linked to the control cylinder and closes the loop around the rudder orders. It is seen that, in actuality, there are two servos in tandem, one positioning the control cylinder, the second the rudder. The first is electro-hydraulic; the second has no electrical connections at all. In most installations the control cylinder servo is of the bang-bang or on-off type. The servo valve is nothing more than a pair of solenoid actuated two-way valves, so that the control cylinder is moving either at maximum speed or not at all. Although this system is still by far the most popular today, it is starting to fall out of favor, due primarily to the high cost of the mechanical differential. Also, due to wear in the differential, it is difficult to keep the actuator dead band sufficiently small for high performance systems.

In order to eliminate the cumbersome mechanical differential, some of the more recently designed merchant ships have a so-called integrated steering system, as shown in Figure 4. Here the stroke control ram strokes the variable delivery pump directly. Two feedback signals are provided, one from the output ram to close the loop, and the other the position of the stroke control ram.

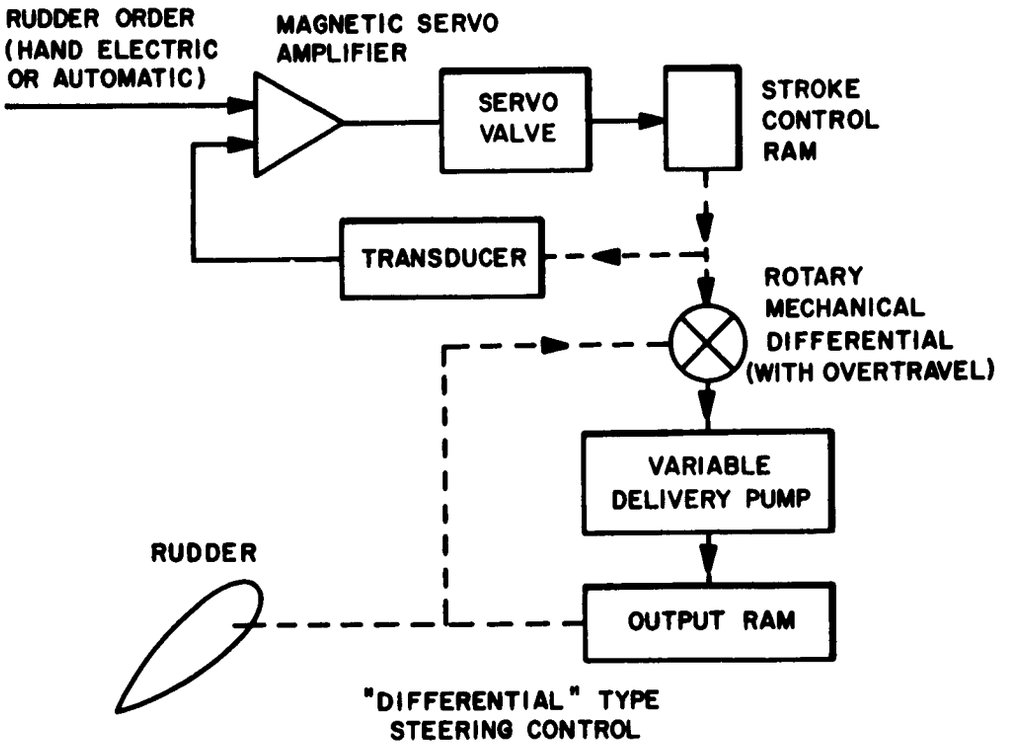
RUDDER ORDER
(HAND ELECTRIC
OR AUTOMATIC)
MAGNETIC SERVO
AMPLIFIER
SERVO
VALVE
STROKE
CONTROL
RAM
TRANSDUCER
ROTARY
MECHANICAL
DIFFERENTIAL
(WITH OVERTRAVEL)
VARIABLE
DELIVERY PUMP
RUDDER
OUTPUT RAM
"DIFFERENTIAL" TYPE
STEERING CONTROL

Figure 3

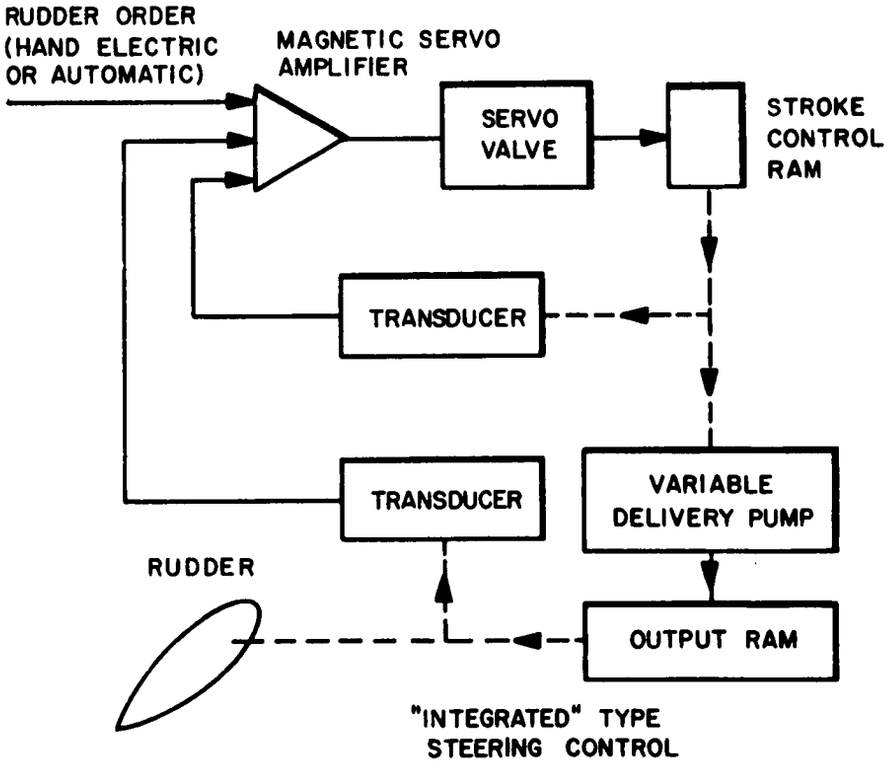
RUDDER ORDER
(HAND ELECTRIC
OR AUTOMATIC)
MAGNETIC SERVO
AMPLIFIER
SERVO
VALVE
STROKE
CONTROL
RAM
TRANSDUCER
TRANSDUCER
VARIABLE
DELIVERY PUMP
RUDDER
OUTPUT RAM
"INTEGRATED" TYPE
STEERING CONTROL

Figure 4

The latter signal is now proportional to pump flow, or rudder rate, and serves to stablize the servo loop. This system, in addition to its comparative simplicity, has the additional advantage of extreme flexibility. By varying the relative signal gradients of the two transducers, the servo response can be varied over an extremely wide range. For research purposes, the integrated steering system provides a much more useful vehicle than does the differential system.

Now let us go from the actuator to the computer. Virtually all autopilots in use today are so-called rate pilots. That is, they use a heading rate signal in addition to a heading error signal. The control computer is set up to solve the control equation shown in Figure 5.

The course error signal is obtained from the difference between signals of heading order and own ships course as obtained from a gyro-compass. In general, these signals are electrical and are derived from potentiometers or synchros. The turning rate signal is obtained from a tachometer geared either to the compass or to a compass repeater. The sensitivities are functions of the ship's characteristics and speed, and of the characteristics of the rudder servo. For simplicity, the sensitivities can be conceived of as varying as follows: The ratio n/m is a function of the hydrodynamic characteristics, primarily the damping coefficient, and theoretically varies inversely as ship's speed. On merchant ships, which operate at essentially constant speed, no provision is made to vary the n/m ratio. Submarines, on the other hand, use their automatic control systems from dead slow to flank speed. To cover this range an automatic speed control input is provided.

The levels of the n and m sensitivities are determined largely by the actuator characteristics (maximum rate and small signal non-linearities) and also by the sea state. A sensitivity control, or weather adjustment, is made available on all systems which serves to reduce the system sensitivities in heavy weather. The function of this weather adjustment is not to improve the course keeping ability, but rather to reduce excessive rudder activity. In general, except for very heavy weather, the course keeping performance improves with increased sensitivity.

Automatic pilots also have the function of making course changes in addition to keeping course. This ability to maneuver automatically is more important in a military than a merchant ship, but the requirements generally exist for both. Designing high performance maneuvering systems presents some interesting challenges. For example, going back to our control equation, if the sensitivities m and n are held constant and step commands are inserted, the

$$\delta_r = mCe + nC^{\circ}$$

WHERE δ_r = ORDERED RUDDER ANGLE

Ce = COURSE ERROR

C° = TURNING RATE

m = RUDDER RATIO

n = RATE SENSITIVITY > SYSTEM SENSITIVITIES

EQUATION OF STEERING CONTROL COMPUTER

Figure 5

resulting ship responses will vary with the signal amplitude as shown in Figure 6. If the response is made optimum for small maneuvers, large maneuvers can be highly underdamped, or even oscillatory. On the other hand, if the response is optimized for large changes, then small changes can be highly overdamped. This phenomenon occurs primarily at higher speeds and is a result of the limited rudder rate. The solution to this problem is a non-linear error, being large for small errors and smaller for large errors. By a proper choice of non-linearity, the response form can be made essentially independent of amplitude.

We now come to the problem of course keeping. Before any automatic control design can be undertaken it is necessary to characterize both the magnitude and frequency of the disturbances acting on the ship, and to compare these to the corrective forces and moments available from the rudder. An example of such a computation will be given now. As will be seen, this computation will be very helpful in understanding both the practical problem of steering in these seas and also the analysis problem facing the designer. For illustrative purposes we will use a Mariner vessel, operating at 20 knots in a state six sea.[1] What we will compute are the yaw moment disturbance and the yaw response of the uncontrolled ship in both bow and quartering seas. For the purposes of the illustration the sway force will be neglected, although this is a significant factor in determining the ultimate control system configuration. As a result of this computation we will be able to formulate a more specific statement of the problem, and also obtain an approach to the solution. In the course of the computation some of the analytic tools we are using will become apparent.

The characteristics of the ship we are using are given in Figure 7. Essentially it is a 528 foot long ship with a displacement of 16, 500 tons. At the speed of 20 knots, maximum rudder displacement produces a moment of approximately 9×10^7 foot-pounds.

We will characterize a state six sea by means of a Neumann spectrum for a 28 knot wind fully arisen sea.[2] This spectrum is illustrated in Figure 8. In a Neumann sea the variation of wave heights is Gaussian in nature. For the illustrated spectrum the average height from crest to trough of the one-third highest waves, the so-called significant height, is 18 feet. Let us consider the significance of this spectral curve. The area under the curve represents the mean square height of the sea above mean water level. Between any two frequencies, the area under the curve represents the mean square height of those waves within the frequency band. From a physical viewpoint the significance of the spectrum is the area under the curve rather than the curve itself.

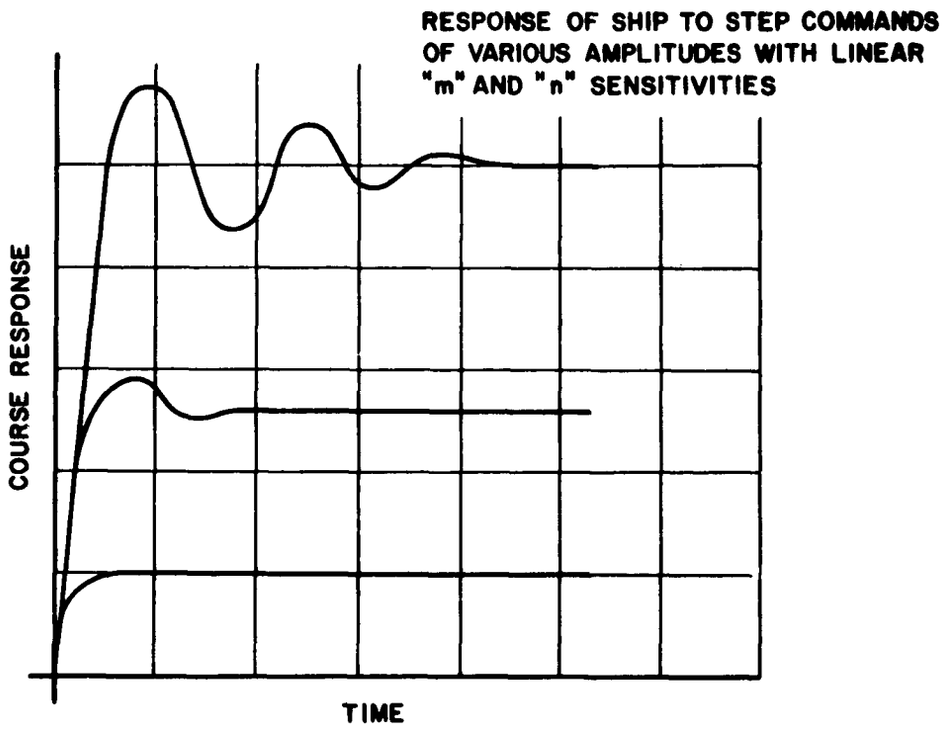
RESPONSE OF SHIP TO STEP COMMANDS
OF VARIOUS AMPLITUDES WITH LINEAR
"m" AND "n" SENSITIVITIES
COURSE RESPONSE
TIME

Figure 6

"MARINER" HULL

LENGTH	= 528 FEET
DISPLACEMENT	= 16,500 TONS
MOMENT OF INERTIA (IN WATER)	= 40×10^9 SLUG FT.^{2}
MAXIMUM RUDDER MOMENT AT 20 KNOTS	= 9×10^7 FT.-LBS.

Figure 7

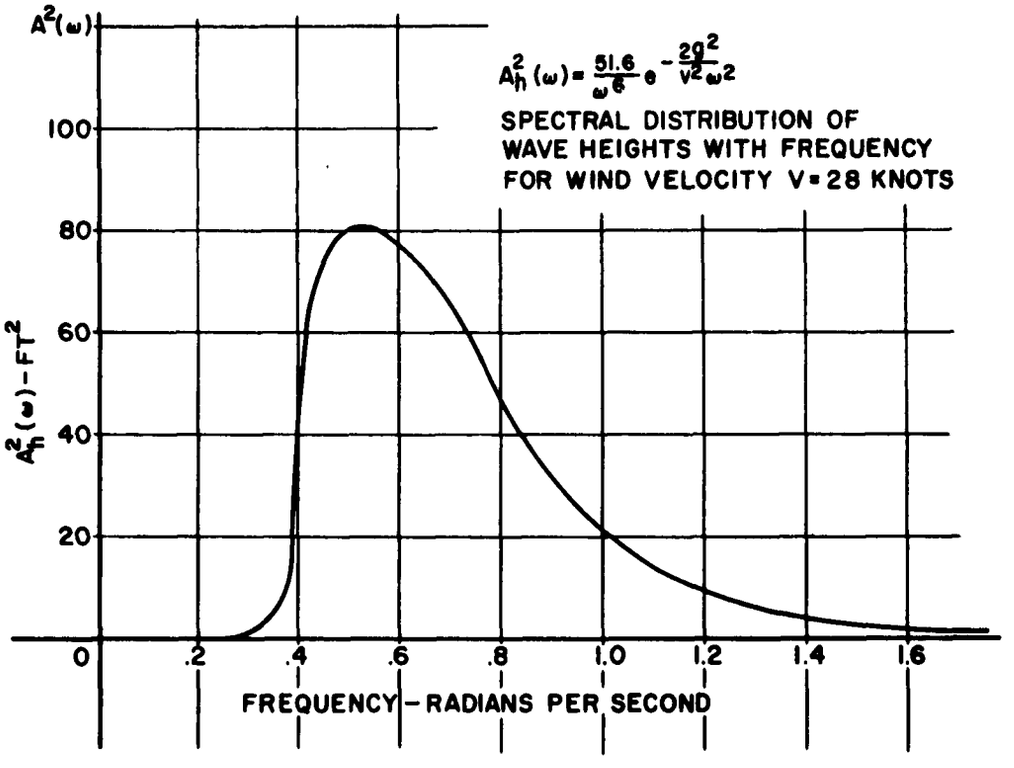
$A^2(\omega)$
$A_h^2(\omega) = \frac{51.6}{\omega^6} e^{-\frac{2g^2}{V^2\omega^2}}$
SPECTRAL DISTRIBUTION OF
WAVE HEIGHTS WITH FREQUENCY
FOR WIND VELOCITY V = 28 KNOTS
100
80
60
40
20
$A_h^2(\omega)$-FT^2
0
.2
.4
.6
.8
1.0
1.2
1.4
1.6
FREQUENCY – RADIANS PER SECOND

Figure 8

The Neumann spectrum is a stationary one, that is the frequencies indicated are those seen by a stationary observer. Aboard a moving ship the frequencies of encounter vary as a function of the relative velocities of the ship and the wave and the sea state spectrum must be revised accordingly. The basis for the revised sea spectra is shown in Figure 9, which illustrates the relationship between the wave length and frequency of a gravity wave as a function of ship speed and relative sea direction. The term $\sqrt{\frac{g\lambda}{2\pi}}$ is called the wave celerity and is the velocity of the wave front. At zero speed it is seen that the frequency of each wave decreases with wave length, while the celerity increases with wave length. Thus, longer waves have a lower frequency, but a higher velocity. As seen by a moving observer the relative velocity of each wave length component is the celerity minus the component of ship's speed in the direction of the wave travel and the encounter frequencies are modified accordingly. In a head sea each wave length component is encountered at a higher frequency. In following seas, the frequencies are lower, and in fact can go negative. What this means is that for a true following sea, waves longer than 225 feet overtake a 20 knot ship, while the ship overtakes all waves shorter than 225 feet. Another interesting phenomenon in a following sea is the fact that the encounter frequency reaches a peak at a wave length which is four times the zero frequency wave length. Starting with very long waves, the length of the wave decreases at a faster rate than the wave velocity and the frequency increases. As we pass 900 feet, the velocity begins to decrease faster than the wave length and the frequency decreases. The effect of this peak in frequency is to distort the encounter frequency spectrum in following seas.

The encounter spectra are shown in Figure 10, for bow, beam and quartering seas. The markings on each spectrum correspond to waves of equal length. The beam sea spectrum is identical to the stationary spectrum. The bow sea spectrum is shifted toward the higher frequencies. The quartering sea spectrum is shifted toward the left, reaches an infinite peak at a frequency of 0.34 radian per second and then reverses direction. The significance of this infinite peak is difficult to appreciate at first glance. However, we recall that the physical significance of the spectrum is in the area under the curve. And, strange as it seems, the areas under all three curves are identical.

Because of the difficulty in visualizing the significance of spectra with infinite peaks, it is far more convenient to do all the work with wave length rather than frequency as the independent variable. The 28 knot wind Neumann spectrum is shown as a function of wave length in Figure 11. The area under this curve is identical to that of the frequency spectrum.

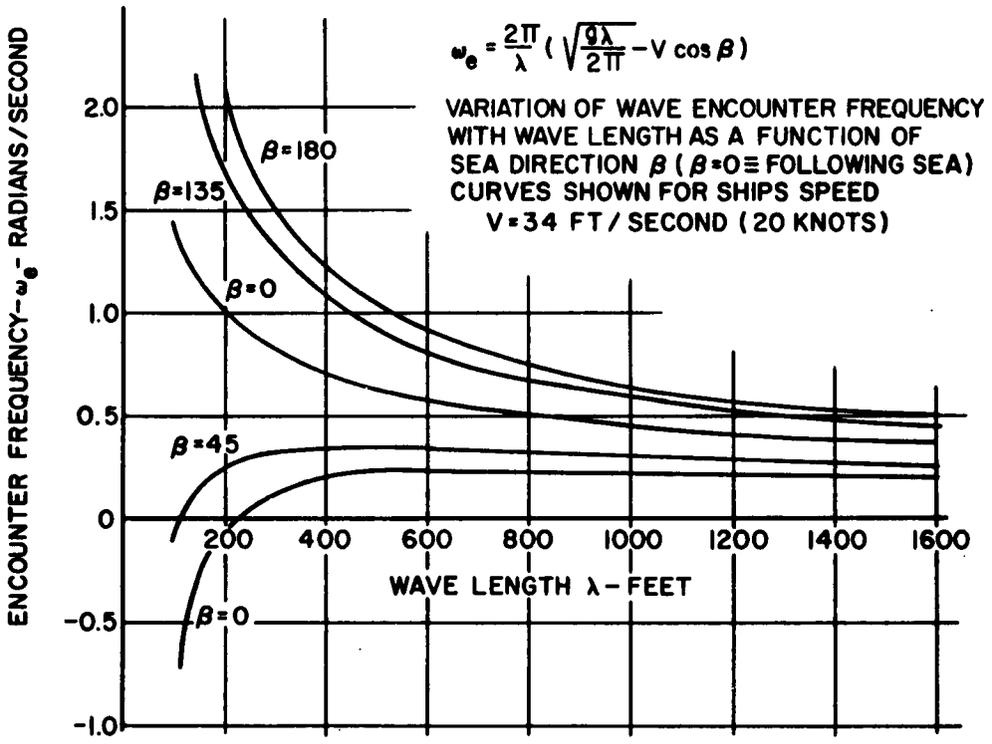
$\omega_e = \frac{2\pi}{\lambda}\left(\sqrt{\frac{g\lambda}{2\pi}} - V\cos\beta\right)$
VARIATION OF WAVE ENCOUNTER FREQUENCY WITH WAVE LENGTH AS A FUNCTION OF SEA DIRECTION β (β=0≡ FOLLOWING SEA) CURVES SHOWN FOR SHIPS SPEED V=34 FT/SECOND (20 KNOTS)
ENCOUNTER FREQUENCY-ω_e- RADIANS/SECOND
2.0
1.5
1.0
0.5
0
-0.5
-1.0
β=180
β=135
β=0
β=45
β=0
200
400
600
800
1000
1200
1400
1600
WAVE LENGTH λ-FEET

Figure 9

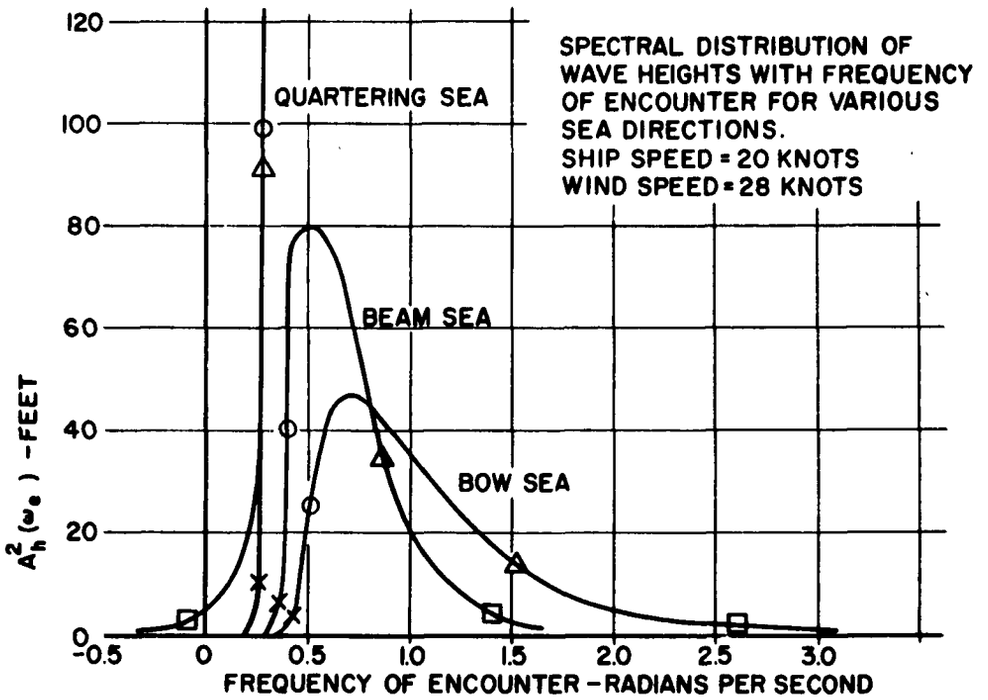
SPECTRAL DISTRIBUTION OF WAVE HEIGHTS WITH FREQUENCY OF ENCOUNTER FOR VARIOUS SEA DIRECTIONS.
SHIP SPEED = 20 KNOTS
WIND SPEED = 28 KNOTS
QUARTERING SEA
BEAM SEA
BOW SEA
$A_h^2(\omega_e)$ - FEET
120
100
80
60
40
20
0
-0.5
0
0.5
1.0
1.5
2.0
2.5
3.0
FREQUENCY OF ENCOUNTER - RADIANS PER SECOND

Figure 10

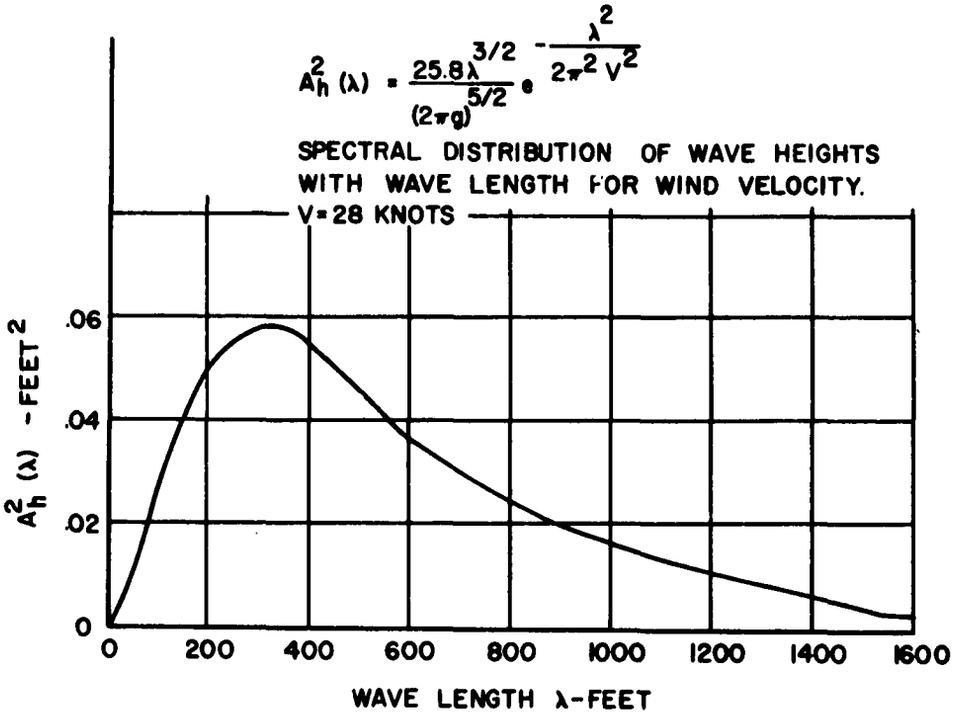
$A_h^2(\lambda) = \frac{25.8\lambda^{3/2}}{(2\pi g)^{5/2}} e^{-\frac{\lambda^2}{2\pi^2 V^2}}$
SPECTRAL DISTRIBUTION OF WAVE HEIGHTS
WITH WAVE LENGTH FOR WIND VELOCITY.
V=28 KNOTS
$A_h^2(\lambda)$ -FEET^2
.06
.04
.02
0
0
200
400
600
800
1000
1200
1400
1600
WAVE LENGTH λ-FEET

Figure 11

Now that we have a representation of the sea, it is necessary to convert this to a moment acting on the ship. The work of Cummins [9] and Korvin-Kroukovsky [8] provide a basis for computing the moment acting on a ship due to a sinusoidal surface wave. In performing the computation used here the hull shape was simplified by assuming a ship symmetrical about the yaw axis, whose submerged cross section is semi-circular. This is a usual assumption made in such computations. The direction of encounter at which a given wave induces a maximum yaw moment on a ship is a function of the relative lengths of the wave and the ship and of the speed of the ship. For illustrative purposes a 45 degree angle of encounter has been used, and the moment associated with each of the wave length components of the spectrum has been computed.

For each of these waves, the yaw moment per unit wave height is shown plotted in Figure 12. As a matter of interest it will be noted that at 45 degrees the wave length for maximum moment is approximately two-thirds the length of the ship. This critical wave length varies with the angle of encounter.

The spectrum for the moment disturbance is obtained by squaring the unit moment curves and multiplying by the wave height spectrum. These moment spectra are shown in Figure 13. The areas under these curves represent the mean square moment applied to the ship, the square root of the area is the root mean square or rms moment. This is seen to be 16×10^7 foot pounds for the quartering sea and 18.6×10^7 foot pounds for the bow sea. With a Gaussian distribution, the moment will be within a factor of two of the rms value 90 percent of the time.

Referring to the ship characteristics, the maximum rudder moment was seen to be 9×10^7 foot pounds, so that in a state six sea the peak moments applied to the hull are in the order of four times the maximum restoring moment available from the rudder. Furthermore, at the frequencies involved, the maximum rudder angle cannot be used due to the limited rudder rate capability. Basically, therefore, it appears that there is very little that can be done to stabilize against state six sea disturbances. The small amount of stabilization that could be achieved by driving the rudder hardover to hardover does not seem worthwhile at all. Before abandoning hope, however, it is worthwhile to compute the ship's motions.

All the disturbance frequencies we have been considering have been in the frequency band above 0.2 radian per second. In this region the ship behaves essentially as a pure inertia. The transfer function of the ship in this region is thus quite simple and the yaw response spectrum can easily be determined from the moment spectrum. This is shown in Figure 14.

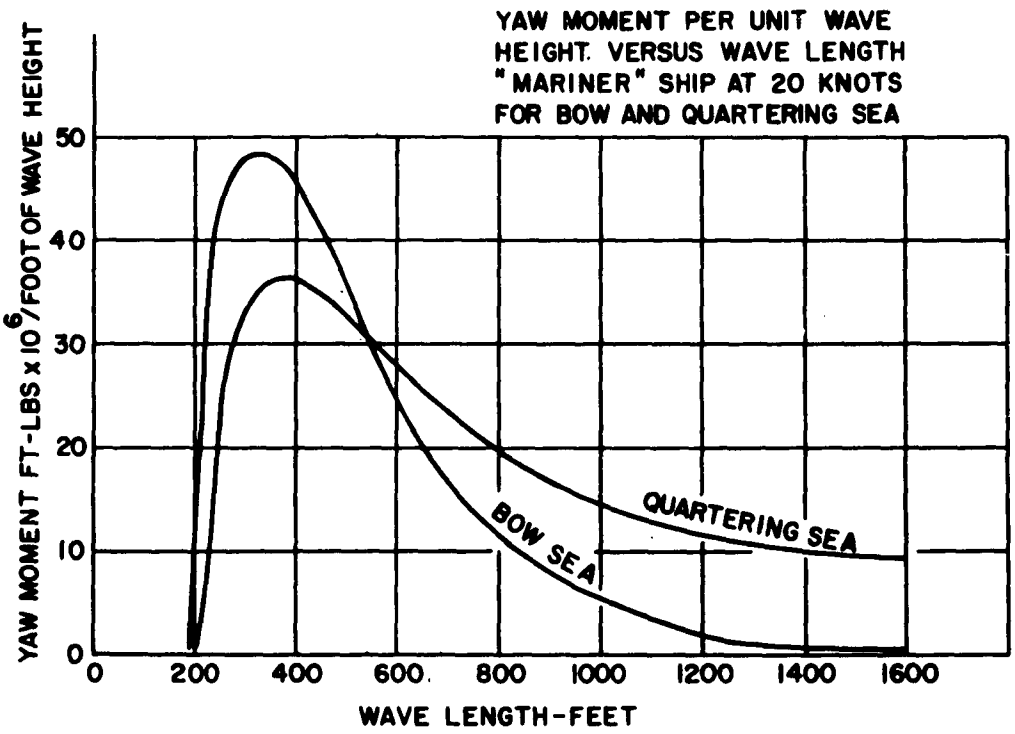
YAW MOMENT PER UNIT WAVE
HEIGHT VERSUS WAVE LENGTH
"MARINER" SHIP AT 20 KNOTS
FOR BOW AND QUARTERING SEA
YAW MOMENT FT-LBS x 10⁶/FOOT OF WAVE HEIGHT
0
10
20
30
40
50
0
200
400
600
800
1000
1200
1400
1600
WAVE LENGTH-FEET
QUARTERING SEA
BOW SEA

Figure 12

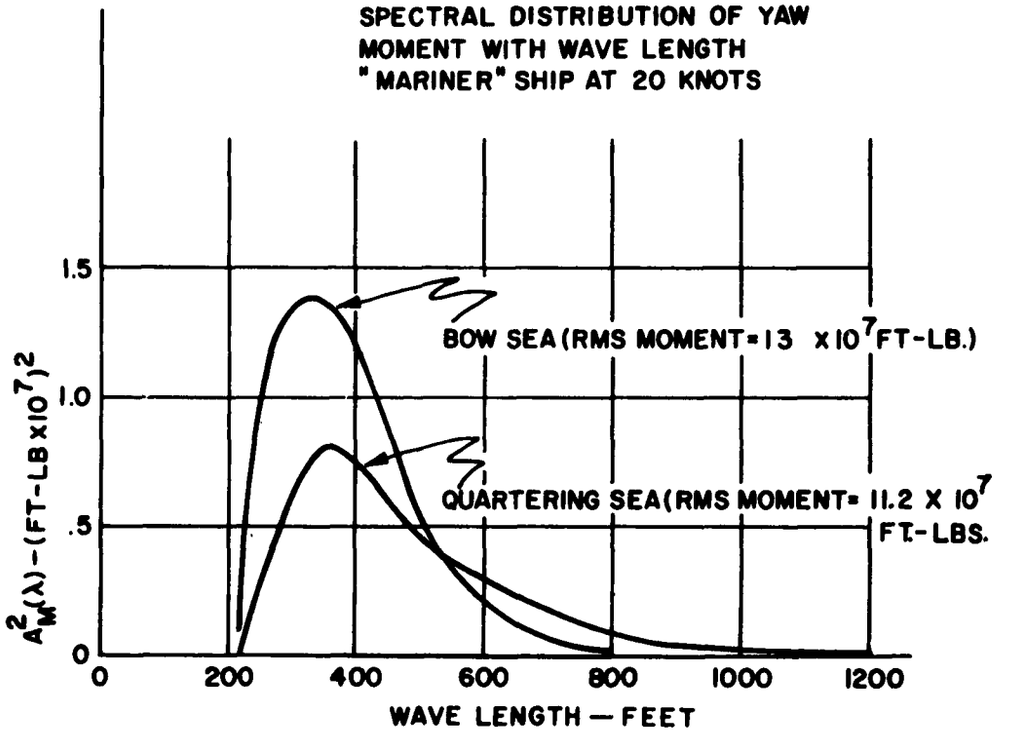
SPECTRAL DISTRIBUTION OF YAW
MOMENT WITH WAVE LENGTH
"MARINER" SHIP AT 20 KNOTS
BOW SEA (RMS MOMENT = 13 X 10^7 FT-LB.)
QUARTERING SEA (RMS MOMENT = 11.2 X 10^7 FT-LBS.
$A^2_{M(\lambda)}$ - (FT-LB X 10^7)^2
1.5
1.0
.5
0
0
200
400
600
800
1000
1200
WAVE LENGTH — FEET

Figure 13

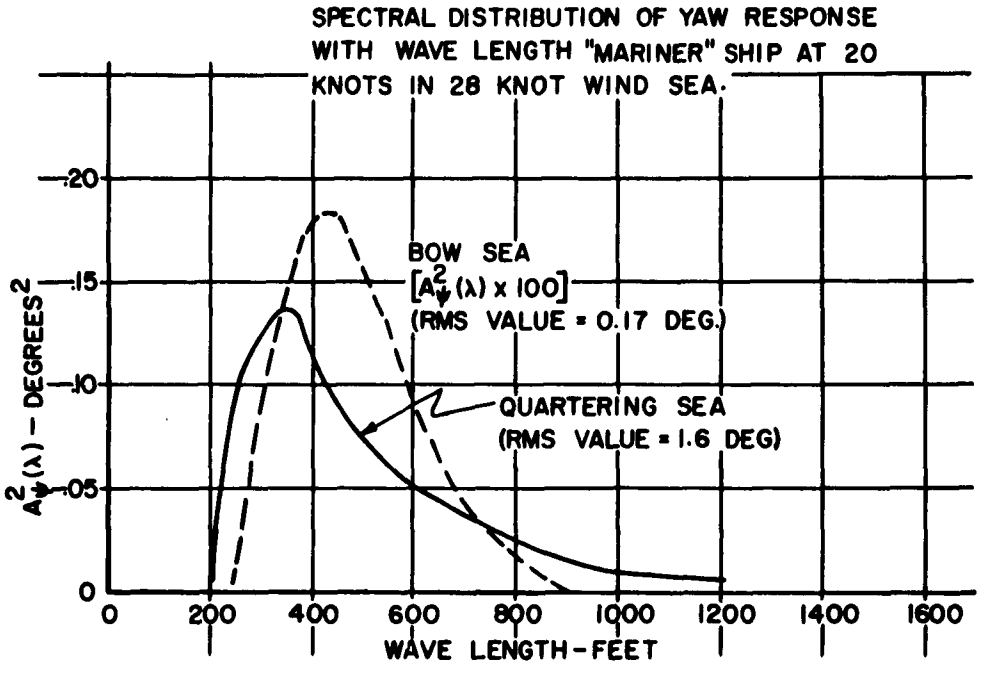
SPECTRAL DISTRIBUTION OF YAW RESPONSE WITH WAVE LENGTH "MARINER" SHIP AT 20 KNOTS IN 28 KNOT WIND SEA.
BOW SEA
$[A^2_{\psi}(\lambda) \times 100]$
(RMS VALUE = 0.17 DEG.)
QUARTERING SEA
(RMS VALUE = 1.6 DEG)
$A^2_{\psi}(\lambda)$ - DEGREES^2
.20
.15
.10
.05
0
0
200
400
600
800
1000
1200
1400
1600
WAVE LENGTH - FEET

Figure 14

Inasmuch as the encounter frequencies for the bow sea situation are much higher than those for the quartering sea, the yaw responses of the bow sea are much smaller. In order to show the two spectral responses on the same illustration it was necessary to multiply the bow sea response by 100. Taking the square root of the area under the two curves, the rms value of yaw angle in a quartering sea is computed to be 2.2 deg, in a bow sea 0.24 degree. Thus, in a bow sea the ship will be off course by less than one-half degree for 90 percent of the time. In a quartering sea, it will be off course by less than 4½ degrees for 90 percent of the time. The bow sea performance is perfectly satisfactory. The quartering sea performance is becoming marginal, particularly if other motions are superimposed on the sea disturbance motions.

It would seem that, in a heavy sea, our best course of action might be to leave the rudder on zero. However, it should be recognized that our brief analysis was by no means complete. First of all, the stability of the Mariner ship is marginal. With zero applied rudder the ship will tend to drift in one direction or the other. Secondly, there are d-c or very low frequency disturbances acting on the ship due to wind and sway forces. The motions due to these disturbances, on an instantaneous basis, are superimposed upon these motions due to the sea forces. An automatic control is required to stabilize against these other disturbances.

Although the spectral responses could be calculated quite readily for the uncontrolled ship, the method is not completely applicable when controls are used. This is due primarily to the non-linearity caused by the rudder rate limit. Statistical techniques, unfortunately, are not directly applicable to non-linear systems. The problem is further complicated if a non-linear control computer is required. The solution to the problem is to conduct the analysis with an analog computer.

Using the wave length domain to generate spectra, the problems of infinite peaks in following sea encounter spectra can be avoided. An approximation of the spectrum using 10 wave components is satisfactory for virtually all applications, and fewer components can generally be used.

Although we have not solved the problem yet, we have learned much which will be useful in obtaining the ultimate solution. Let us review what we have learned.

First of all, we have a method of predicting uncontrolled motions in a seaway which is valid not only for the Neumann spectrum but for any spectrum which might be found to be valid. The ability

to predict uncontrolled motions provides the basis for devising performance criteria. Lack of suitable criteria has been one of the biggest stumbling blocks in evaluating the performance of on-board systems.

The second important fact we have learned is that it is not worthwhile trying to stabilize against high frequency disturbances. From this point of view, disturbance frequencies of 0.3 radian per second are considered high.

We can therefore expect that the ultimate computer configuration will include a low pass filter. This will not solve the entire problem inasmuch as it is difficult to design a filter with exactly the proper attenuation characteristics which will simultaneously provide a stable control loop. Further, very severe filtering will also seriously inhibit the turning or maneuvering capability of the ship.

It is probable that the ultimate control computer configuration will include a dead zone in one or another of the signal channels. Dead zones have been used rather successfully as weather adjustments. A dead zone is built into an on-off control system, so that a reduction in sensitivity is accompanied by an increase in the system dead zone. On one type of submarine steering control, a dead zone was inserted in the rate signal, with reasonable success.

The big design problem is to obtain a control which will function satisfactorily in both course keeping and course changing with a minimum of adjustments for sea conditions. We do not have the system yet. However, we are working on it, and I hope to be able to report results by the next seminar.

The author wishes to express his appreciation to Mr. Tom Noble of Sperry Piedmont Company for his assistance in performing the computations and preparing the illustrations associated with the ship motion computations.

J. Bentkowsky

REFERENCES

1. R.V. Morse and D. Price - Maneuvering Characteristics of the Mariner Type Ship (USS Compass Island) in Calm Seas-Final Report Contract NOnr 3061(00), Dec. 1961.

2. H.E. Landsberg - Advances in Geophysics-Academic Press, Inc. 1955.

3. W.E. Cummins - Hydrodynamic Forces and Moments Acting on a Slender Body of Revolution Moving under a Regular Train of Waves-DTMB Report 910, December 1954.

4. B.V. Korvin-Kroukovsky - Theory of Seakeeping - Society of Naval Architects and Marine Engineers, 1961.

MOTIONS OF SUBMERGED BODIES IN REGULAR AND IRREGULAR WAVES

Daniel Savitsky,
Head, Applied Mechanics Group
Davidson Laboratory

and

Dennis Lueders,
Head, High-Speed Test Facility
Davidson Laboratory

SUMMARY

The motions of a submerged body at zero forward velocity in regular and irregular waves are defined as a function of wave size, wave direction, and depth of submergence. It is found that in regular waves the submerged body acts essentially as a water particle at depth and that the heave and surge motions are those of a water particle at the center of gravity of the body. In beam seas the hydrodynamic roll moment is proportional to the wave slope at depth. All roll motions are determined using this effective wave slope, the natural roll frequency and damping of the body, and the standard dynamic equations of motion of a linear, single degree-of-freedom oscillator. In head seas, the heave and surge motions are equal to those of a water particle at the center of gravity when the wave length is greater than approximately four times the model length. The pitch amplitude of the body is equal to the effective wave slope at depth when the wave size is greater than approximately two times the model length. Results of energy spectrum analysis in irregular waves shows that the "principle of linear superposition of component responses" is also applicable in predicting the irregular spectrum of motions of submerged bodies in head and beam seas.

I. INTRODUCTION

Hydrodynamicists have for many years been concerned with analytical and experimental studies of the motions of

surface ships when running at various headings in regular and irregular wave systems. The literature contains numerous papers on this subject including the works of St. Denis and Pierson,[1] Fuchs and MacCamy,[2] Lewis and Numata,[3] Williams,[4] etc. The general conclusion of these studies is that the ship response to regular waves is governed by the dynamics of a system composed of the ship with its inertia and damping characteristics acted upon by a forcing function associated with the height and length of the regular wave. The irregular response of a ship to an irregular wave form is equal to the summation of its responses to the component waves.

It was believed that the results of ship motion theory would also be applicable to the case of submerged bodies in a wave system. To evaluate the applicability of this assumption model tests were conducted at the Davidson Laboratory, Stevens Institute of Technology, on a submerged, asymmetrical finned body at zero velocity when acted upon by regular and irregular long-crested waves approaching the body from various directions. It is expected that the results presented in this paper would serve the following purposes:

1. To describe the general characteristics of the motions of a submerged body and their relations to the disturbing regular and irregular wave system.

2. To provide guidance and experimental data useful in analytical solutions of motions of submerged bodies.

3. Determine the extent of applicability of the principle of superposition to the study of submerged body motions in irregular seas. This principle states that "the sum of response of a ship to a number of simple sine waves is equal to the response of the ship to the sum of the waves."[1]

Test apparatus and models are considered first, then results of experiments are presented, followed by a discussion of results and specific conclusions. Although tests were made at various wave headings, only beam and head sea results are presented in this paper since it is believed that these headings best serve to provide the information consistent with the objectives of this presentation. For the purposes of generalizing the presentation all results are presented in non-dimensional form.

II. APPARATUS AND TEST PROCEDURE

A. Test Model The test model was an asymmetric finned body whose center of gravity and pitch and roll inertias could be easily adjusted by an internal ballast arrangement. Also, the dimensions of the vertical fin located on the top of the body could be adjusted to provide a desired positive metacentric height and roll damping of the body. The weight of the model was ballasted for neutral buoyancy in the submerged condition and for a desired center of gravity position. A simplified sketch of the test model is given in Fig. 1.

B. Test Apparatus The submerged model was supported on a unique test apparatus which allows a model to have six degrees of freedom with virtually no restraints. This so-called "Davidson Lab. Motions Apparatus" was originally designed for surface ship motion studies in oblique seas and was modified to be applicable in submerged body tests. A sketch of this apparatus is given in Fig. 2 and is described in detail in ref. 5. Briefly, the function of the motions apparatus is to follow (by means of servo-control) the model continuously and to provide a means of recording the six components of motion with a minimum of restraint. The vertical support post of the motions apparatus was connected to the center of gravity of the submerged model through a special low friction universal pivot which allowed the model to have freedom in pitch and roll. Freedom in heave and yaw was provided by the free moment of the vertical rod while freedom in surge and sway were provided by the servo-mechanism on the support carriage. The vertical support rod was of small diameter, thin walled, and free flooding in order to provide a minimum heave restoring force.

C. Test Procedure The model was set at a prescribed initial heading and submerged in smooth water. The desired regular or irregular wave system was then passed over the submerged model and time histories of the six components of model motions and the surface wave profile at the center of gravity were recorded. Tests were first made in regular long-crested waves of various heights and lengths in order to establish the response amplitude operators of the model. Tests were then made in irregular waves whose energy spectrum covered the range of regular wave test frequencies.

III. RESULTS AND DISCUSSION

A. Natural Frequencies and Damping of Submerged Model

The natural frequencies and damping characteristics of the model were obtained by submerging it in smooth water to a depth corresponding to the test conditions in waves and then applying an initial disturbance separately in roll and in pitch. The time histories of the resultant free oscillations were then analyzed to define the natural periods and damping characteristics in roll and pitch. These results included, of course, the hydrodynamic effects of the entrained fluid masses. In all cases the test submergences were deep enough so that the free water surface effects were negligible. The envelopes of the roll amplitude and pitch amplitude decay curves are shown in Fig. 3. The damping ratio, ζ, is obtained by combining results such as given in Fig. 3 with the natural frequency of the test body in either roll or pitch. It is seen that for moderate angles of roll and pitch the damping is essentially linear but becomes significantly nonlinear for large roll angles. The wave test conditions discussed in this paper are confined to the cases where the angular motions of the test model were essentially within the range of linear damping. The magnitudes of the roll and pitch periods and damping ratios are functions of specific hull geometries and hence are not defined in this presentation which is intended to be general in its discussions and conclusions.

B. Behavior of Submerged Body in Regular Waves

1. Beam Sea Condition. When submerged in beam sea conditions the only observable motions of the test body were in heave, sway, and roll--all of which were oscillatory motions having a frequency equal to that of the wave frequency. The model heading remained constant in all beam sea tests. The vectorial sum of the oscillatory heave and sway motions was essentially constant during this cyclic motion and was equal to the orbital radius of a wave particle at the center of gravity of the body. Figure 4 is a plot of the calculated heave and sway motions compared with the experimental results. The ordinate of the plot is the ratio of the heave or sway amplitude divided by the orbital radius of a water particle at a depth equal to the submergence of the center of gravity. The theoretical value of this ratio is equal to 1.0. It is seen that the agreement between theory and experiment is excellent. In effect, then, for a beam sea the neutrally buoyant submerged body orbits as a water particle located at its center of gravity and hence its heave and sway motions are readily calculated for any wave height, wave length, and depth of submergence. The maximum up heave occurs under a

wave crest while the maximum sway displacement occurs under a wave nodal point. The simple formulation for the orbital radius of the combined oscillatory heave and sway motion of the submerged body is:

$$r = a\, e^{-\frac{2\pi h}{\lambda}} \qquad (1)$$

where: r = maximum heave or sway displacement
a = wave amplitude
h = submergence of center of gravity
λ = wave length

The heave and sway velocities of the submerged body were also found to be consistent with the heave and sway velocities of a water particle effectively located at the center of gravity of the body. The formation for the maximum velocity is given by the usual deep water wave equations:

$$v_{max} = u_{max} = Kace^{-Kh} \qquad (2)$$

where: v_{max} = maximum vertical velocity

u_{max} = maximum horizontal velocity

K = wave number = $2\pi/\lambda$

c = wave celerity = $\sqrt{g\lambda/2\pi}$

The heave and sway motions and velocities of the submerged body are always in phase with the water particles effectively located at the center of gravity of the body.

Figure 5 presents a plot of the roll amplitude-wave amplitude ratio versus ratio of wave frequency to natural roll frequency of the submerged body in beam seas. It is seen that the roll response curve is sharply "tuned" at wave frequencies equal to the roll frequency. This is a typical characteristic of lightly damped systems such as was the case for the present test model. Within the roll angle range of linear damping, the roll angle is directly proportional to the wave height for all wave lengths and submergences. Also presented on Fig. 5 is a plot of computed roll angle amplitude as a function of frequency ratio. The computed curve is based on the following considerations.

The roll motions of the submerged body are considered to be the result of the motions of a damped, linear, single degree of freedom oscillating system. The hydrodynamic roll

moment is proportional to the wave slope at depth and, in the absence of dynamic effects, the roll angle of the submerged body is taken to be equal to the effective wave slope at a depth corresponding to the vertical distance of the center of the vertical fin below the level water surface. Combining these assumptions with the usual dynamic amplification factor for a damped, linear, single degree of freedom oscillating system results in the following expression for the roll amplitude of a submerged body in beam seas.

$$\theta = \frac{2\pi a}{\lambda} e^{-2\pi h/\lambda} \left[\frac{1}{\left[1 - \left(\frac{\omega}{\omega_n}\right)^2\right]^2 + \left[2\zeta \frac{\omega}{\omega_n}\right]^2} \right] \qquad (3)$$

where: θ = roll amplitude

ω_n = natural roll frequency of submerged body

ω = wave frequency

h = depth to center of vertical fin

ζ = damping ratio in roll

The results of eq. 3 are also plotted in Fig. 5. It is seen that the agreement between computed and experimental results is excellent. This agreement confirms the assumption of a linear, single degree of freedom system for moderate roll angles. The assumption of the "effective" wave slope at depth of vertical fin is somewhat arbitrary. However, since the vertical fin is primarily responsible for the roll motions of an otherwise symmetrical body, it is believed that the assumption is reasonable. For more complicated body forms, the establishment of an "effective" depth will require further consideration.

Figure 6 shows the effect of depth of submergence on the roll motions of a submerged body. It is seen that the roll angle is attenuated with depth in accordance with the wave exponential decay relations associated with deep water waves. The variation in roll angle with depth is given by the following formulation:

$$\frac{\theta_1}{\theta_2} = \frac{e^{-2\pi h_1/\lambda}}{e^{-2\pi h_2/\lambda}} \qquad (4)$$

where: θ_1 = roll amplitude at vertical depth of center of fin equal to h_1

θ_2 = roll amplitude at vertical depth of center of fin equal to h_2

The points on Fig. 5 are computed for a CG depth of 1.5d using eq. 4 and the data on the curve for a CG depth of 1.0. It is seen that the computed values agree very well with the experimental values confirming the expected exponential decay with depth.

Figure 7 presents the phase relation between maximum roll angle and maximum wave slope. The result is typical of linear, single degree of freedom, oscillator systems. For wave frequencies much less than the roll frequency, the roll motion is in phase with the wave slope. At wave frequencies equal to the roll frequency, there is a 90° phase shift, i.e., the maximum roll of the submerged body occurs under a crest. For wave frequencies much larger than the roll frequency the maximum roll angle is 180° out of phase with the maximum wave slope. It can easily be shown that the wave hydrodynamic forces produce a rolling moment on the submerged body which is in phase with the wave slope. In all cases, the model rolled at a frequency equal to that of the disturbing regular wave system.

It is concluded from the previous discussion that, if the system can be assumed to be linear, all the beam sea motions of a submerged body at zero speed can be simply obtained from a knowledge of the natural roll frequency and damping of the submerged body. These elemental characteristics can easily be obtained from the time history decay of the free oscillation of the body when subjected to an impulsive function.

2. Head Sea Conditions. In head sea test conditions the only motions of the submerged model were in heave, surge and pitch. In all cases the motions were oscillatory of frequency equal to the wave disturbance. Figure 8 presents a plot of the ratio of heave amplitude to orbit radius versus the ratio of wave length to model length. The orbit radius corresponds to that of a water particle at a depth equal to the CG submergence of the body. It is seen that for wave lengths less than 75 percent of the model length, the heave oscillations are quite small. With increasing wave length-model length ratio the heave oscillations increase. For wave lengths greater than approximately 4 times the model length, the heave amplitude oscillations are equal to the orbital radius of a water particle at the center of gravity of the model. The center of gravity motion of the submerged model was always in phase with the wave system, i.e., the maximum up motion always occurred when a wave crest was over the center of gravity.

Considering the pitch motions in head seas, the present conditions of test were such that the test wave frequencies were always larger than at least twice the natural pitch frequency of the submerged model. Referring to the dynamics

of simple linear oscillator systems, then, the maximum pitch amplitude should be in phase with the maximum wave slope since the pitch moment forcing function is 180° out of phase with the maximum wave slope. Further, for such large frequency ratios, the attenuation effects for the dynamic system are nearly constant over a wide range of imposed frequencies. A study of the model test data did indeed demonstrate the 0° phase relation between model pitch and wave slope, i.e., the maximum pitch of the submerged body occurred at the time of maximum wave slope. Figure 9 presents a plot of pitch amplitude-wave amplitude ratio versus wave length-model length ratio. It is seen that the pitch motions first increase as the model length-body length ratio is decreased from values less than 5, and reach a maximum when the wave length is equal to nearly twice the model length. The pitch motions then decrease rapidly for wave lengths shorter than twice the model length. A comparison was made between the maximum pitch amplitude and the "effective" wave slope at a depth corresponding to the center of gravity submergence of the test model. The effective maximum wave slope, α, at a depth, h, is defined by:

$$\alpha = \frac{2\pi}{\lambda} a \, e^{-\frac{2\pi h}{\lambda}} \qquad (5)$$

The ratio α/a as a function of wave length-model length ratio is also plotted on Fig. 9. It is seen that the computed variation of α/a with wave length is generally similar to the test results. Further it is seen that the experimental values of the pitch angle are nearly equal to the effective wave slope at depth for wave lengths larger than twice the length of the test model. For wave lengths shorter than twice the model length, the pitch angles are much less than computed by Eq. 5. This is an expected result since for these short waves the model cannot align itself with the maximum wave slope. For wave lengths much shorter than the body length the pitch angle approaches zero.

In summary, then: for head sea operation, the pitch angles are directly proportional to wave amplitude, are attenuated with depth in accordance with the usual exponential decay relation for deep water waves, and, for wave lengths larger than twice the body length, the pitch angles are equal to the effective wave slope at a depth corresponding to the center of gravity submergence of the body. Further, the pitch angle is always in phase with the wave slope when the wave frequencies are higher than the natural pitch frequency of the submerged body.

C. Behavior of Submerged Body in Irregular Waves

Tests were made in irregular, long-crested waves whose energy spectrum was designed to be consistent with those developed by Pierson, Neumann and James in ref. 6. The time histories of the irregular heave, roll and pitch motions in beam and head seas were measured and compared with the calculated values obtained by combining the response amplitude operators obtained in regular sea tests with the spectrum of the test irregular sea.

1. Irregular Long-Crested Waves Used in Tests. The theoretical irregular wave spectrum is given by:

$$\left[r(\omega)\right]^2 = \frac{c}{\omega^6} e^{-2g^2/v^2\omega^2} \qquad (6)$$

where: $\left[r(\omega)\right]^2$ is the energy spectrum, ft^2sec

c is a constant 51.6 ft^2/sec^5

ω is the wave frequency, rad/sec

g is 32.2 ft/sec^2

v is the wind velocity, ft/sec

The wave generator in the test tank was programmed in an attempt to generate an irregular wave spectrum corresponding to that of Eq. 6. A comparison between the computed spectrum and actual test wave spectrum is given in Fig. 10. It is seen that the actual test spectrum is nearly like the computed except for a secondary peak that the test spectrum contains at low frequencies. For the purposes of the following analyses, the characteristics of the model test spectrum are used throughout. Also plotted on Fig. 10 are relative frequencies corresponding to maximum roll response operator and maximum pitch response operator obtained in the regular wave tests. It is seen that these maximum response frequencies were lower than the frequency corresponding to maximum energy in the irregular sea test spectrum.

2. Experimental Spectrum of Model Motions. As previously described, simultaneous records were taken of the irregular surface wave pattern and the corresponding heave, pitch, and roll motions of the submerged body in head and beam seas. The automatically controlled wave pattern produced nearly identical wave conditions for all tests. The test data were automatically digitized at time intervals equal to approximately 1/2 of the shortest apparent period in the irregular wave record. The total length of record analyzed was taken to be consistent with the Davidson Laboratory

standards on establishing confidence limits in spectral analysis. The spectrum of surface waves and model motions were obtained using the Tukey autocorrelation method[7] which has been programmed for numerical computation on the IBM 1620 digital computer.

The experimental energy spectrum for heave and roll motions in beam seas is given in Fig. 11 and the spectrum for heave and pitch motions in head seas are given in Fig. 12. Comparing these motion spectra with the energy spectra of the test wave (Fig. 10), it is seen that the maximum energy in roll and pitch motions occur at frequencies corresponding to those at which the response operators in roll and pitch are a maximum. In both cases the frequency at which maximum motions occur is less than the frequency of maximum wave energy. Examining the heave spectrum in beam and head seas again it is seen that the maximum energy of heave motions occurs at a frequency smaller than the frequency corresponding to maximum wave energy. This result is consistent with the characteristics of the heave response operator shown in Figs. 4 and 8 which indicated large attenuations in the heave motion at regular wave frequencies corresponding to the frequency of maximum wave energy in the test irregular sea.

3. Computed Motion Spectra. The principle of superposition of component responses[1] indicates that the spectrum of model response--as in pitch, heave, or roll--can be predicted if the sea spectrum and the "response amplitude operator" are known. In the present case, the sea spectrum is defined in Fig. 10 while the response operators in pitch, heave, and roll have been found from regular wave tests. The predicted energy spectrum of the motions in waves is then obtained by multiplying the ordinates of the sea spectrum curve by the ordinates of the model response amplitude operator curve at corresponding frequencies. The predicted spectra of pitch, heave and roll in beam and head seas is also plotted in Figs. 11 and 12. Agreement between computed and experimental motion spectra is excellent. It is concluded that, for linear systems, the superposition technique is equally applicable to the case of submerged body motions as it has been shown to be in the case of surface ship motions in irregular seas.

IV. CONCLUSIONS

The following conclusions are presented as a result of Davidson Laboratory model studies on the motions of asymmetrical

finned bodies submerged in regular and irregular beam and head seas. The conclusions are limited to the case of linear responses of the submerged body.

A. Beam Seas (Regular Waves)

1. The submerged body acts essentially as a water particle orbiting in a radius equal to that of a water particle effectively located at the center of gravity of the submerged body.

2. The amplitudes of the heave and roll motions are proportional to surface wave height and are attenuated with depth in an exponential manner consistent with deep water wave relations.

3. The amplitude of the roll angle in any wave is equal to the effective wave slope at depth amplified by the usual dynamic relations of a damped, linear, single degree of freedom oscillator. Hence the beam sea motions are completely defined from a knowledge of the natural frequencies and damping.

4. For wave frequencies less than the natural roll frequency of the submerged body, the maximum roll angle is in phase with the maximum wave slope. For wave frequencies greater than the natural roll frequency, the roll angle is 180° out of phase with the surface wave slope.

5. All motions are harmonic of frequency equal to the disturbing wave frequency.

6. In beam seas the only motions of the submerged body are heave, roll, and sway.

B. Head Seas (Regular Waves)

1. The only motions of the submerged body are pitch, heave, and surge.

2. In the present tests, the wave frequencies were always much higher than the natural pitch frequency of the submerged body. Hence, the heave and pitch motions of the body were always in phase with the wave height and wave slope respectively.

3. For wave lengths larger than approximately 4 times the model length,the heave and surge motions of the submerged body are essentially equal to the motions of an equivalent water particle at a submergence equivalent to the CG position of the submerged body.

4. For wave lengths larger than approximately twice the model length, the pitch motions of the submerged body are equal to the effective wave slope of the wave at a submergence corresponding to the center of gravity submergence. The pitch motions are reduced considerably for wave lengths less than twice the model length.

5. The pitch, heave, and surge motions were directly proportional to wave amplitude and were attenuated with depth in accordance with the usual exponential decay relation.

C. Irregular Head and Beam Seas

1. Results of energy spectrum analysis of wave and motion records are presented and applied to the evaluation of the "principle of linear superposition of component responses." It was shown that the computed and experimentally obtained motion spectra in heave, roll and pitch were in excellent agreement.

V. REFERENCES

1. St. Denis, M. and Pierson, W. J., Jr.: "On the Motions of Ships in Confused Seas," Transactions of the Society of Naval Architects and Marine Engineers, 1953.

2. Fuchs, R. A. and MacCamy, R. C.: "A Linear Theory of Ship Motions in Regular Waves," University of California, Institute of Engineering Research, Series 61, No. 2, July 1953.

3. Lewis, E. V. and Numata, E.: "Ship Model Tests in Regular and Irregular Seas," Davidson Laboratory, Stevens Institute of Technology Report 567, July 1957.

4. Williams, A. J.: "An Investigation into the Motions of Ships at Sea," Transactions of the Institution of Naval Architects, 1952.

5. Lewis, E. V. and Numata, E.: "Ship Motions in Oblique Seas," Transactions of Society of Naval Architects and Marine Engineers, 1960.

6. Pierson, W. J., Neumann, G. and James, R. W.: "Practical Methods for Observing and Forecasting Ocean Waves," U.S. Navy Hydrographic Office Publication No. 603, 1956.

7. Tukey, J. W.: "The Sampling Theory of Power Spectrum Estimates," Symposium on Applications of Autocorrelation Analysis to Physical Problems," Woods Hole, Mass., 1949.

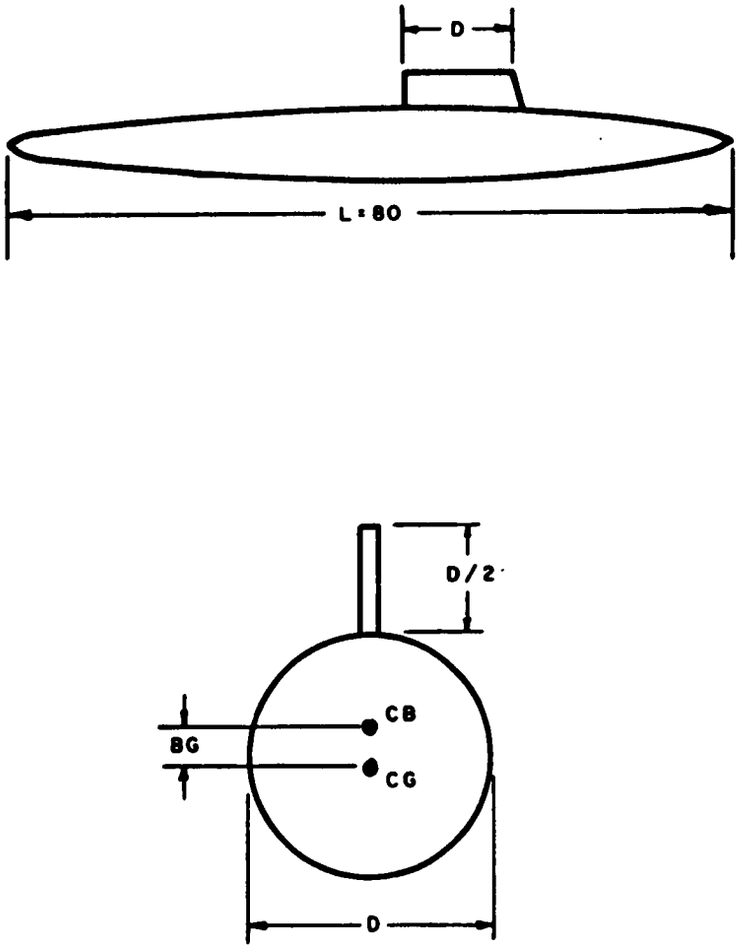

FIGURE 1. LINE SKETCH OF TEST MODEL

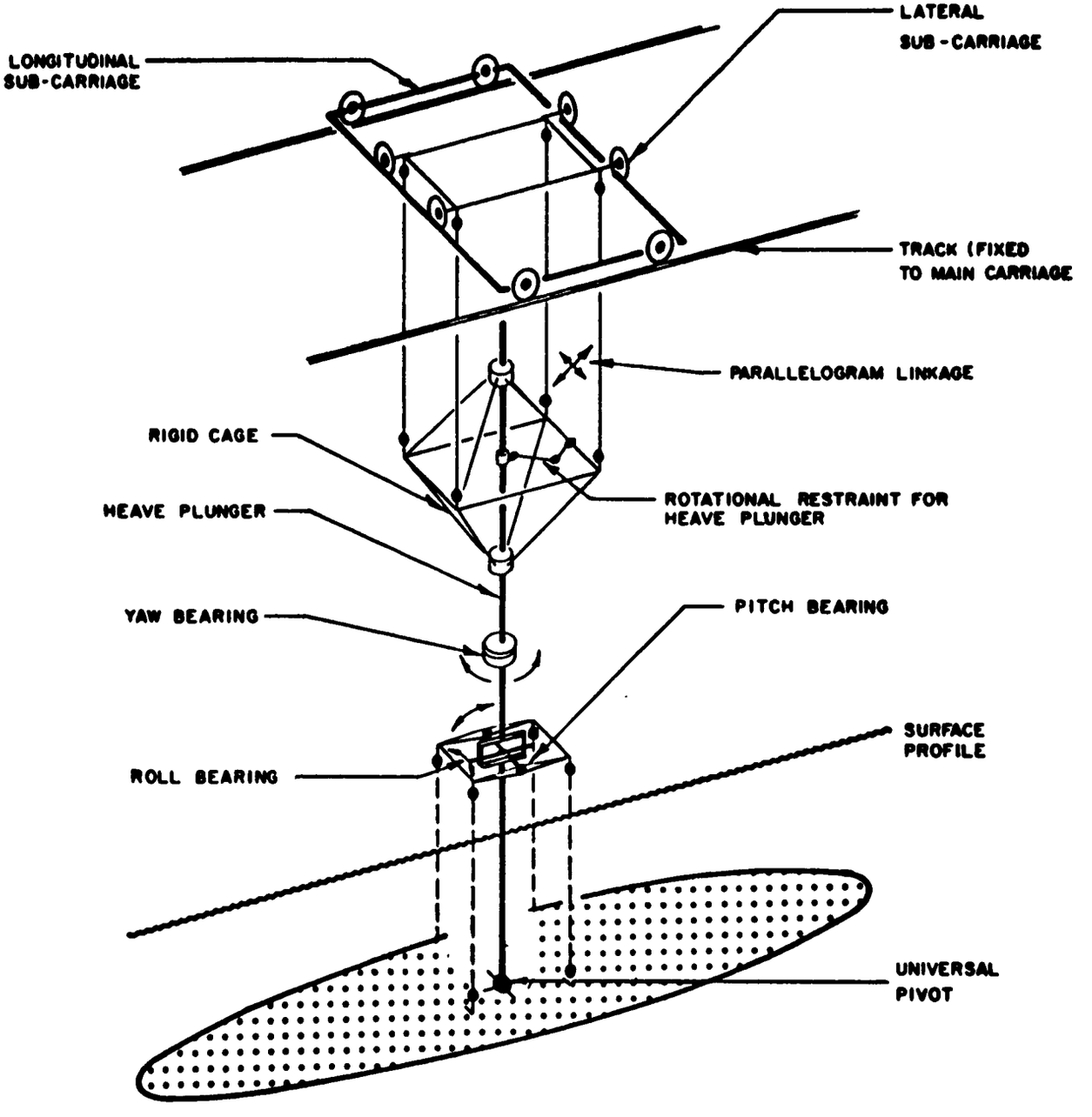

FIGURE 2. DAVIDSON LABORATORY MOTIONS APPARATUS AND EXPERIMENTAL SET - UP

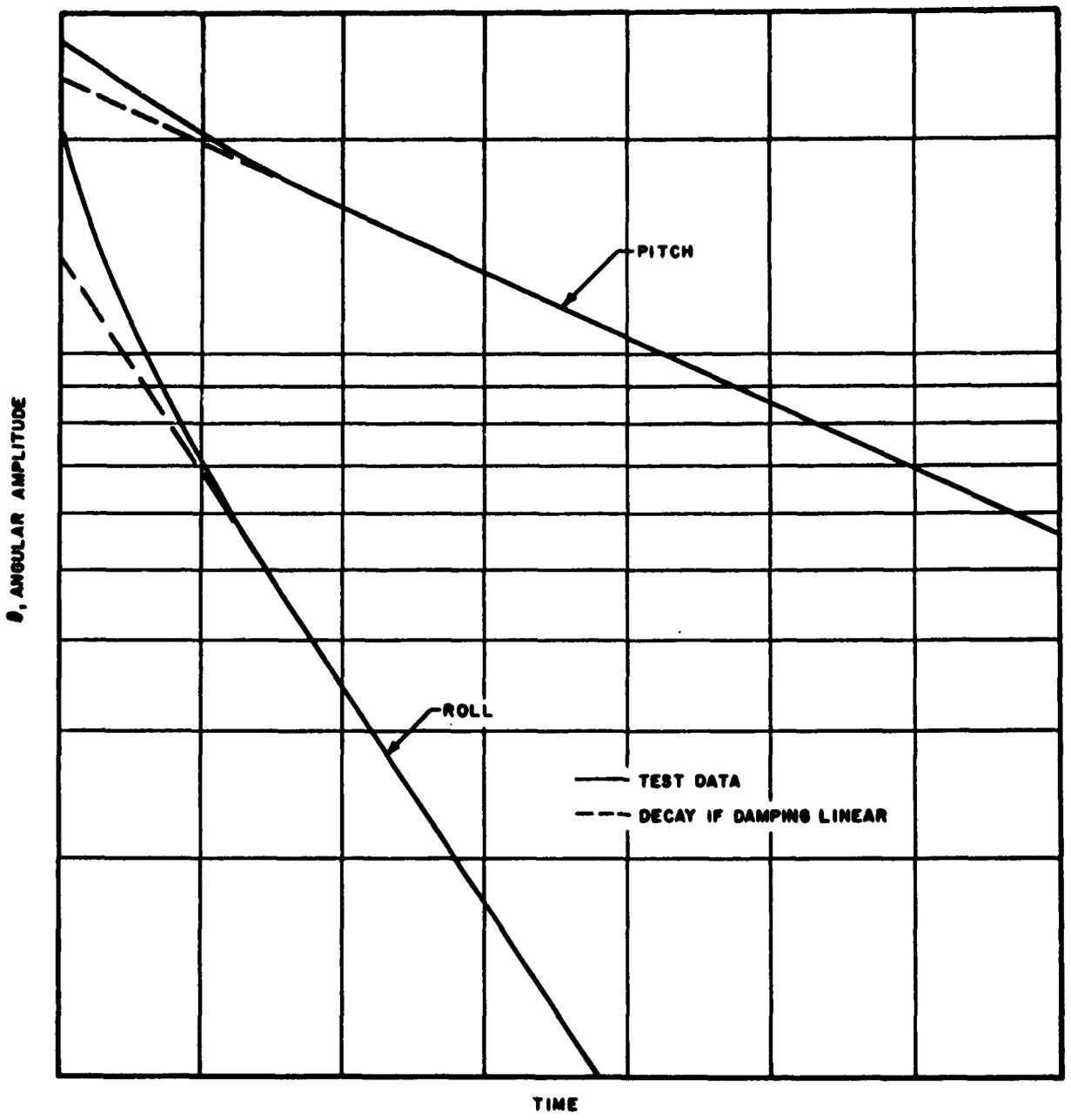

FIGURE 3. ROLL AND PITCH AMPLITUDE DECAY FREE OSCILLATIONS

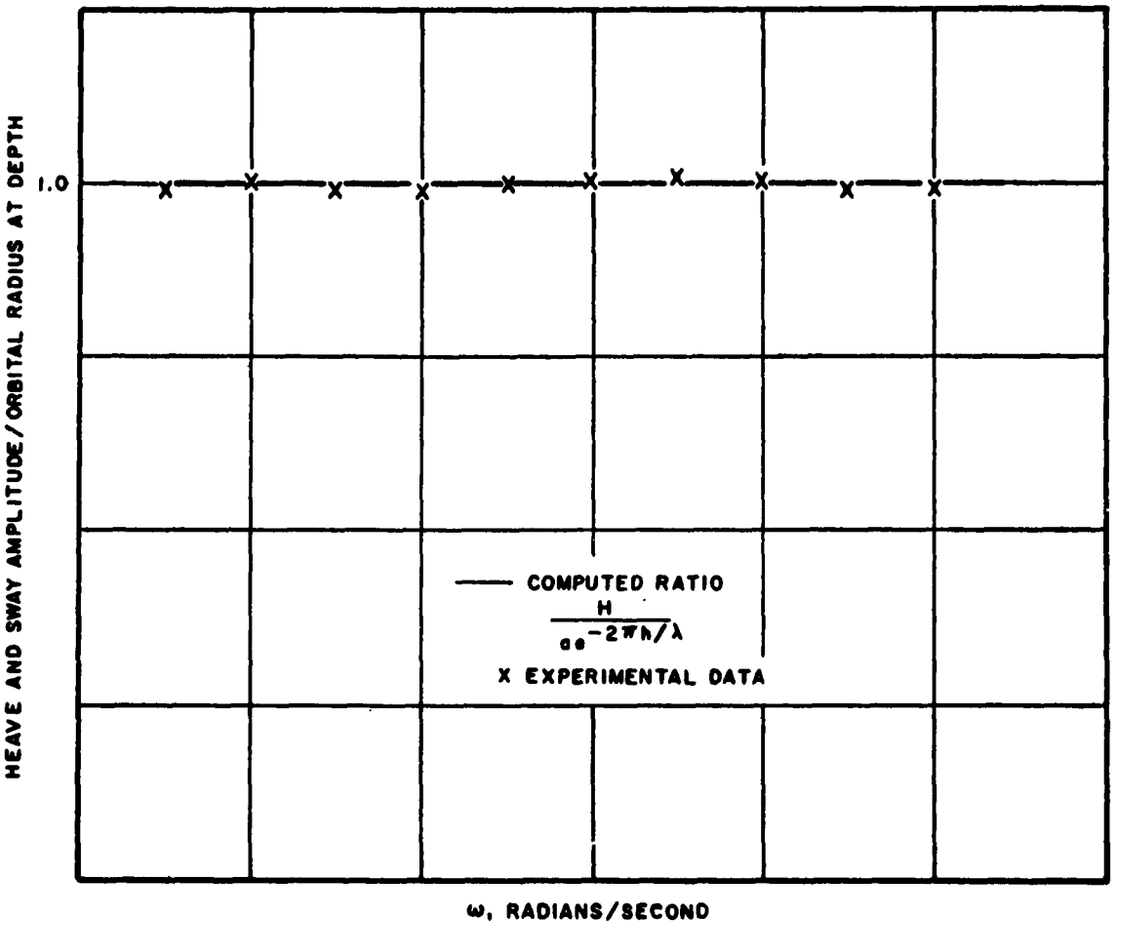

FIGURE 4. HEAVE AND SWAY MOTIONS VERSUS WAVE FREQUENCY REGULAR BEAM SEAS

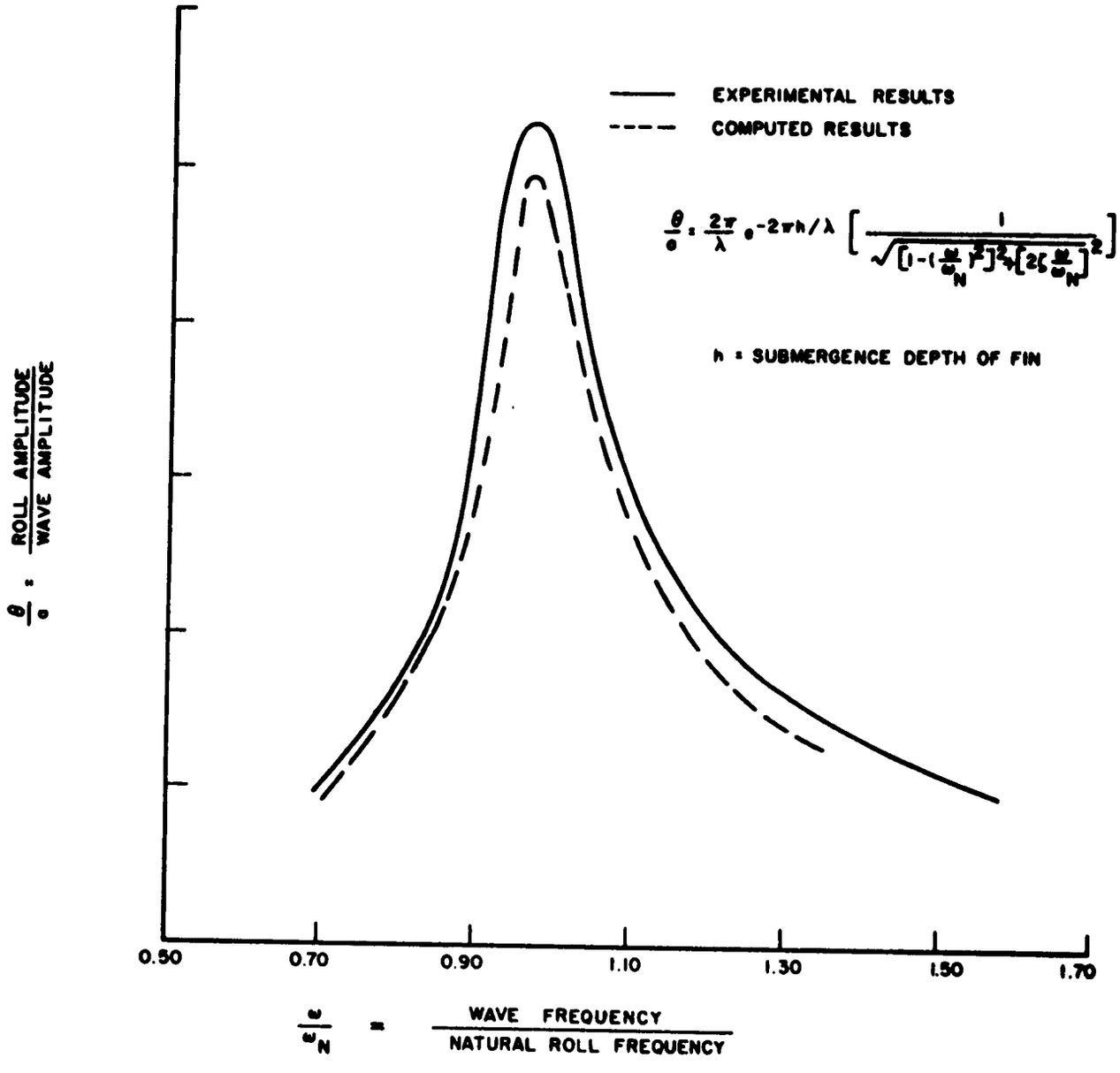

FIGURE 5. COMPARISON OF COMPUTED VERSUS ROLL ANGLE IN REGULAR BEAM SEAS

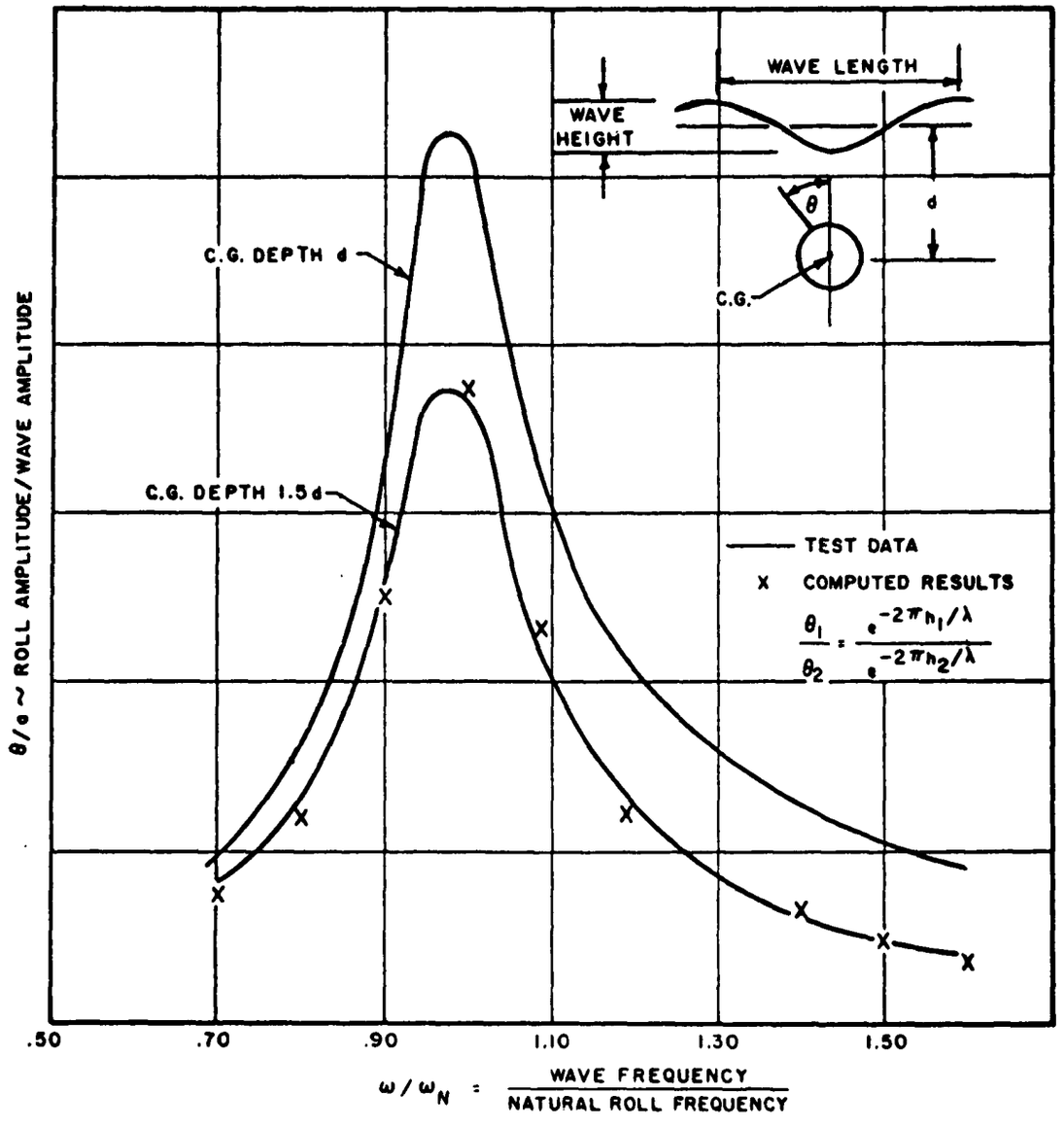

FIGURE 6. ROLL ANGLE AMPLITUDE VERSUS FREQUENCY RATIO FOR UNIT WAVE AMPLITUDE REGULAR BEAM SEAS

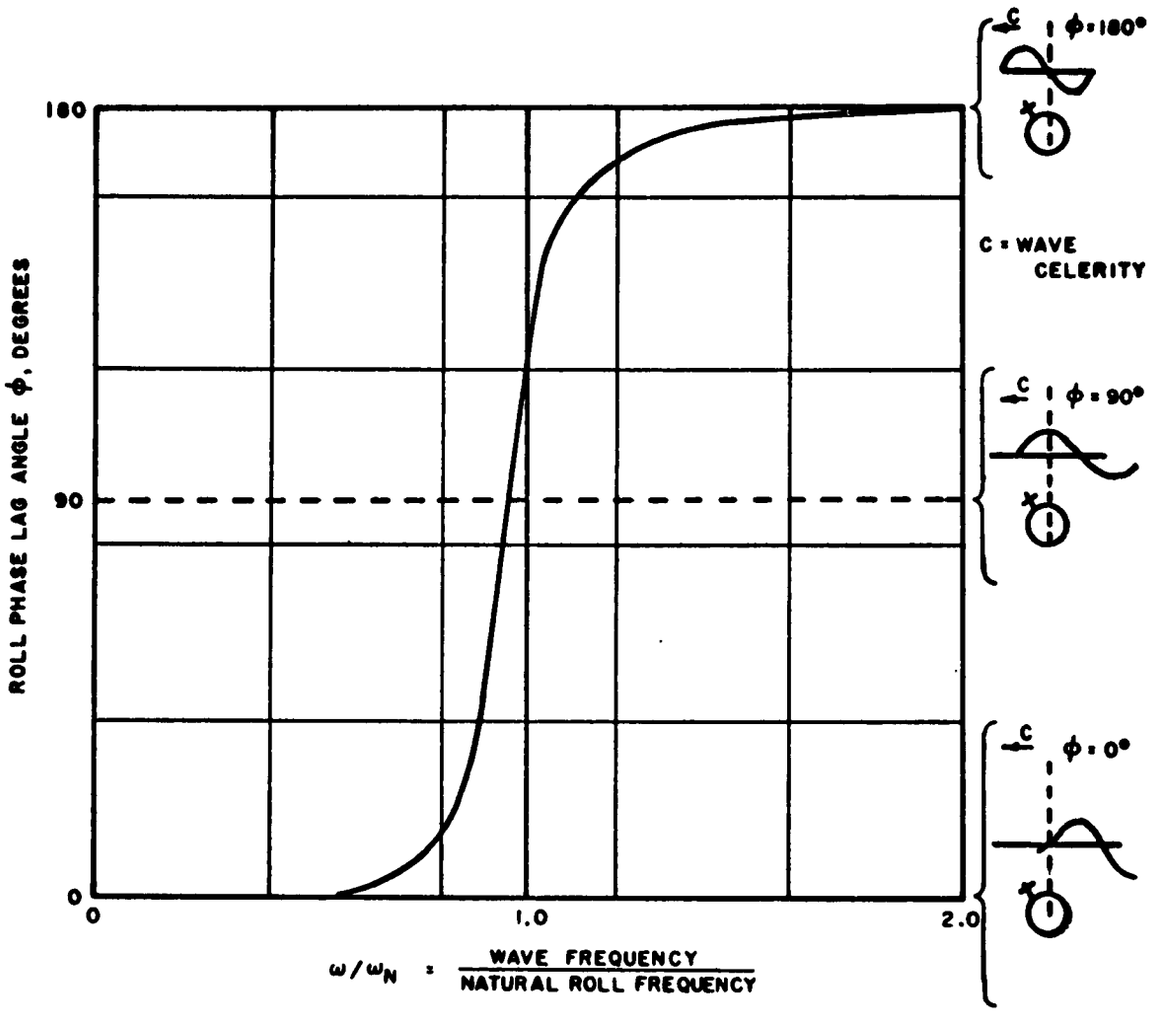

FIGURE 7. PHASE ANGLE BETWEEN MAXIMUM ROLL AND MAXIMUM WAVE SLOPE REGULAR BEAM SEAS

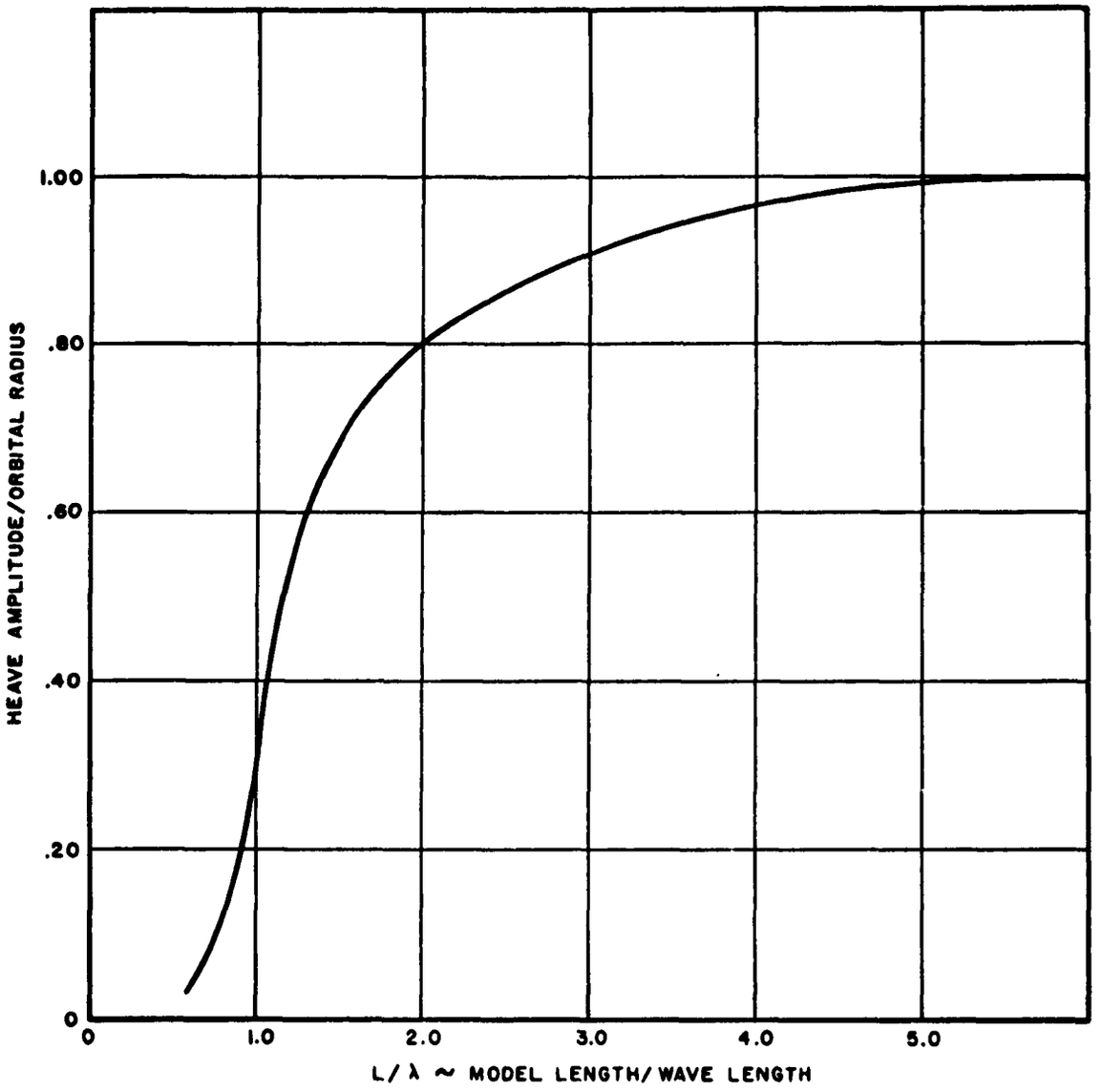

FIGURE 8. $\frac{\text{HEAVE AMPLITUDE}}{\text{ORBIT RADIUS}}$ VERSUS $\frac{\text{MODEL LENGTH}}{\text{WAVE LENGTH}}$ REGULAR HEAD SEAS

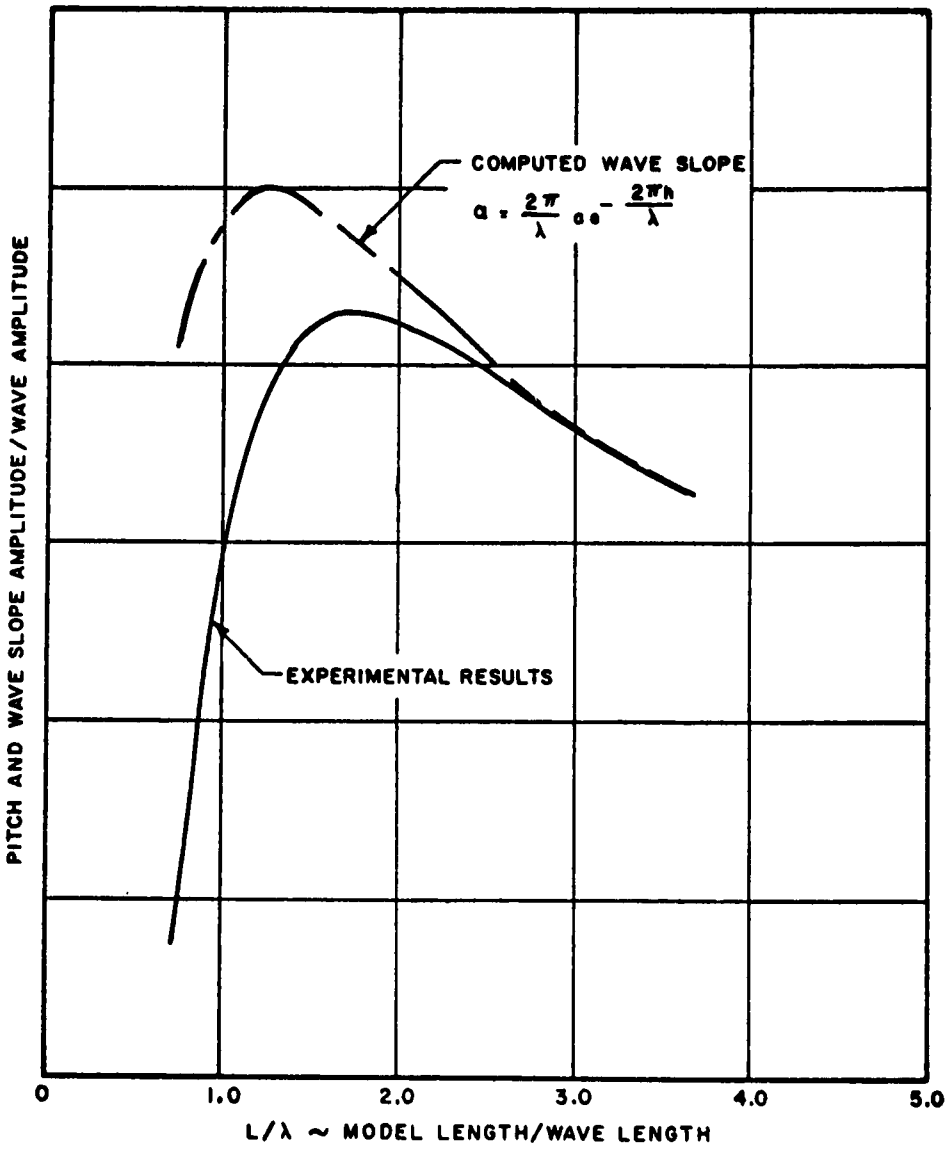

FIGURE 9. PITCH ANGLE AND EFFECTIVE WAVE SLOPE AT DEPTH VERSUS WAVE LENGTH REGULAR HEAD SEAS

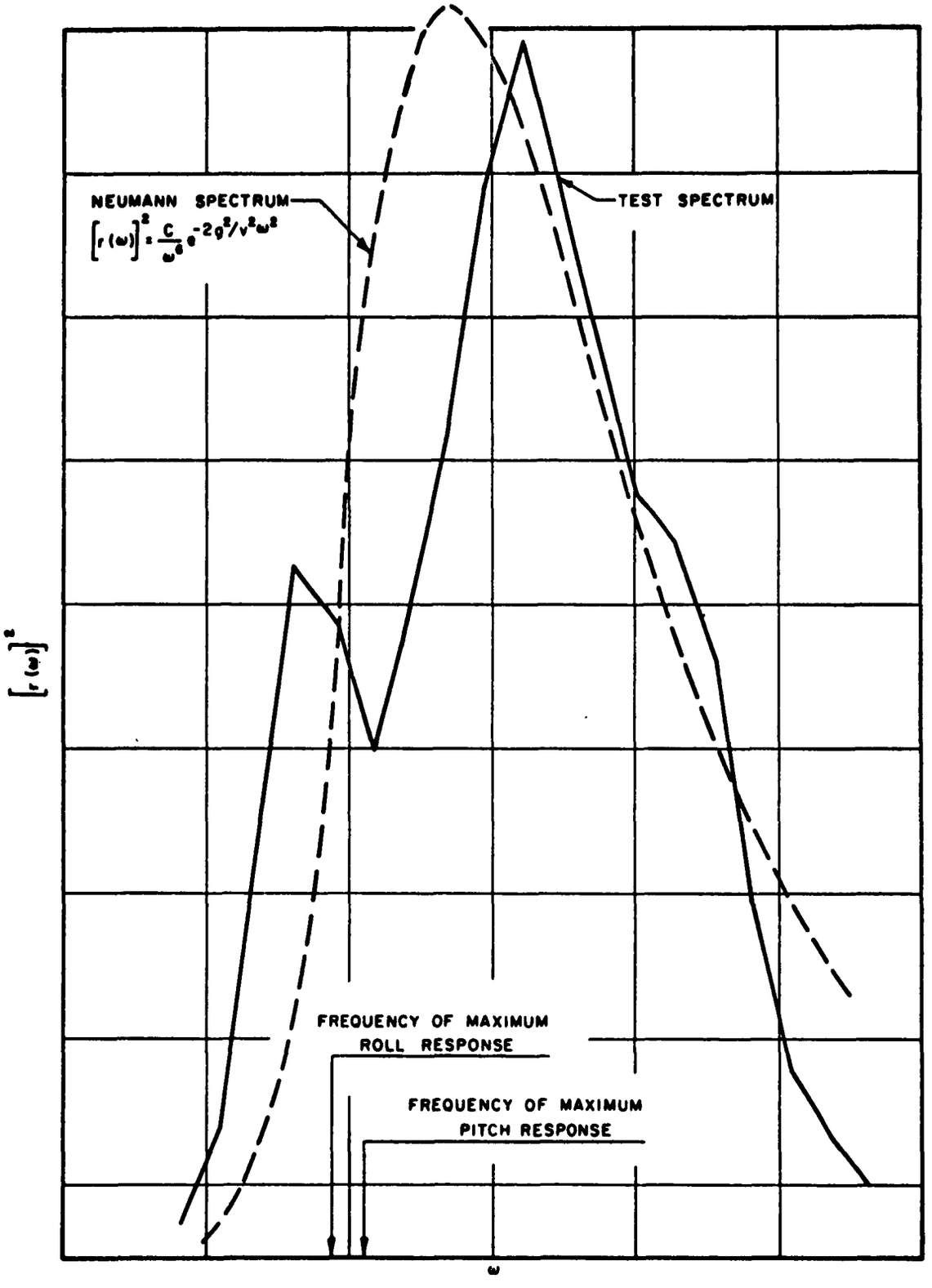

FIGURE 10. ENERGY SPECTRUM IN IRREGULAR WAVE TESTS

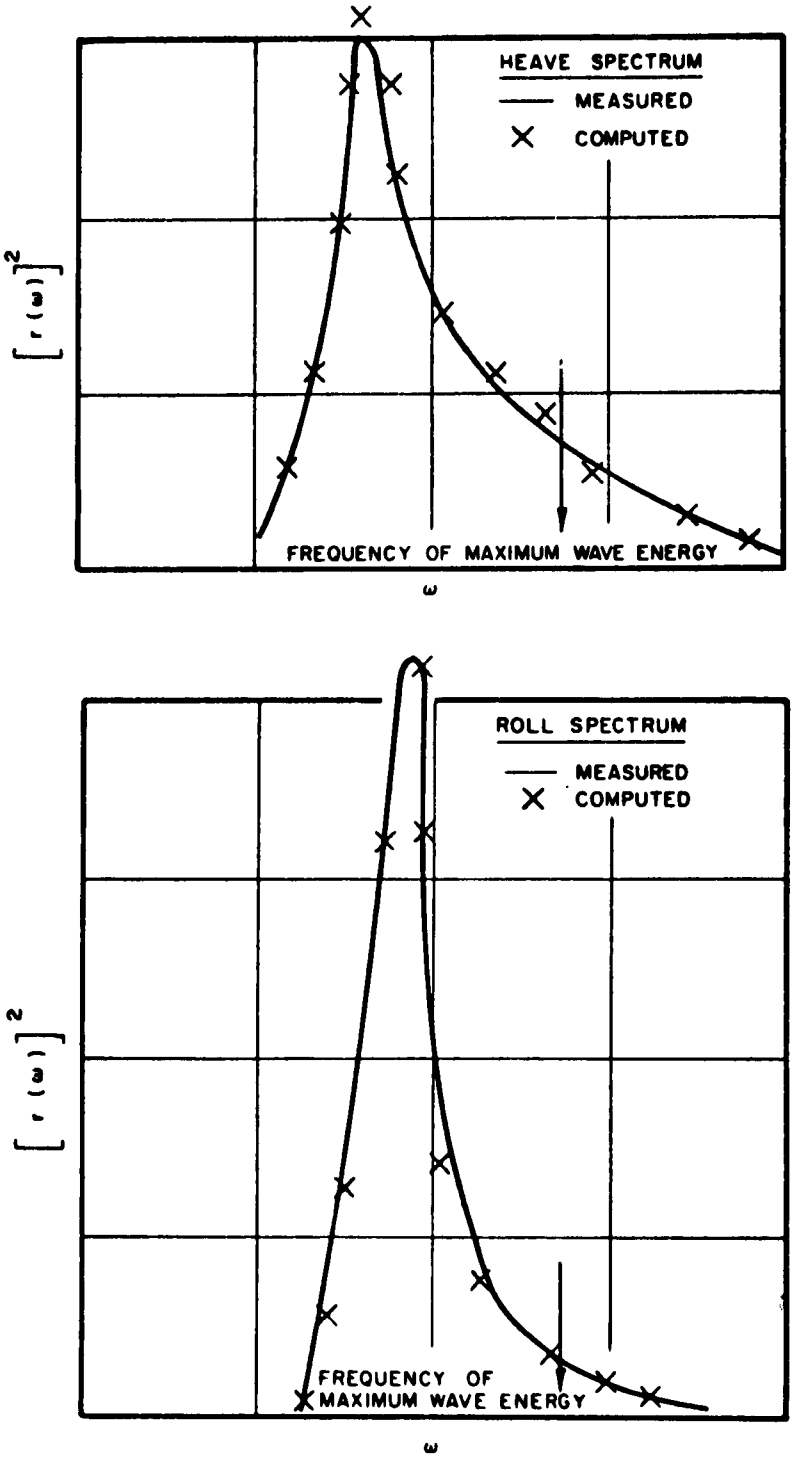

FIGURE 11. MEASURED AND COMPUTED MOTION SPECTRA IN IRREGULAR BEAM SEAS

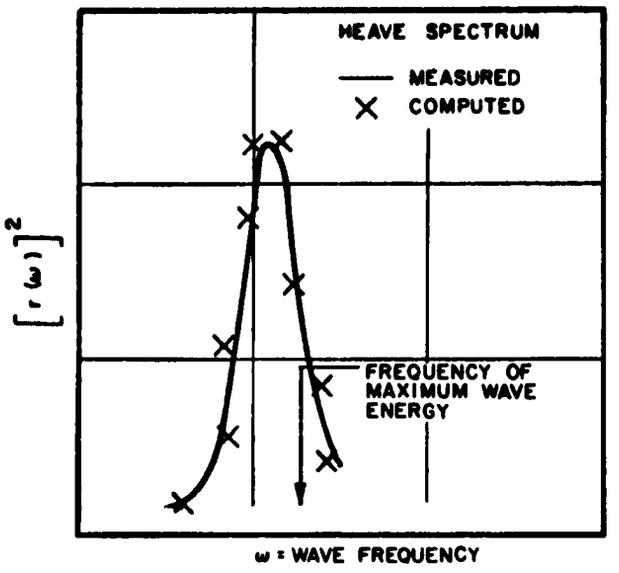

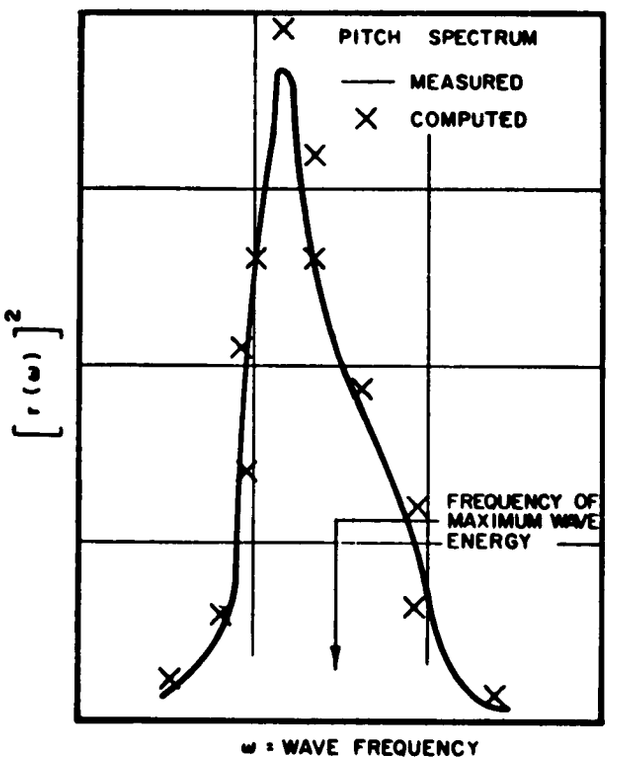

FIGURE 12. MEASURED AND COMPUTED MOTION SPECTRA IN IRREGULAR HEAD SEAS

RESEARCH ON HIGH SPEED SHIP FORMS

Earl M. Uram
Staff Scientist
Davidson Laboratory
Stevens Institute of Technology

I. INTRODUCTION

In recent years ship designers and hydrodynamists have been directing increased efforts to the problem of obtaining higher speeds for ships at sea. As we know, there are at least two things of major interest; the horsepower required to attain a given ship speed in calm and rough waters and the maintainance of tolerable ship motions at high speeds in a rough sea. It is this latter requirement that most times dictates speed limitations of small, high performance ships in the 3,000 ton displacement class such as destroyers. It is well known that the major contribution to the calm water horsepower requirement for ships at high speeds is that required to overcome wave making. Naturally any methods used to reduce the wave-making resistance of a ship should not adversely affect the ship motions and, if possible, should tend to decrease the ship motions under rough sea conditions. Figure 1 illustrates the directions taken in attempts to develop high speed ship forms using the destroyer as a basis. It is well known that for a same displacement just lengthening the ship reduces the wave-making resistance and gives the ship somewhat better motion characteristics at a given speed. The limitations of this approach are quite obvious. Another way to achieve the higher speed is to design the hull so that it planes at the higher speeds thus making use of the dynamic pressure available at those speeds. However, planing boats suffer from severe motions even in the lowest sea states and are quite limited in size. The next logical step would be to get the ship out of the water such as is done with the hydrofoil craft. Such craft have excellent horsepower to displacement characteristics and also have very acceptable motion characteristics in reasonable seas but their size appears to be quite limited. Current estimations of the largest-size hydrofoil craft feasible are in the vicinity of 500 to 1,000 displacement.

The technique of reducing ship wave resistance at a given speed by the use of large forward or aft bulbs, or combinations of the two, has received much attention in recent years. Work done here at Davidson Laboratory and by Inui[2] in Japan has shown that this is a successful means of attenuating wave resistance. However, attenuation is achieved only in a narrow speed band. P. Van Mater[3] of Davidson Laboratory has investigated the motion and powering characteristics of a large double bulbed ship and has found that improvements in resistance as well as pitching motions are definitely realized. However, detrimental heave motion characteristics had been introduced for the particular model used. This technique appears to warrant further serious investigation. Another direction in reducing the motion characteristics in a sea of a destroyer type hull is to run the conventional hull submerged as in the semi-submerged ship concept of Lewis and Odenbret.[4] This effectively puts more damping into the system and reduces the motions. However, as seen in Fig. 2 the penalty paid in the horsepower requirement is prohibitive.

Present nuclear power plants become large and unacceptable for the power required in the vicinity of 45 knots for a ship displacement of the size under consideration. Keeping in mind the desire to continue using air-breathing power plants, the concept of operating a ship completely submerged as a conventional submarine although offering the best seakeeping and horsepower characteristics at reasonably deep depth will, at present, be ruled out. It is, however, included in Fig. 2 for comparison. The attenuation of wave resistance with depth as well as the reduced effect of the surface characteristics on the motion of a shallow running craft make such a concept quite attractive. The horsepower requirements for several versions of such craft are indicated in Fig. 2. The shark form suggested by Boericke[5] with the large strut extending over almost the entire length of the ship is very unattractive from a resistance standpoint alone. However, reduction in the size of the strut does make the shallow running submercible quite attractive from the horsepower standpoint. Mandel[6] further encouraged the use of such a vehicle in a recent investigation by noting that a shallow running submercible such as item F with a large strut showed extremely good speed attenuation characteristics under waves. This type of vehicle also provides the attraction of being able to operate at Froude numbers, say, in the vicinity of 1 which could not be achieved with a surface craft unless it were a planing design. At Froude numbers in this range the wave resistance of a submerged vehicle running shallow is extremely attenuated and no longer is the major contributing factor in the horsepower requirements.

A most serious problem connected with the semi-submarine concept is the fact that the vehicle has to operate with very limited depth excursions in order not to broach the surface or not to submerge its air-breathing apparatus. Therefore, the inherent stability and control characteristics of such a vehicle at high speeds is most important. It is apparent that the semi-submarine with a single strut emerging from the water for the air supply is a most unstable vehicle unless provided with a very sophisticated automatic control. During the past year at Davidson Laboratory we have been investigating a configuration which should provide inherent stability in the craft in the roll, pitch and heave motions. Since a drag penalty must be paid for the surface piercing elements in order to handle the air-breathing apparatus, it is proposed that this surface piercing element should be a surface piercing dihedral hydrofoil system large enough to supply the required air to the engines but designed to provide forces only for control purposes rather than for support of the entire craft-as is the case with a hydrofoil craft. Figure 3 is an illustration of this concept referred to as the Hydrofoil-Semi-Submarine. The remainder of this paper will be directed to the investigation of this type of craft conducted here at Davidson Laboratory which has been supported jointly by the Bureau of Ships and the Office of Naval Research.

II. THE HYDROFOIL SEMI-SUBMARINE

The stability and control characteristics of the envisioned hydrofoil semi-submarine, Fig. 3, are of prime importance, since the vehicle must operate in a very restricted manner in the vertical plane. It is also, however, of major importance to determine desirable configuration characteristics from a power requirement standpoint. An initial study was made of streamlined bodies of revolution in order to determine the resistance characteristics relative to the requirements of this particular study. That is, to determine, for a given displacement, whether or not there exists an optimum fineness ratio for a body operating at the anticipated design speeds from the standpoint of horsepower required. It was also of interest to know whether available air-breathing power plants such as the marine version of the aircraft gas turbine could be used to supply sufficient power for such vehicles. This study indicated that the wave-making resistance of such bodies moving near the surface at Froude number near unity can be taken to be practically independent of the fineness ratio of the body. Also, the wave-making resistance coefficient of such streamlined bodies in the Froude number range of interest is approximately 25% of their frictional resistance coefficient. It was therefore inter-

esting to look at the effective horsepower required for such bodies at deep submergence for varying fineness ratio with constant displacement. Figure 4 contains curves of the specific horsepower as a function of body length with fineness ratio and velocity as parameters. Two separate sets of curves are shown, one for 45-knot and one for 60-knot speeds. The parameter for the solid curves on the plot is the fineness ratio of the body. Since the velocity is constant for the family of fineness ratio curves shown in each curve set, it is possible and informative to associate with the length variable a corresponding Froude number for that particular velocity. A secondary scale of Froude number is included in the abscissa of the figure. It should be kept in mind that in the Froude number range between 0.8 and approximately 1.4 it is possible to assume that the wave-making resistance for near surface operation of a streamline body of revolution is roughly 25% of its deep submergence frictional coefficient. The dashed curves show constant displacement parametric curves.

It is apparent that for a design displacement of 3,000 tons and a design Froude number of operation of 1.0 that there is an optimum fineness ratio that one should consider using for a 45 knot craft: that fineness ratio being L/d of 5. It was estimated that using an L/d of 5 and accounting for the additional resistances of the hydrofoil system and the stern planes that the required horsepower for a 3,000 ton vehicle would be in the vicinity of 90,000 horsepower. It is conceivable that such a horsepower requirement could be met by a complex of four converted aircraft gas turbine engines, each producing in the vicinity of 30,000 horsepower. This is in keeping with the current state of the art for such power plants.

The next part of the study involved determining the size and position of the main hydrofoil system as well as the stern control planes and their sizes. Under most conditions, it is desirable to operate the craft with its body axis in a horizontal position for all velocities. It was therefore necessary to determine the balance of the static forces and moments on the craft to maintain a zero-pitch trim condition at all speeds. It is timely to recall at this point that not only must the hydrodynamic forces and moments generally experienced by such a craft be taken into account, but one must also include the forces induced as a result of the proximity of the free water surface to the vehicle. The craft is subjected to a vertical force as well as a pitching moment due to the free surface condition, Figs. 5 and 6. As seen from the figures, the vertical force changes sign and magnitude depending upon the Froude number involved. It also changes magnitude with the depth of submergence. For a body of the

fineness ratio chosen for this configuration, the pitch moment is seen not to change sign but, in general, would change sign at low Froude numbers. The pitch moment, also, is a function of Froude number and the depth of submergence as indicated in the figures. The static trim force and moment equations were programmed on a digital computer with the output devised to maintain zero trim and yield information concerning the location of the main foil system, the size of the horizontal stern plane necessary and the amount of variable ballast that the ship would need. The configuration was selected so that the variable ballast to maintain trim should not exceed 5% of the boat displacement. The additional requirement that the angles of the dihedral foil system and horizontal stern plane be kept to a minimum was imposed so as to induce as little drag as possible from these devices.

It is of interest to note here the configuration of the stern planes. The horizontal stern plane is located off the centerline - a distance of one maximum body radius below the axis of the craft. This puts the horizontal stern plane outside the boundary layer of the ship which makes it more effective for its size and takes advantage of the pitching moment induced by the drag on the plane.

It was of further interest, before proceeding with the construction of a model of this configuration, to investigate the dynamic stability of the vehicle. The pitch and heave equations of motion, discussed by prior papers during this symposium, can be put into the form shown in Fig. 7. The best estimates in keeping with the current state of the art of the hydrodynamic forces and moments encountered and their derivatives, were inserted in the equations after they were programmed for the analog computer at Davidson Laboratory. The response of the boat due to an initial disturbance was determined. It was found, as demonstrated in Fig. 8, that this configuration when operating without the influence of a free surface is quite stable dynamically. However, because of the change in sign of the vertical force at the very low Froude numbers, it is possible that the vehicle would not be stable if one included the free surface effects. Figure 9 shows the response of the vehicle one might expect at the low Froude number and indicates that the vehicle is quite stable in pitch, but because of the unbalance in vertical forces there is a net tendency of the craft to broach. This can be overcome by including in the computer program (and in the ship) a proportional control for the stern planes. This study indicated to us that it was advisable to build a model for investigation which would have stern plane control built into it.

The final dimensions and characteristics of the craft that was decided upon is indicated in Table 1. The model

TABLE I

HYDROFOIL SEMI-SUBMARINE

PRINCIPAL DATA

	SHIP		MODEL
LENGTH	168.5 FT		3.75 FT
MAXIMUM DIAMETER	33.75 FT		0.75 FT
DISPLACEMENT	2700 TONS		62.25 LBS
HYDROFOIL			
CHORD	15 FT	(20% FLAP)	0.33 FT
SPAN (PLANFORM)	80.4 FT		1.785 FT
DIHEDRAL	35°		35°
PLANFORM ASPECT RATIO	5.36		5.36
HORIZONTAL STERN PLANE			
CHORD	15 FT		0.33 FT
SPAN	34 FT		0.756 FT
ASPECT RATIO	2.26		2.26

Earl M. Uram

contains a variable volume ballast tank on its centerline designed such that ballast of the model can be varied to within 5% of the model displacement without changing the center of gravity of the model. Also included in the design are stern planes that can be servo-controlled proportional to excursions in the vertical plane. The model, constructed in the Davidson Laboratory shop, was completed in April of this year and checked out for testing by the first week of June.

The test program incorporates plans to test the model under restraint of all degrees of freedom to determine the forces and moment on the ship in such a manner to discern the contributions from each of the various appendages on the model. Upon completion of this, the craft will undergo tests in motion studies to determine its motion characteristics in calm seas and regular and irregular ahead and following seas. The initial restrained conditions tests of the model were completed last week and I am therefore able to present some preliminary data which is of considerable interest.

Data reduced to date are relative to measurements of the total resistance and EHP requirements and the vertical force. Figure 10 shows the behavior of the vertical force coefficient versus the Froude number. The dashed curve represents the vertical force coefficient for a spheroid with a submergence-to-length ratio of 0.3. This is equivalent to the centerline 1-1/2 diameters below the surface. We see that the curve for the hydrofoil semi-submarine crosses the axis (that is vertical force changes sign) much before that for the spheroid and the coefficient magnitude is substantially larger at high Froude numbers. Both the deviation from a spheroid of the hull geometry and the significant hydrofoil configuration contribute to this behavior. The hydrofoil making a major contribution since its Froude number is much higher than the hull and it is substantially closer to the surface than the hull. Figure 11 is the usual calm water total resistance coefficient versus Reynolds number plot on which the Schoenherr friction resistance curve is also shown. In order to estimate the effective horsepower required and to extrapolate this to the Reynolds number of the full scale ship, an increment of 30% of the Schoenherr resistance of the bare body was added to account for the frictional resistance of the foils, stern planes and fairing. The resulting scaled-up total resistance coefficient is also shown in this figure. The dashed curve above the solid one would be the total resistance coefficient if the residual resistance were calculated without the 30% allowance for the appendages. Figure 12 is a comparison of the effective horsepower required for the hydrofoil semi-submarine in calm water with that required by several of the ship forms pre-

viously discussed. All information on this figure is taken from experimental model data and includes two comparable destroyers, the large bulb ship and the semi-submerged ship. We see that the hydrofoil semi-submarine, above approximately 30 knots, is substantially better than any of the others as far as the effective horsepower is concerned. In particular, at the designed speed of 45 knots, the effective horsepower required by the more conventional surface ships is some 45% more than that required by the hydrofoil-semi-submarine. We do notice, however, in the low speed range between 18 and 30 knots, that the hydrofoil-semi-submarine horsepower requirements are larger than the others. This is a result of the Froude numbers corresponding to that speed range being those at which this particular craft generates the largest amount of wave resistance. It is possible, however, to overcome this problem.

As part of this investigation, an analytical study was made in order to determine methods by which the wave resistance of such a craft might be attenuated in any part of the Froude number range, especially in the part where it compares unfavorably with conventional or modified surface ships. Dr. Pung Hu and Mr. King Eng of our laboratory conducted this part of the analytical work by investigating the characteristics of spheroids moving in the proximity of a free surface. They found by perturbing the geometry of the body that it is possible to substantially reduce the wave resistance over a rather large Froude number range.

Figure 13 shows a spheroid represented by a doublet distribution along its axis. The perturbations of the doublet distribution from the one representing the spheroid are indicated by the various values of the parameter A. The constraint put on the problem were that the configuration must have a constant volume. That is, the perturbation to the doublet distribution must not contribute or detract from the displacement of the original body. The net effect of the perturbation is essentially to neck down the body in the region of the center of the body. It was not possible to find a closed form solution to the integral containing the doublet distribution for calculating the wave resistance of the body. Therefore, the problem was programmed for the IBM 1620 computer. The results obtained relative to the particular configuration we are speaking about here are shown in Figure 14. Actually a range of fineness ratio and depth to length ratio was covered during the study and the behavior of the wave resistance behavior due to these perturbations were studied in a much more complete manner.

However, for our purposes, we see in Fig. 14 that the wave resistance coefficient versus Froude number plot for

the original spheroid is the heavy line on the figure and the effect of the perturbations for variations in the parameter A are shown with the other curves. It is seen that above a Froude number of 0.3 a substantial reduction in the wave-making resistance of such a body moving in the proximity of the surface is realizable. The reduction in many cases in the Froude number range between 0.35 and .5 is in the vicinity of 40 to 60% of the resistance. However, a penalty is paid at a lower Froude number. A judicious choice must be made of the perturbation parameter so that the wave resistance is not unacceptably increased at particular Froude numbers.

Figure 15 is a photograph of the model running in the towing tank. One can see the surface piercing hydrofoil configuration as well as the model (under water) and the six component balance used to measure forces and moments. It is planned to complete the constrained model tests and to use the force and moment measurements in oder to get a more realistic prediction of the necessary equilibrium trim settings for the ballast and hydrofoil system for the craft during the contemplated motion studies.

III. ACKNOWLEDGMENT

I would like to acknowledge the most able contributions made during the course of this project by Mr. Young Chey of the Davidson Laboratory. Figures 1 and 2 are from ref. 7.

IV. REFERENCES

1. Lewis, E. V. and Breslin, J. P.: "Semi-Submerged Ships for High Speed Operation in Rough Seas," Third Symposium on Naval Hydrodynamics Scheveningen, Netherlands, September 1960.

2. Michelsen, F. C. and Kim, H. C.: "Three Recent Papers by Japanese Authors on the Effect of Bulbs on Wave-Making Resistance of Ships," Dept. of Naval Architecture and Marine Engineering, University of Michigan, Ann Arbor, Michigan.

3. Van Mater, P.: "Preliminary Evaluation of a Large Bulb Ship for Operation in Calm and Rough Water," Davidson Laboratory, Stevens Institute of Technology to be published.

4. Lewis, E. V. and Odenbrett, C.: "Preliminary Evaluation of a Semi-Submerged Ship for High Speed Operation in Rough Seas," SNAME Journal of Ship Research, Vol. 3, No. 4, March 1960.

5. Boericke, H., Jr.: "Unusual Displacement Hull Forms for High Speed," International Shipbuilding Progress, Vol. 6, 1959.

6. Mandel, P.: "The Potential of Semi-Submerged Ships in Rough Water Operation," New England Section, SNAME March 1960.

7. Lewis, E. V. and Breslin, J. P.: "Semi-Submerged Ships for High-Speed Operation in Rough Seas," Presented at Third Symposium on Naval Hydrodynamics, ONR-Netherlands Ship Model Basin, Scheveningen, The Netherlands September 1960

FIG. 1

POSSIBLE DIRECTIONS TO SEEK HIGHER SPEEDS AT SEA

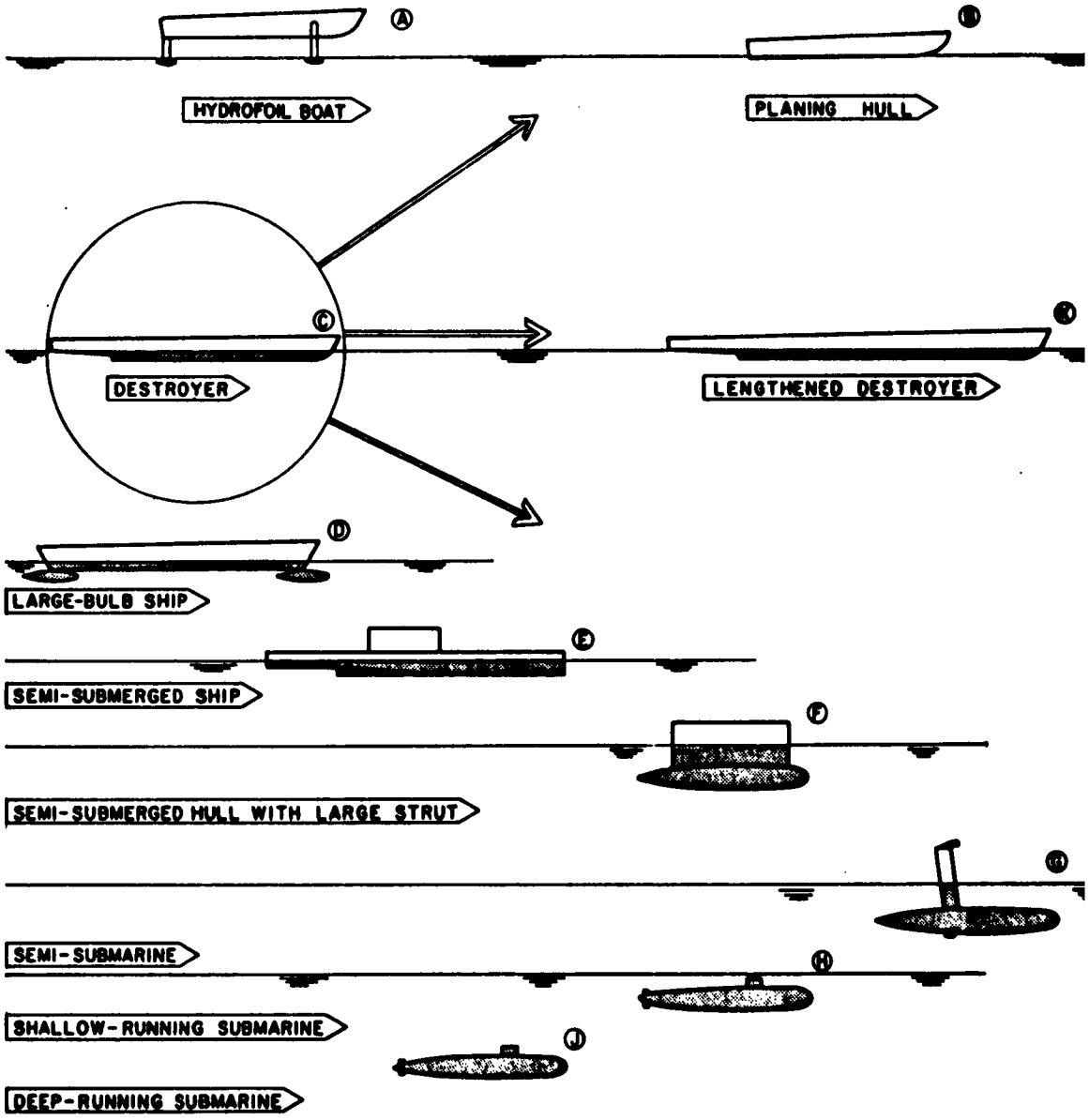

FIG. 2

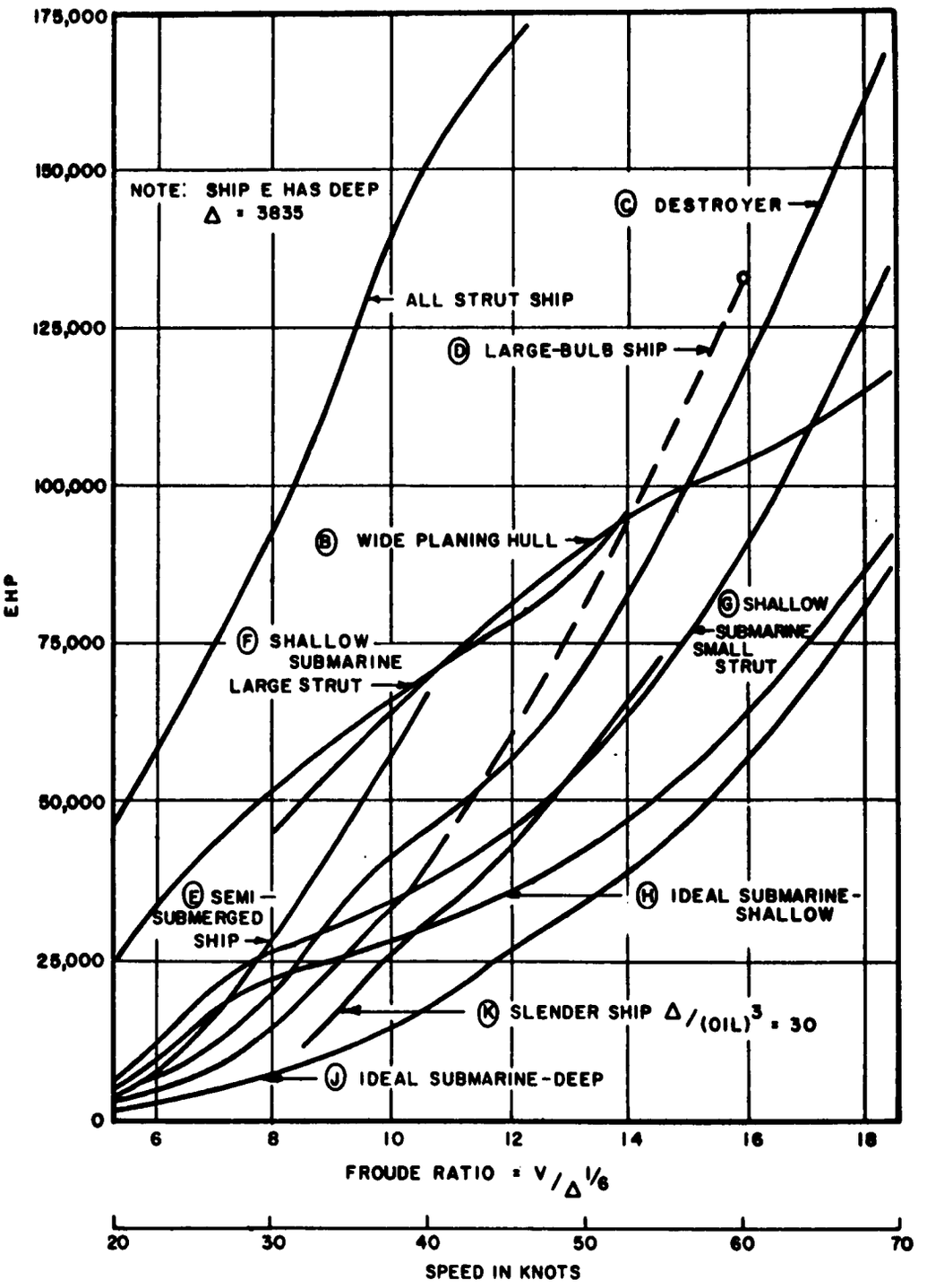

HORSEPOWER REQUIRED FOR VARIOUS SHIP FORMS
(Δ = 2844 TONS)

Earl M. Uram

FIG. 3

HYDROFOIL-SEMI-SUBMARINE

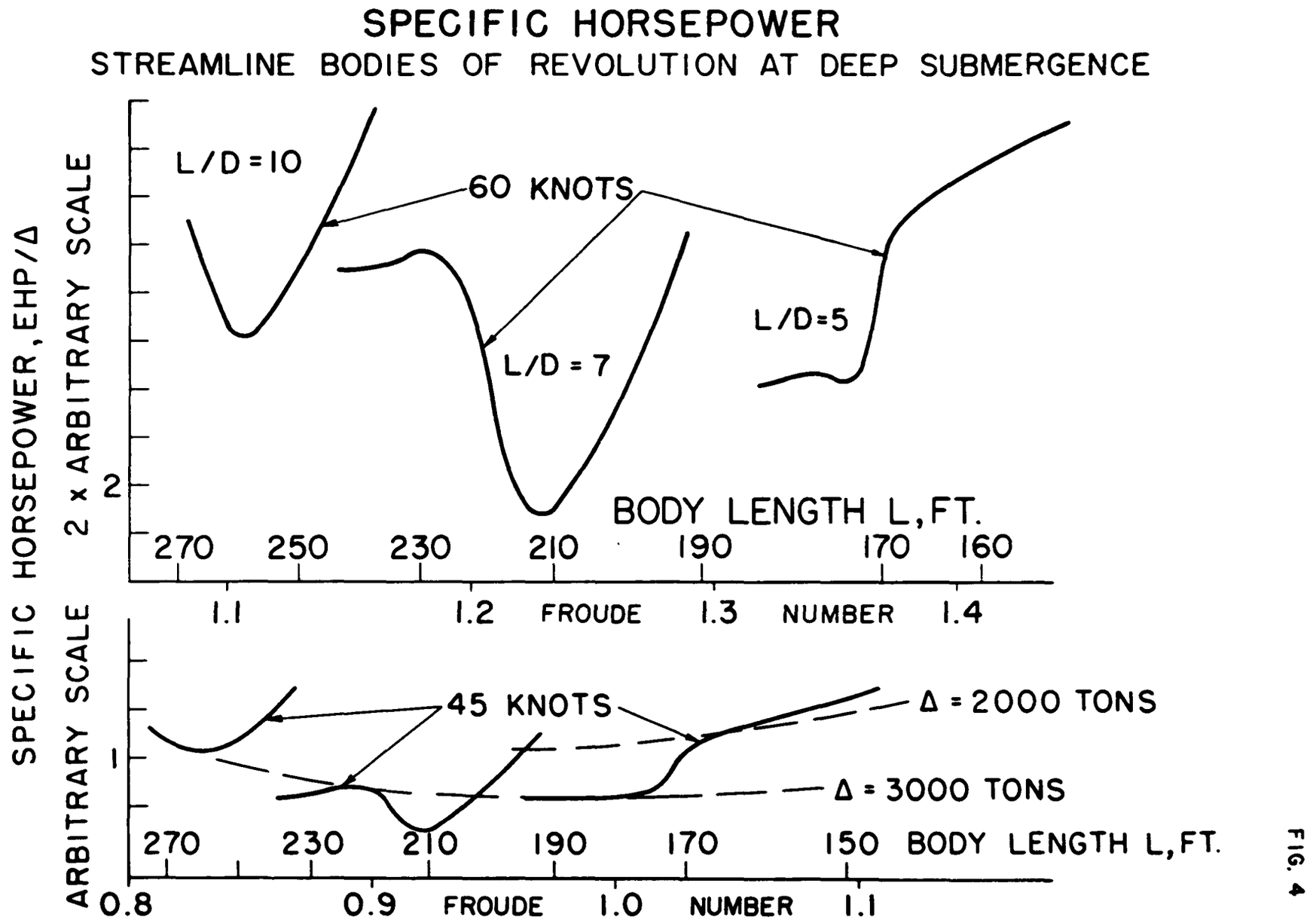
SPECIFIC HORSEPOWER
STREAMLINE BODIES OF REVOLUTION AT DEEP SUBMERGENCE
SPECIFIC HORSEPOWER, EHP/Δ
2 x ARBITRARY SCALE
L/D = 10
60 KNOTS
L/D = 7
L/D = 5
2
BODY LENGTH L, FT.
270 250 230 210 190 170 160
1.1 1.2 FROUDE 1.3 NUMBER 1.4
ARBITRARY SCALE
1
45 KNOTS
Δ = 2000 TONS
Δ = 3000 TONS
270 230 210 190 170 150 BODY LENGTH L, FT.
0.8 0.9 FROUDE 1.0 NUMBER 1.1

FIG. 4

FIG. 5

VERTICAL FORCE COEFFICIENT
(SPHEROID L/D = 5)
SUBMERGENCE z/L = 1.5
FROUDE NUMBER
0
0.4
0.8
1.2
1.6
2.0
2.4
2.8
3.2
3.6
4.0
VERTICAL FORCE COEFFICIENT z'
2
1
0
-1
VERTICAL FORCE DERIVATIVE ∂z'/∂(zL)
10
0
-10

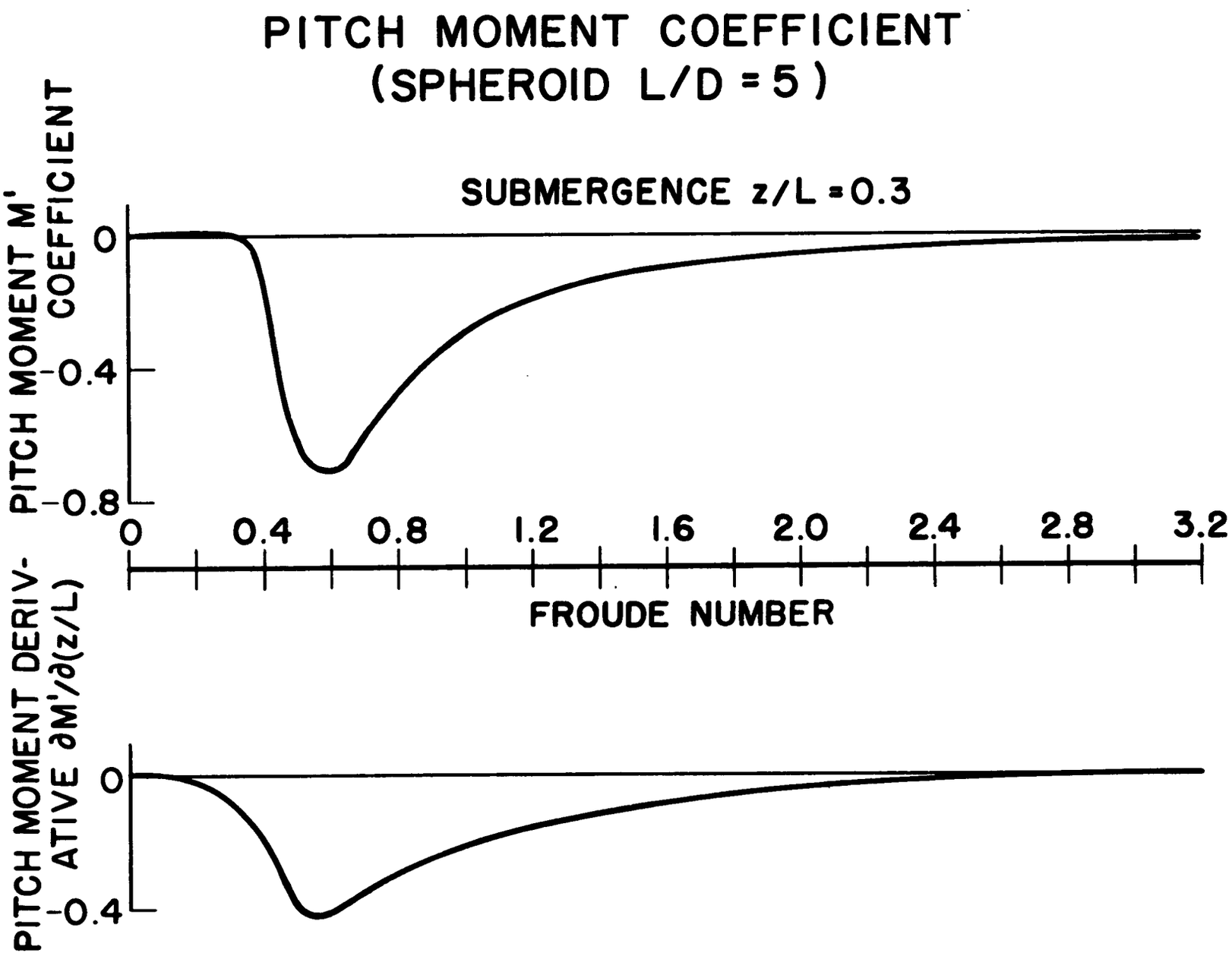
PITCH MOMENT COEFFICIENT
(SPHEROID L/D = 5)
SUBMERGENCE z/L = 0.3
PITCH MOMENT M' COEFFICIENT
0
-0.4
-0.8
0
0.4
0.8
1.2
1.6
2.0
2.4
2.8
3.2
FROUDE NUMBER
PITCH MOMENT DERIV-ATIVE ∂M'/∂(z/L)
0
-0.4

FIG. 6

MOTION EQUATIONS

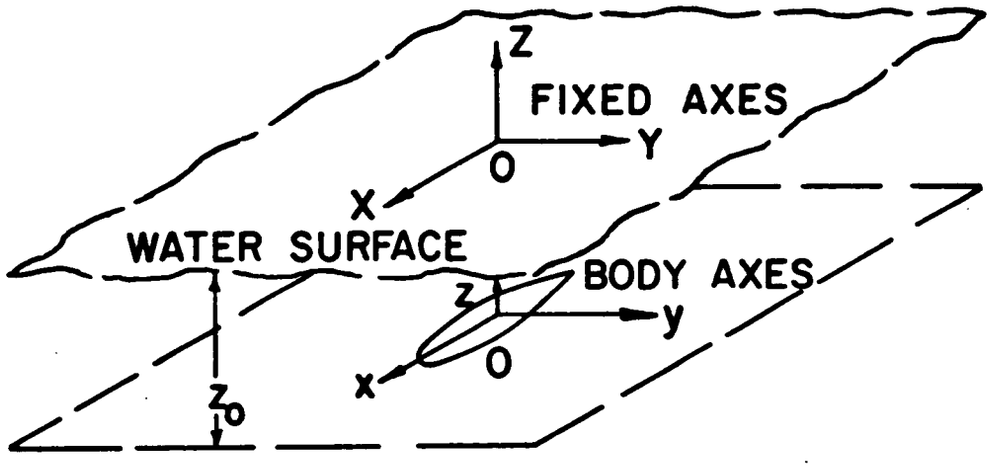

$$0 = a\ddot{z}_o + \left(\frac{\partial F_z}{\partial w}\right)\dot{z}_o + \left(\frac{\partial F_z}{\partial z_o}\right)z_o + \left(\frac{\partial F_z}{\partial \dot{\theta}}\right)\ddot{\theta} + \left(\frac{\partial F_z}{\partial \dot{\theta}} - V\frac{\partial F_z}{\partial \dot{w}}\right)\dot{\theta} + \left(\frac{\partial F_z}{\partial \theta} + V\frac{\partial F_z}{\partial w}\right)\theta$$

$$0 = A\ddot{\theta} + \left(\frac{\partial M}{\partial \dot{\theta}} - V\frac{\partial M}{\partial \dot{w}}\right)\dot{\theta} + \left(\frac{\partial M}{\partial \theta} + V\frac{\partial M}{\partial w}\right)\theta + \left(\frac{\partial M}{\partial \dot{w}}\right)\ddot{z}_o + \left(\frac{\partial M}{\partial w}\right)\dot{z}_o + \left(\frac{\partial M}{\partial z_o}\right)z_o$$

$$w = \dot{z}_o - V\theta + (\xi\dot{\theta})$$

$$\dot{w} = \ddot{z}_o - V\dot{\theta} + (\xi\ddot{\theta} - V\dot{\theta})$$

V = CONSTANT

FIG. 7

Earl W. Uram

SEMI-SUBMARINE STABILITY

RESPONSE TO PITCH DISTURBANCE
SURFACE EFFECTS NEGLECTED

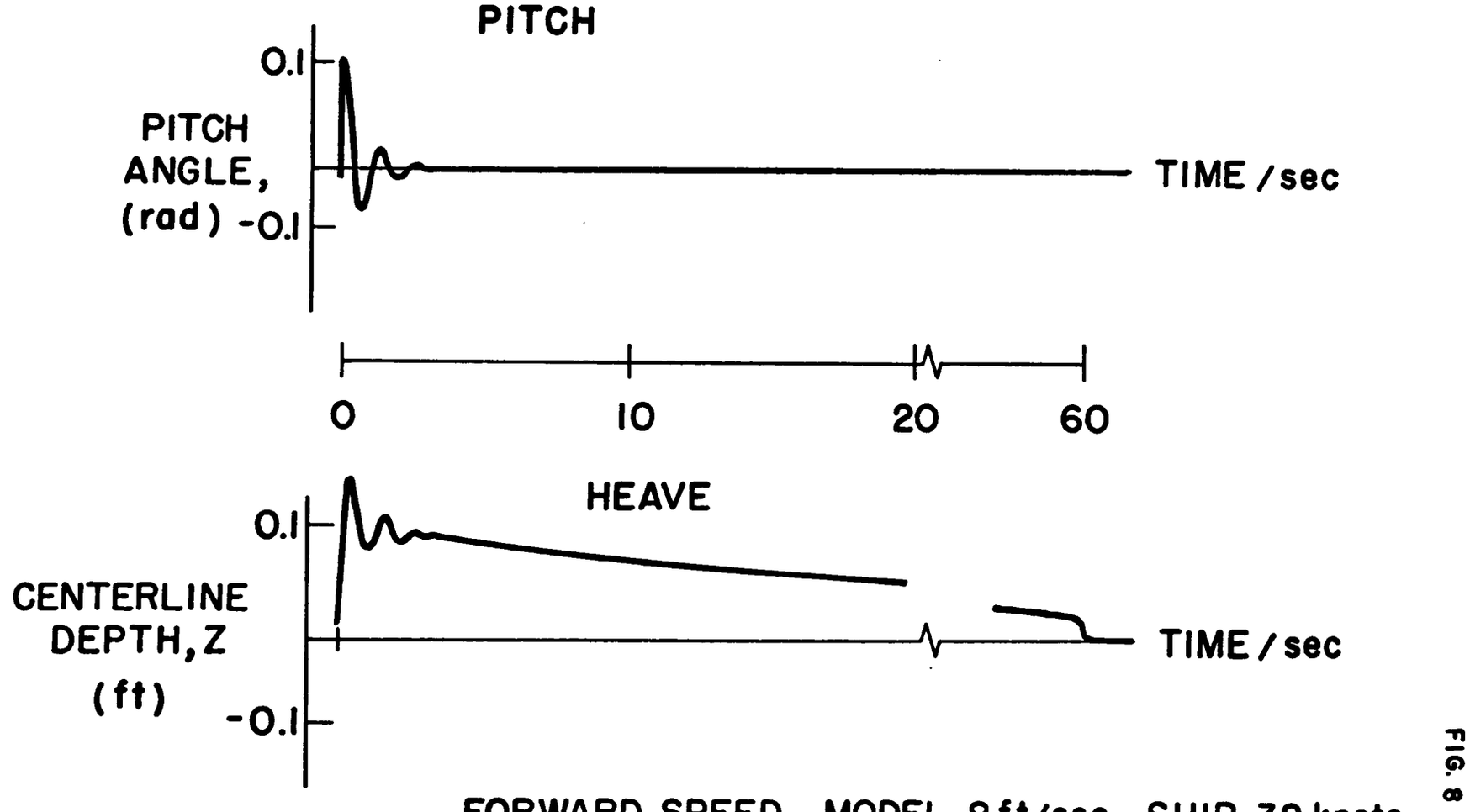

FORWARD SPEED MODEL 8 ft/sec , SHIP 32 knots

FIG. 8

SEMI-SUBMARINE STABILITY

RESPONSE TO PITCH DISTURBANCE

SURFACE EFFECTS INCLUDED

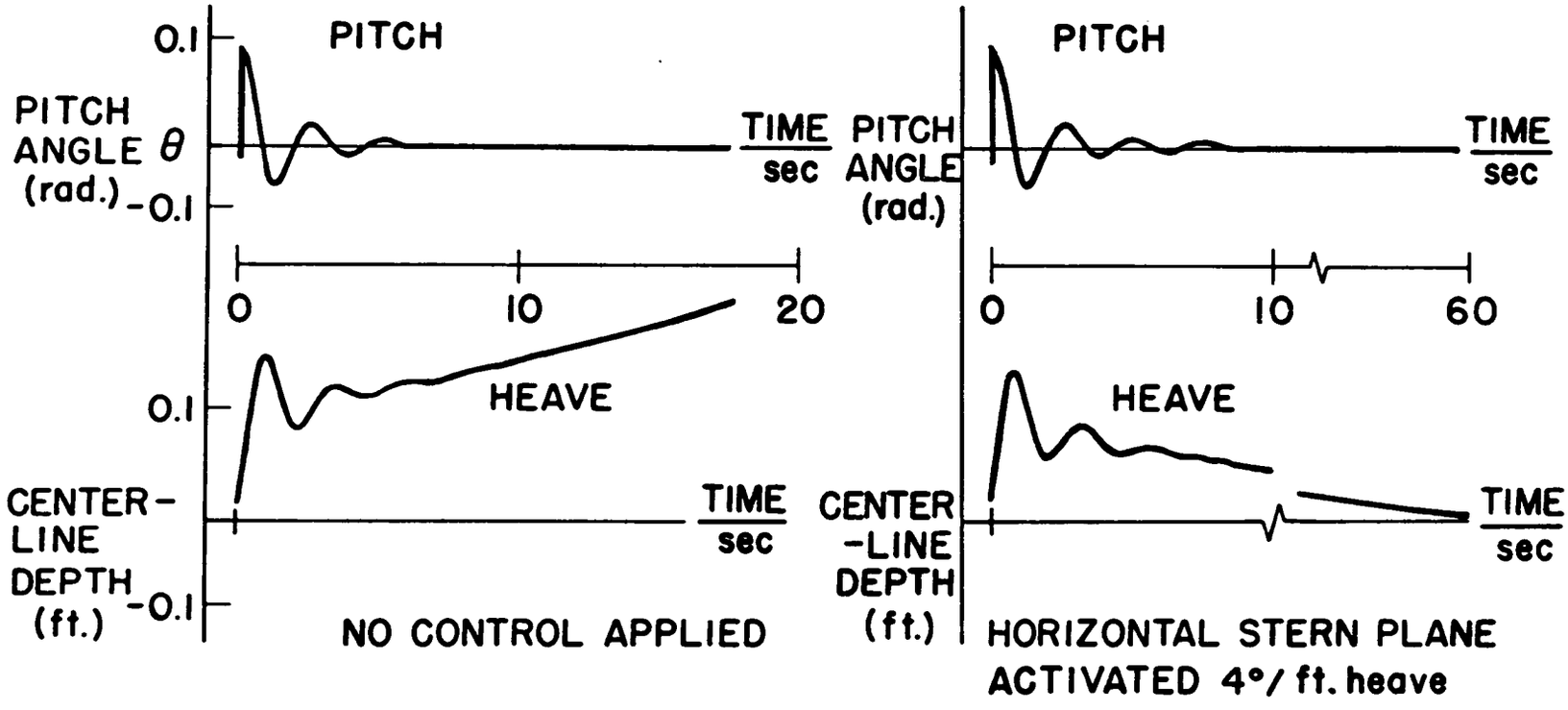

FIG. 9

VERTICAL FORCE
(z/L = 0.3)

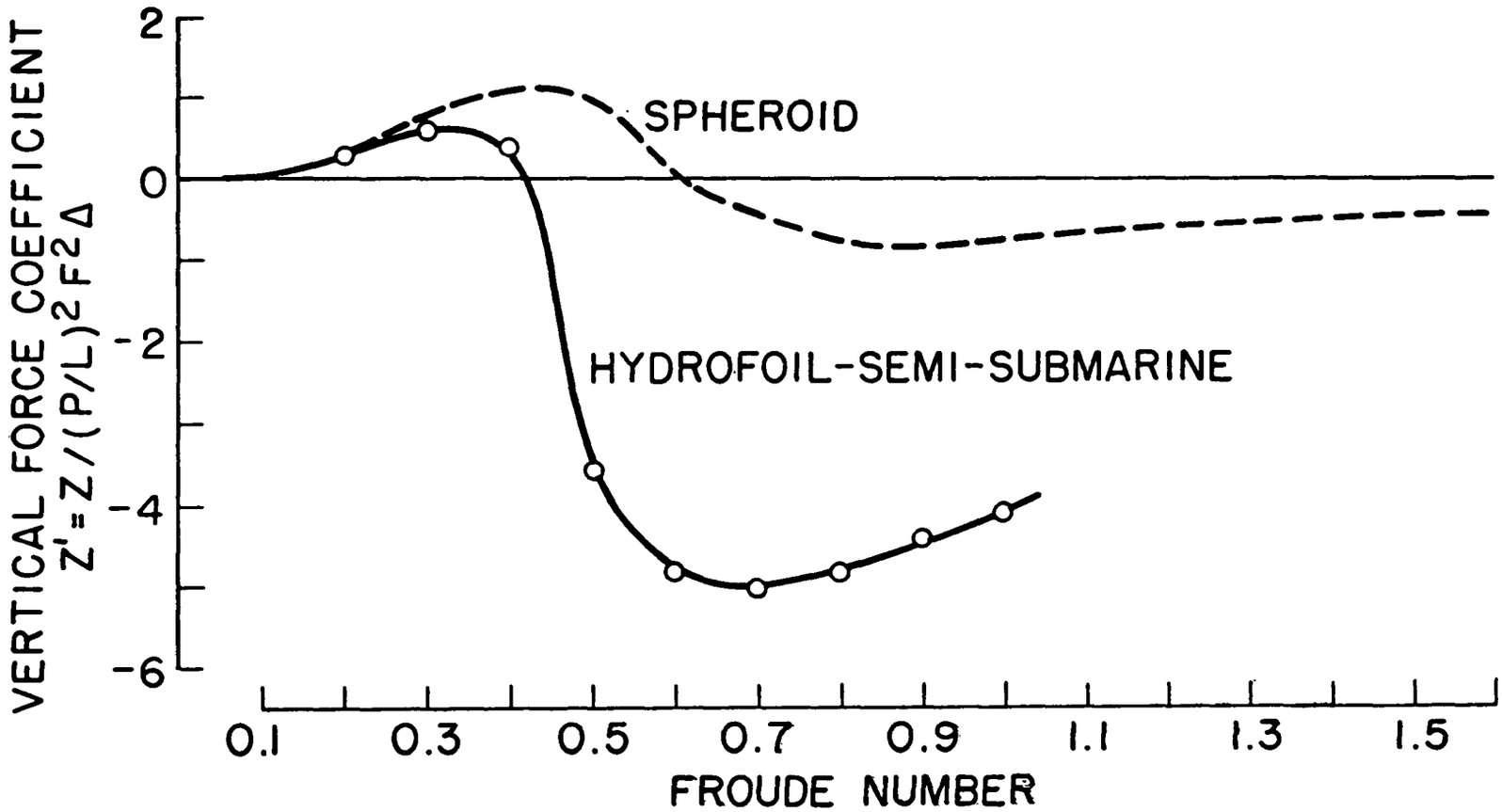

FIG. 10

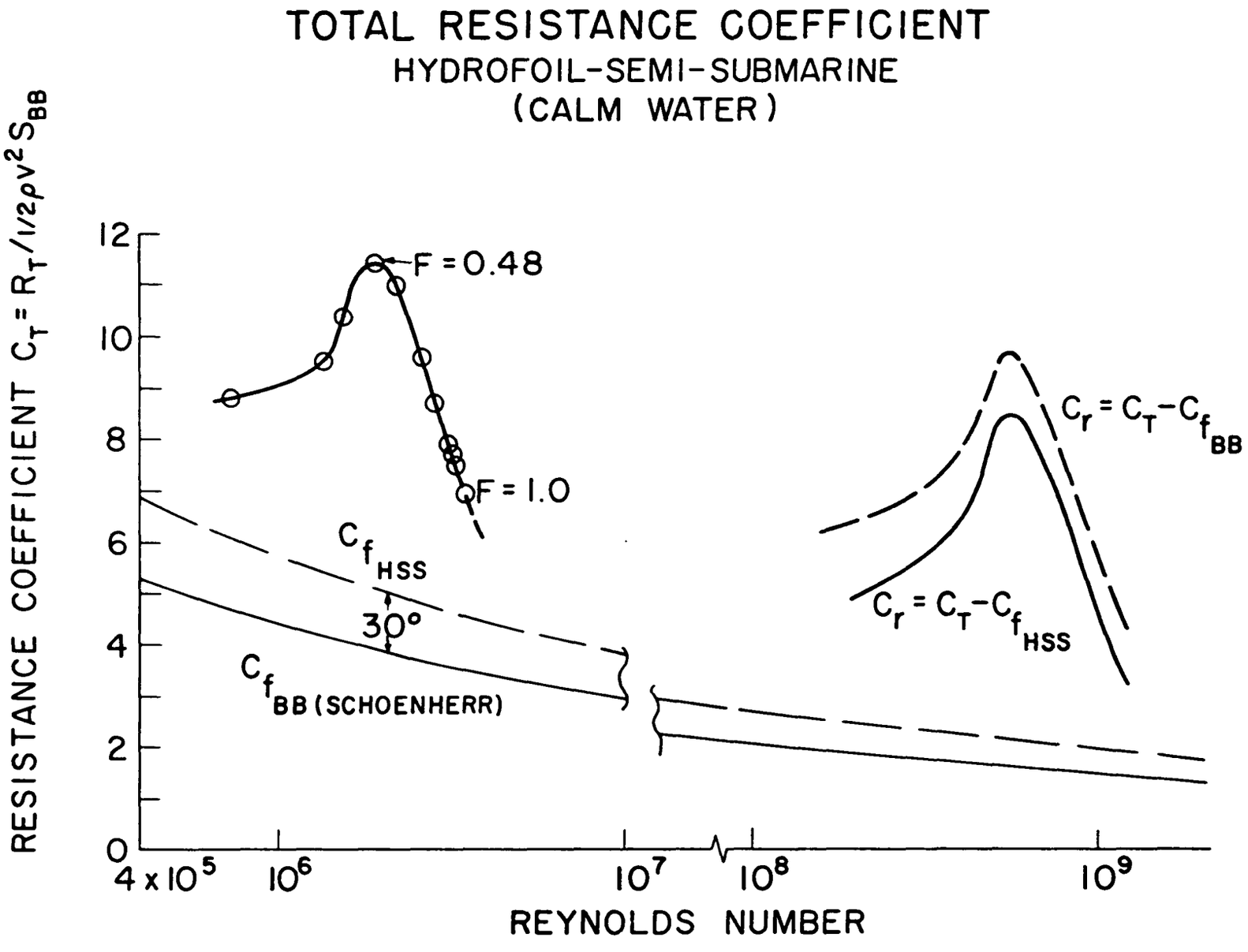
TOTAL RESISTANCE COEFFICIENT
HYDROFOIL-SEMI-SUBMARINE
(CALM WATER)
RESISTANCE COEFFICIENT $C_T = R_T/1/2\rho V^2 S_{BB}$
12
10
8
6
4
2
0
F = 0.48
F = 1.0
$C_{f_{HSS}}$
30°
$C_{f_{BB\ (SCHOENHERR)}}$
$C_r = C_T - C_{f_{BB}}$
$C_r = C_T - C_{f_{HSS}}$
4×10^5
10^6
10^7
10^8
10^9
REYNOLDS NUMBER

FIG. 11

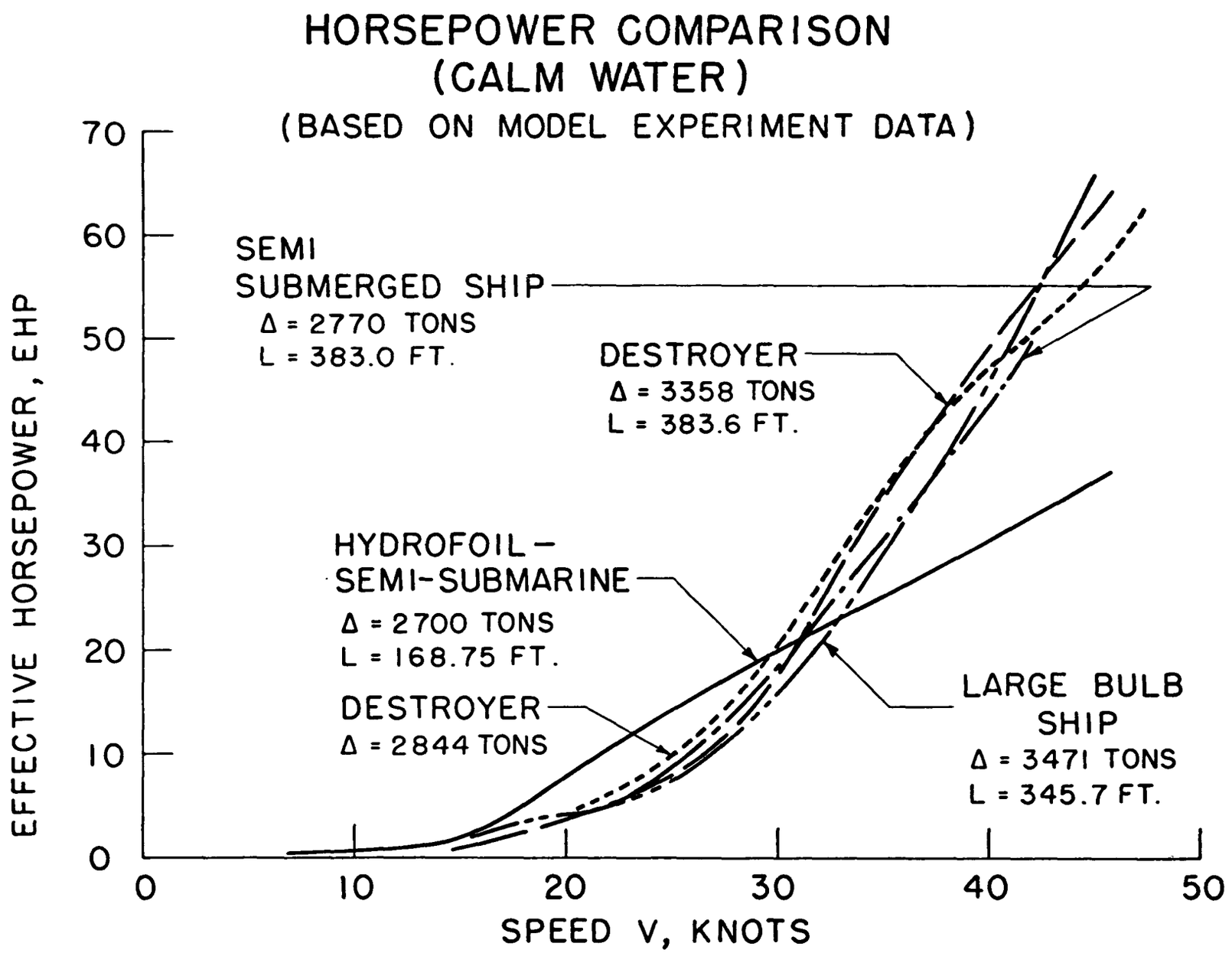
HORSEPOWER COMPARISON
(CALM WATER)
(BASED ON MODEL EXPERIMENT DATA)
EFFECTIVE HORSEPOWER, EHP
SPEED V, KNOTS
0
10
20
30
40
50
60
70
SEMI
SUBMERGED SHIP
Δ = 2770 TONS
L = 383.0 FT.
DESTROYER
Δ = 3358 TONS
L = 383.6 FT.
HYDROFOIL –
SEMI-SUBMARINE
Δ = 2700 TONS
L = 168.75 FT.
DESTROYER
Δ = 2844 TONS
LARGE BULB
SHIP
Δ = 3471 TONS
L = 345.7 FT.

FIG. 12

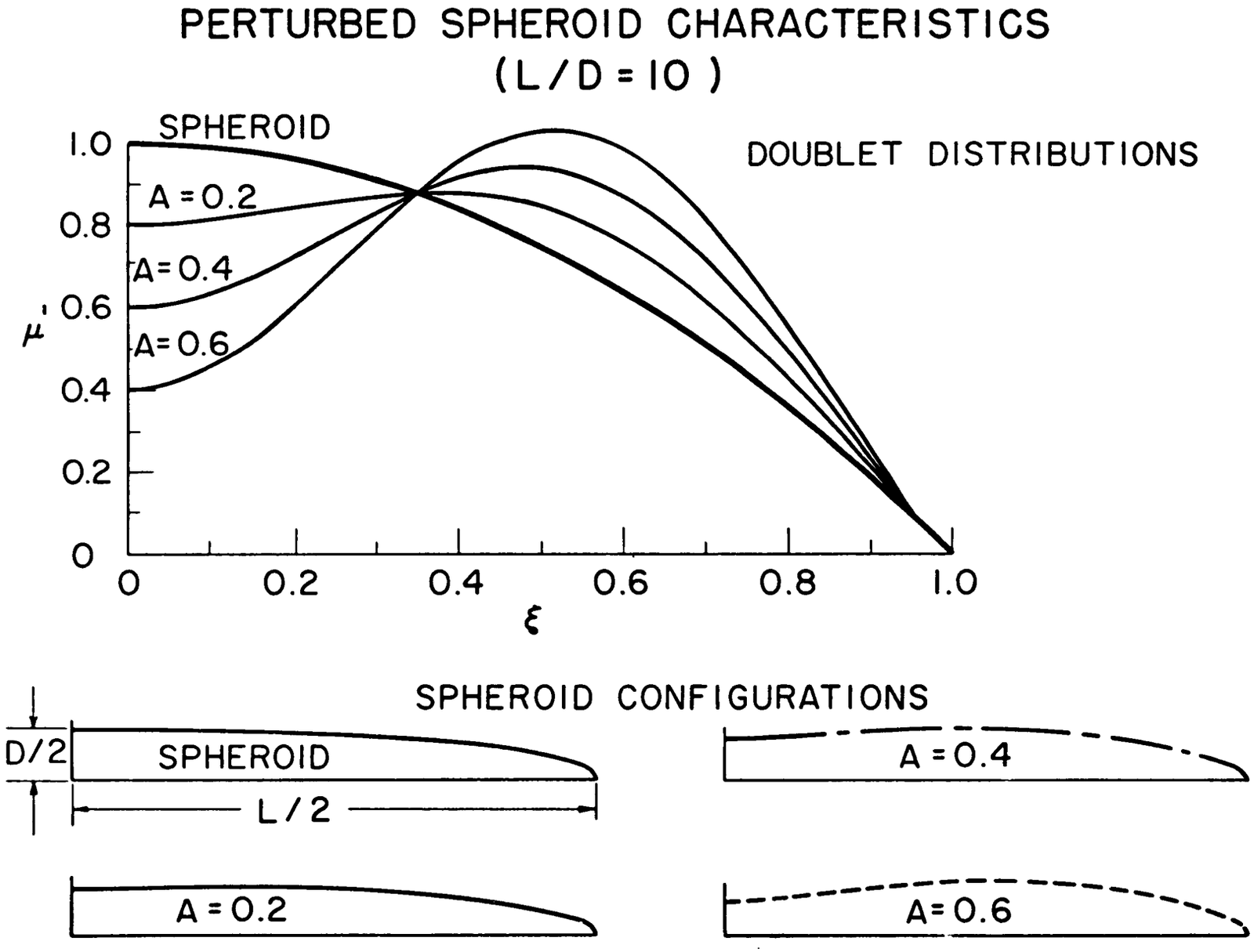
PERTURBED SPHEROID CHARACTERISTICS
(L/D = 10)
DOUBLET DISTRIBUTIONS
SPHEROID
A = 0.2
A = 0.4
A = 0.6
μ'
1.0
0.8
0.6
0.4
0.2
0
0
0.2
0.4
0.6
0.8
1.0
ξ
SPHEROID CONFIGURATIONS
D/2
SPHEROID
L/2
A = 0.4
A = 0.2
A = 0.6

FIG. 13

FIG. 14

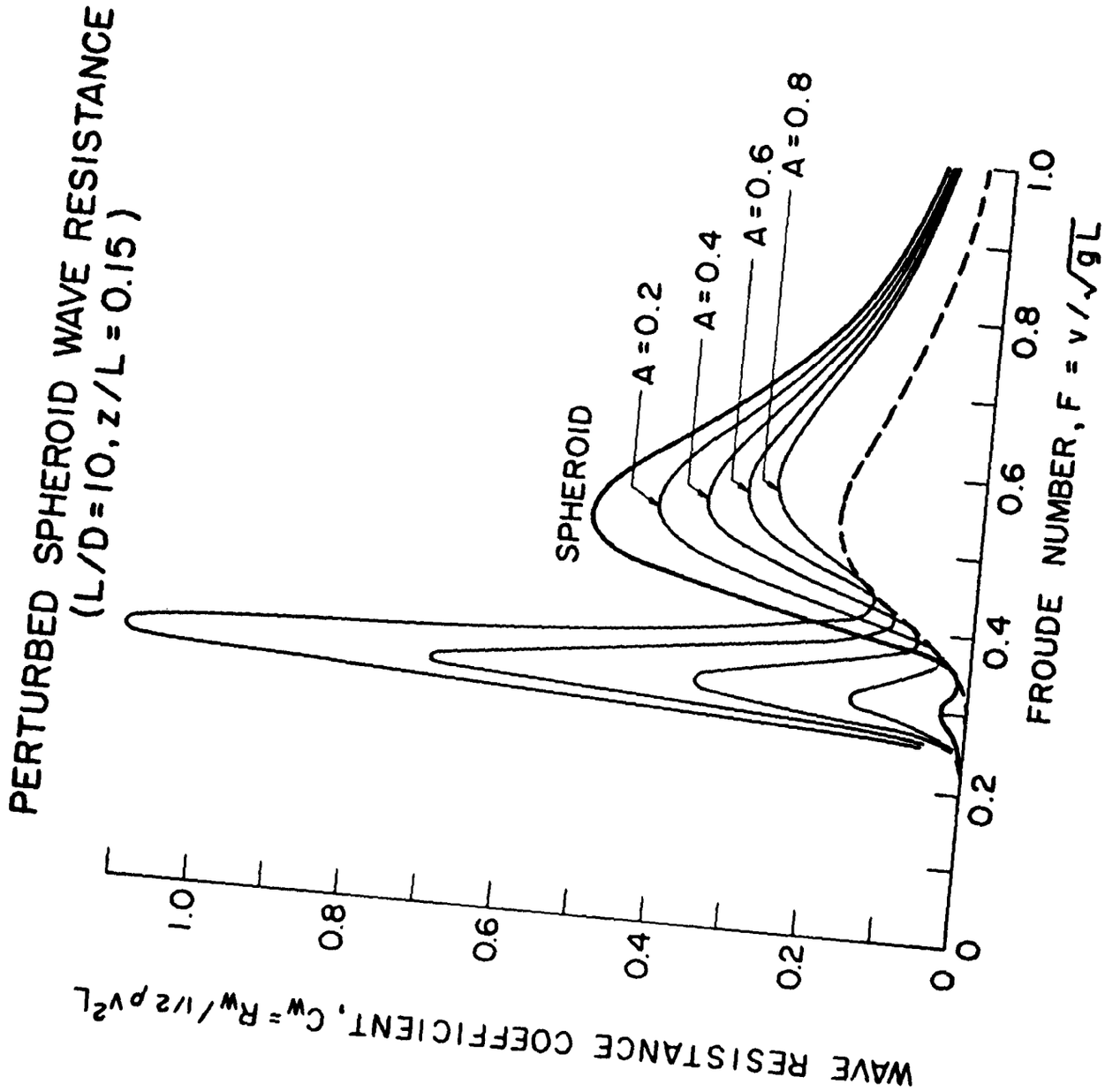
PERTURBED SPHEROID WAVE RESISTANCE
(L/D=10, z/L=0.15)
SPHEROID
A=0.2
A=0.4
A=0.6
A=0.8
FROUDE NUMBER, F = v/√gL
0
0.2
0.4
0.6
0.8
1.0
WAVE RESISTANCE COEFFICIENT, Cw = Rw/1/2 ρ v²L
0
0.2
0.4
0.6
0.8
1.0

FIG. 15

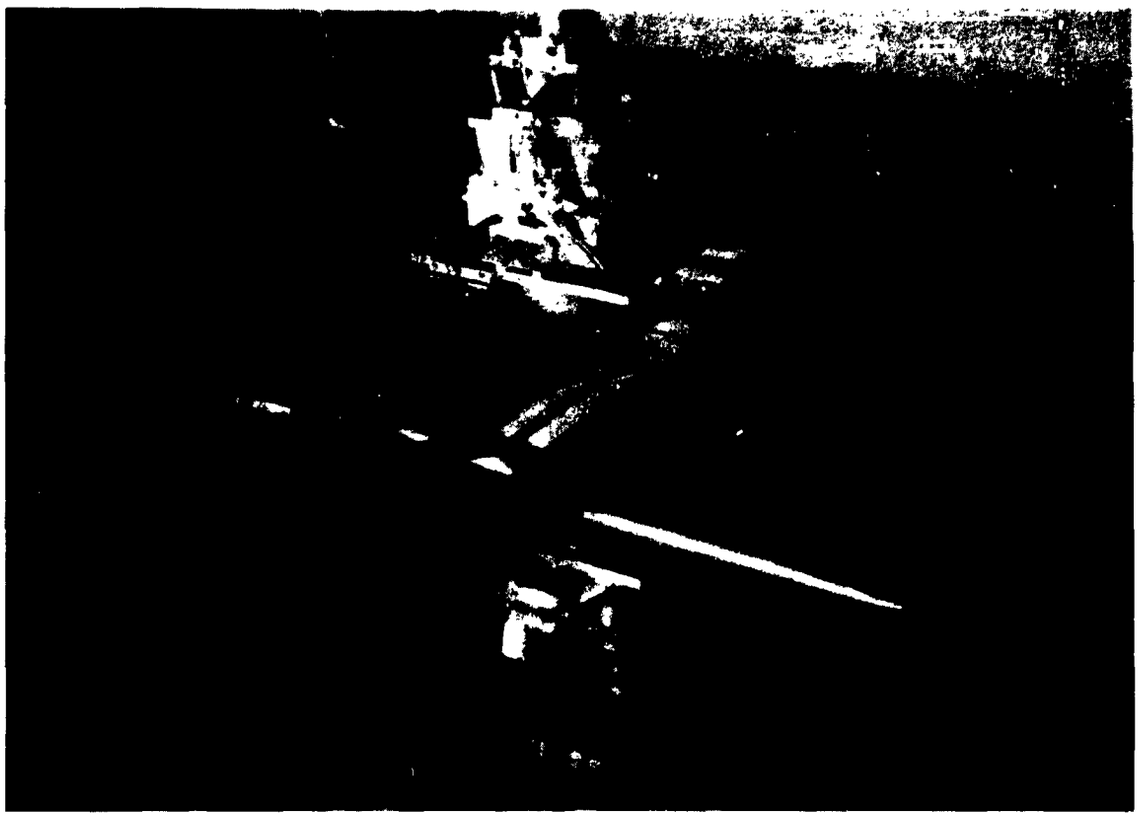

PROPULSIVE PERFORMANCE IN WAVES

Prof.ir J. Gerritsma
Delft Shipbuilding Laboratory
Netherlands

I. INTRODUCTION.

The resistance increase of a ship, due to seawaves, results in many cases in a considerable loss of speed. In general this added resistance depends on the dimensions, the form and the weight-distribution of the ship but the quantative knowledge of resistance and propulsion in a seaway is still rather scarce. The present conventional shipform has been developed by emperical methods in combination with experimental work on shipmodels. There is no doubt that the optimum hullform for normal cargo and passengerships, sailing in still water, is closely approximated but with the present state of knowledge a naval architect cannot claim that his design has an optimum propulsive performance in waves. It is possible that also in this respect the long experience and the practical insight of the profession has led to ships that cannot be improved very much. In my opinion, however, a definite answer to this question cannot be given at the moment because systematic research in this area started only a few years ago.

Logbook analysis and seakeeping trials showed us the order of magnitude of the power increase which is necessary to maintain a certain ship speed in a seaway. In a head sea and windforce 5 a normal cargoship needs 30% to 60% extra power to maintain the still water speed. At windforce 6 the extra power is approximately 50% to 100%. The usual power reserve of a ship is much smaller and in these conditions the ship has to travel with reduced speed. On the North Atlantic windforce 5 is not an exception; in fact this value is exceeded in about 50% of the time. In moderate head seas a speed loss of 1 to 3 knots is not unusual for normal cargoships at full power. Therefore the investigation of the propulsive performance of a ship in waves seems worthwile.

When we limit ourselves to theoretical work and model experiments the research on resistance and propulsion of a ship in waves is mostly of recent date. Without being complete I mention the investigations of Havelock[1], Hanaoka[2], Maruo[3] and the model experiments carried out in this country, Japan, Great Britain and the Netherlands.

In particular the recent modeltests carried out at the Wageningen Seakeeping Tank can be regarded as a more systematic

approach to the problem, in which the influence of the shipform on the resistance and power increase in waves has been studied.

Almost without exception the experimental work has been done in regular waves. Until recently the relation between resistance and power in regular waves and in irregular waves was not known to the profession. In 1957 a method was given by Maruo, to determine the mean resistance increase of a ship in irregular waves when the resistance increase in regular wave components is known[3]. Model experiments carried out in the Delft Towing Tank have shown that Maruo's method can be used with sufficient accuracy to predict the propulsive performance of a ship in longitudinal irregular waves[4]. Some of the results of this investigation are the subject of this paper.

The possibility to determine the resistance and the power of a ship in a given wavespectrum allows a significant comparison of different hull forms. It is known that such a comparison based on regular wavetests only, may be difficult. In regular head waves of moderate height and a length which is approximately equal to the length of the ship the power increase may be in the order of 200% to 300%. The question of a shipowner how he could use such "unpractical information" led to our experimental investigation.

II. RESISTANCE AND PROPULSION IN REGULAR WAVES.

Theory and experiments have shown that the resistance increase of a ship in waves is mainly due to the heaving and pitching motions and the phases of these motions with respect to the waves. Reflection effects also add to the resistance but relatively these effects seem to be small.

Other secondary effects such as steering resistance in oblique waves and the influence of a mean yawing angle in oblique waves may be mentioned too. The increase in power depends on the increase in resistance, the change in propulsive efficiency due to the increased loading and the influence of the shipmotions on the operation of the propeller. With a linear theory Maruo found that the resistance increase R_r of a mathematical shipform can be written as follows:

$$R_r = \rho_r \rho g r^2 B^2 / L$$

where ρ is the density of the water, g is the acceleration of gravity, r is the wave amplitude, B is the breadth and L is the length of the ship.

The resistance increase coefficient ρ_r is given as a function of the heave and pitch amplitudes (z_o and ψ_o), the wave amplitude and the phases of heave and pitch with respect to the wave(ε_{zr},

$\varepsilon_{\psi r}$), namely:

$$\rho_r = D_{11}(\frac{z_o}{r})^2 + D_{22}(\frac{\psi_o}{kr})^2 + D_{12}(\frac{z_o}{r})\ (\frac{\psi_o}{kr})\ \cos\ (\varepsilon_{zr} - \varepsilon_{\psi r})$$

$$+ D_{13}(\frac{z_o}{r})\ \cos\ \varepsilon_{zr} + D_{23}(\frac{\psi_o}{kr})\cos\ \varepsilon_{\psi r} + D_{33}$$

Maruo found that the resistance increase in waves is independent of the still water resistance. Furthermore it appeared that pitching motions are the main cause for resistance increase. Reflection effects, represented by the coefficient D_{33} are small. This is illustrated by figure 1 which is taken from Maruo's paper. For small motion amplitudes the reflection effects are relatively more important but then the absolute magnitude of the resistance increase is very small. The same conclusion can be derived from model experiments: in short waves the motions and the resistance increases are both small even in relatively high waves.

The largest resistance is found in the region of pitch and heave resonance and this region may differ from that where maximum motion amplitudes occur.

In order to study the various aspects of the performance in waves in more detail extensive model experiments were carried out with a 7½ feet model of the "Maasdam", one of the ships of the Holland America Line (figure 2). This ship is 145 m long and is built on conventional lines corresponding to a still water speed of about 17½ knots. The blockcoefficient is 0.65 and the longitudinal radius of gyration is 23% of the length. Resistance and propulsion tests were carried out in still water and in regular waves of different lengths and heights. In each wave condition the mean values of speed, thrust and torque were measured at constant revolutions of the propeller. The results for a waveheight equal to the shiplength are shown in figure 3. In total six wavelengths were considered covering the range $\lambda/L = 0.6$ to $\lambda/L = 1.6$.

It is important to note that the propulsion tests were carried out with constant revolutions. That means that at a certain speed the revolutions did not vary as a result of the varying propeller loading which is caused by shipmotions and wave action. Various authors have proposed three alternative methods for propulsion tests in waves namely: constant revolutions, constant torque and constant power. In each of these cases an electronic control of the propeller motor is necessary.

Model experiments carried out at the seakeeping tank at Wageningen have shown that within the experimental errors the three methods give the same results with regard to motions and propulsion. These results are given in figure 4.[5] The constant revolutions method was preferred for our tests because of the simple and accurate control system.

The other values such as speed, thrust and torque show cyclic variations as a result of the model motions and the action of the waves. Their mean values are used in the analysis. An impression of the magnitude of the torque fluctuations is given in figure 5. A comparison with the torque fluctuations measured on board of the Japanese cargoship "Nissei Maru" shows that the same order of magnitude is found in practice[6] (see figure 6).

The fluctuations of torque and thrust do not have a high correlation with the heaving and pitching motions. Probably the variation of horizontal flow in the propeller resulting from surging and the orbital motion in the waves is the main cause for the variations in torque and thrust[6]. Unfortunately the surging motions were not measured and therefore a further analysis of these effects could not be made.

The tests in waves were analysed in the following way. First of all the increases of resistance, thrust, torque and revolutions with regard to the still water values were divided by the squared wave amplitude. For resistance this seemed a logical approach since theory has indicated that such a resistance increase coefficient must be constant for constant speed and wavelength. The experimental data confirm that this assumption is valid within the experimental accuracy as shown in figure 7 where the dimensionless resistance coefficient ς_r is given for one particular speed as a function of wavelength. In the same figure the dimensionless increase coefficients for thrust, torque, revolutions and power, as introduced by Vossers[5] are given viz:

$$\tau_r = \frac{T_r}{\rho g r^2 \frac{B^2}{L}} \quad , \quad K_r = \frac{Q_r}{\rho g r^2 \frac{B^2}{L} D} \quad , \quad \nu_r = \frac{n_r D^3 V}{\rho g r^2 \frac{B^2}{L}}$$

$$\pi_r = \frac{P_r}{\rho g r^2 \frac{B^2}{L} V}$$

Obviously all the increases are approximately proportional to the square of the waveheight. That means that at constant speed the increases of thrust, torque, revolutions and power must be approximately proportional to the resistance increase. To investigate this in more detail the measured values of thrust, torque, revolutions and power in waves have been plotted in figure 8 on a base of resistance at constant speed. Also the still water values corresponding to the self-propulsion point of the ship are indicated in this figure and consequently the increase due to the waves can be read off easily in each case. In addition the results of overload tests in still water are given.

It is clearly shown that the thrust and torque increase is proportional to the resistance increase. With acceptable error the same applies to the increase of power and revolutions. Some remarks may be added to this result. The thrust is related to the resistance by the well known formula:

$$R = T(1 - t).$$

In general the thrust deduction factor is not constant; it depends on the propeller loading and on the non-stationnary effects caused by the ship motions.

If constant propeller characteristics in waves are assumed, the analysis of the wake fraction and thrust deduction factor reveals that their values decrease with increasing ship motions. As a first approximation, however, an average linear relation between thrust and resistance at constant speed may be accepted.

A possible explanation of the almost linear relation between resistance and torque could be as follows. The propulsive efficiency can be written as follows:

$$\frac{R.V.}{2\pi Q n} = \frac{1 - t}{1 - \psi} \eta_p \eta_r$$

or:

$$\frac{R}{Q} = \frac{2\pi}{V} n \frac{1 - t}{1 - \psi} \eta_p \eta_r$$

where η_p is the propeller efficiency and η_r is the relative rotative efficiency. At constant speed an increase of resistance corresponds to higher revolutions and lower propeller efficiency. These two effects seem to compensate each other and as the variation to the other factors is relatively small the torque is proportional to the resistance at constant speed.

The revolutions are certainly not proportional to the resistance or the thrust. In the usual range of propeller loading we may assume a linear relation between the thrust constant:

$$K_T = \frac{T}{\rho n^2 D^4}$$

and the advance coefficient:

$$\Lambda = \frac{V_e}{nD}, \text{ viz:}$$

$$\frac{T}{\rho n^2 D^4} = c_1 + c_2 \frac{V_e}{nD}$$

When thrust deduction factor and wake fraction are assumed to be constant it follows that:

$$R = (1 - t)T = c_1 n^2 + c_2 Vn$$

The experiment shows however, that also in this case the increase of revolutions is approximately proportional to the resistance increase at constant speed and wavelength. The same applies for the power increase. This seems more or less unlogical, but the combination of revolutions and torque appears to give a slightly curved power resistance curve and the straight line approximation for the power increase can be accepted as an average solution.

It is remarkable that the still water overload points plot very well in line with the regular wave points. Although the individual wave results show some scatter it may be concluded that the average propulsive characteristics are not greatly affected by the action of the waves.

Finally the influence of resonance is clearly demonstrated in figure 9 where as an example the thrust increase coefficient for various model speeds is plotted on a base of frequency of encounter. Maximum values are found in the vicinity of pitch and heave resonance.

III. RESISTANCE AND PROPULSION IN IRREGULAR WAVES.

According to Maruo the mean increase of resistance in a given wave spectrum can be determined when the resistance increase in regular wave components is known. The ordinates of the wave spectrum $G_{rr}(\omega_e)$ are related to the amplitudes $r(\omega_e)$ of the wave components by the well known formula:

$$G_{rr}(\omega_e)\, d\omega_e = \sum_{\omega_e}^{\omega + d\omega_e} \tfrac{1}{2} r^2(\omega_e)$$

When the resistance increase coefficient for regular waves: $\frac{R_r}{r^2}$ is given as a function of the frequency of encounter for constant speed the mean increase of resistance is:

$$R_r = 2\int_0^\infty G_{rr}(\omega_e)\, \frac{R_r}{r^2}(\omega_e)\, d\omega_e$$

or:

$$R_r = 2\rho g B^2/L \int_0^\infty G_{rr}(\omega_e)\, \rho_r(\omega_e)\, d\omega_e$$

Based on the approximately linear relation between resistance increase on the one hand and the increase of thrust, revolutions and power on the other hand, similar expressions are valid for thrust, revolutions and power. Figure 10 illustrates the procedure for torque: the ordinates of the wave spectrum and the torque increase coefficient are multiplied and the surface of the resulting curve is proportional to the mean increase of torque. It has to be remarked that the method cannot be used to determine the resistance increase coefficients from the mean resistance in irregular waves of which the energy spectrum is known. In this respect there is a difference with ship motions analysis where the concept of a motion spectrum is used to this purpose.

Maruo's method has been confirmed experimentally for torque, power and revolutions. This was done as follows. In irregular long crested head waves the mean torque and the revolutions were measured for a range of speeds. Two wave spectra were considered: spectrum 1 with a significant wave height $H_{1/3} = 4.15$ cm corresponding to 9 feet full scale and spectrum 2 with $H_{1/3} = 6.3$ cm corresponding with the full scale value $H_{1/3} = 14$ ft. For the same speed range the torque and the revolutions were predicted by using the results of the regular wave tests and the measured wave spectra. A comparison of the predicted and the directly measured values is given in figure 11. Apparently the agreement is good. It should be mentioned that in spectrum 1 a model speed of 1.04 m/s corresponds approximately to the attainable ship speed. In spectrum 2 this speed amounts to 0.95 m/s.

The curves in figure 11 are determined without using a friction correction on the propeller loading. The tests in regular waves were carried out by using the I.T.T.C. friction line correction but it appeared that this complication is not necessary because, within the experimental accuracy the increase of thrust, torque and revolutions is not influenced by the friction correction. As the thrust dynamometer was damaged during one of the first runs no measurements of thrust in irregular waves were available.

IV. ANALYSIS OF SERVICE PERFORMANCE DATA.

A large number of service performance data of the ship was available. They were collected on the North Atlantic route in the course of one and a half year. Each set of data contained the following observations and measurements:

a). log speed of the ship
b). wind velocity and wind direction
c). waveheight and wave direction
d). shaft horsepower, measured with a torsionmeter
e). propeller revolutions
f). course of the ship.

At the beginning and at the end of each voyage the draft forward and aft was measured and the displacement for each series of observations could be estimated. Also the results of propulsion tests with a 6 meter model in still water were available. With the aid of these data the tank horsepower for each specified condition of the ship with regard to speed and displacement could be determined. The variation of displacement did not exceed 15% and therefore it was assumed that the tank horsepower at constant ship speed varied as $(\text{displacement})^{2/3}$.

Out of the 900 available sets of data, three groups were selected, namely:

1). smooth sea, no waves, light wind
2). light sea, coming in on the beam, light to moderate winds
3). waves on the bow, direction of propagation within a sector from 30° starboard to 30° port.

With the data of group "1" the mean ship speed under ideal conditions was determined. For all of the data in the groups 1, 2 and 3 the measured shaft horsepower was corrected for wind resistance. The wind resistance can be expressed as:

$$R_w = \zeta \tfrac{1}{2} \rho_a V_r^2 A$$

where:

ζ = a coefficient depending on the direction of the relative wind and the type of superstructure.
ρ_a = the density of air
V_r = relative wind velocity
A = projected area above the waterline.

The power which corresponds to the wind resistance is:

$$P_w = \frac{\xi \, \frac{1}{2} \rho_a V_r^2 A V_s}{75. \, \xi} = C_w V_r^2 V_s$$

where ξ = the total propulsive efficiency. The coefficient C_w was estimated from published windtunnel experiments and the known values of A and ξ.

Secondly a mean roughness allowance could be determined from the data of group "1" and "2" where the influence of the sea waves on the total resistance could be neglected. It could be clear that the roughness allowance in this particular case is assumed to be the difference between the measured power, corrected for shaft friction (3%) and the sum of the power allowance for wind and the tank horsepower. Due to this definition it is possible that our "roughness" allowance contains also a relatively small "correlation" allowance.

For each voyage the mean value of $\frac{\text{roughness allowance}}{(\text{speed})^3}$ has been determined.

This procedure is justified when the roughness resistance varies as the square of the speed. For small variations of the speed a deviation from this assumption has only a small influence on the final result. In this way a mean roughness allowance could be determined as a function of the ship speed.

The data of group "3" were arranged according to the waveheight. To begin with the relation between the mean speed and the observed waveheight was determined, see figure 12. Then the power increase due to the waves was found by deducting the tank horsepower and the allowances for shaft friction, wind resistance and roughness from the measured shaft horsepower. The mean power increase due to wave action as a function of the observed waveheight is shown in figure 13. It should be mentioned that in all the analysed conditions approximately the full power of the machinery was used to propel the ship. There was no speed reduction necessary form the point of view of excessive shipmotions or slamming. To allow a comparison with the experimental results two assumptions of a somewhat disputable nature had to be made, viz:

a). for the conditions under consideration the ship has been moving in irregular unidirectional head seas, definable by the Neumann spectrum family,

b). the observed waveheight corresponds to the average value of the one-third highest waves of the Neumann spectrum.

For five wind speeds up to 30 knots the Neumann spectra for fully developed seas were used to predict the power increase at sea. For that purpose the power increase coefficients derived from the modeltests in regular waves were used. The results are shown

in figure 14 where the power increase are labelled with the mean of the one-third highest waves. In combination with the speed - observed waveheight (figure 12) relation, the power increase as a function of the waveheight could be determined as given in figure 13. Obviously the power increase derived from the service performance data agrees very well with the predicted values.

In figure 15 the total horsepower, consisting of tank horsepower and the allowances for wind, roughness and waves is shown as a function of waveheight. The total power developed is independent of the waveheight. For waveheights exceeding 4 meter no reliable observations were available; in this range the speed-waveheight curve was estimated. It is probable however, that for higher waves the speed has to be reduced because of the shipmotions.

It is agreed that the two assumptions with regard to the form of the wave spectrum are of a somewhat arbitrary nature and consequently not too much value should be attached to one particular case. Very recently however, the thrust and power in seawaves of the British ship "Weather Reporter" were analysed by using a directly measured sea state. It was reported that the predictions agreed satisfactorily with the measured values[7].

The conclusions of the investigations may be that a reliable method for the prediction of the propulsive performance in a given sea state is now available. The method can be used to compare the performance of various hull and propeller designs in specified waveconditions.

REFERENCES.

1. T.H. Havelock.
   "The damping and pitching motion of a ship".
   Phil. Mag. 33, 1942.

2. T. Hanaoka.
   "Theoretical investigation concerning ship motion in regular waves".
   Proceedings Symposium on the Behaviour of Ships in a Seaway, Wageningen 1959.

3. H. Maruo.
   "The excess resistance of a ship in rough seas".
   Int. Shipb. Progress, 1957.

4. J. Gerritsma, J.J. v.d. Bosch, W. Beukelman.
   "Propulsion in regular and irregular waves".
   Int. Shipb. Progress, 1961.

5. G. Vossers, W.A. Swaan.
   "Some seakeeping tests with a Victory model".
   Int. Shipb. Progress, 1960.

6. "Investigation into the sea-going qualities of the single screw cargo ship "Nissei Maru" by actual and model ship experiments 1954". Shipbuilding Research Association of Japan.

7. H.J.S. Canham, D.E. Cartwright, G.J. Goodrich, N. Hogben.
   "Seakeeping trials on O.W.S. Weather Reporter".
   TRINA 1962.

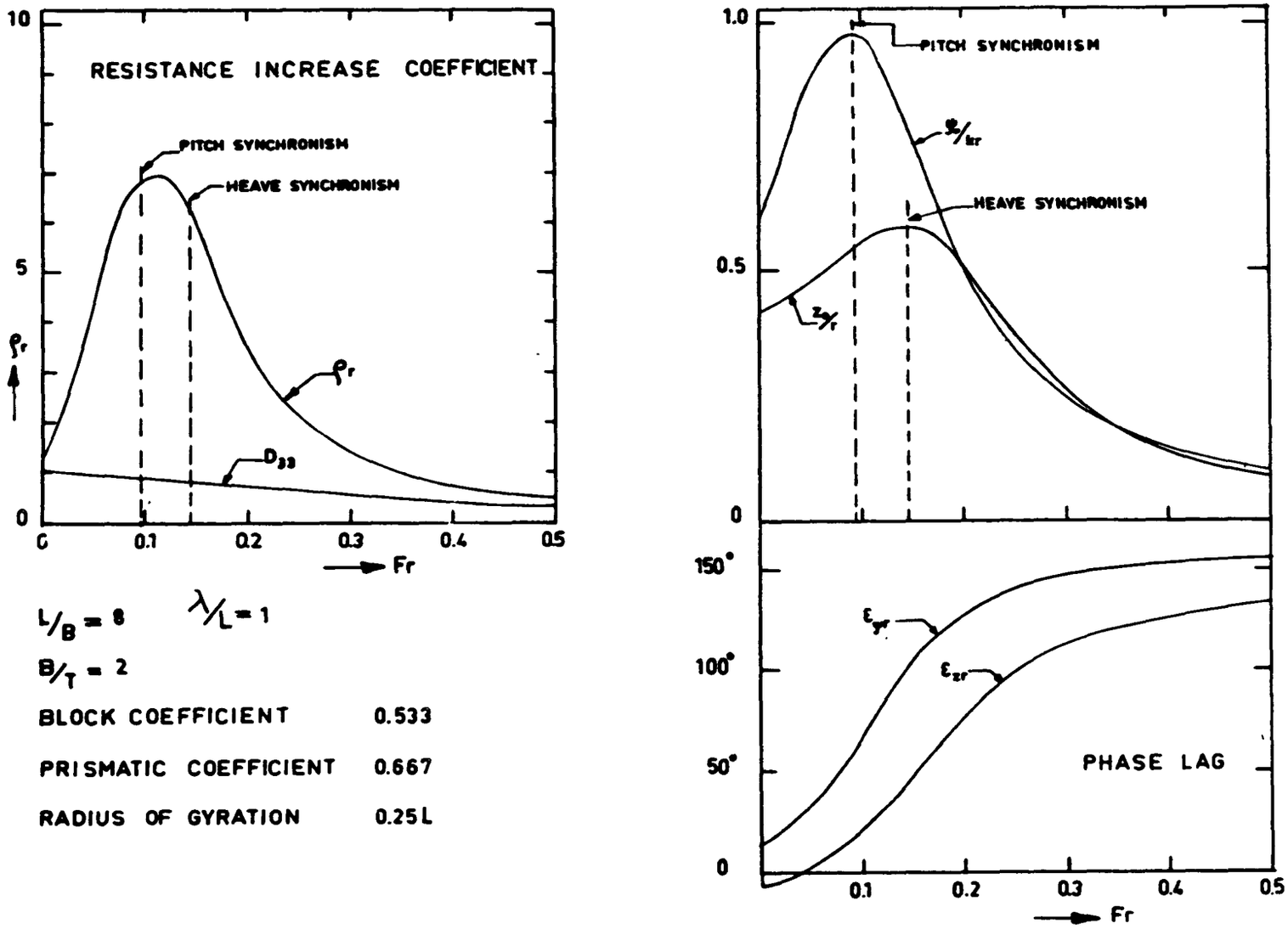

Fig. 1. Resistance increase and motions of a mathematical ship form in waves (reference 3)

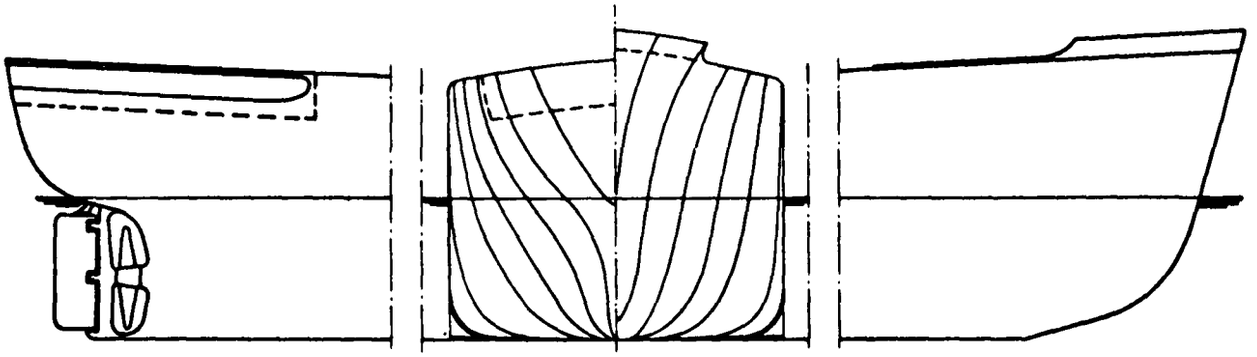

Fig. 2. Body plan

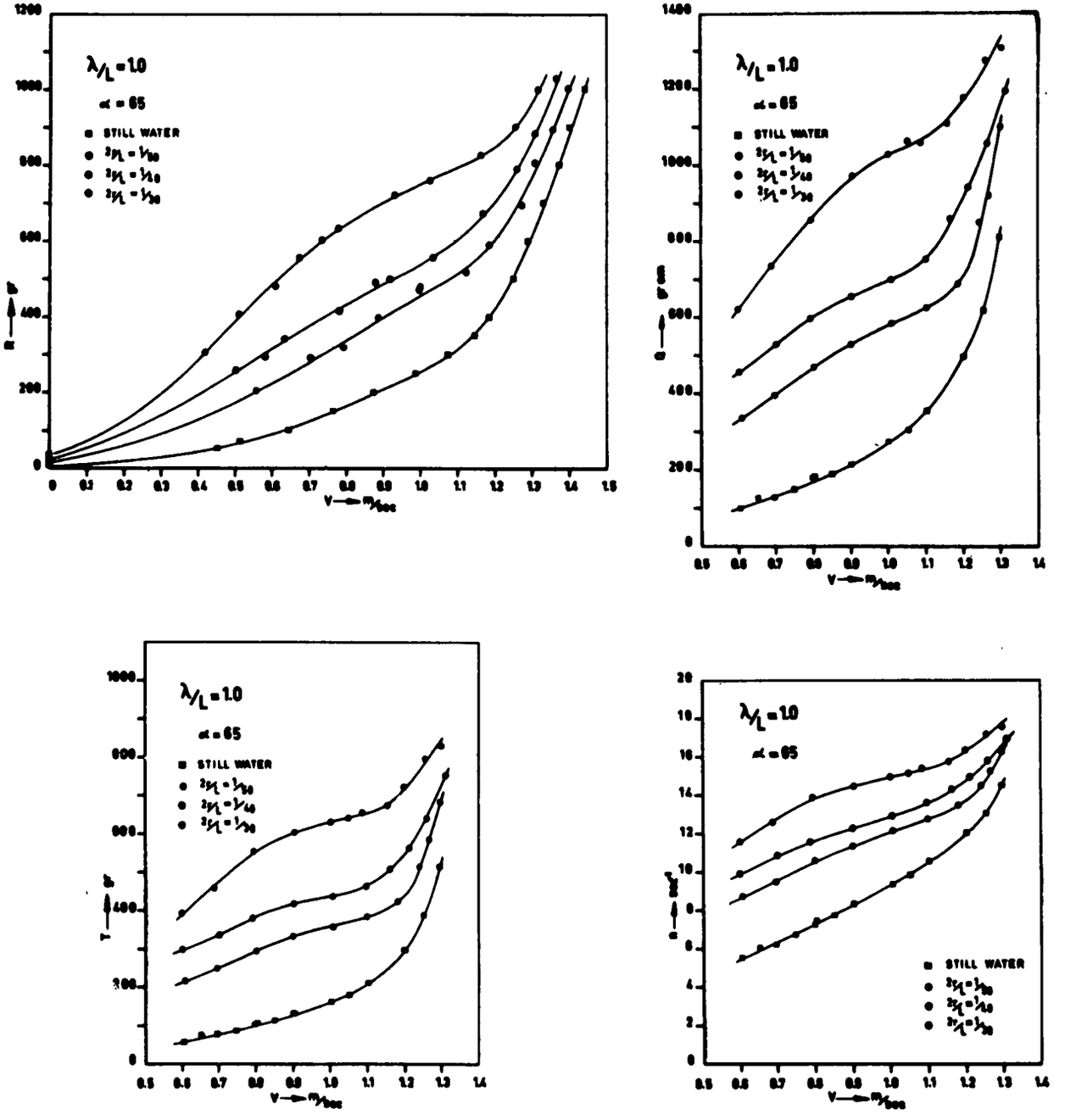

Fig. 3. Resistance and propulsion in regular waves.

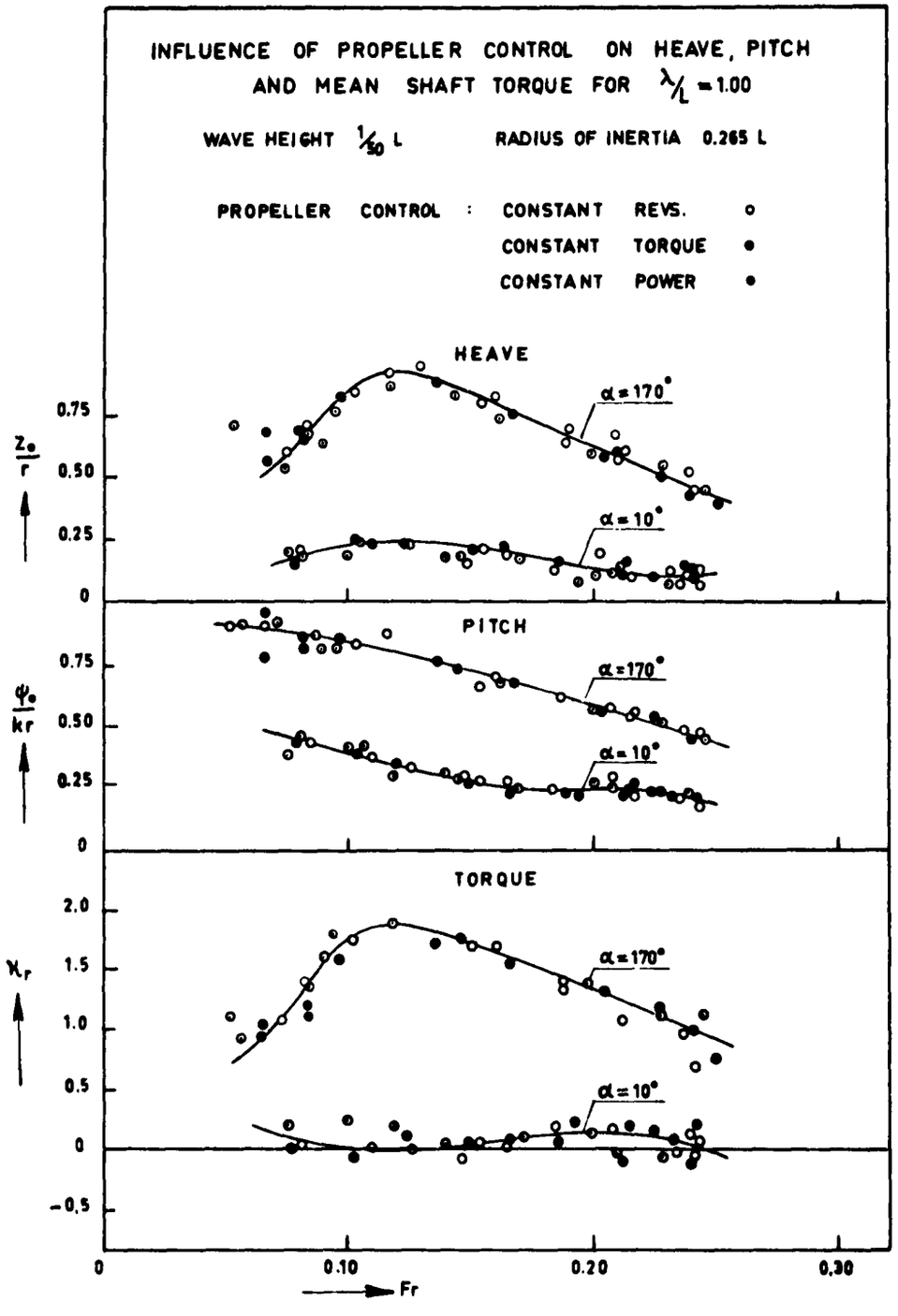

Fig. 4. Influence of propeller control on ship motions and thrust increase in regular waves

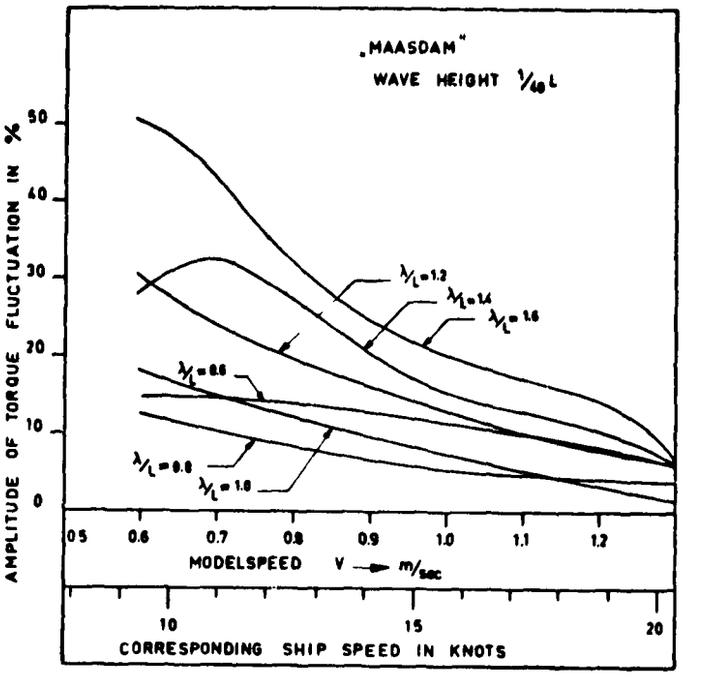

Fig. 5. Torque fluctuation in regular waves

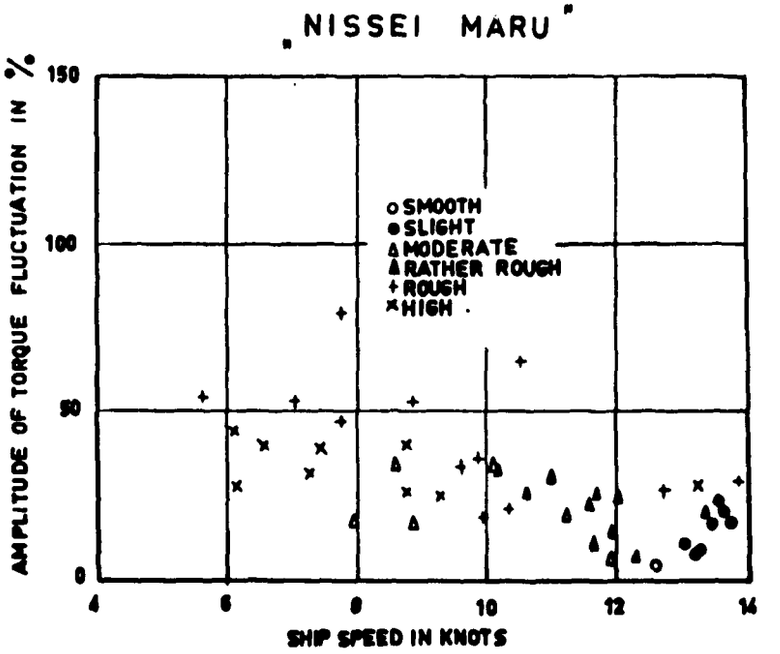

Fig. 6. Torque fluctuation of the "Nissei Maru" at sea (reference 6)

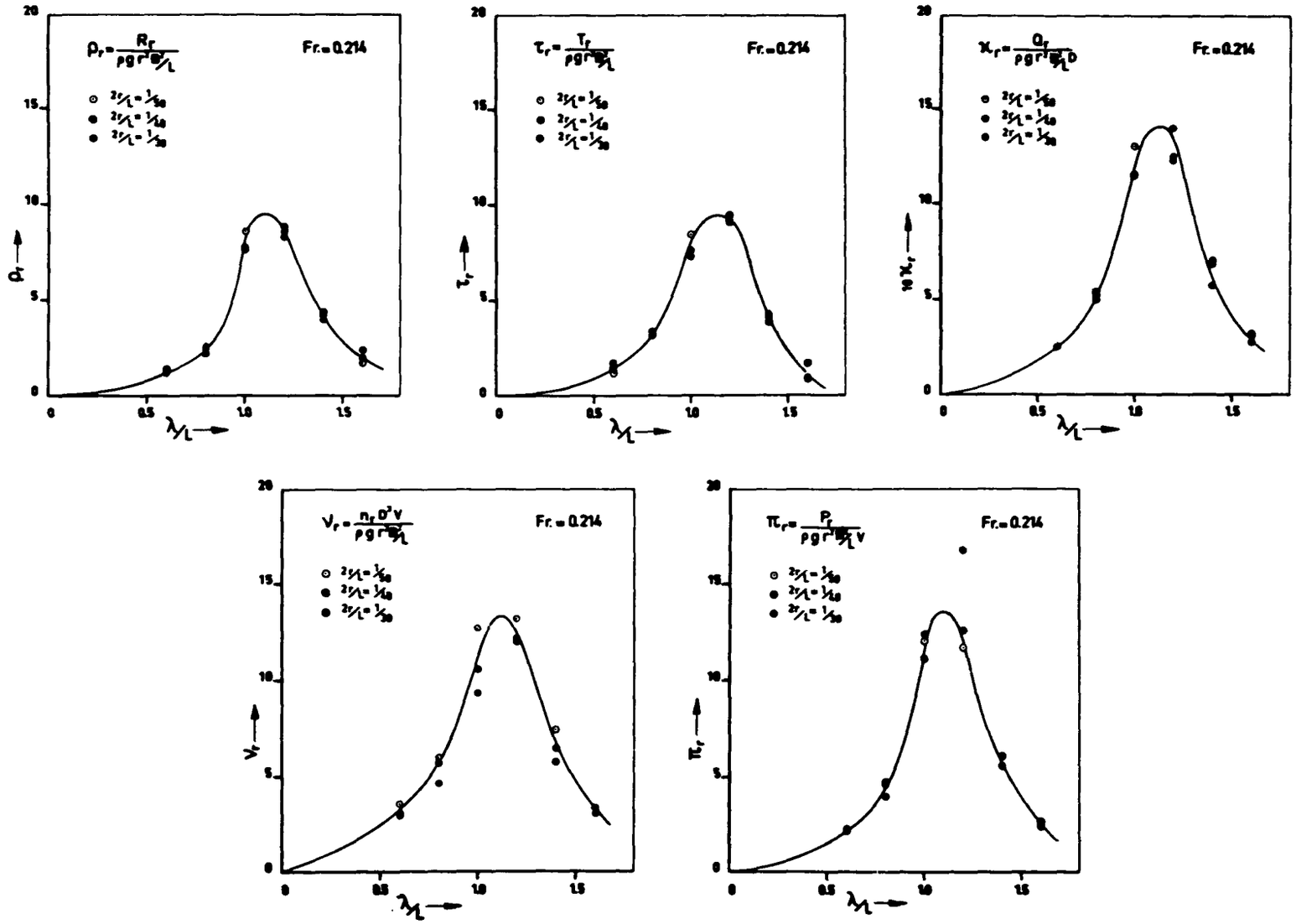

Fig. 7. Mean increase of resistance, thrust, torque, propeller revolutions and power in regular waves

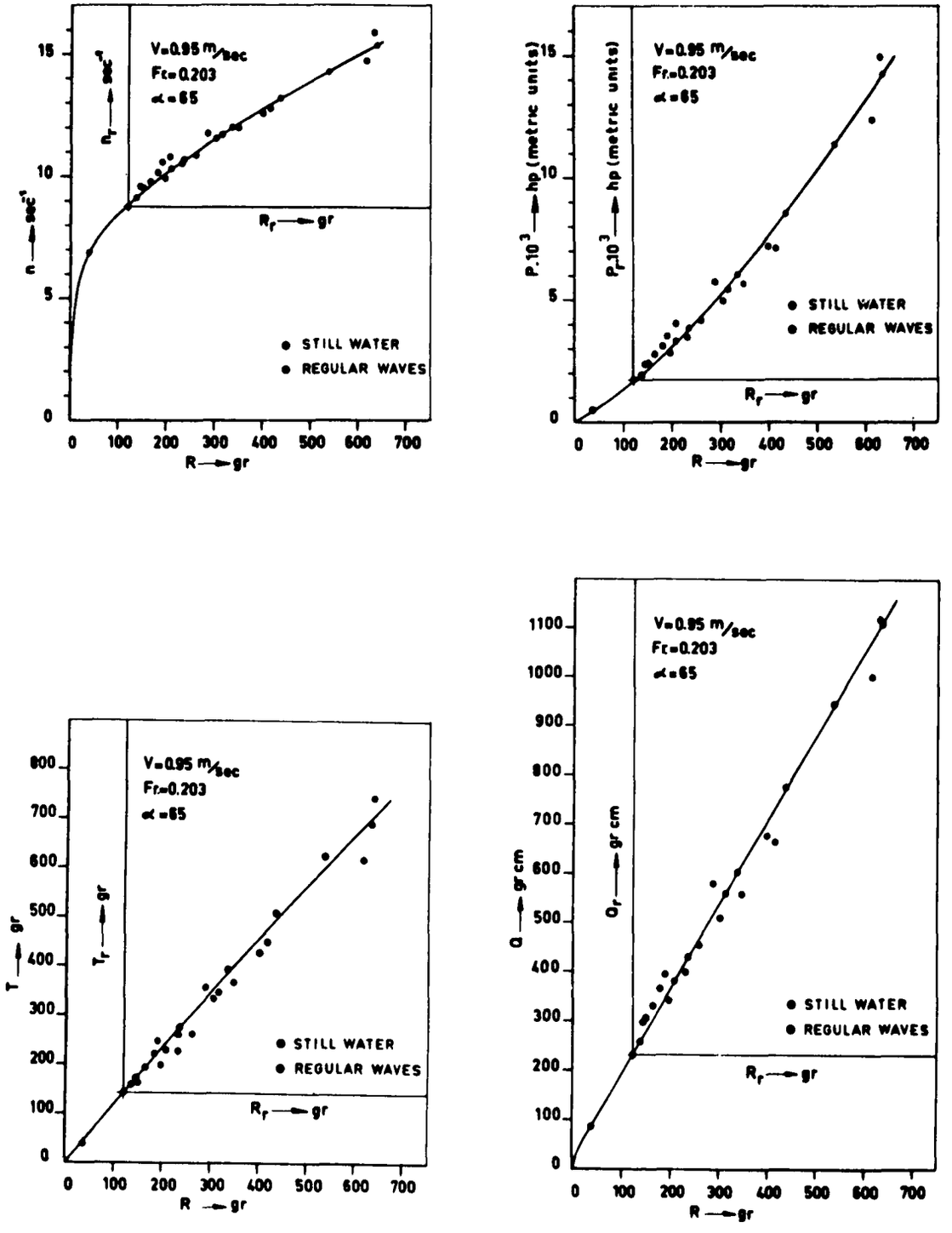

Fig. 8. Results of a resistance and propulsion test in still water and in regular waves at constant speed

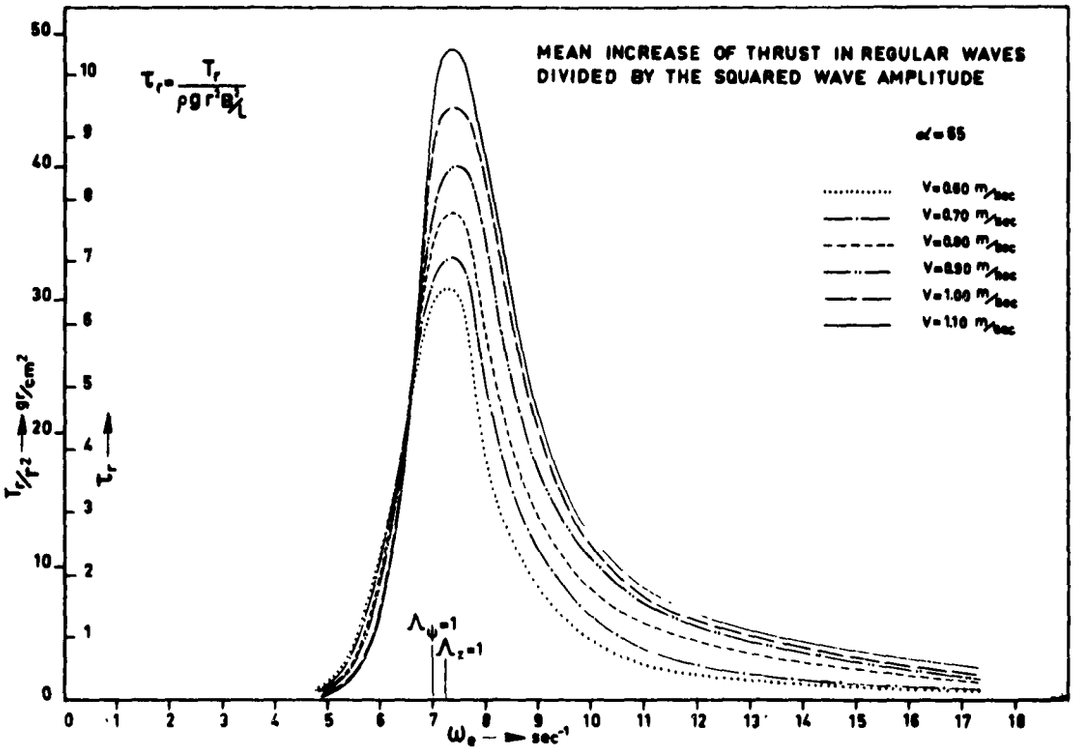

Fig. 9. Transfer function for thrust increase

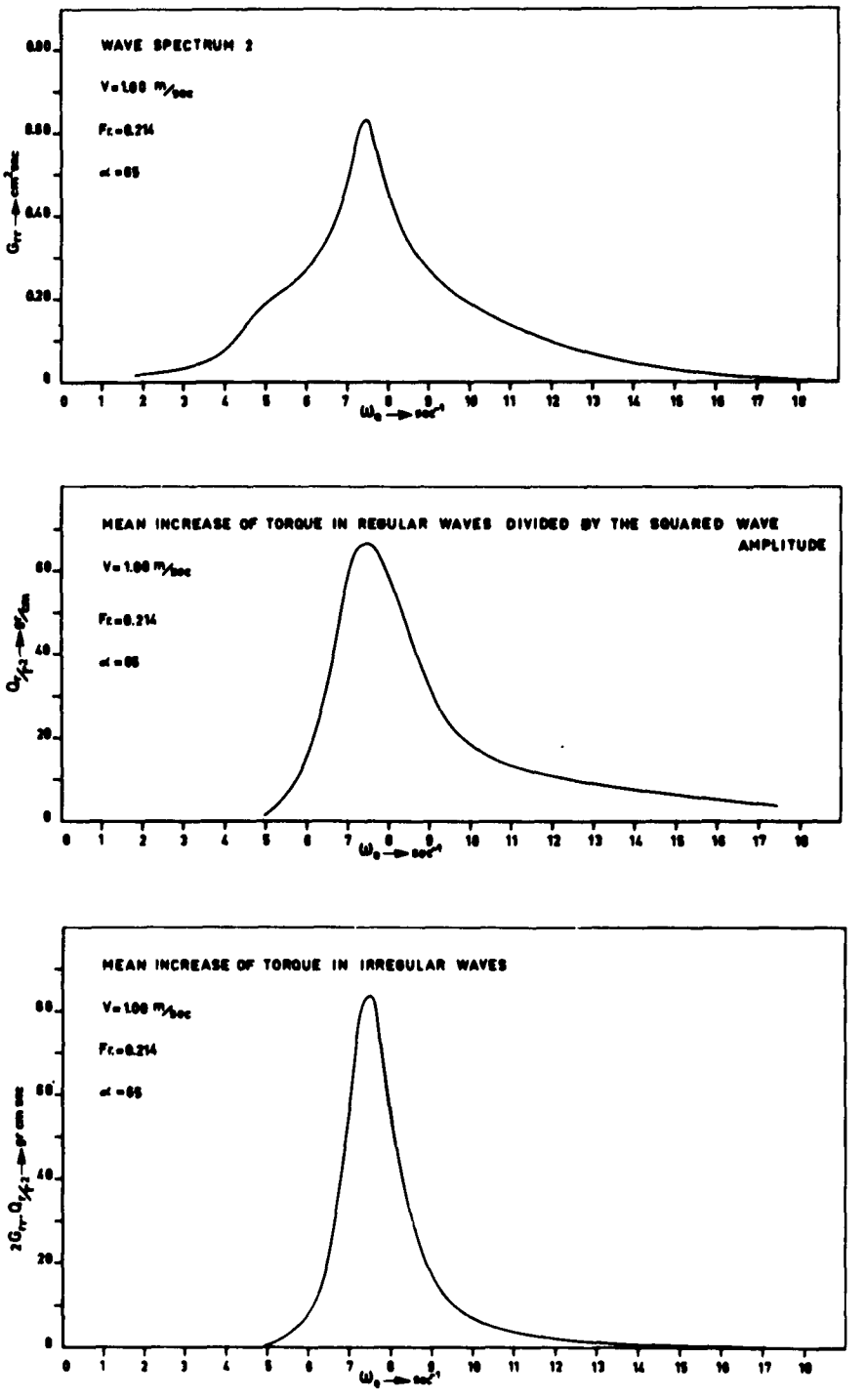

Fig. 10. Evaluation of mean increase of torque in irregular waves

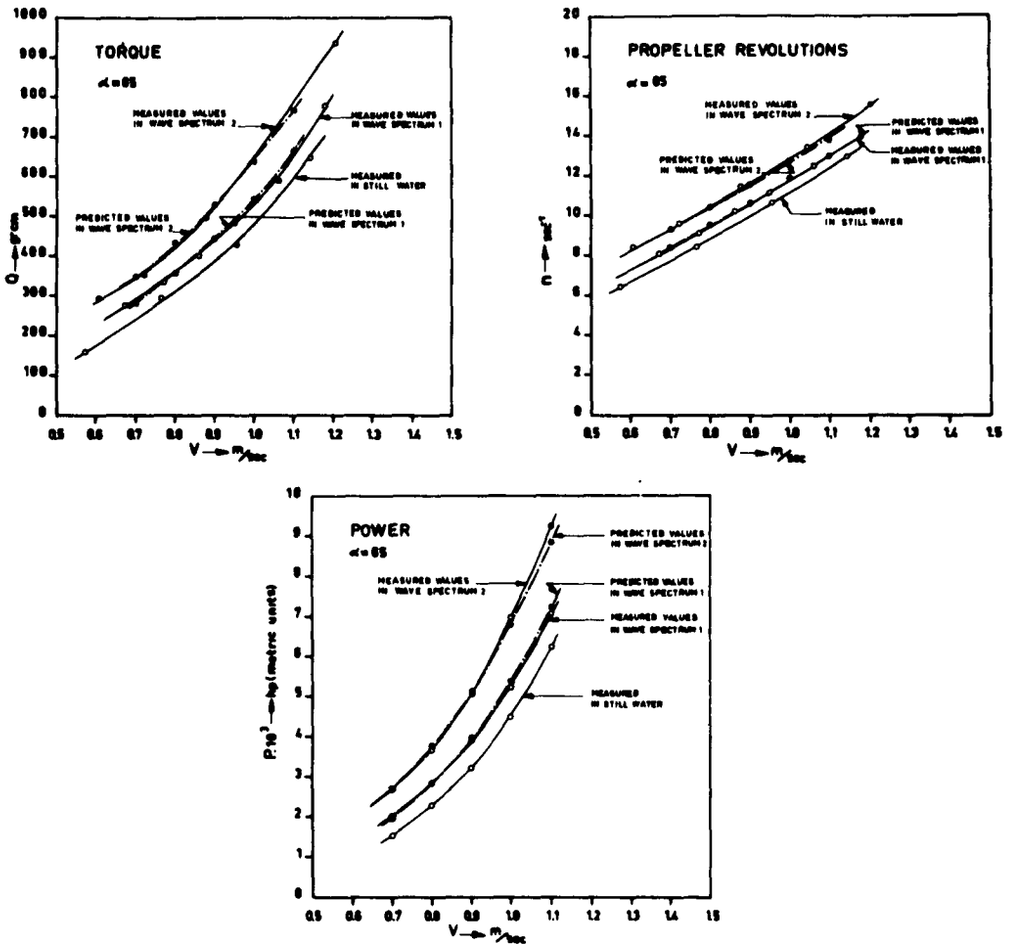

Fig. 11. Comparison of measured and predicted values of torque, propeller revolutions and power in irregular waves

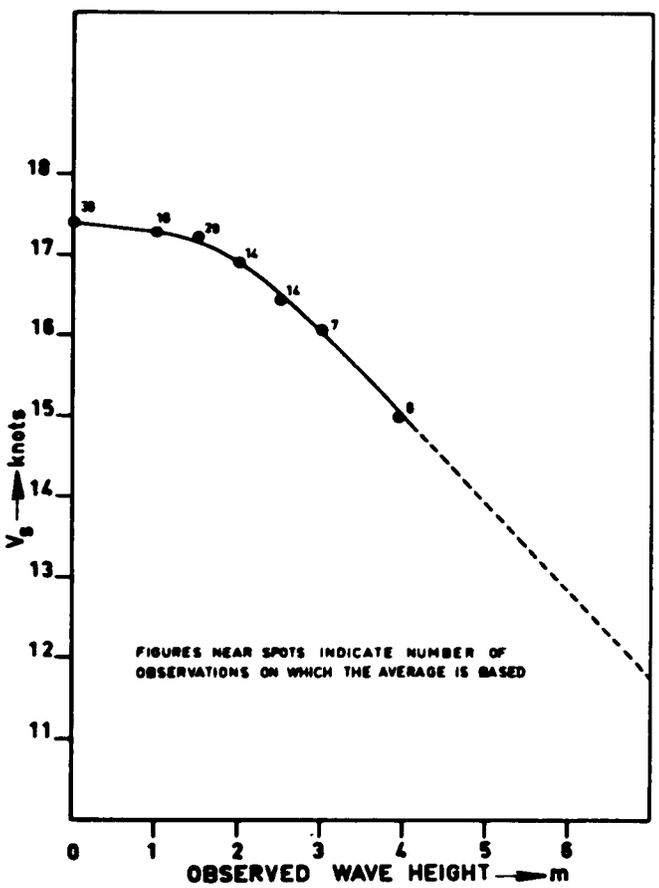

Fig. 12. Ship speed as a function of wave height, derived from service performance data

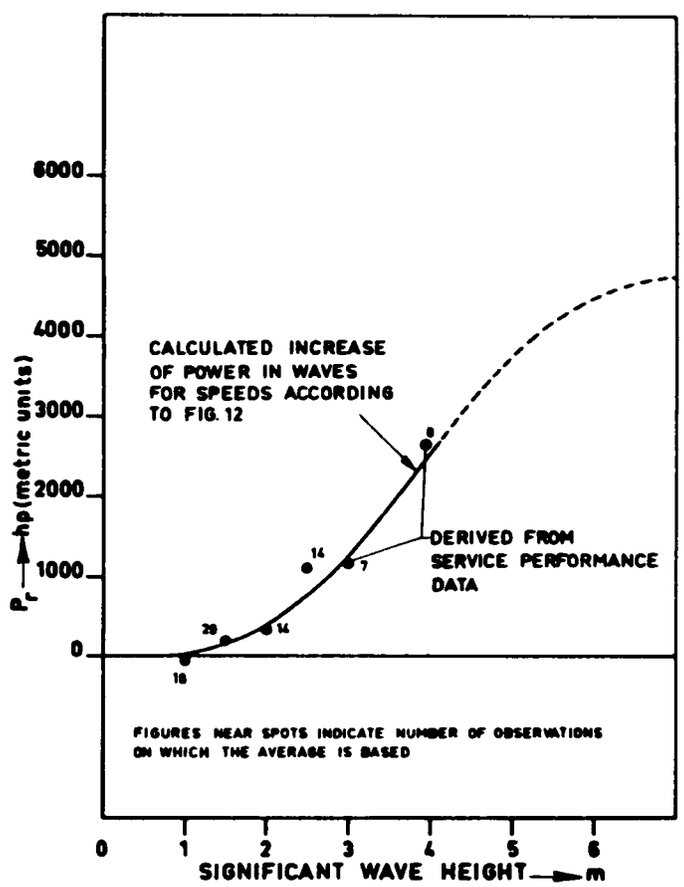

Fig. 13. Comparison of calculated power increase in waves with service performance data

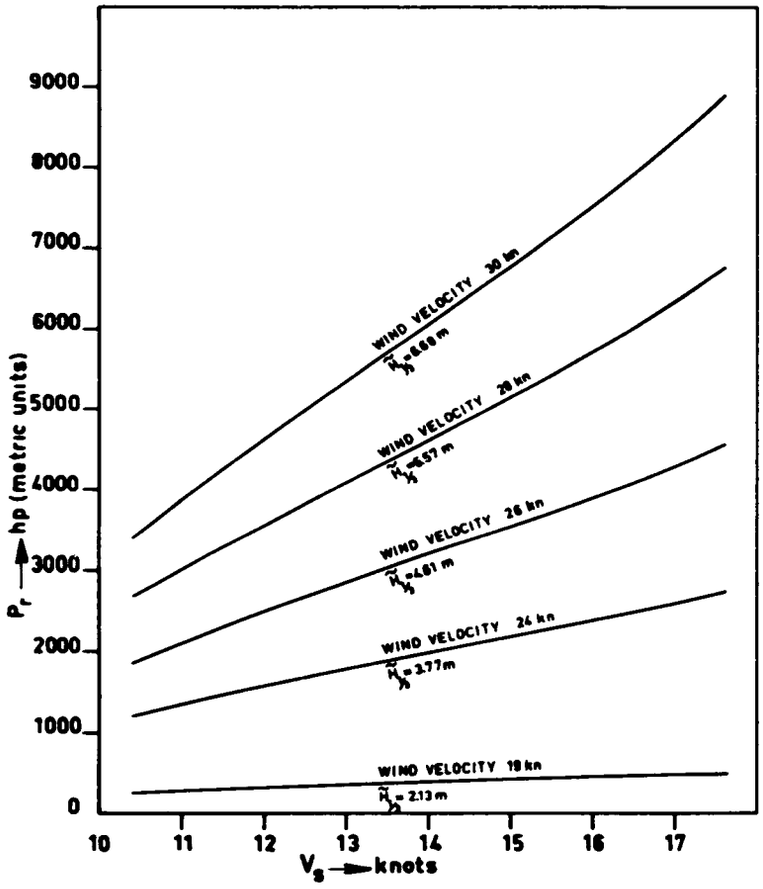

Fig. 14. Calculated increase of power due to unidirectional head seas (Neumann spectrum)

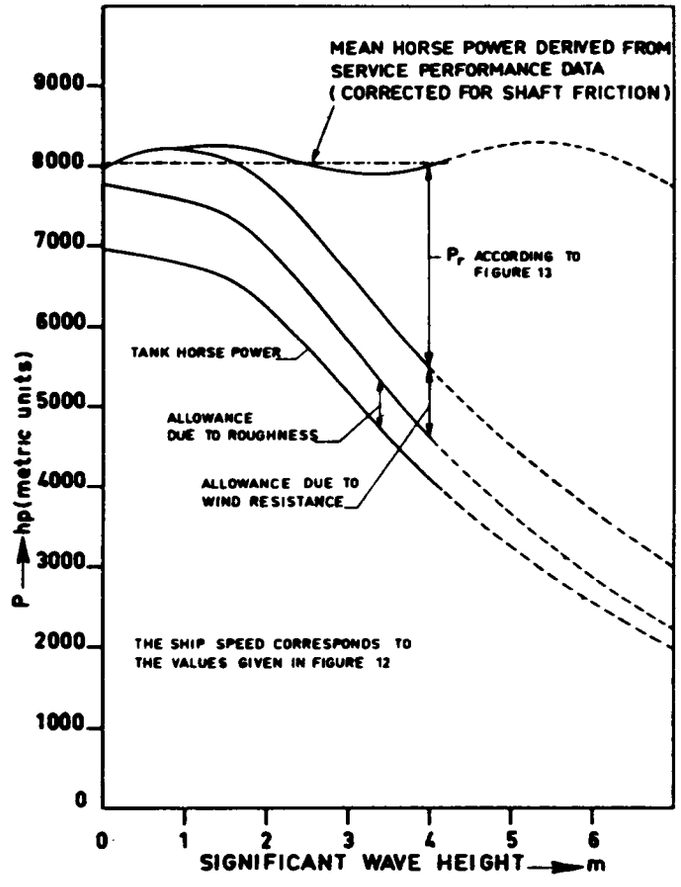

Fig. 15. Sub-division of total power

BENDING MOMENTS IN EXTREME WAVES

by John F. Dalzell
Head, Ship Hydrodynamics Division
Davidson Laboratory

I. INTRODUCTION

"In order to made possible the safe and economic structural design of larger and faster ships and to provide greater economy in conventional ships, a more rational method of designing is essential."* A rational method means, in part, that all the loads that can be expected in service should be determined and combined. This project, sponsored by the Ship Structure Committee, National Academy of Sciences-National Research Council, deals with one of the problems of loading--that is, wave bending loads. On the basis of a pilot study carried out at DL* it was suggested that some upper limit on longitudinal bending loads might exist: limit which is reached prior to some limiting sea state. This approach contrasts to that followed most extensively in research on wave bending moments and which is of a statistical nature. This approach, in principle, recognizes the possibility that wave bending loads and wave heights may achieve any value.

The project at hand was initiated to study the midship bending moments experienced by ship models in head and following waves of extreme steepness. The investigation was to include a range of wave lengths, wave heights up to the maximum possible wave height, and moderate heading and speed variations. A study was to be made of the effect on midship bending moments of weight distribution variation and freeboard variation, for a conventional merchant ship type. Also, two additional ship types were to be studied. It was felt that

---

*Lewis, E. V. and Gerard, G.: "A Long Range Program in Ship Structural Design," Ship Structure Committee Report SSC-124, National Academy of Science-National Research Council, 1959.

such a program would indicate whether or not an upper limit existed in general on wave bending moments before the limiting wave steepness occurred.

II. MODELS

At the outset of the investigation it was determined that as much change as possible in model variables was to be made to avoid the chance of submerging differences in the large scatter of data which would result from tests in extreme waves. Table I summarizes the characteristics of all the models tested. The ship selected for the merchant ship model was the Mariner, which represents good current practice in merchant ship design. On this model various changes were made to study the effect of weight distribution, and the effect of freeboard on the extreme bending moments.

The first column of Table I shows the characteristics of the Mariner design; the second column shows the characteristics of the Mariner with as much weight as possible shifted to midships (cargo). The third column of the table shows the Mariner with as much weight as possible shifted to the ends (cargo at ends). The weight distribution comparison between the Mariner, Mariner with cargo at midships, and Mariner with cargo at ends, is shown at the bottom of Fig. 1.

The second major variation on the Mariner was that of a radical increase in freeboard. The characteristics of the Mariner with increased freeboard are shown in the fourth column of Table I. The weight distribution for the model with increased freeboard was kept the same as that of the parent or original Mariner. Thus the first four models in Table I comprise an investigation of the effect of freeboard and the effect of weight distribution on one ship type.

Two other models were also selected to investigate the effect of ship type. These were a giant tanker design (shown in the fifth column of Table I), and a destroyer design (shown in the last column). The ship type investigation thus comprises the Mariner with a block coefficient of .61 and a displacement length ratio of 140; the destroyer with a block coefficient of .55, displacement length ratio of 60; and the giant tanker with a block coefficient of .80 and displacement length ratio of 170. Weight distribution curves for the tanker, the Mariner and the destroyer are shown at the top of Figure 1. All curves are plotted for ship or models of the same length.

TABLE I - MODEL CHARACTERISTICS

Model Number	2251A-V-1	2251A-V-2	2251A-V-3	2251B	2251D	2130
Design	Mariner	Mariner	Mariner	Mariner with Increased Freeboard	Giant Tanker	Destroyer
Weight Distribution	Design	Cargo ▮	Cargo-Ends	Design	Design	Design
Ship L.B.P., Feet	520.0	520.0	520.0	520.0	895.0	383.0
MODEL CHARACTERISTICS						
Nominal Model Scale	1:104	1:104	1:104	1:104	1:179	1:67.09
Length on 20 Stations, inches	60.00	60.00	60.00	60.00	60.00	68.5
Beam, inches	8.76	8.76	8.76	8.76	8.85	7.30
Draft inches	3.20	3.20	3.20	3.22	3.28	2.33 Fwd 2.68 Aft
Displacement, Pounds, F.W.	38.1	38.1	38.1	38.1	52.0	25.1
B/H	2.72	2.72	2.72	2.72	2.70	2.92
C_b	0.61	0.61	0.61	0.61	0.80	0.55
$C_{▮}$	0.98	0.98	0.98	0.98	0.99	-
$\Delta/(L/100)^3$, Design	140	140	140	140	172	62
LCB, % Station Length From ▮	1.42 Aft	1.40 Aft	1.45 Aft	1.44 Aft	0.32 Fwd	3.33 Aft
Gyradius, % Station Length	24.3	15.9	30.3	24.2	22.7	23.4
Natural Pitching Period, Sec.	0.70	0.60	0.80	0.70	0.70	0.60
Natural Heaving Period, Sec.	0.75	0.75	0.80	0.75	0.80	0.65
Natural Frequency of Vibration, CPS	16.5	17.2	14.1	16.5	13.7	10.7
Freeboards: Aft, inches Fwd, inches	2.30 4.05	2.30 4.05	2.30 4.05	5.48 5.48	1.56 2.52	1.37 3.44
V.C.G., inches	3.34	3.14	3.36	3.39	2.62	1.23
HALF MODEL, FWD SECTION						
Weight, lbs.	17.9	17.9	17.9	17.9	26.6	11.2
LCG Fwd ▮, inches	12.10	6.04	15.88	12.10	11.46	12.88
VCG, inches	3.32	3.46	3.43	3.34	2.60	1.06
K_o, % Station Length/2	26.9	24.8	28.2	26.8	23.2	23.9
HALF MODEL, AFT SECTION						
Weight. lbs.	20.2	20.2	20.2	20.2	25.4	13.9
LCG Aft ▮, inches	12.32	6.93	15.72	12.33	11.59	14.56
VCG, inches	3.37	2.86	3.30	3.44	2.65	1.37
K_o, % Station Length/2	25.5	21.8	32.0	25.5	25.2	25.6

III. INSTRUMENTATION

The method used to measure bending moment was that used previously at DL: wooden models, split in half and connected only by a balance capable of yielding a signal proportional to the bending moment. The models were towed on an apparatus in Tank No. 3 (300 x 12 x 6 ft) and allowed freedom in pitch, heave and surge. Roll, sway and yaw motions were restrained. Records obtained were of midship bending moment, pitch, heave and wave elevation ahead of the model.

IV. TEST PROGRAM

Each model was tested in five wave lengths, ranging in length from half the model length to 1-3/4 its length. The wave heights for each wave length were varied from approximately ($\lambda/30$) up to the maximum obtainable, which generally ranged between ($\lambda/11$ and $\lambda/8$). Four or five wave heights were used with each wave length. The test program included five speed-heading combinations, as follows:

1. head seas, forward speed at a Froude No. of about .13,
2. head seas, zero speed,
3. head seas, drifting astern at the speed produced by the highest wave generated for each wave length,
4. following seas, zero speed, and
5. following seas, a forward speed corresponding to about twice the astern drifting speed obtained in that case in head seas.

The total program including all models, wave lengths, wave heights, and all speed-heading combinations for each model consisted of some 650 good runs.

V. DATA REDUCTION

The average amplitudes of wave, pitch, heave and midship bending moment for each model in each test were calculated by measuring maxima and minima of between 10 and 18 moment and motion cycles on the oscillograph records. These were averaged and

converted to non-dimensional form. Notation and details on the non-dimensionalizing are in the Appendix. Because the resulting data made up about 600 plots of response vs. wave steepness, curves were fitted to the experimental points by a computer in order to avoid subjectivity in fairing of the data. The form of equation used to fit all of the data was

$$Y = a\left(\frac{h}{\lambda}\right) + b\left(\frac{h}{\lambda}\right)^N$$

where, N = 2, 3 or 4 (according to which yielded the least mean square error)

h/λ = wave steepness

λ = wave length

Y = average amplitude of response.

Sample basic test results are shown (Figs. 2 to 4) with the resulting fitted curves. Sagging moment and pitch amplitudes are plotted above the middle axis of each plot, hogging moment and heave below.

VI. PLOTS OF FITTED CURVES

Figures 5 through 10 show plots of faired mean bending moments and motions amplitudes for the parent Mariner model only. These are shown as functions of wave steepness for various wave lengths. Numbers shown on the plot signify the wave length to ship length ratio. The first set of two plots is for head seas at forward speeds, the second set for head seas at zero speed, and the third set for head seas drifting astern. The static calculations indicated on the bending moment plots with the notation "L/20 Static" etc., are for the static calculation in a 1.0L wave of height noted and do not include Smith effect. The scales at the right of the plot labeled μ_{HA} and μ_{AA} are scales of absolute bending moment. This is simply the wave bending moment scale translated in the proper direction to account for the still water bending moment.

It is interesting to note from the plots of the bending moments that moments exceeding the L/20 static calculation were measured in all three cases shown. These occurred primarily in the longer wave lengths at wave steepnesses above about 1/12th. This observation holds equally well for all

other models and variations tested. It is also interesting to note that no consistent indication of an upper bound is shown. In Fig. 7, for example, for bending moments, the line for the sagging moment in a 1.25L wave shows considerable curvature and tends to flatten out at about a wave steepness of 1/10th. Similar trends on the same figure can be noted for hogging moments in the longer waves. Considering all models tested, no consistent indication has so far been found of an upper bound on wave bending moments reached prior to a limiting wave steepness. For the same model, indications of an upper bound are found in some wave lengths and not in others.

VII. CROSS PLOTS OF BENDING MOMENTS AND MOTIONS DATA

Figures 11 to 22 are cross-plots of faired bending moment motions data for a wave steepness of 1/10th. Bending moments and motions are plotted as functions of wave length for all six models. Figures 11 through 14 show results for head seas at forward speed; Figs. 15 through 18 show results for head seas at zero speed; and Figs. 19 through 22 show results for head seas drifting astern. The vertical scales on these figures are similar to those preceeding; all bending moments are in non-dimensionalized form as are the heaving amplitudes. Where possible, L/20 static calculations are shown. The vertical scales on the right-hand side of the bending moment figures show the zeros for the absolute bending moment scale. Thus it is seen in Fig. 11, for example, that the Mariner with cargo amidships case in waves of steepness of 1/10th has bending moments which are always sagging, whereas for the cargo-at-ends case, bending moments are always hogging. It can be noted at this point that for waves of steepness ratio of 1/10th a Froude No. of around .13 is an extremely high speed, and in fact it is estimated that none of the models tested could maintain this speed with the power normally installed in the full scale ships.

Because the realism or validity of the tests in head seas at forward speeds could be questioned, the following remarks on the effects of variations in model parameters on extreme moments are confined to the results at zero and the drifting speed.

1. Weight Distribution Investigation. When weight is shifted toward amidships, it appears that the result is higher bending moment amplitudes and lower pitching amplitudes than those of the parent model. Conversely, shifting weight to the ends of the model results in lower bending moments and larger pitching amplitudes (See Figs. 15, 17, 19, 21).

2. Freeboard Investigation. Motion amplitudes appear to be approximately the same in both the high freeboard model and the parent model. However, some difference in bending moments is seen: that is, the same or lower hogging moments and perhaps somewhat greater sagging moments than experienced by the parent model.

3. Ship Type Investigation. The non-dimensionalized moment amplitudes generally seem to increase in this order: destroyer, Mariner, tanker--although some exceptions to this progression are shown. The hogging and sagging bending moment amplitudes as experienced for the destroyer and the Mariner, and the sagging amplitude for the tanker are similar in magnitude. The hogging moments for the tanker, however, are noticably larger than those of either Mariner or destroyer. This large hogging moment in the tanker probably does not have much significance because the still water bending moment of the tanker is a hogging moment (see Fig. 16, for example), and the controlling design moment for the tanker would very likely be a sagging moment.

No final conclusions have been drawn at present concerning the effect of weight distribution or model type but it has been shown that the variation of weight distribution is at least of equal importance as details of hull form. Within the same ship, radical variations of the distribution of weights can produce as wide a variation in wave bending moments as experienced by ships of quite different form.

VIII. FINAL REMARKS

It appears that an upper limit to wave bending moments--considering all possible combinations of variables investigated--will probably be dictated, in general, by the heights of the waves. When the waves reach a physical upper limit, bending moments will also do so. Also, wave bending moments exceeding the L/20 standard static calculation values were quite commonly measured in the experiments.

APPENDIX: NOTES ON FIGURES AND NON-DIMENSIONALIZING

1. Bending Moment Amplitudes:

All results are presented as non-dimensional bending moment coefficients:

$$\mu = \frac{\text{Bending Moment}}{\rho g \, L^3 B}$$

where, ρg = weight density of water

L = model length (LBP)

B = maximum model beam

The symbols μ_S and μ_H stand for wave sagging and hogging moment coefficients respectively. The condition $\mu_S = \mu_H = 0$ corresponds to the midship moment existing in the model afloat in calm water.

The symbols μ_{SA} and μ_{HA} stand for "absolute" sagging and hogging moment coefficients respectively. Scales of μ_{SA} and μ_{HA} were obtained by translating the origin of the $\mu_S - \mu_H$ scales by the calculated bending moment in still water.

These scales have the frame of reference ordinarily used in design.

2. Motion Amplitudes:

The symbol $(2\theta_o)$ or (2θ) stands for the double amplitude of pitch in degrees.

The symbol $2Z_o/L$ is a non-dimensionalized heaving double amplitude.

3. Wave Lengths and Steepness:

Wave length (λ) is expressed as wave length to ship length ratio, (λ/L) times (L).

Wave steepness is expressed as the wave height to length ratio (h/λ).

4. Heading:

In accordance with the usual towing tank convention, head and following seas are denoted by heading angles of 180° and 0° respectively.

5. Speeds:

The standard test program included five speed-heading combinations:

Head seas (180°)

1. forward speed: $V/\sqrt{gL}$ about .13 ±.01
2. zero speed
3. drifting backwards at the speed produced by the highest wave generated for each wave length.

Following seas (0°)

1. zero speed
2. forward speed corresponding to about twice the drifting speed in 3 above.

All speeds quoted in the figures are in terms of Froude number. Table II gives the conversions of the Froude numbers quoted in the figures to speed-length ratio and knots for a 500-foot ship.

TABLE II - SPEED CONVERSION

Heading	$V/\sqrt{gL}$	$V_K/\sqrt{L}$	Knots for 500-ft ship (approx.)
180°	0.12 to .14	.40 to .47	9.0 to 11
180°	0.0	0.0	0
180°	- .08 to -.15	-.27 to -.50	-6 to -11
0°	0.0	0.0	0
0°	.16 to .26	.54 to .87	12 to 20

The rather wide speed ranges shown for the drifting and high speed following-sea cases in Table II are a consequence of the test speed being dependent on wave length. Once the drifting speed in the highest wave for each wave length was established, test Froude numbers in less steep waves were held within ±.02 or about ±2 knots for a 500-foot ship. Differences in drifting speed for different models in the same wave length were within the test tolerance above.

The actual speed ranges obtained in each wave length are tabulated in Table III.

TABLE III - SPEED RANGES, ALL MODELS

Heading, Condition	180° Forward Speed	180°, Drifting	0°, Forward Speed About twice the Drift Speed
λ/L = 0.75	$V/\sqrt{gL}$ = .12 to .14	-.08 to -.12	.16 to .20
1.00	$V/\sqrt{gL}$ = .12 to .14	-.10 to -.14	.19 to .23
1.25	$V/\sqrt{gL}$ = .12 to .14	-.11 to -.15	.22 to .26
1.50	$V/\sqrt{gL}$ = .12 to .14	-.11 to -.15	.21 to .25
1.75	$V/\sqrt{gl}$ = .12 to .14	-.10 to -.14	.19 to .23

6. Static Calculations:

All available results of static bending moment calculations are plotted in the applicable figures with the notation "L/20 Static," "L/10 Static," etc.

All results are for the static calculation in a 1.0L wave of height noted and do not include Smith effect.

Notes for Figures 5 to 10:

The labels on each mean line refer to wave length.

Only the points for the sagging static calculation are labeled, results for the hogging calculation are plotted in the same manner.

No hogging calculation for the large tanker was available.

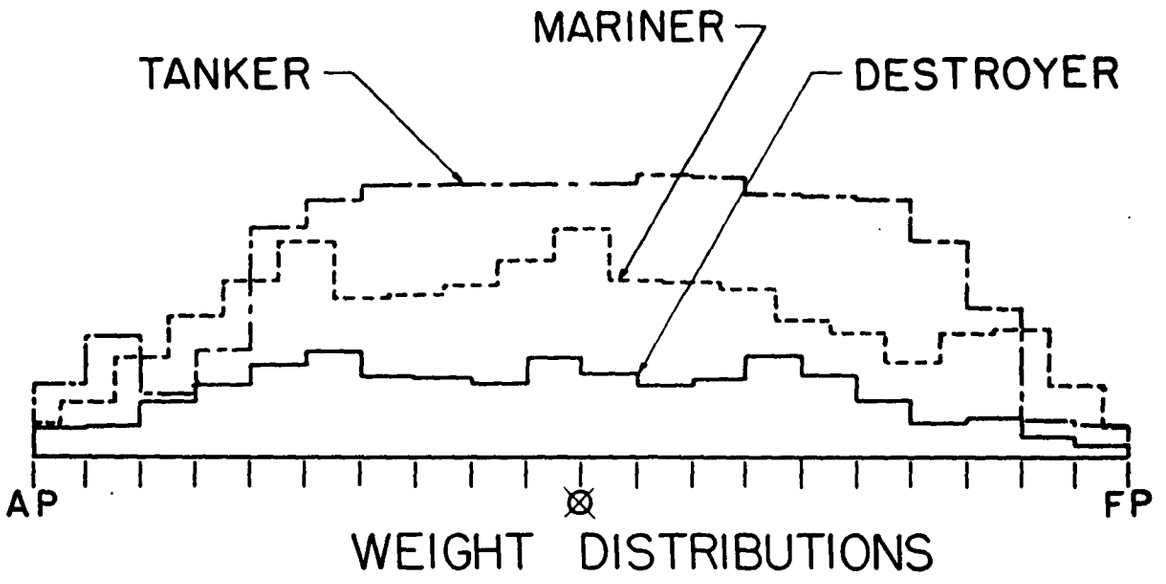
MARINER
TANKER
DESTROYER
AP
FP
WEIGHT DISTRIBUTIONS

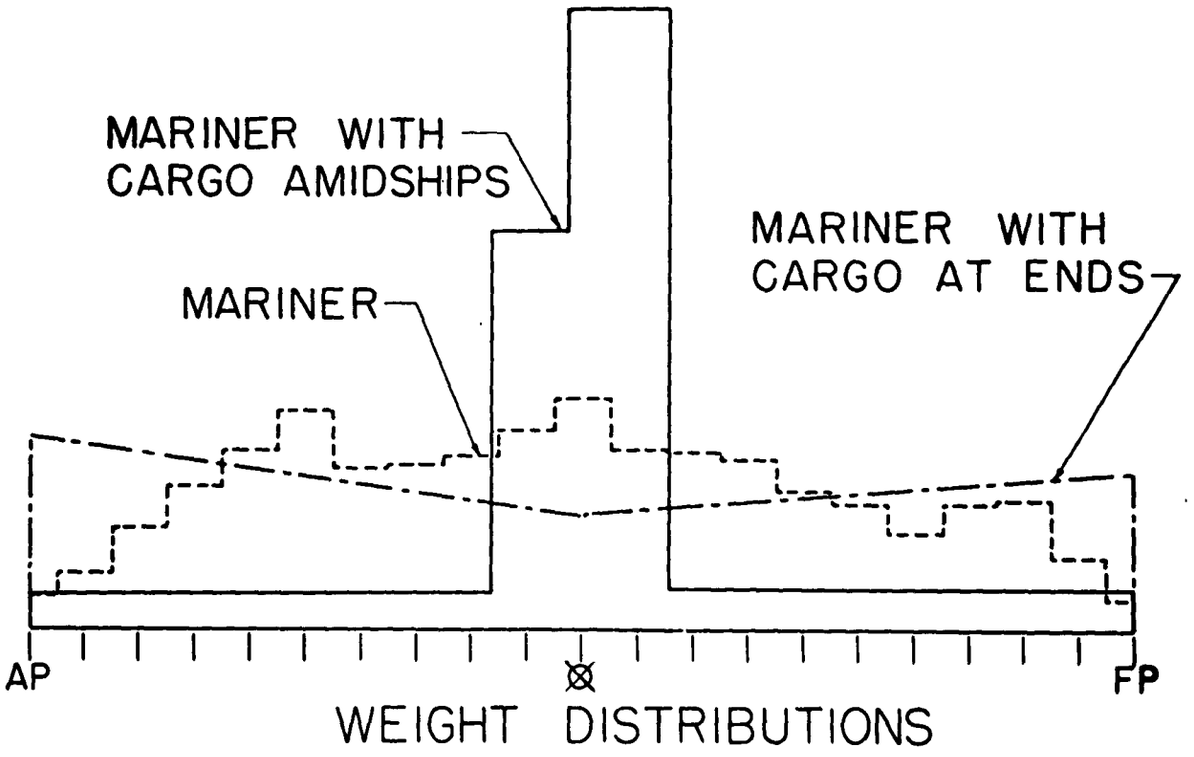
MARINER WITH
CARGO AMIDSHIPS
MARINER WITH
CARGO AT ENDS
MARINER
AP
FP
WEIGHT DISTRIBUTIONS

FIGURE 1

MODEL: 2251A-VI TEST GROUP: 1.1111075

WAVE LENGTH: 0.75 L MODEL HEADING: 180°

APPROX. MODEL SPEED: $v/\sqrt{gL}$ = 0.0

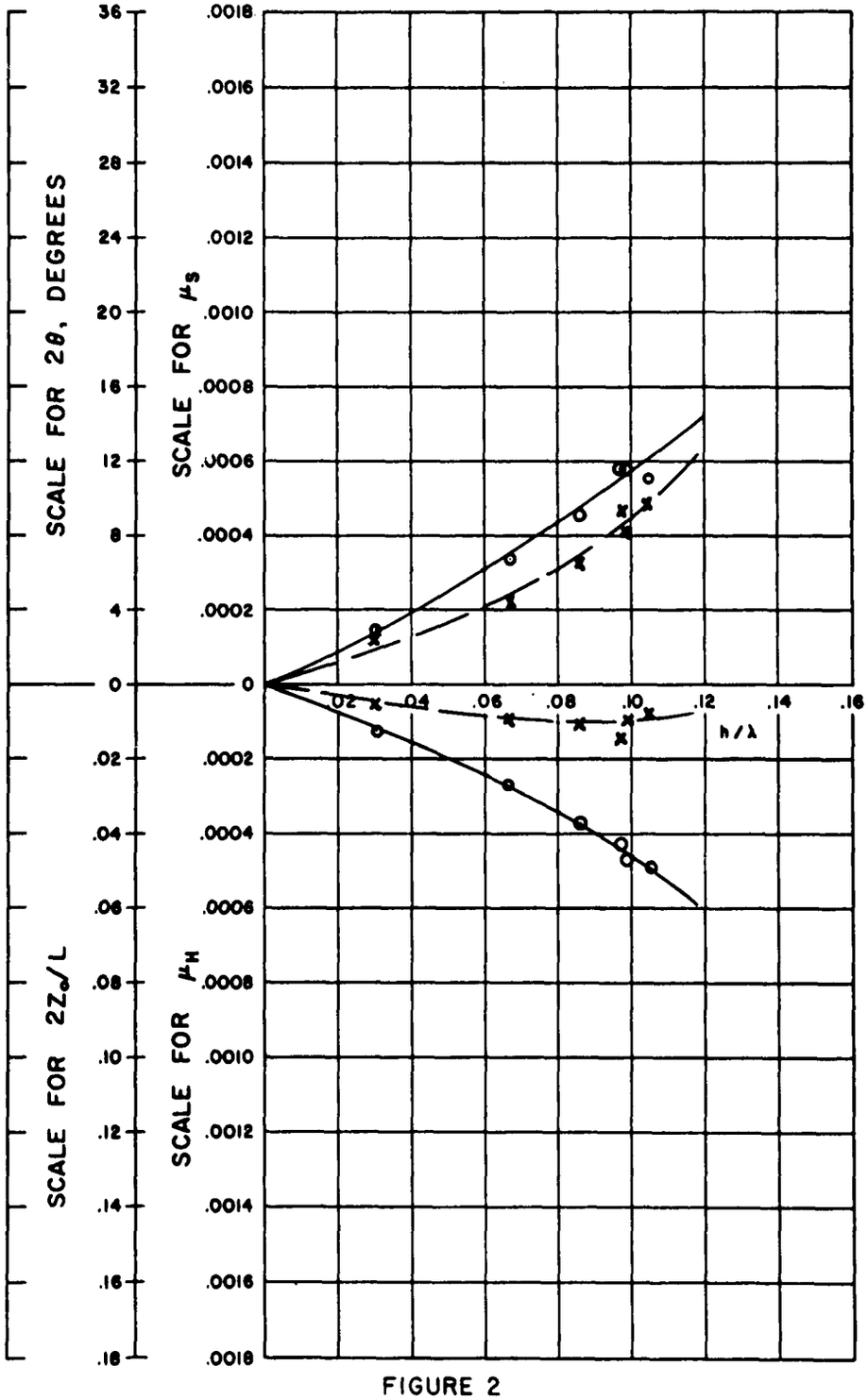

FIGURE 2

MODEL: 2251 A-VI TEST GROUP: 1.1111100

WAVE LENGTH: 1.00 L MODEL HEADING: 180°

APPROX. MODEL SPEED: $v/\sqrt{gL}$ = 0.0

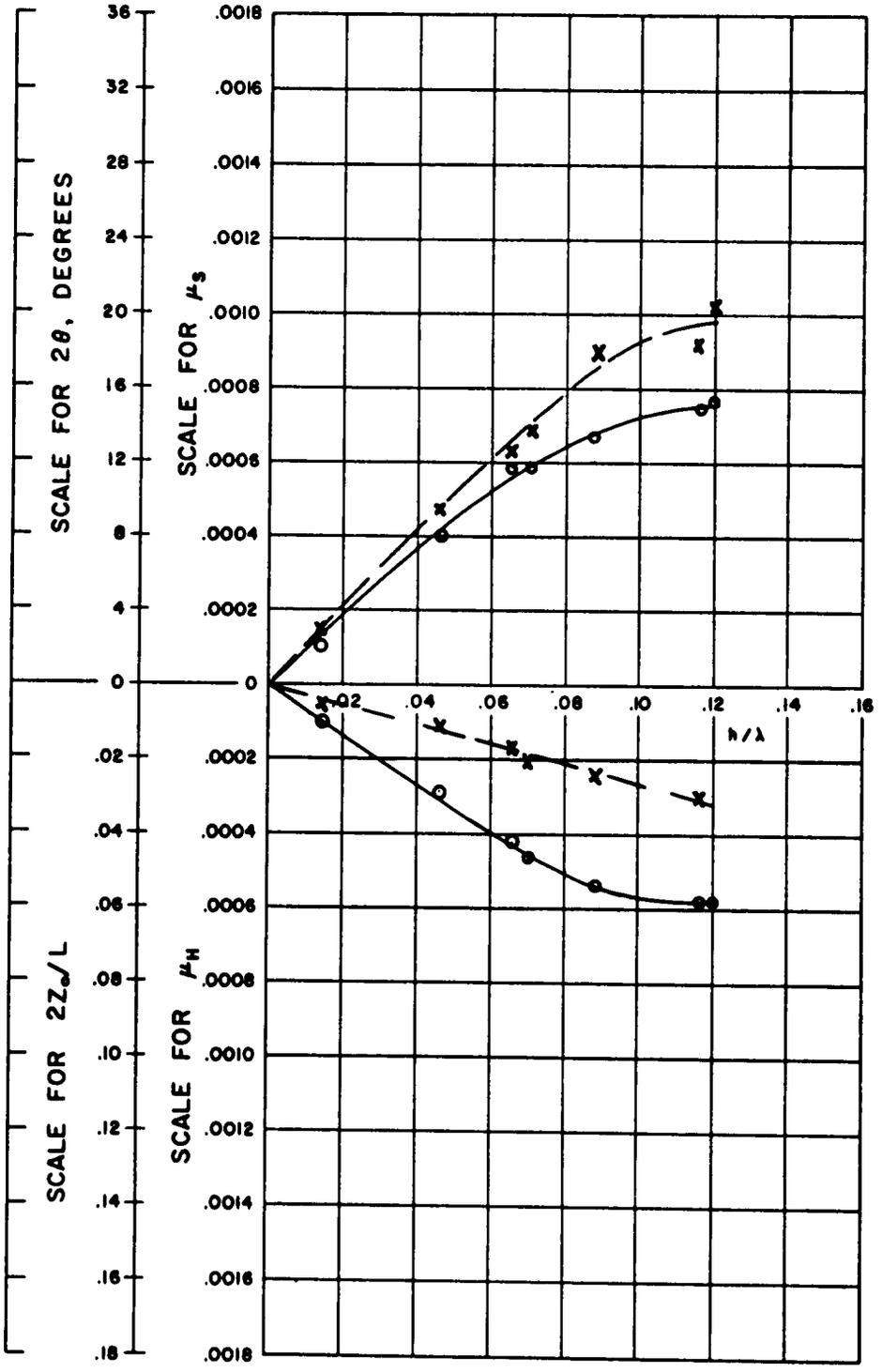

FIGURE 3

MODEL: 2130 TEST GROUP: 2.1022125

WAVE LENGTH: 1.25 L MODEL HEADING: 180°

APPROX. MODEL SPEED: $v/\sqrt{gL}$ = 0.12 TO 0.14

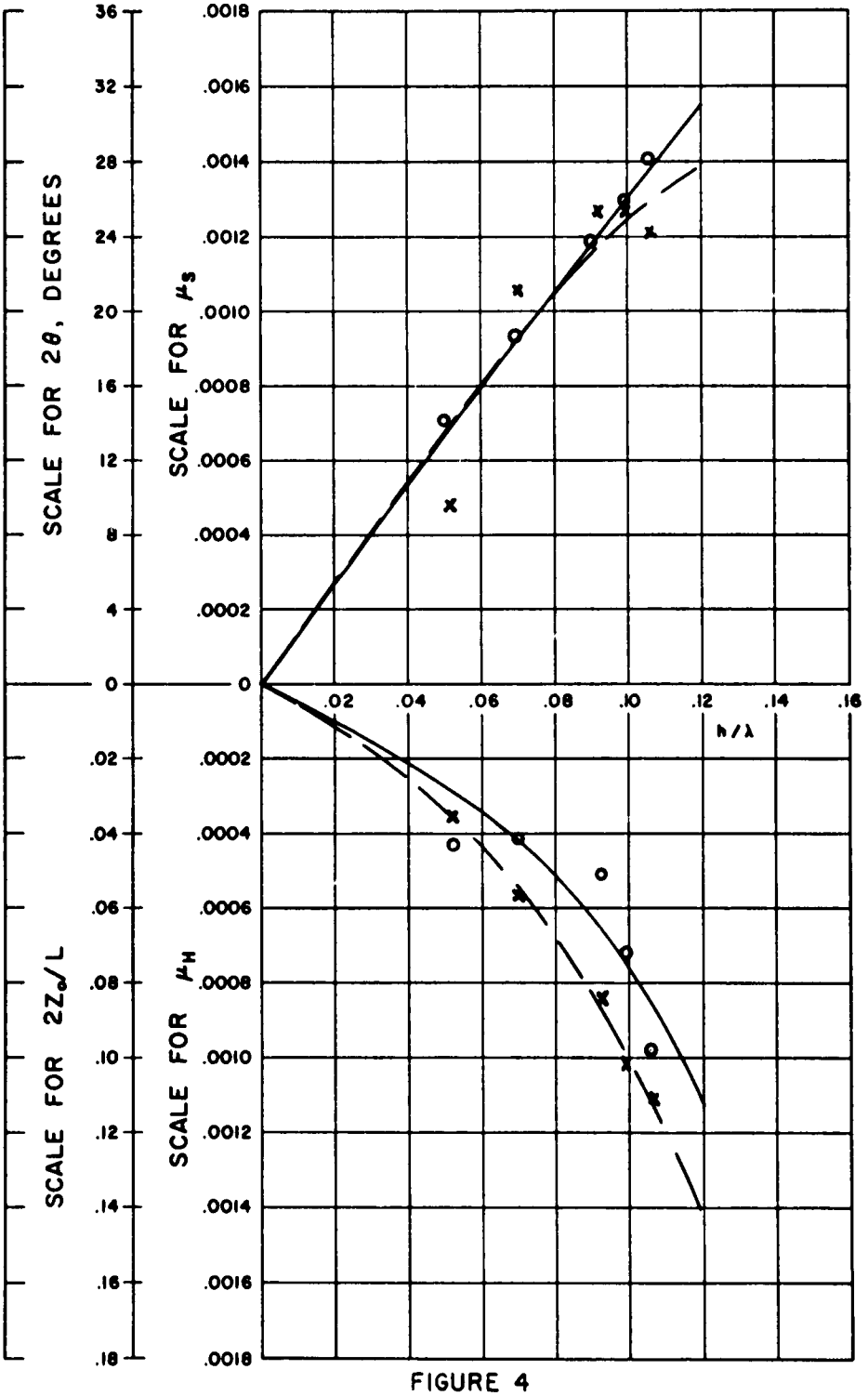

FIGURE 4

MODEL: 2251A-VI, MARINER

MODEL HEADING: 180°

APPROX. MODEL SPEED: $v/\sqrt{gL}$ = 0.12 TO 0.14

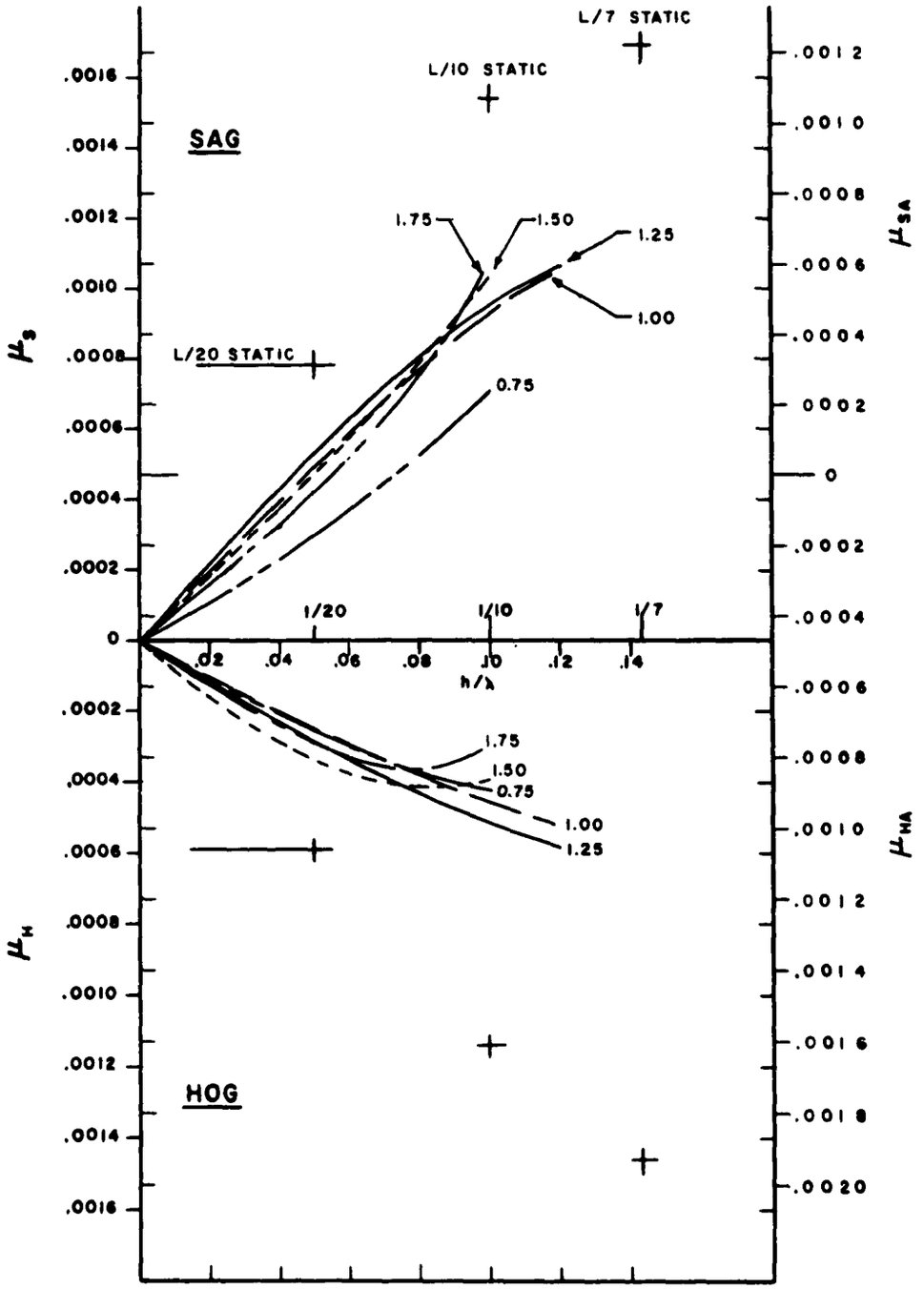

FIGURE 5

MODEL: 2251A-VI, MARINER

MODEL HEADING 180°

APPROX. MODEL SPEED: $v/\sqrt{gL}$ = 0.12 TO 0.14

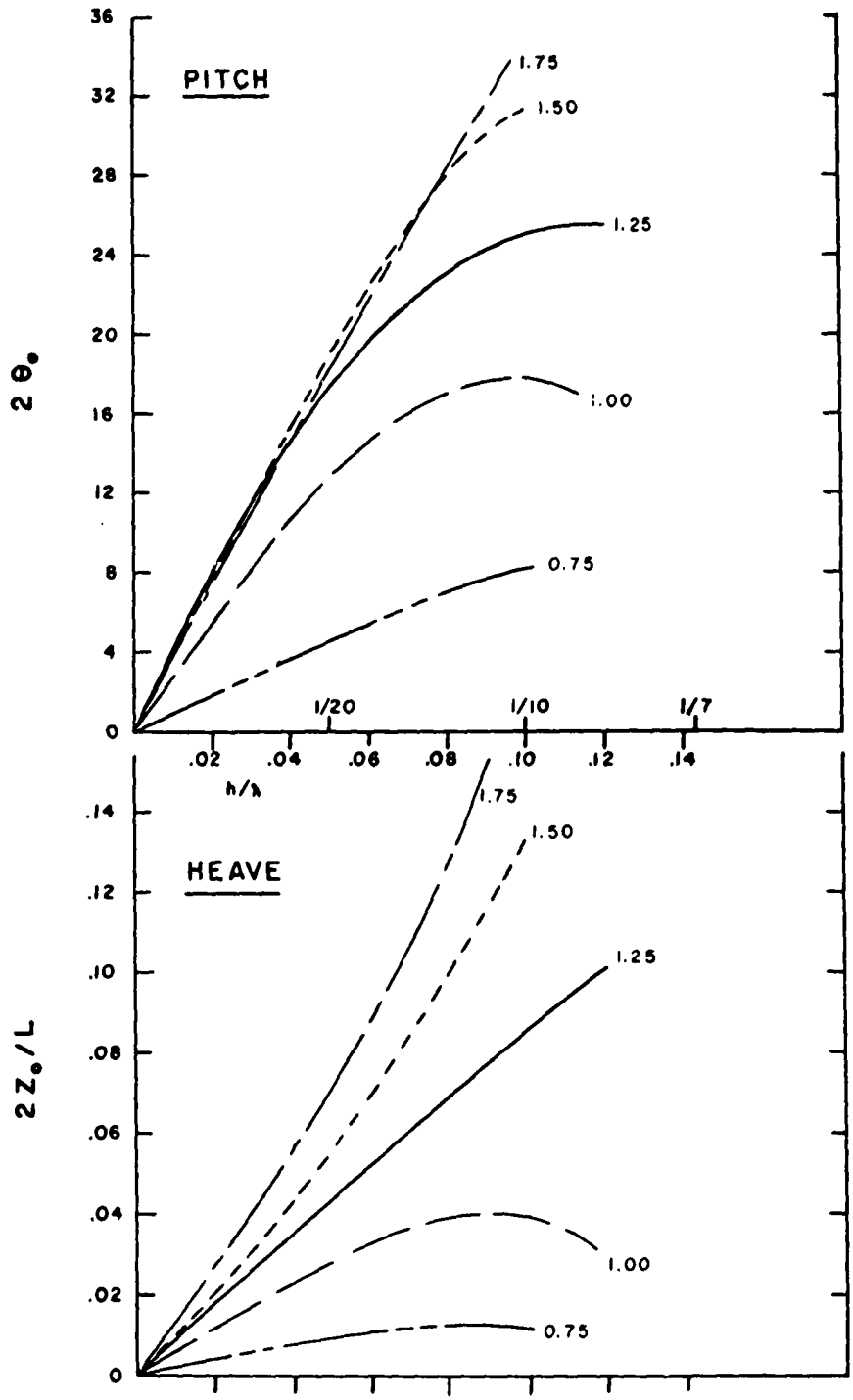

FIGURE 6

MODEL: 2251A-VI, MARINER

MODEL HEADING: 180°

APPROX. MODEL SPEED: $v/\sqrt{gL}$ = 0.0

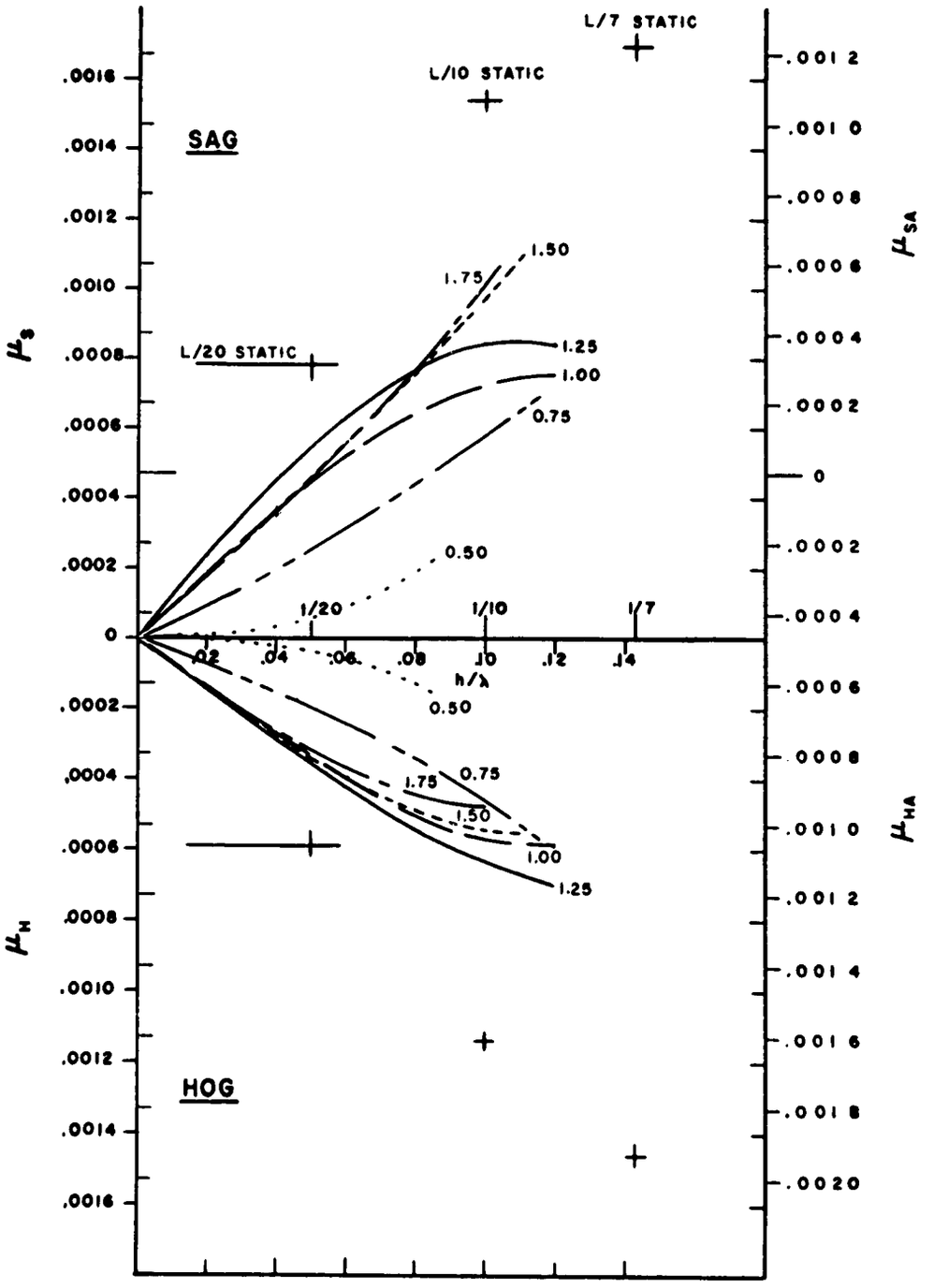

FIGURE 7

MODEL: 2251A-VI, MARINER

MODEL HEADING 180°

APPROX. MODEL SPEED: $v\sqrt{gL}$ = 0.0

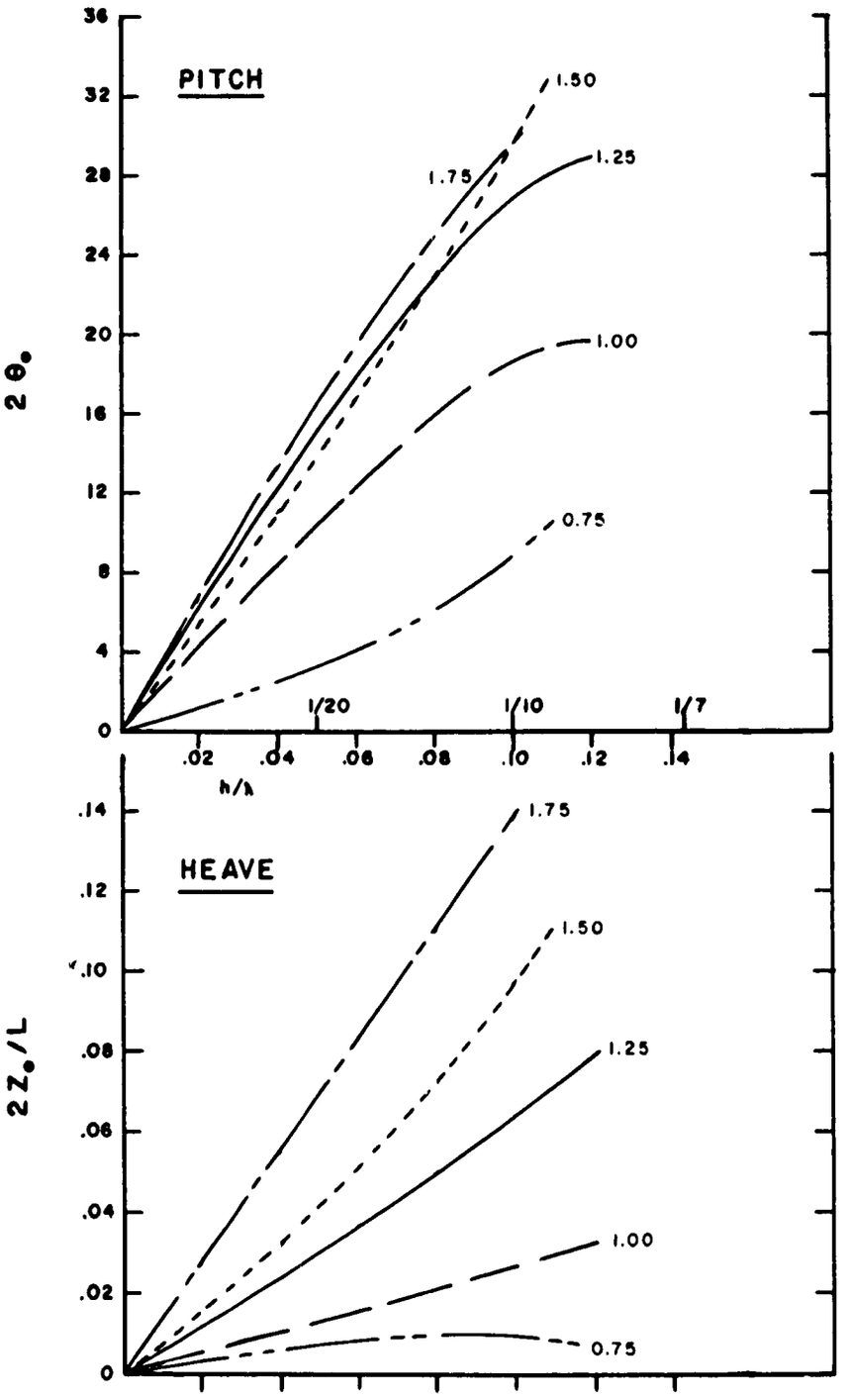

FIGURE 8

MODEL: 2251A-VI, MARINER

MODEL HEADING: 180° (DRIFT)

APPROX. MODEL SPEED : $v/\sqrt{gL}$ = -0.08 TO -0.15

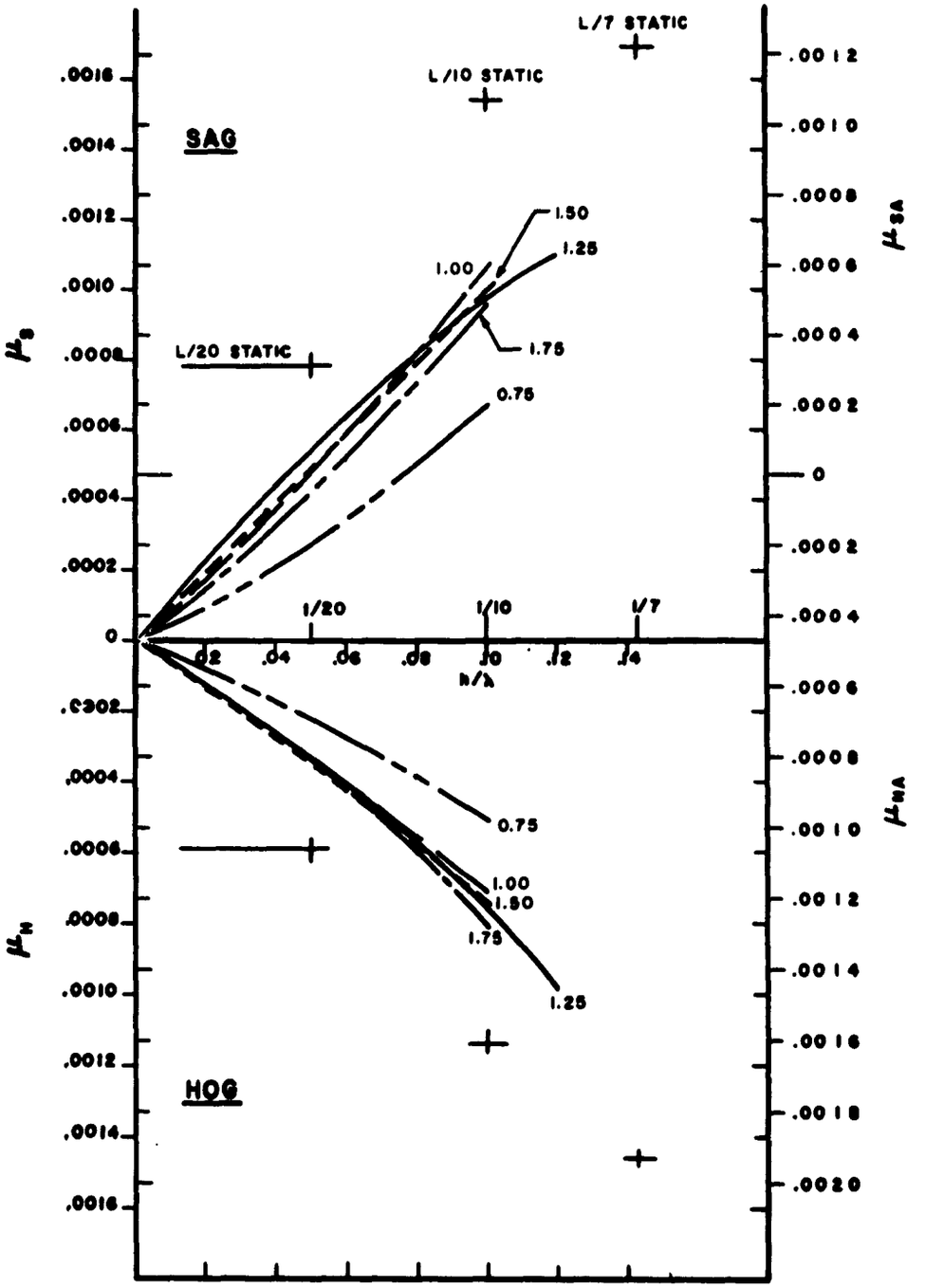

FIGURE 9

MODEL: 2251A-VI, MARINER

MODEL HEADING 180° (DRIFT)

APPROX. MODEL SPEED: $v/\sqrt{gL}$ = -0.08 TO-0.15

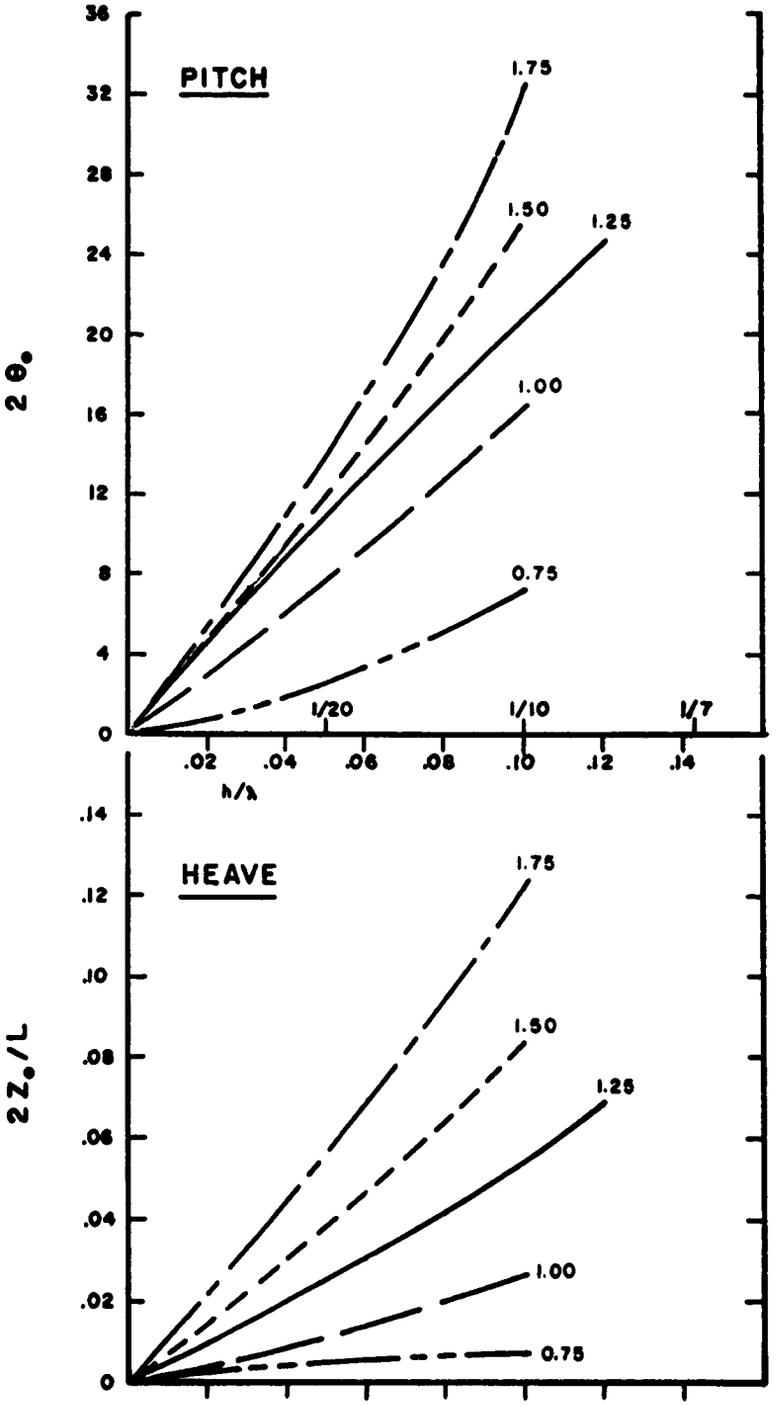

FIGURE 10

CROSS PLOT OF FAIRED BENDING MOMENTS

MARINER VARIATIONS

WAVE HT. 1/10 LENGTH HEADING 180°

SPEED: $V/\sqrt{gL}$ = 0.12 TO 0.14

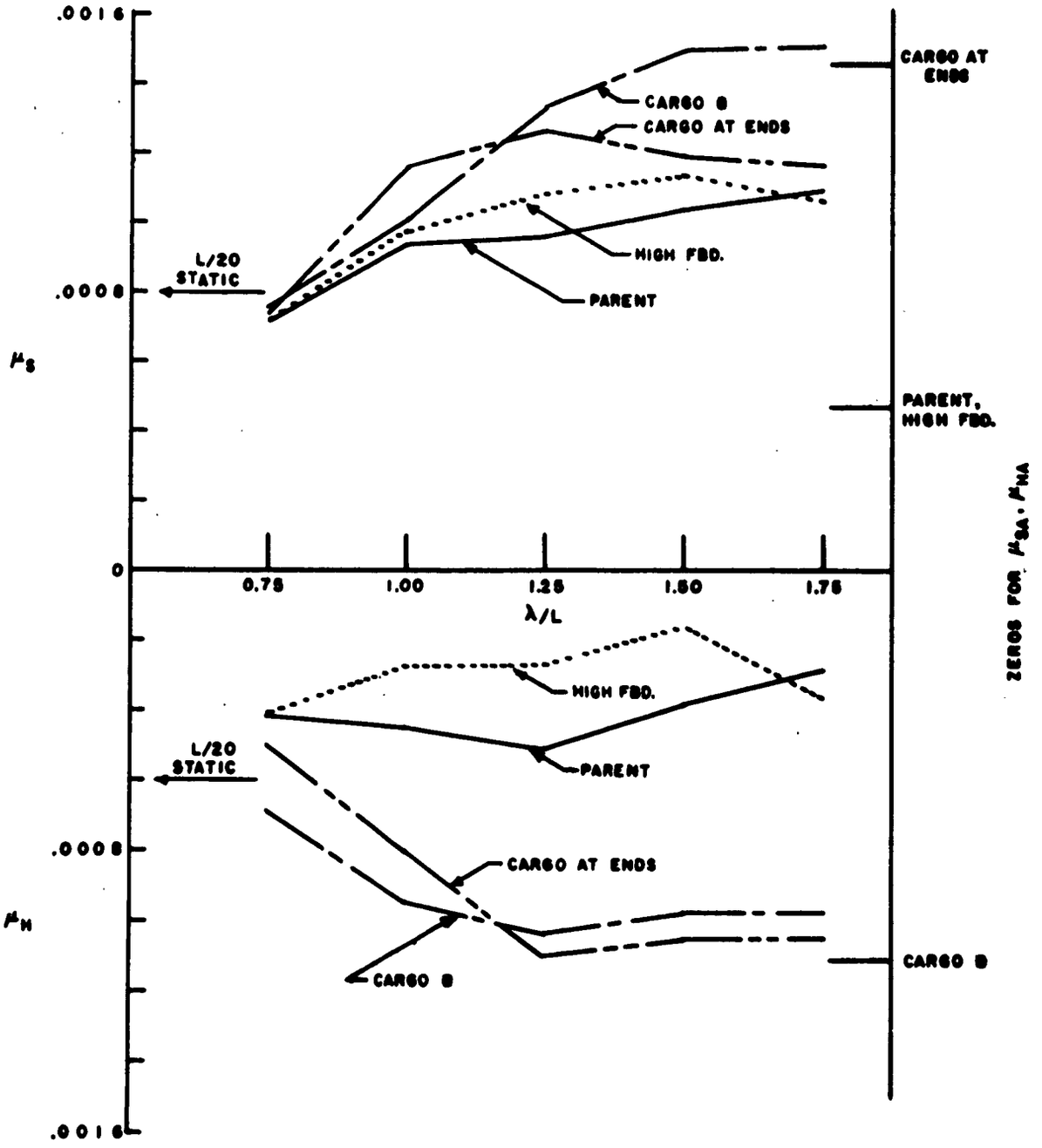

FIGURE 11

CROSS PLOT OF FAIRED BENDING MOMENTS
WAVE HT. 1/10 LENGTH, HEADING 180°
SPEED: $V/\sqrt{gL}$ = 0.12 TO 0.14

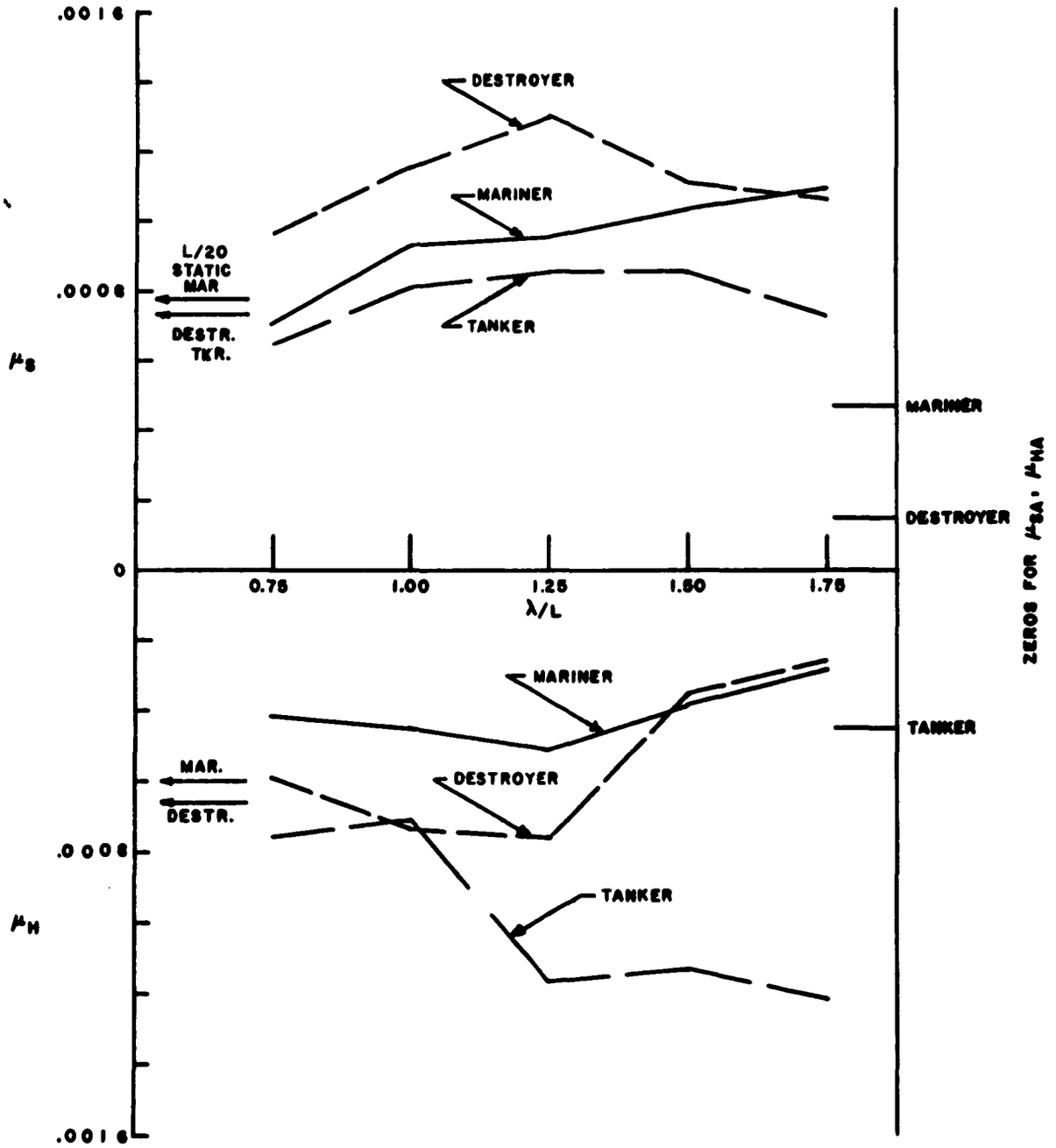

FIGURE 12

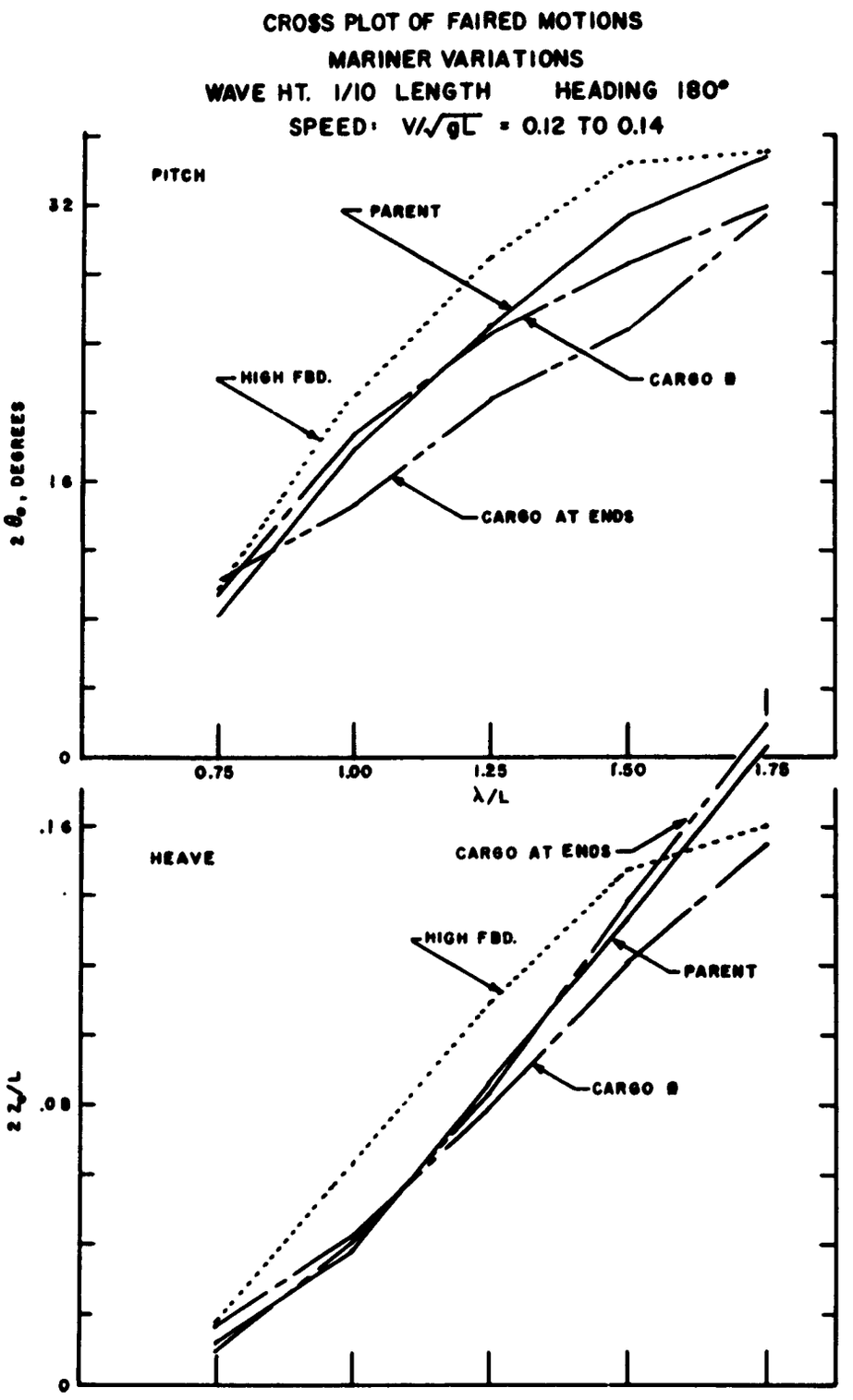
CROSS PLOT OF FAIRED MOTIONS
MARINER VARIATIONS
WAVE HT. 1/10 LENGTH HEADING 180°
SPEED: V/√gL = 0.12 TO 0.14
PITCH
PARENT
HIGH FBD.
CARGO B
CARGO AT ENDS
2θ₀, DEGREES
32
16
0
0.75
1.00
1.25
1.50
1.75
λ/L
HEAVE
CARGO AT ENDS
HIGH FBD.
PARENT
CARGO B
2z₀/L
.16
.08
0

FIGURE 13

CROSS PLOT OF FAIRED MOTIONS
WAVE HT. 1/10 LENGTH HEADING 180°
SPEED: $V/\sqrt{gL}$ = 0.12 TO 0.14

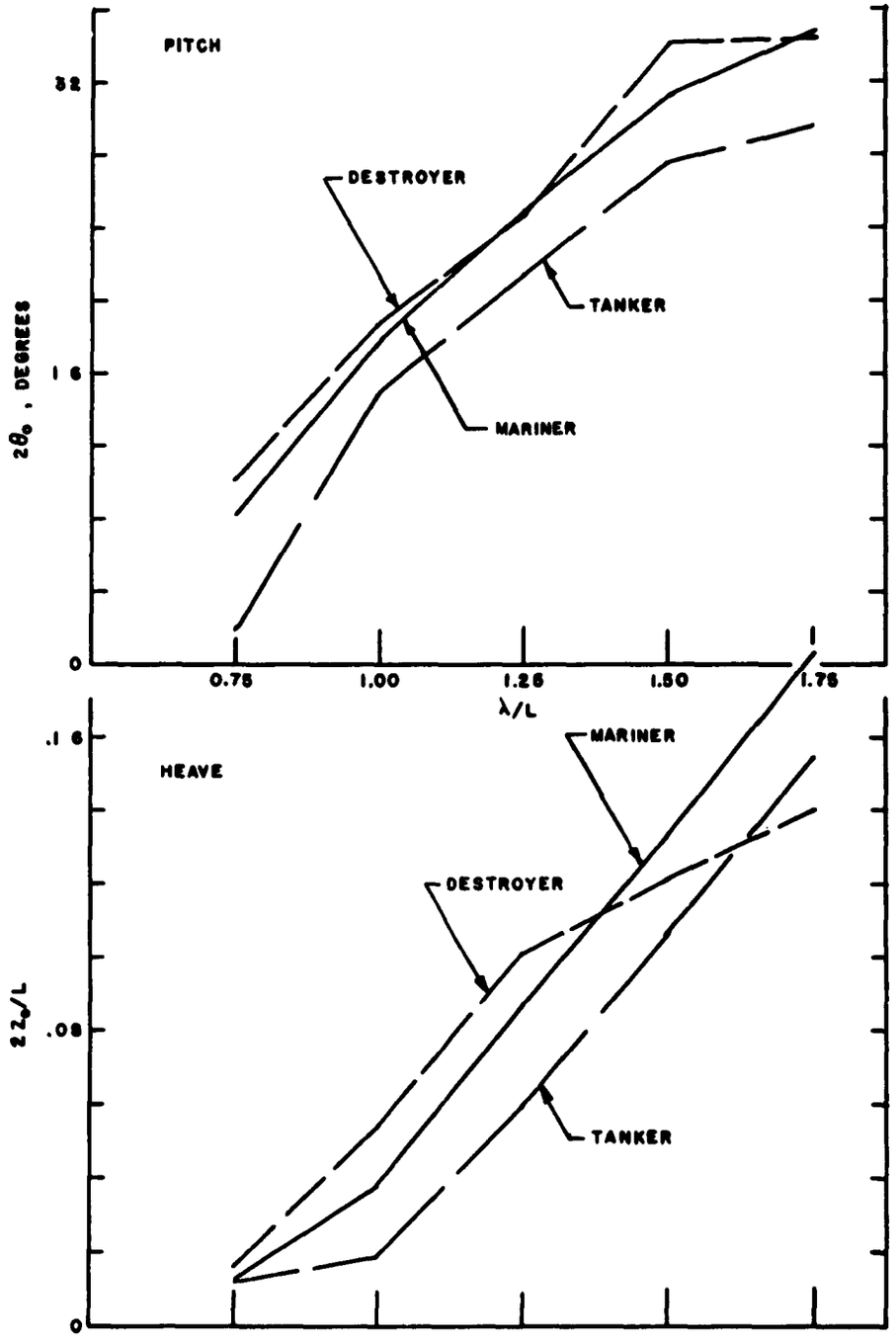

FIGURE 14

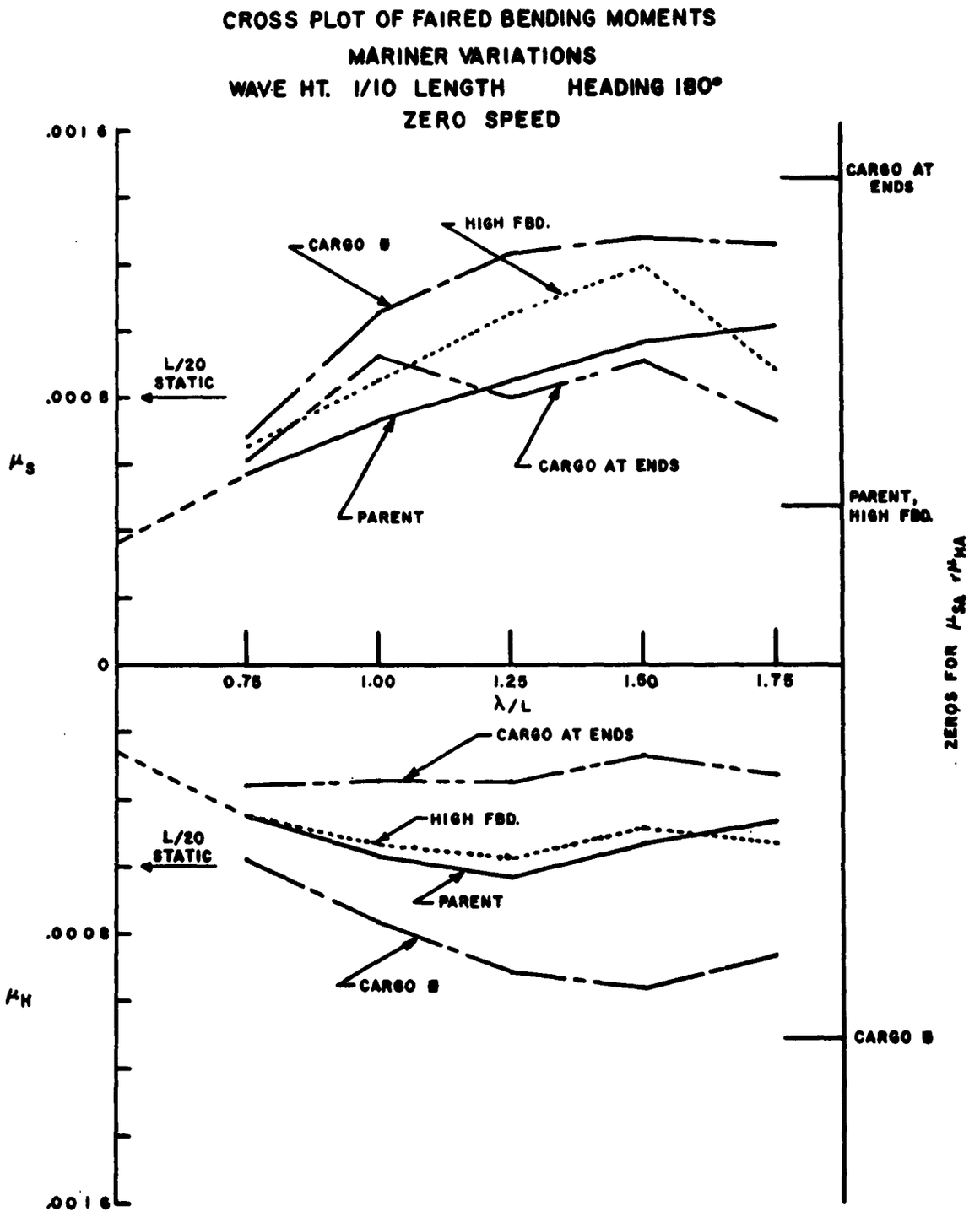
CROSS PLOT OF FAIRED BENDING MOMENTS
MARINER VARIATIONS
WAVE HT. 1/10 LENGTH HEADING 180°
ZERO SPEED
.0016
.0008
0
.0008
.0016
μ_S
μ_H
L/20 STATIC
L/20 STATIC
CARGO B
HIGH FBD.
CARGO AT ENDS
PARENT
CARGO AT ENDS
HIGH FBD.
PARENT
CARGO B
0.75
1.00
1.25
1.50
1.75
λ/L
CARGO AT ENDS
PARENT, HIGH FBD.
CARGO B
ZEROS FOR μ_{SA} & μ_{HA}

FIGURE 15

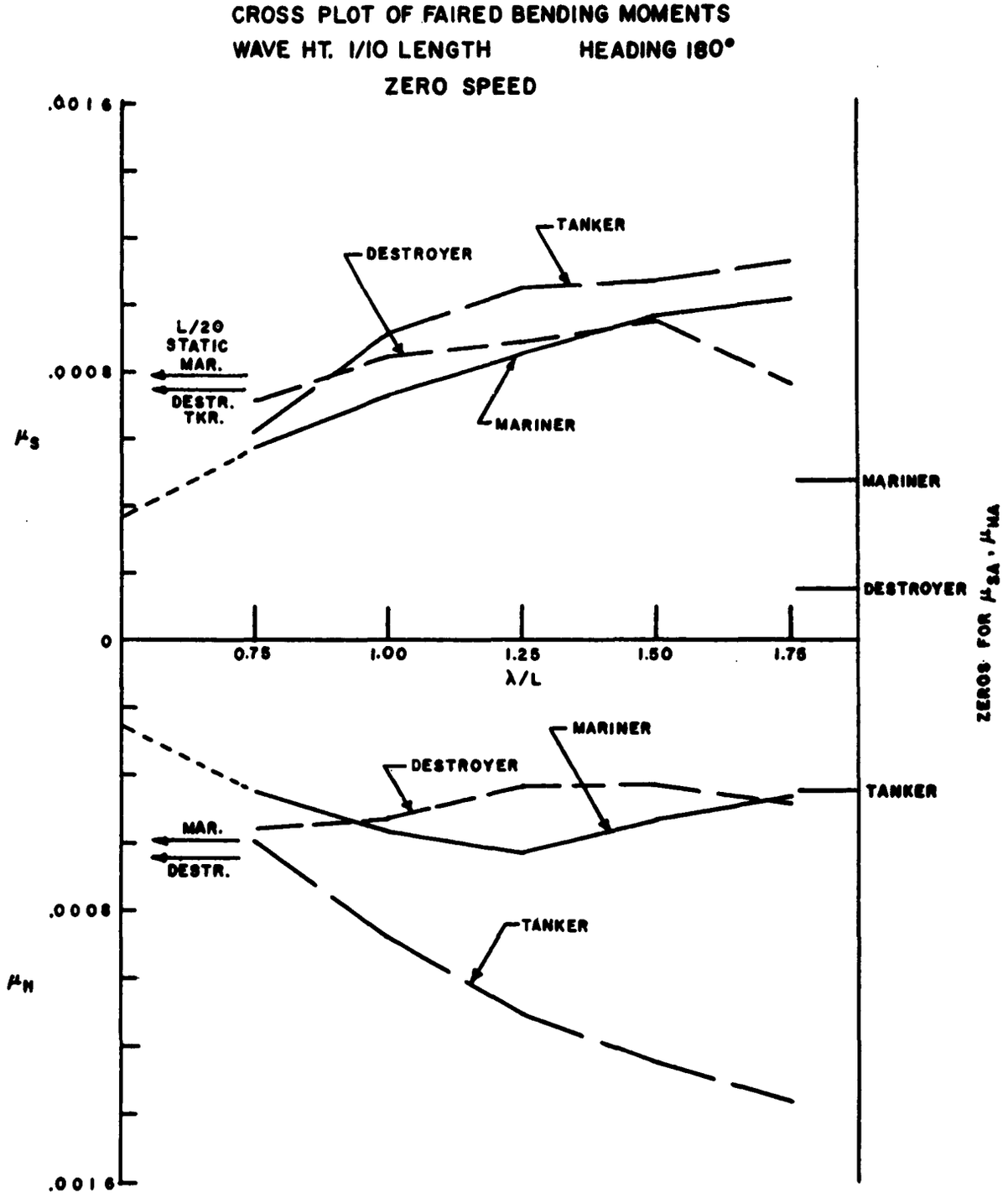
CROSS PLOT OF FAIRED BENDING MOMENTS
WAVE HT. 1/10 LENGTH HEADING 180°
ZERO SPEED
.0016
.0008
0
.0008
.0016
μ_S
μ_H
L/20 STATIC MAR.
DESTR. TKR.
DESTROYER
TANKER
MARINER
MARINER
DESTROYER
0.75
1.00
1.25
1.50
1.75
λ/L
MARINER
DESTROYER
TANKER
MAR.
DESTR.
TANKER
ZEROS FOR μ_{SA}, μ_{HA}

FIGURE 16

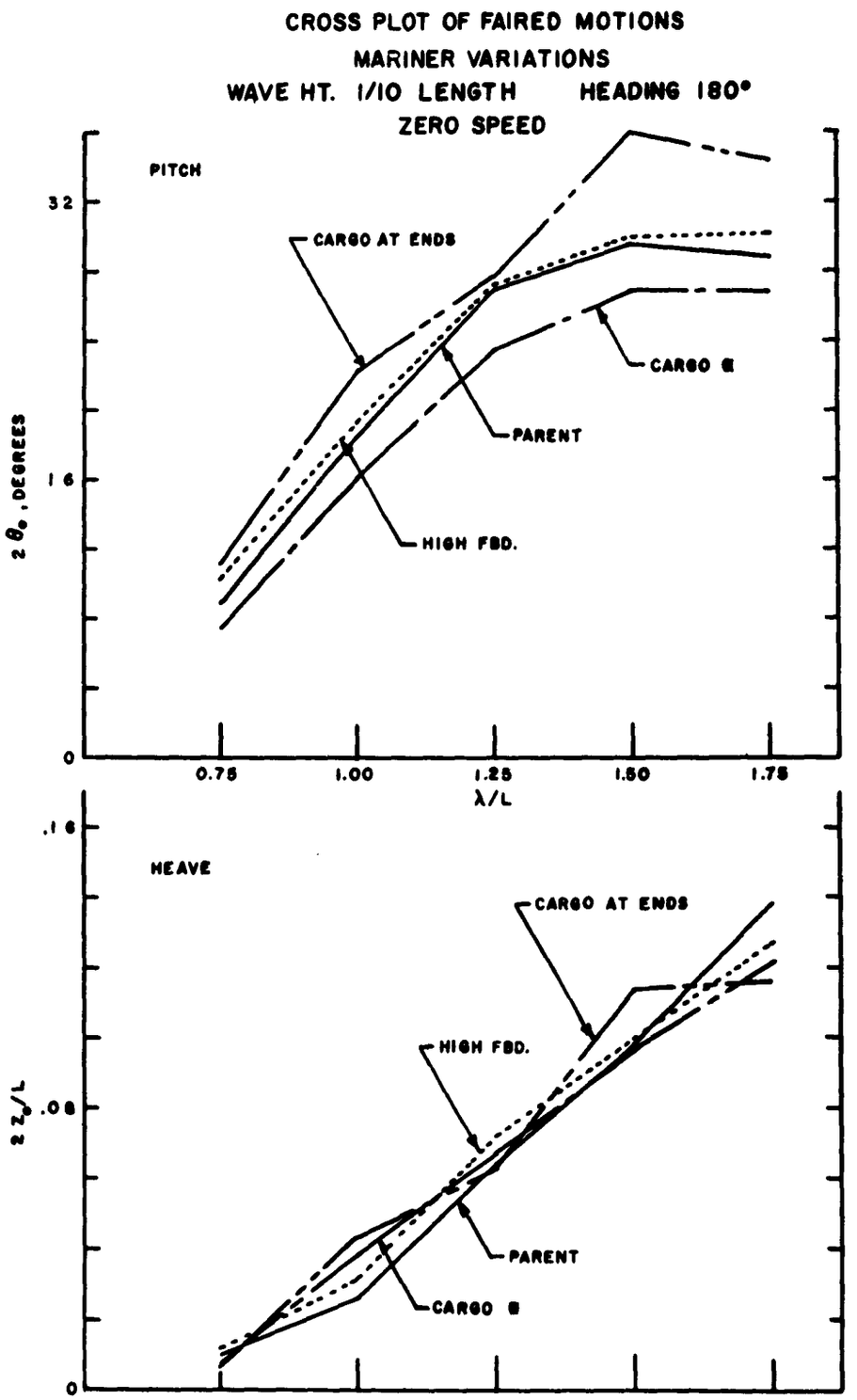
CROSS PLOT OF FAIRED MOTIONS
MARINER VARIATIONS
WAVE HT. 1/10 LENGTH HEADING 180°
ZERO SPEED
PITCH
3.2
1.6
0
2θ₀, DEGREES
CARGO AT ENDS
CARGO E
PARENT
HIGH FBD.
0.75
1.00
1.25
1.50
1.75
λ/L
.16
.08
0
2z₀/L
HEAVE
CARGO AT ENDS
HIGH FBD.
PARENT
CARGO E

FIGURE 17

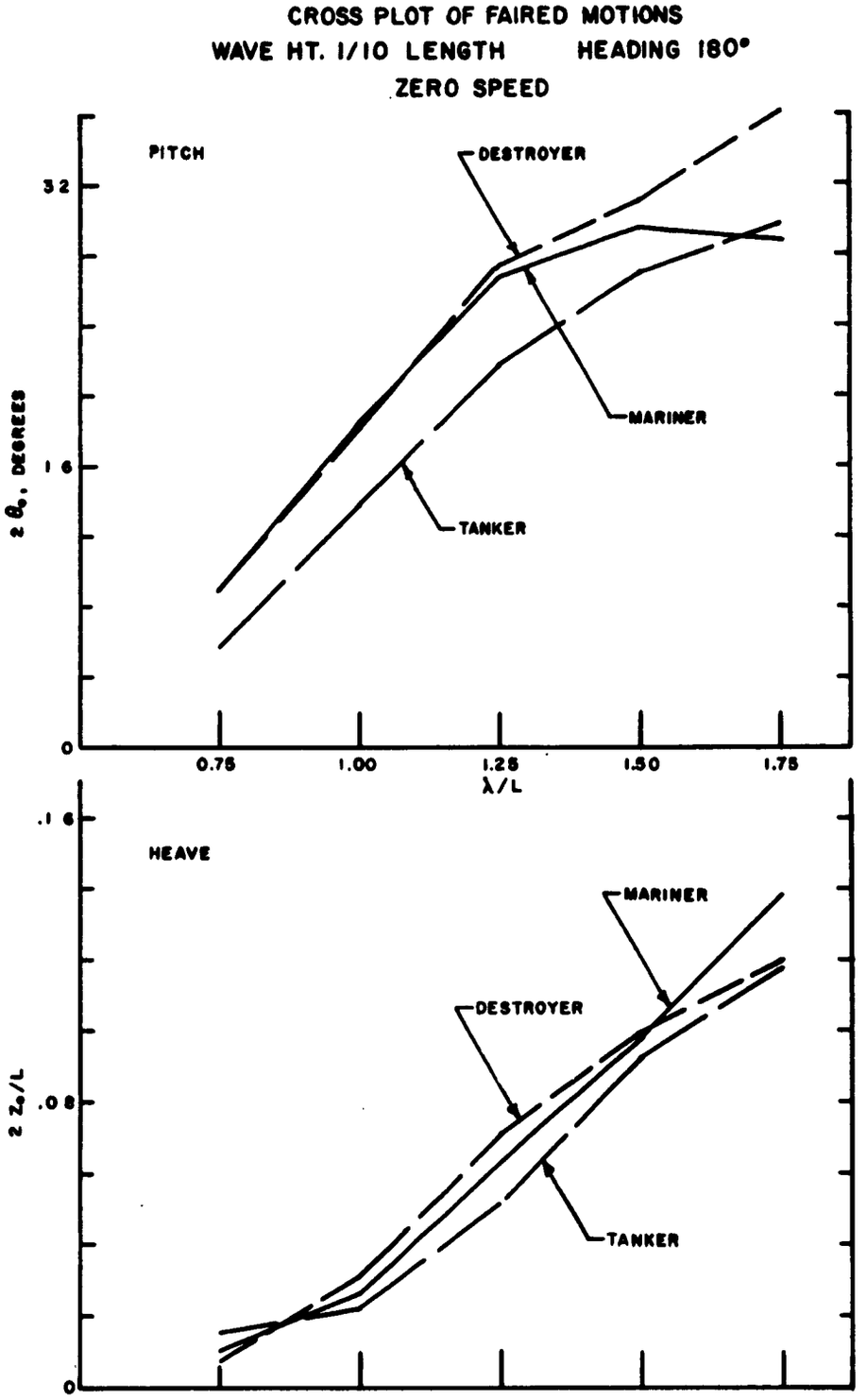
CROSS PLOT OF FAIRED MOTIONS
WAVE HT. 1/10 LENGTH HEADING 180°
ZERO SPEED
PITCH
DESTROYER
MARINER
TANKER
2θ₀, DEGREES
32
16
0
0.75
1.00
1.25
1.50
1.75
λ/L
HEAVE
MARINER
DESTROYER
TANKER
2Z₀/L
.16
.08
0

FIGURE 18

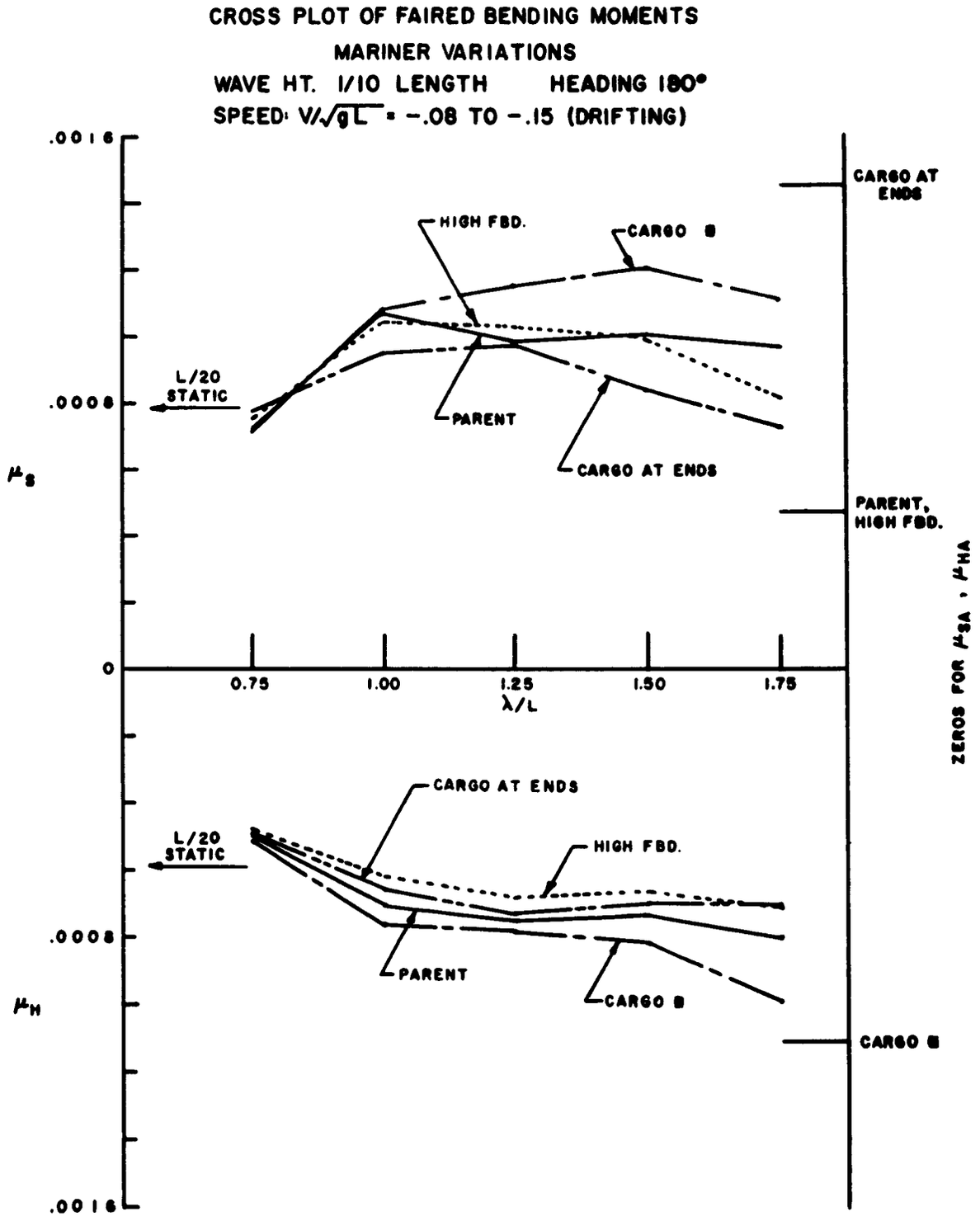
CROSS PLOT OF FAIRED BENDING MOMENTS
MARINER VARIATIONS
WAVE HT. 1/10 LENGTH HEADING 180°
SPEED: $V/\sqrt{gL}$ = -.08 TO -.15 (DRIFTING)
.0016
.0008
0
.0008
.0016
μ_S
μ_H
L/20 STATIC
L/20 STATIC
HIGH FBD.
CARGO B
PARENT
CARGO AT ENDS
CARGO AT ENDS
HIGH FBD.
PARENT
CARGO B
0.75
1.00
1.25
1.50
1.75
λ/L
CARGO AT ENDS
PARENT, HIGH FBD.
CARGO B
ZEROS FOR μ_{SA}, μ_{HA}

FIGURE 19.

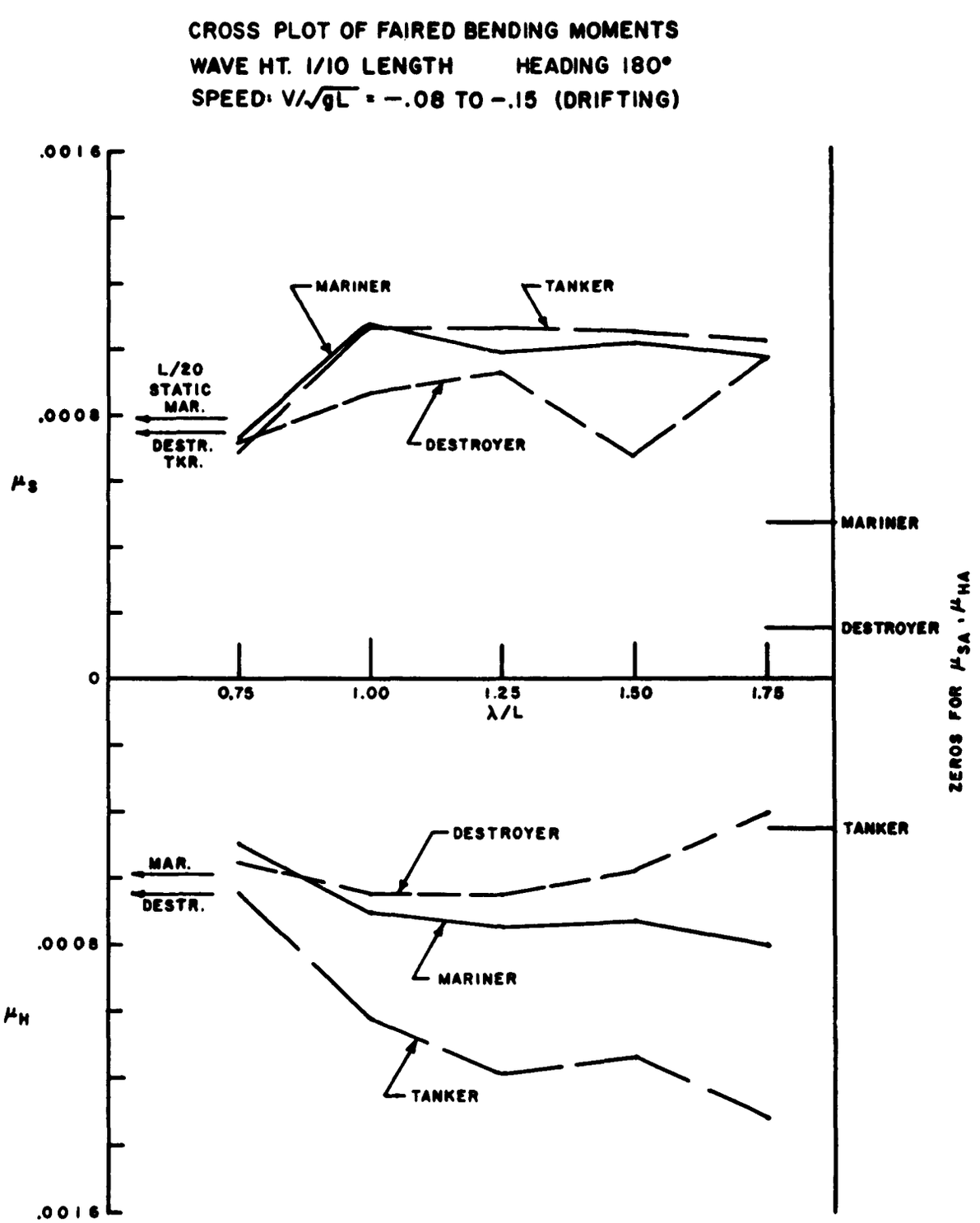
CROSS PLOT OF FAIRED BENDING MOMENTS
WAVE HT. 1/10 LENGTH HEADING 180°
SPEED: V/√gL = −.08 TO −.15 (DRIFTING)
.0016
.0008
0
.0008
.0016
μ_S
μ_H
MARINER
TANKER
DESTROYER
L/20 STATIC MAR.
DESTR. TKR.
MAR.
DESTR.
0.75
1.00
1.25
1.50
1.75
λ/L
MARINER
DESTROYER
TANKER
ZEROS FOR μ_{SA}, μ_{HA}

FIGURE 20.

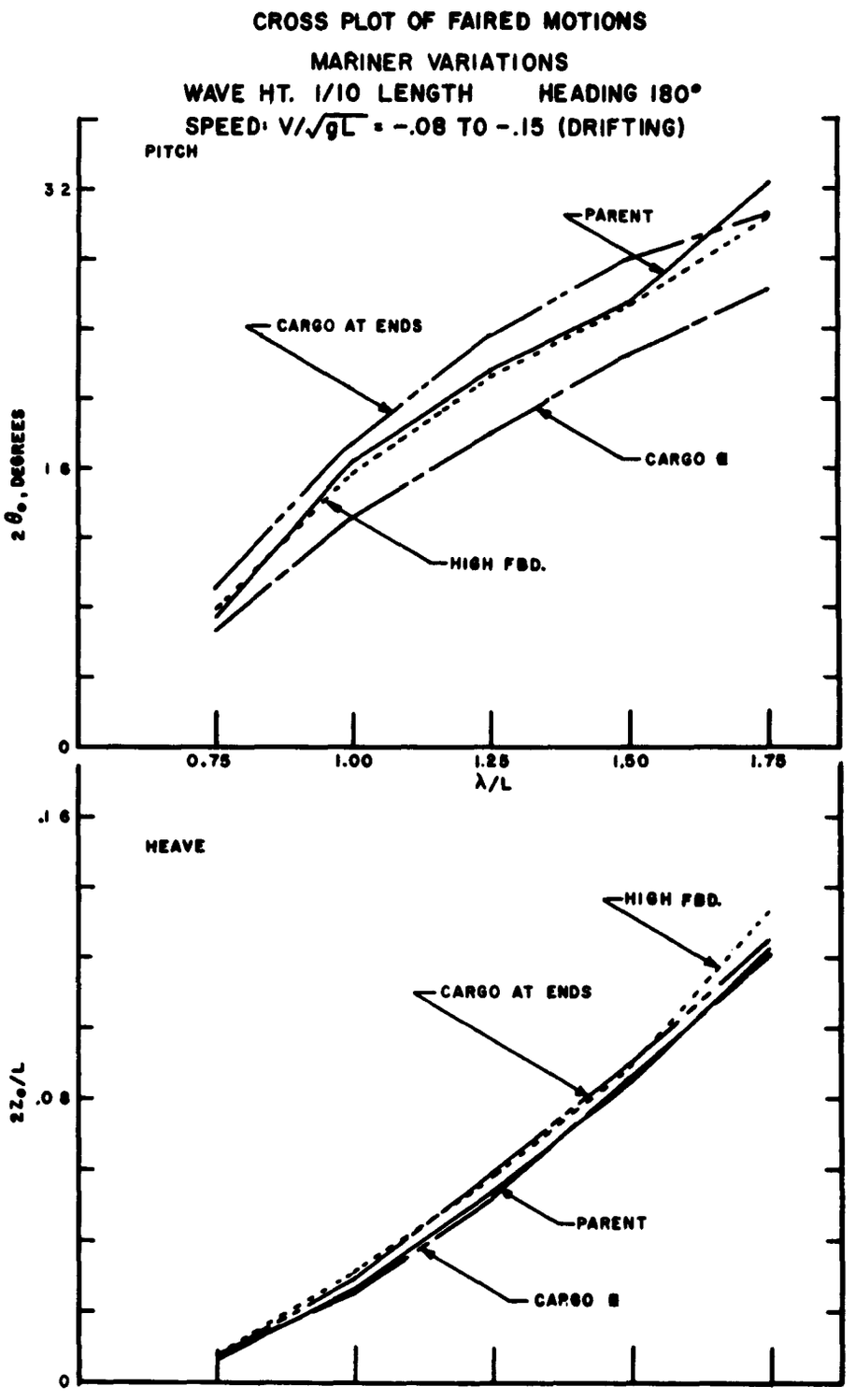
CROSS PLOT OF FAIRED MOTIONS
MARINER VARIATIONS
WAVE HT. 1/10 LENGTH HEADING 180°
SPEED: V/√gL = -.08 TO -.15 (DRIFTING)
PITCH
3 2
1 6
0
2θ₀, DEGREES
PARENT
CARGO AT ENDS
CARGO @
HIGH FBD.
0.75
1.00
1.25
1.50
1.75
λ/L
.1 6
.0 8
0
2Z₀/L
HEAVE
HIGH FBD.
CARGO AT ENDS
PARENT
CARGO @

FIGURE 21

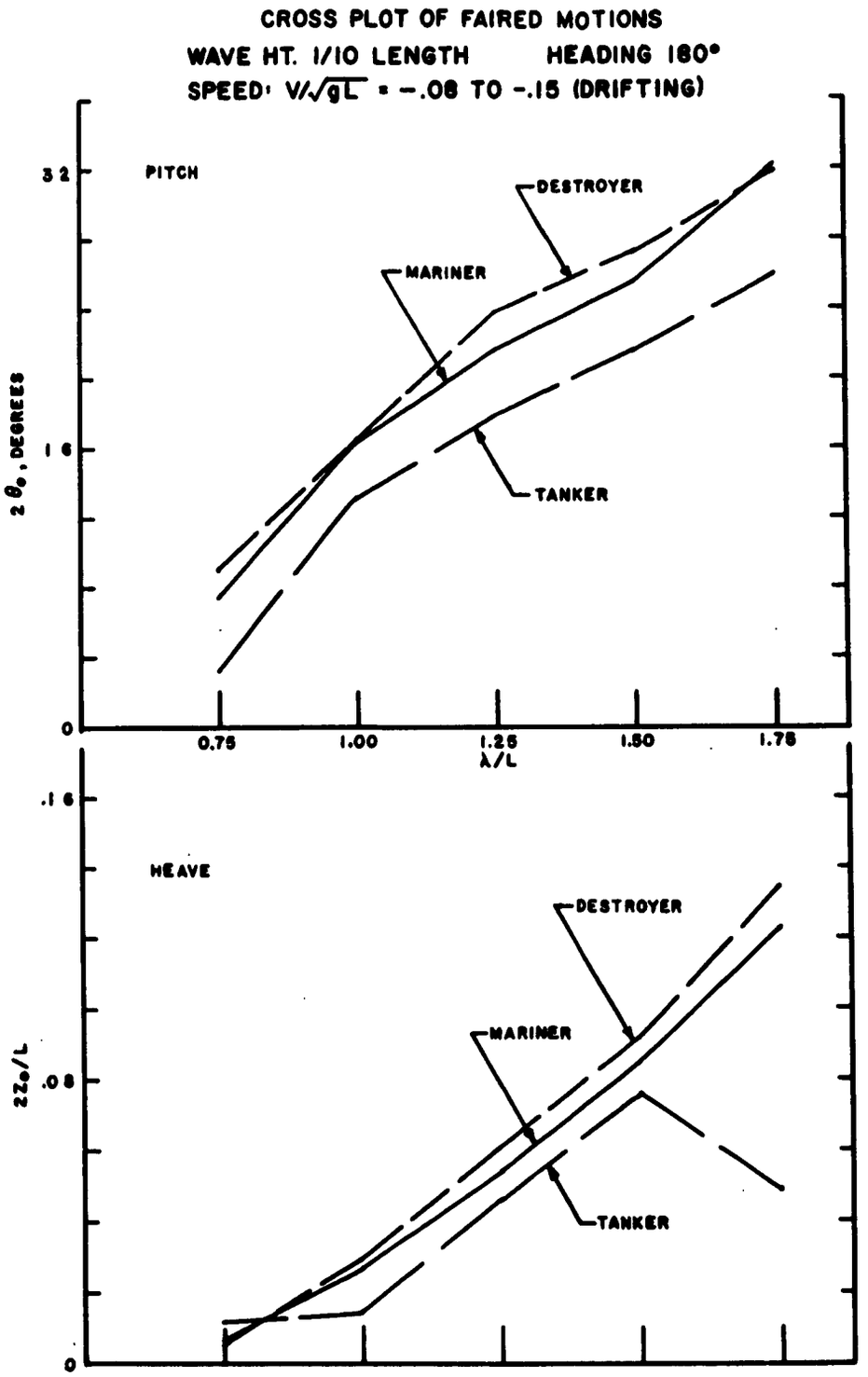
CROSS PLOT OF FAIRED MOTIONS
WAVE HT. 1/10 LENGTH HEADING 180°
SPEED: $V/\sqrt{gL}$ = -.08 TO -.15 (DRIFTING)
PITCH
DESTROYER
MARINER
TANKER
$2\theta_a$, DEGREES
3.2
1.6
0
0.75
1.00
1.25
1.50
1.75
λ/L
HEAVE
DESTROYER
MARINER
TANKER
$2Z_a/L$
.16
.08
0

FIGURE 22.

TRENDS OF BENDING MOMENTS IN IRREGULAR WAVES

Edward V.Lewis
Assistant to President
Webb Institute of Naval Architecture
Glen Cove, New York

I. INTRODUCTION

A great deal of research has been done in recent years on the problem of wave-induced longitudinal bending moments on a ship's hull. By means of full-scale strain measurements, model tests, and theoretical developments the effects of ship and wave motions have been clarified. But the incompleteness of our knowledge of the sea, particularly under severe storm conditions, has prevented the new knowledge from being applied directly to the design of ship structures or to the establishment of more rational strength standards.

Meanwhile, the basis for design remains a standard bending moment calculation for the ship poised statically on a wave of its own length. Wave height and allowable stress are determined on an empirical basis, in order to allow for the effects of ship size and other characteristics.

Such a semi-empirical design procedure would undoubtedly be satisfactory if there were no change in the size and speed of ships. But there has been a remarkable trend in recent years toward larger tankers and bulk cargo carriers, and the end is not in sight. Not only are waves of the length of these large ships less frequent, but their heights are known to be generally not so great as those of shorter waves. Some reduction in design wave height therefore seems permissible, but the question is, how much? As stated by Mr. David P. Brown, Chairman of the Board, American Bureau of Shipping, in his half-yearly statement of July, 1961, "there still remains the very important question as to the degree to which recognition may be given to what might be termed the diminishing relative severity of storm conditions as the sizes of ships increase."

At the same time naval and general cargo ships have shown a continuing upward trend in speed, without the spectacular size increases noted for the bulk cargo ships. Questions have been raised as to the effect of speed itself on the wave bending moments, as well as to the influence of the finer form coefficients which accompany the higher speeds. Some of the classification societies now take block coefficient into account in their strength standards.

In Mr. Brown's report, he added: "The development of new facilities for model testing in wavemaking tanks and of instrumentation to be applied to ships at sea is providing increasing opportunities to obtain information on these vexatious problems." It is the purpose here to describe initial results in a project at Webb Institute of Naval Architecture, sponsored by the American Bureau of Shipping, to make use of model test results to predict trends of bending moments on ships in realistic irregular seas. Variables to be considered in the study are severity of the sea, size of ship, speed, heading, and fullness. However, this discussion will deal mainly with the effect of ship size, since this is the only variable studied at the time of this Seminar. A tanker type hull of 0.80 block coefficient series 60 form is considered, at a speed-length ratio of 0.675 and Froude No. = 0.20 (16½ knots for a 600-ft. ship) heading directly into one severe storm sea. No attempt is made to determine the maximum possible bending moment that might be experienced at sea, since our knowledge of the sea is still inadequate for this purpose. But the aim is to determine comparative bending moments for different sizes of geometrically similar ships in one very severe sea condition.

The procedure followed is to make use of the principle of superposition, described in an introductory lecture at this Seminar, to predict in statistical terms the expected bending moments in an irregular storm sea for which the spectrum is known.[1]

II. THE SEA

The best available storm sea data are given in a paper by Pierson,[2] who presents an analysis of records taken by means of a shipborne wave recorder on the British Weather Ship "Weather Explorer" during an extratropical cyclone on November 15-16, 1953. The wind blew quite steadily for about 18 hours at 37-45 knots and 7 hours at 52 knots. The height of the storm was reached 9 hours

later after the wind had blown at 62 knots for 4½ hours. At the time of the analysis in 1959 it was believed that these waves were "probably among the highest significant waves yet recorded by means of an instrument." The peak of the computed spectrum was found to be at a wave length of about 1400 feet, and the longest significant wave component was about 2200 feet. The waves reached a significant height of 42 feet.

The one-dimensional spectrum at the height of the storm is shown in Fig. 1. It is compared in this figure with the ideal Neumann spectrum of a fully-developed sea produced by a 40-knot wind blowing for at least 42 hours.[3] These curves indicate the distribution of wave energy among the theoretically infinite number of wave components present in the sea.

The fairing of the upper end (large ω) of the Pierson spectrum was done on the basis of maintaining reasonable wave slope values for the short wave components, and hence the curve falls below the computed points. It is apparent that the computation method resulted in unreasonably high values here.

These spectra give no indication of the direction of the components and hence of the short-crestedness of the sea. It was necessary, therefore, to apply a "spreading function" to distribute the energy over a range of directions in a reasonable manner. Available information[3] suggested using a relationship in which the energy varies as $\cos^2\alpha_w$, where α_w is the wave direction in relation to the wind direction (assumed to be constant). The factor may be expressed,

$$f(\alpha_w) = \frac{2}{\pi} \cos^2\alpha_w$$

It leads to the following factors by which the one-dimensional spectrum is to be multiplied:

α_w	0°	$\pm 20^\circ$	$\pm 40^\circ$	$\pm 60^\circ$	$\pm 80^\circ$	$\pm 90^\circ$
$f(\alpha_w)$	.636	.562	.373	.159	.019	0

It is clear from this table that most of the wave energy lies within $\pm 45^\circ$ of the wind direction. This seemed reasonable in relation to limited available information, including recent British results in less severe seas,[4] but it must be considered to be tentative.

Edward V. Lewis

Figure 2 shows the observed 62-knot spectrum after applying the above spreading factor. The curve marked 40°, for example, represents the total energy between $\alpha_w = 30^\circ$ and $\alpha_w = 50^\circ$. Integrating with respect to α_w will yield the single curve of Fig. 1.

The two-dimensional spectrum can also be represented as a contour plot, Fig. 3. Sections through this plot at various angles will yield the curves of Figure 2.

III. RESPONSE AMPLITUDE OPERATORS

Although considerable strides have been made in the computation of forces on a body in waves, available theoretical methods are not yet believed to be satisfactory, especially when the effects of ship speed and heading to waves are to be considered. Comprehensive and consistent model tests in regular waves are believed to be most suitable for the present purpose.

The most complete series of oblique seas model test results for bending moments appears to be those reported by Vossers, et.al, in 1961.[5] All bending moments response data used in the calculations are taken from those results. Curves passing through all test spots were used (Figure 4) rather than making any attempt to fair out humps and hollows in the curves.

IV. BENDING MOMENT SPECTRA

The response amplitude operator for bending moments is defined by $(M_V/\zeta)^2$ or the square of the bending moment values plotted in Figure 4. The product of this operator and the directional component of the sea spectrum at the appropriate wind-to-wave angle (α_w) is the bending moment spectrum component,

$$\frac{M_V^2}{\delta\omega_e}\, d\omega_e \quad \text{(ft.-ton)}^2\text{-sec.}$$

A plot of this operation for a typical case (L = 600 feet; V = 16½ knots; $\alpha_w = 0^\circ$) is shown in Figure 5, where the sea spectrum component, bending moment response amplitude operator, and resulting bending moment spectrum are plotted against the frequency of encounter (ω_e) and wave length. Vertical scales are different for each curve.

Figure 6 shows the bending moment spectrum components for L = 600 feet, V = 16½ knots, at the various wind-to-wave angles.

V. BENDING MOMENTS

Integration of the bending moment spectra over the significant frequency range and over wind-to-wave angles of -90° to +90° leads to the cumulative density for bending moment, "R". From values of R for each ship size the average value of the highest expected amplitude of wave bending moment (hog or sag) out of a total of N oscillations may be calculated from the expression,

$$B.Mt. = C\sqrt{R},$$

where the multiplier C takes different values depending on the number of oscillations considered, For example:

Average Bending Moment amplitude = $0.866\sqrt{R}$

Average of 1/10 highest Bending Moments = $1.80\sqrt{R}$

Expected value of highest B.Mt. in 100 oscillations = $2.28\sqrt{R}$

Expected value of highest B.Mt. in 1000 oscillations = $2.73\sqrt{R}$

Expected value of highest B.Mt. in 10,000 oscillations = $3.145\sqrt{R}$

The following results were obtained:

Ship Length, Feet	Speed, Knots	Amplitude of Wave Bending Mt., tons - ft	
		Ave. of 1/10 highest	Expected highest in 10,000 cycles
300	11.6	26,000	45,400
600	16½	296,000	519,000
900	20.2	1,180,000	2,060,000
1200	23.4	2,800,000	4,900,000

The above bending moment amplitudes do not take into account the initial still water bending moment, but show only the effect of waves for the particular weight distribution of the models tested.[5] In general there was a shift of the mean value measured in waves from the initial zero bending moment for the model at rest in still water. This resulted in part from the wave formed by the forward motion of the ship and in part from non-linearity of the wave hydrodynamic forces, which usually results in the hogging moment being greater than sagging. The magnitudes of the zero shift in regular waves were given for the model test results in regular waves.[5] The effect of the ship's own wave was assumed to be the same in irregular waves as in calm water. The non-linear effect was computed for irregular waves on the assumption that the response amplitude operators at each wave frequency were increased by the amount of the zero shift (Fig. 6A). Using these fictitious amplitudes should lead to an approximately correct prediction of hogging moment in irregular waves, but reduced fictitious amplitudes would be necessary to predict sagging.

The corrected wave bending moments for hogging only are then:

Ship Length, Feet	Speed, Knots	Amplitude of Hogging B.Mt. tons - ft	
		Ave. of 1/10 highest	Expected highest in 10,000 cycles
300	11.6	29,600	50,600
600	16.5	349,000	590,000
900	20.2	1,407,000	2,357,000
1200	23.4	3,453,000	5,753,000

VI. BENDING MOMENT TRENDS WITH SHIP SIZE

We come finally to the question of comparing the above computed bending moments with tentatively adopted standards for the variation of wave bending moment with ship size. Since the usual procedure is to specify a wave height to be used for static wave bending moment calculation, with wave length equal to ship length, it seems appropriate to convert the computed irregular wave moments into effective or equivalent static wave heights.

Accordingly, an equivalent wave height was defined as follows:

$$h_{equiv.} = \frac{M_{calc}}{M_{std}} \; h_{std}$$

where $h_{equiv.}$ = equivalent wave height

M_{calc} = bending moment calculated by methods outlined above, including still water ahead speed bending moment and mean value shift

M_{std} = quasi-static bending moment in ship length, $L/20$ trochoidal waves, Smith effect excluded. Values from Ref. 5.

h_{std} = $L/20$

Equivalent wave heights for the following statistical measures of the calculated bending moments are plotted on Figure 7: average of 1/10 highest bending moment, highest expected bending moment in 1,000 cycles and highest expected moment in 10,000 cycles. The same figure also includes other commonly used wave height-to-length relationships for comparison.

VII. CONCLUSIONS

The results shown in Fig. 7 indicate that <u>for this particular severe storm</u> the effective wave height falls off more rapidly than the various commonly used wave height functions. However, examination of Fig. 1 shows that there is a very sharp cut off in wave energy at about $\omega = 0.3$ for this particular storm sea. In other words, there is very little energy in waves longer than about 2200 feet. If the wind had blown for a longer time at 62 knots, we would expect longer wave components to develop. Consequently, the extreme bending moments plotted in Fig. 7 would then not drop off so fast with length.

Work of John Dalzell of the Davidson Laboratory,[6] not yet published, explores this matter further for destroyer hulls on the assumption that ideal fully-developed seas

can be assumed for any wind velocity. He obtains a family of curves similar to those shown in Figure 7 for different wind velocities. They all show a tendency to reach a maximum and ultimately a reduction as length increases. But the point of maximum wave height moves to higher and higher wave lengths as the severity of the sea increases.

Hence, we may conclude at this point that conventional trends of wave height with length seem reasonable, subject to further checking with records of more severe seas recorded on rough weather trade routes. It should be noted also that the effect of lateral bending moments on deck edge stresses have not yet been included.

VIII. SUPPLEMENTARY DATA

Since the Seminar, additional bending moment trends have been obtained. Figure 8 shows the variation with heading for 600 foot ships of 0.60 and 0.80 block coefficient. Surprisingly large values were obtained in beam seas, largely as a result of the short-crestedness of the sea.

Figure 9 shows the variation of bending moment with ship speed and block coefficient in head seas. It is clear that a speed reduction may reduce the wave bending moment somewhat when speed is high, but in other cases may actually increase it.

Figure 10 shows the wave bending moment variation with ship length in head seas, and includes all of the calculated values at the various block coefficients and Froude numbers. Note that in this graph the bending moment scale is logarithmic.

The bending moment values in Figures 8, 9 and 10 represent the amplitudes of wave bending moments and do not specify the amount that the mean values differ from the initial zeros.

ACKNOWLEDGMENTS

The assistance of Professor Robert B. Zubaly is gratefully acknowledged for carrying out the calculations on which this lecture was based. Messrs. W. Lindenmuth

and M. Silber, Seniors at Webb Institute of Naval Architecture, assisted him in the computations for the supplementary results presented in Figures 8, 9 and 10.

The interest and encouragement of the American Bureau of Shipping in supporting this work was greatly appreciated. Mr. David P. Brown, President, has kindly permitted the presentation and publication of this progress report.

REFERENCES

1. Lewis, E.V., "A Study of Midship Bending Moments in Irregular Head Seas." Journal of Ship Research, Vol. 1, no. 1, April, 1957.

2. Pierson, W.J., "A Study of Wave Forecasting Methods and of the Height of a Fully Developed Sea on the Basis of Some Wave Records Obtained by the O.W.S. Weather Explorer During a Storm at Sea." Deutsche Hydrographische Zeitschrift, Band 12 Heft 6, 1959.

3. Pierson, W.J., G. Neumann, and R.W. James, "Practical Methods for Observing and Forecasting Ocean Waves by Means of Wave Spectra and Statistics." H.O. Publication 603, U.S. Navy Hydrographic Office, 1955.

4. Canham, H.J.S., D.E. Cartwright, G.S. Goodrich, and N. Hogben, "Seakeeping Trials on O.W.S. Weather Reporter." Trans R.I.N.A., March 1962.

5. Vossers,G., W.A. Swaan, and H. Rijken, "Vertical and Lateral Bending Moment Measurements on Series 60 Models." International Shipbuilding Progress, Vol. 8, No. 83, July, 1961.

6. Dalzell, J.F., "Trends with Speed, Ship Length and Sea Severity of Midship Bending Moments of a Destroyer Type Ship in Head Seas." Report R-892 of the Davidson Laboratory, Stevens Institute of Technology, May, 1962.

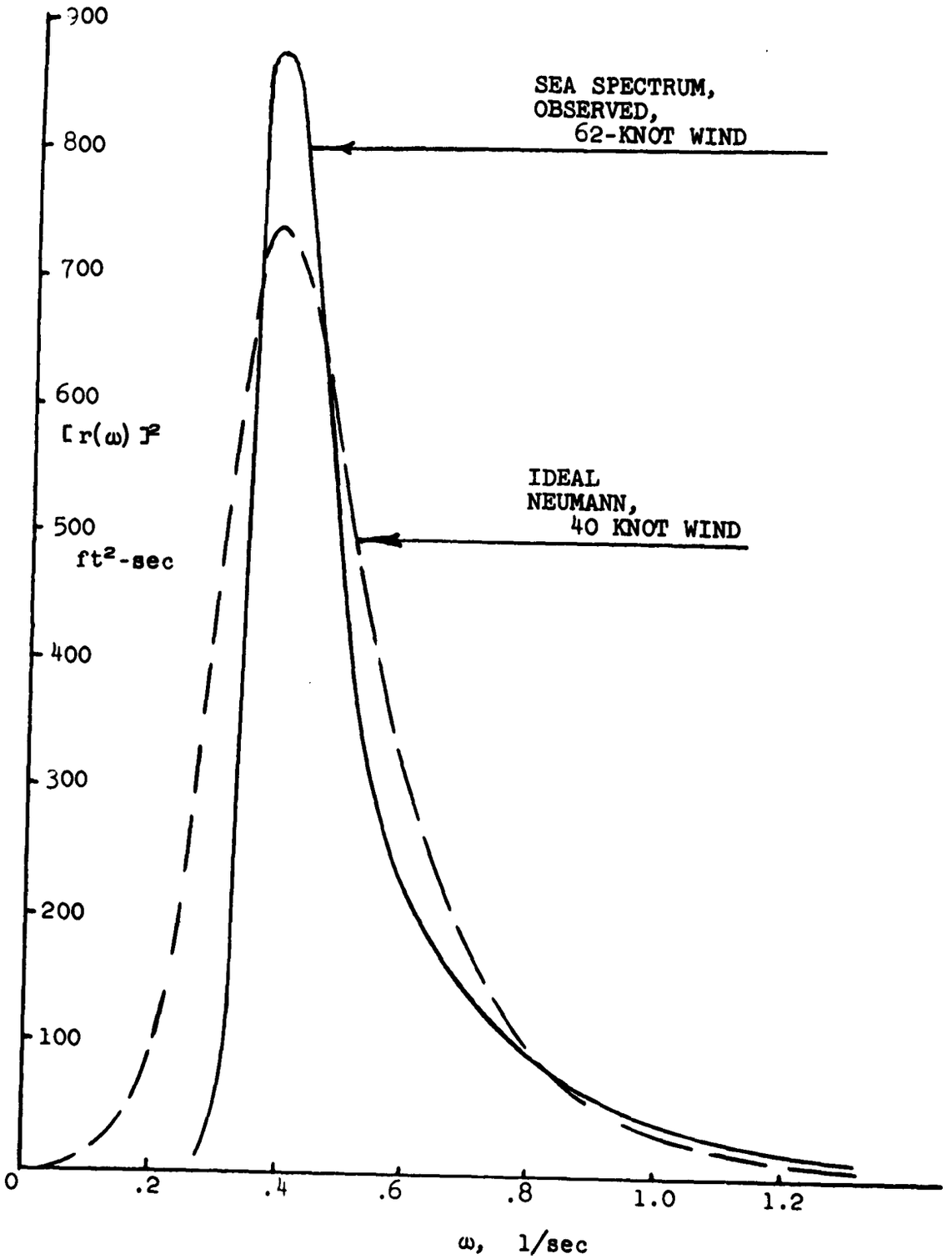

FIGURE 1. SPECTRA OF THE SEA AT A FIXED POINT

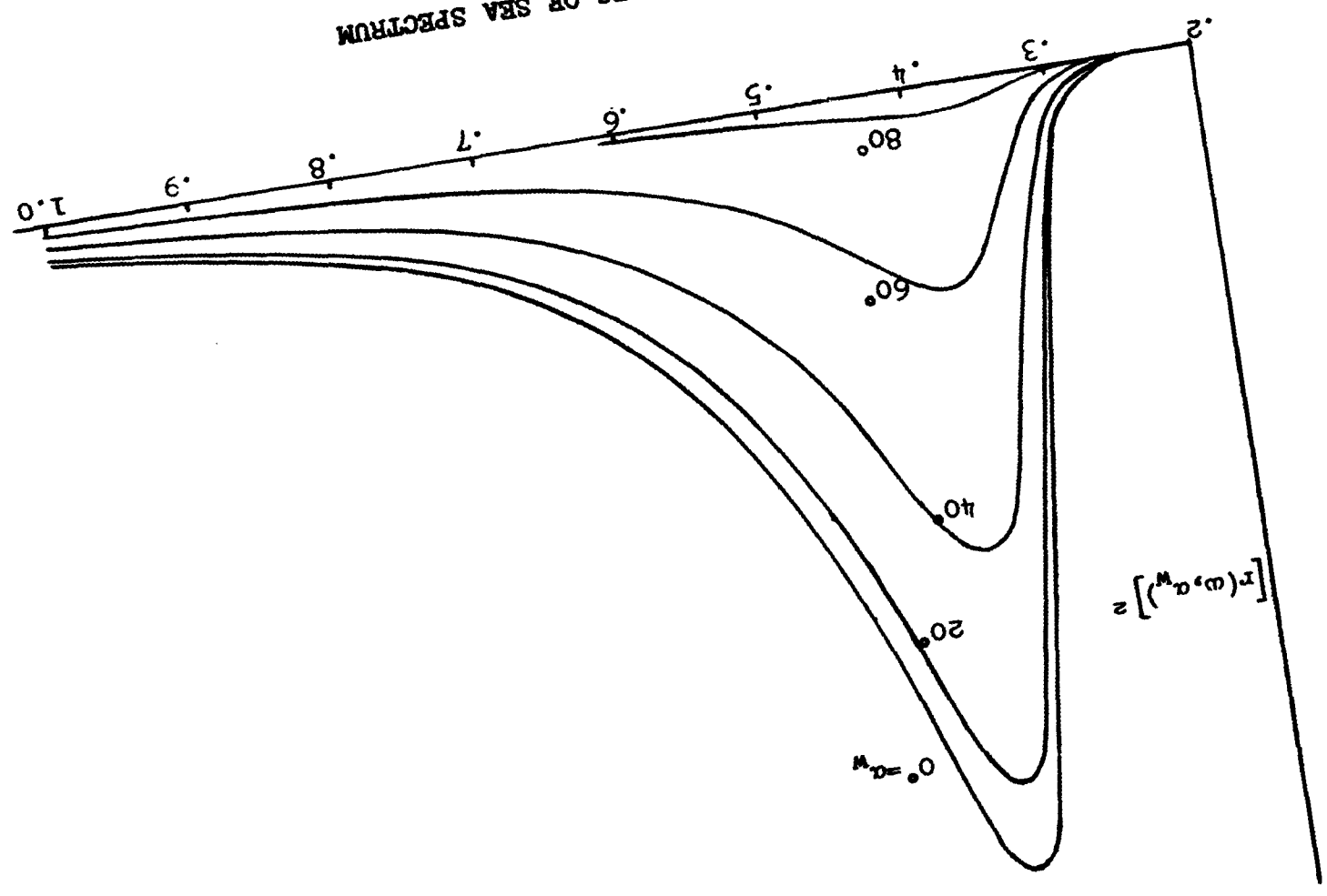

FIGURE 2. ANGULAR COMPONENTS OF SEA SPECTRUM

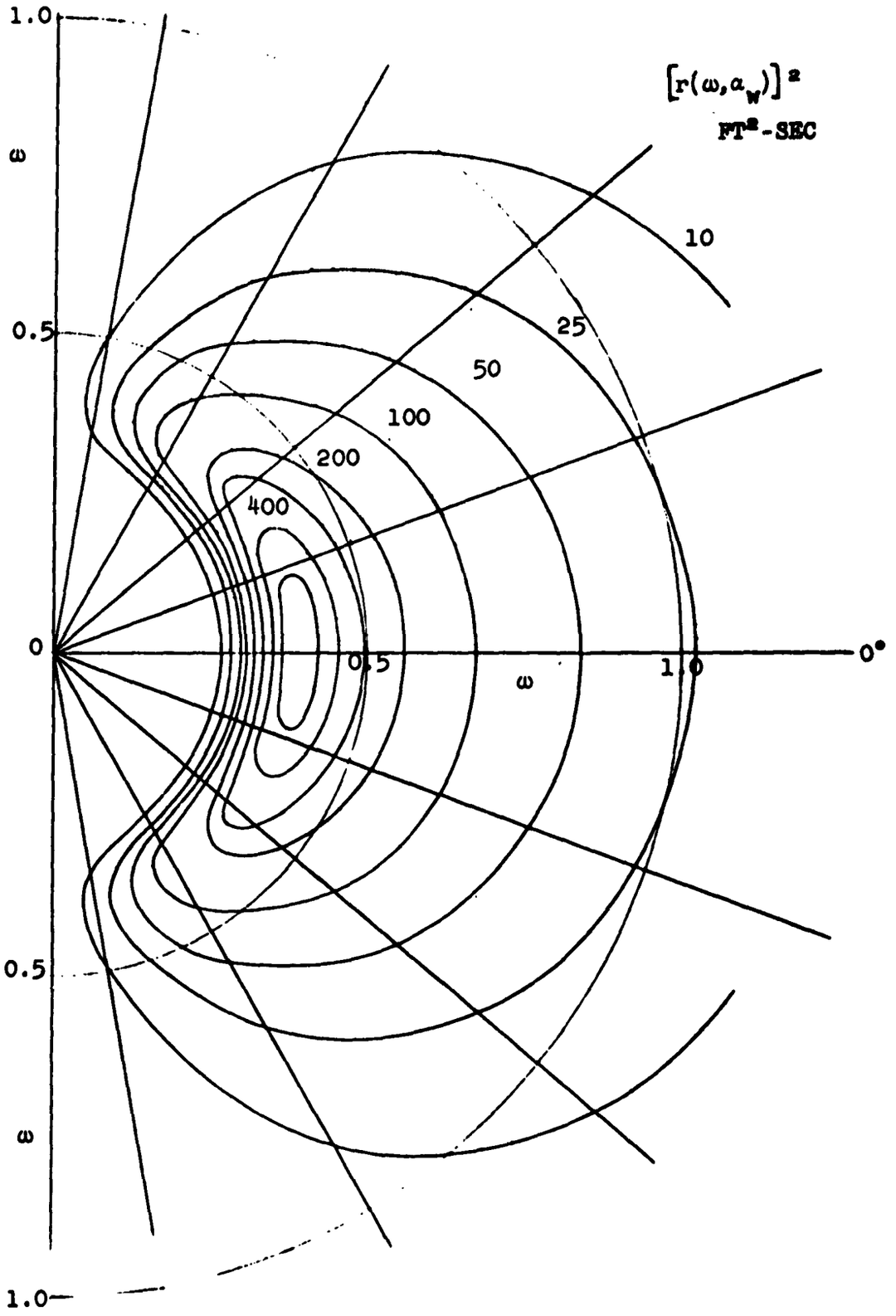

FIGURE 3. TWO-DIMENSIONAL SEA SPECTRUM

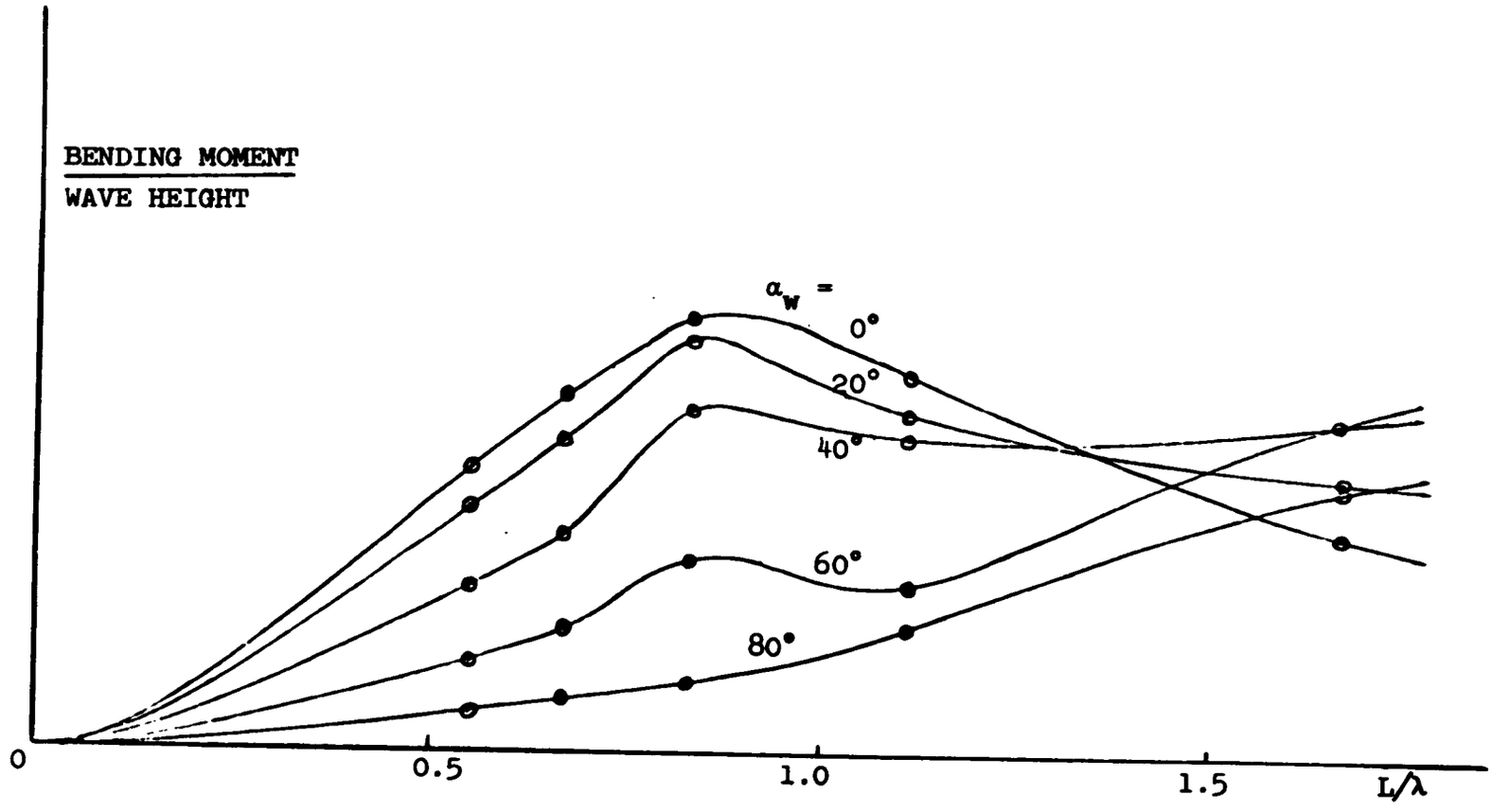

FIGURE 4. BENDING MOMENT RESPONSE OPERATORS FROM MODEL TESTS

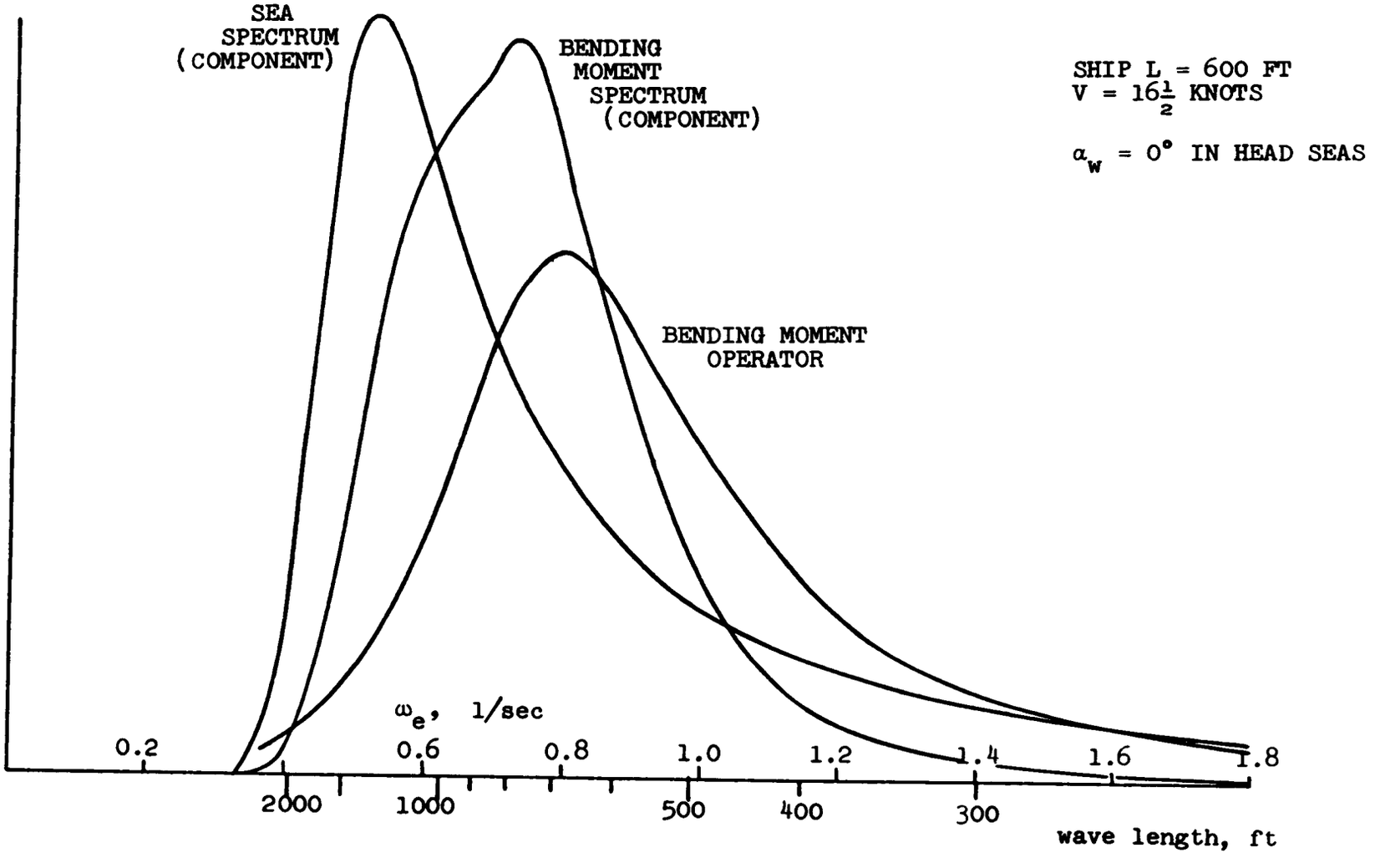

FIGURE 5. BENDING MOMENT SPECTRUM COMPONENT AND CURVES FROM WHICH IT IS DERIVED

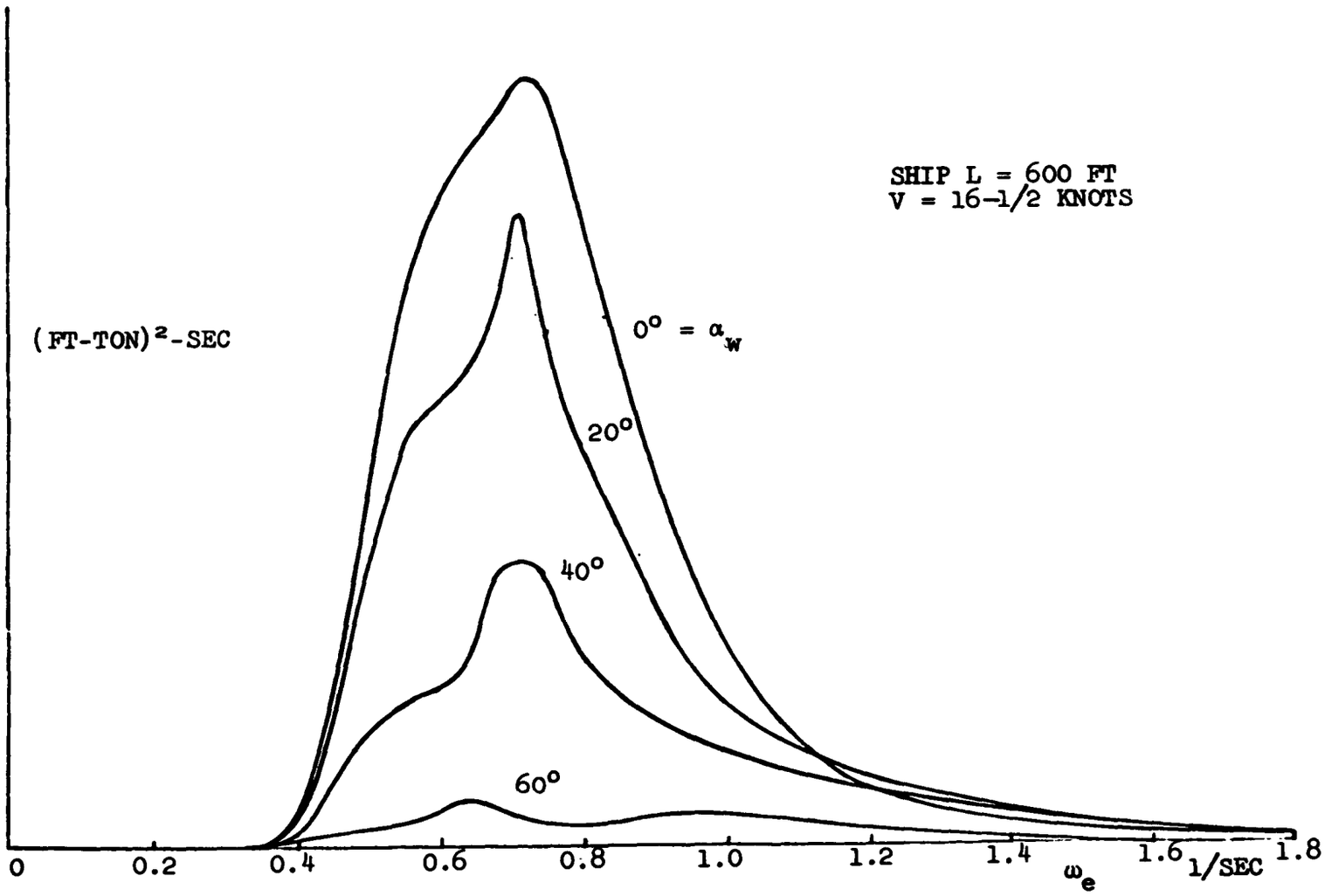

FIGURE 6. ANGULAR COMPONENTS OF BENDING MOMENT SPECTRUM

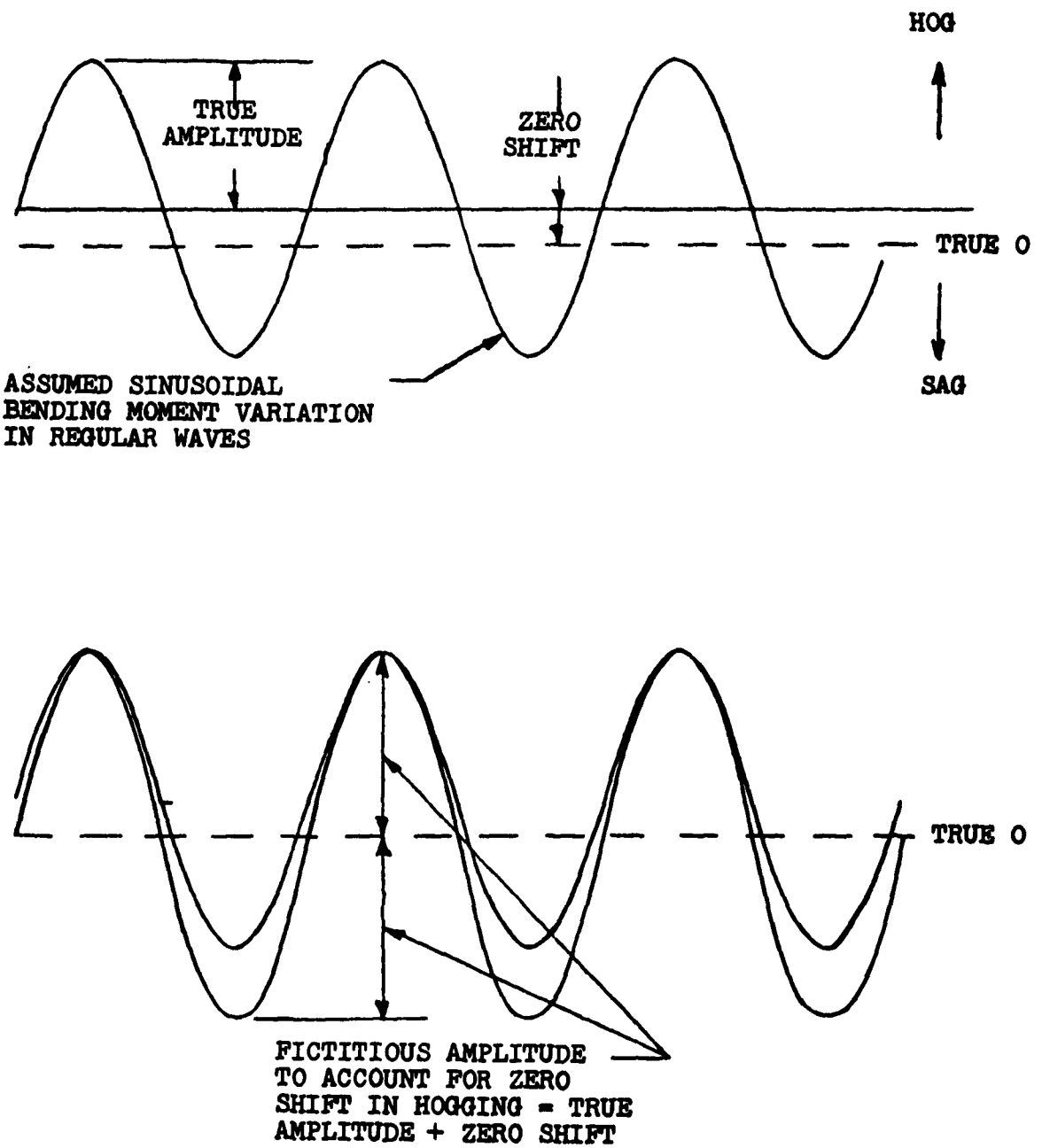

FIGURE 6-A. METHOD OF CORRECTING FOR SHIFT OF BASE LINE IN BENDING MOMENT RESPONSE TO REGULAR WAVES

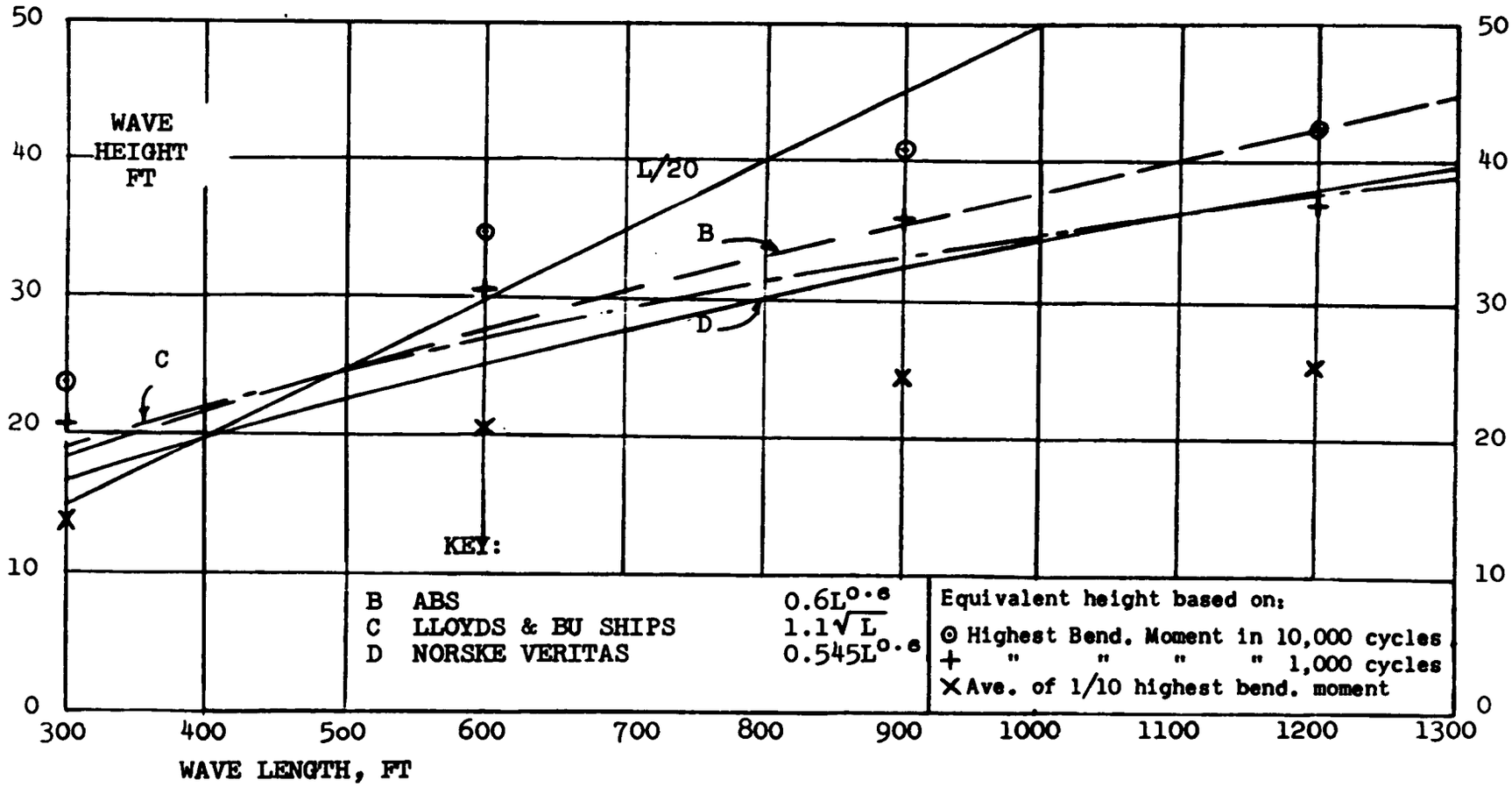

FIGURE 7. EQUIVALENT WAVE HEIGHT
AS A FUNCTION OF SHIP (OR WAVE) LENGTH

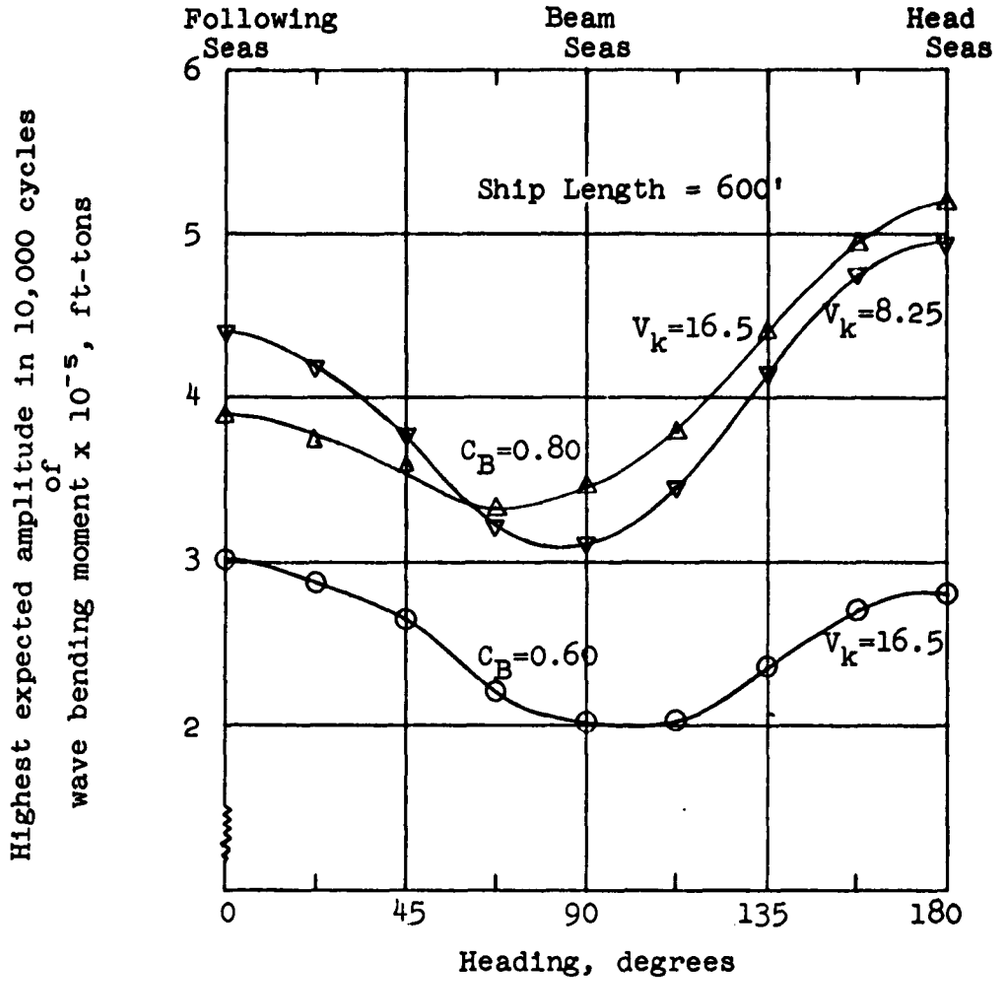

FIG.8. VARIATION OF WAVE BENDING MOMENT WITH HEADING

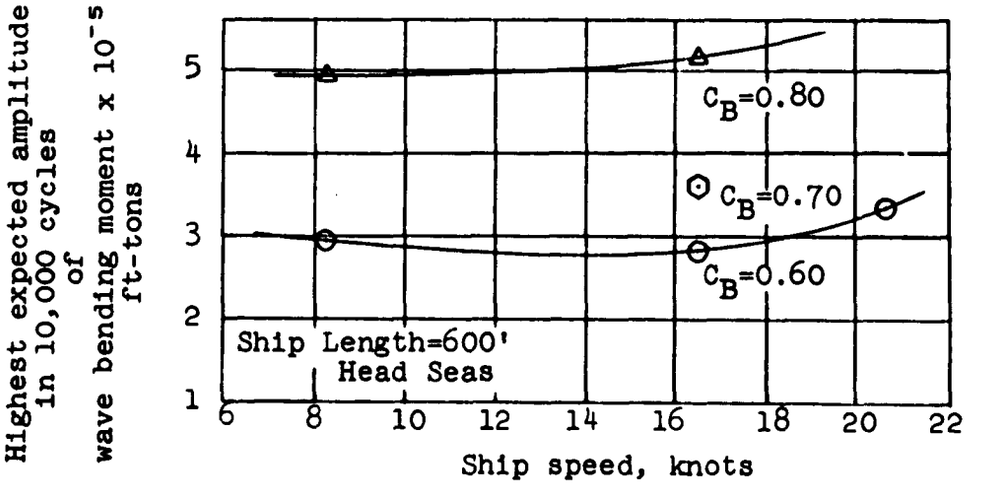

FIG.9. VARIATION OF WAVE BENDING MOMENT WITH SPEED AND C_B

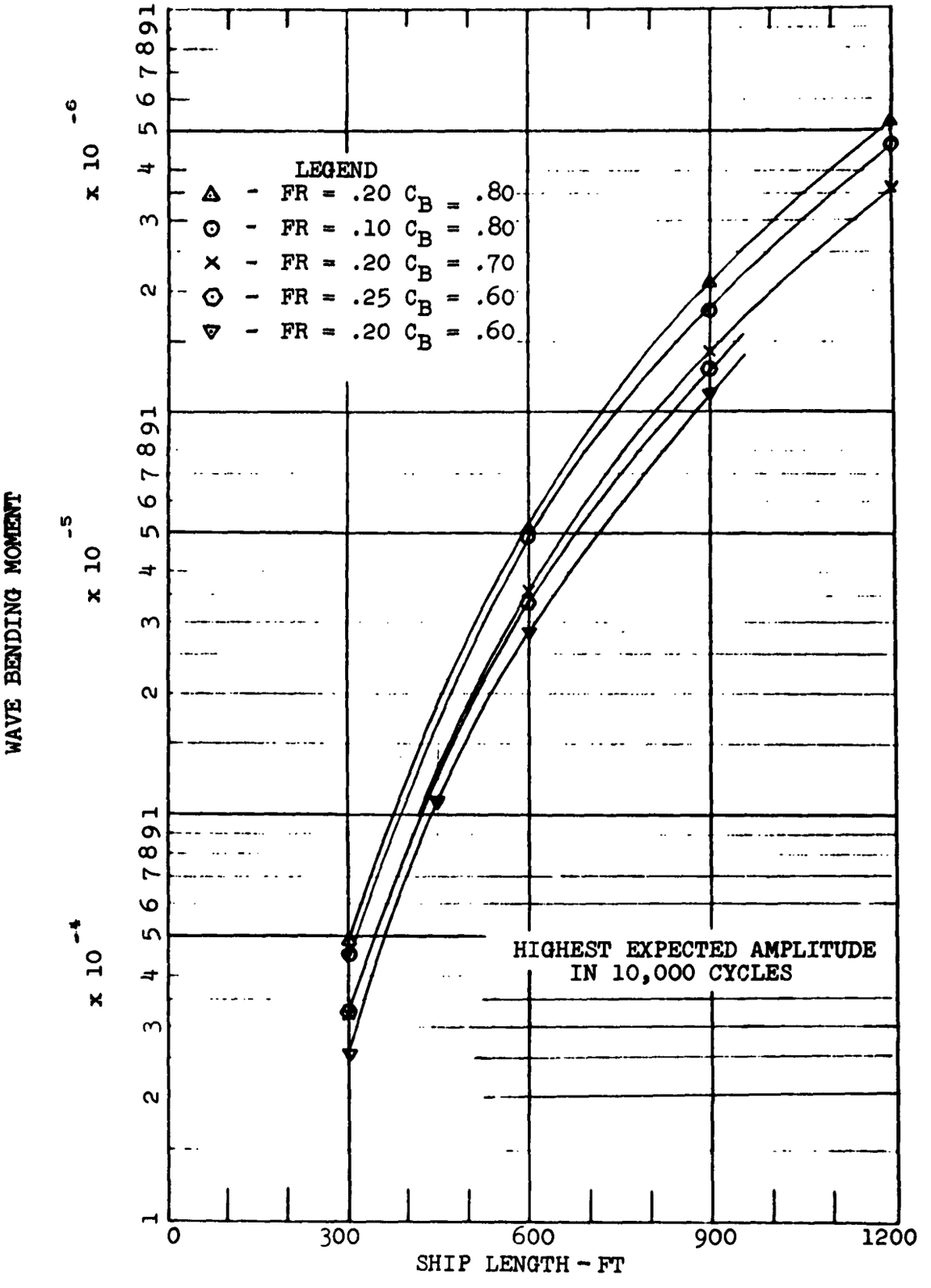

FIGURE 10. WAVE BENDING MOMENTS IN HEAD SEAS

Attendants
Seminar on
SHIP BEHAVIOR AT SEA
June 11-15, 1962

Dr. Wm. E. Cummins
David Taylor Model Basin

Geoffrey J. Goodrich
Natl Physical Lab, England

Prof. Ir. J. Gerritsma
Shipbldg Lab, Netherlands

Prof. B. V. Korvin-Kroukovsky
Consultant

Henry R. Ask
United Aircraft Corporation

J. Bentkowsky
Sperry Piedmont Co

Prof. E. V. Lewis
Webb Inst of Naval Architect

Alfred J. Giddings
Bureau of Ships

Dr. John P. Breslin
Davidson Laboratory

Richard P. Bernicker
Davidson Laboratory

C. Lincoln Crane, Jr.
Davidson Laboratory

Haruzo Eda
Davidson Laboratory

Stephen C. Chen
Davidson Laboratory

John F. Dalzell
Davidson Laboratory

Tadeusz Kowalski
Davidson Laboratory

Daniel Savitsky
Davidson Laboratory

Earl M. Uram
Davidson Laboratory

Raymond Kaufman
M. Rosenblatt and Son

Frank M. Schwartz
David Taylor Model Basin

Michael D. Pearlman
Massachusetts Inst of Tech

Hermann A. Allen
American Export Lines

John M. Ashfield
Royal Canadian Navy

Nathan Kinney Bales
David Taylor Model Basin

R. A. Barr
Hydronautics

Hans Edward Baumgardt, Jr.
Coast Guard

Donald C. Brown
Hamilton Standard

Sheldon B. Fidelman
J. J. McMullen Assn

Ernst Frankel
Massachusetts Inst of Tech

Donald J. Fritch
Lessells and Assoc

Peter A. Gale
Bureau of Ships

William Gray
Bethlehem Steel

Marvin I. Haar
Martin Marietta Corporation

Philip A. Hamill
Natl. Research Council,Canada

N. A. Hamlin
Bethlehem Steel

Kristian Haslum
Massachusetts Inst. of Tech.

John L. Hess
Douglas Aircraft

Thomas A. Holgate
Boeing Company

Richard M. Hopkins
General Dynamics/Convair

William C. Hurt III
Boeing Company

Leon Kaplan
Edo Corp.

Edward E. Kawahara
San Francisco Naval Shipyard

Dr. Jack Kotik
Tech Research Group, Inc.

R. M. Langer
JRM Begs Co.

George H. Levine
Bethlehem Steel

J. Levy
Aerojet

Julius Marcus
U.S. Navy Hydrographic Office

John A. Mercier
Hydronautics

Donald R. Miller
AiResearch Mfg. Co.

Sam A. Naff
Newport News Shipbuilding

Hitoski Narita
Massachusetts Inst. of Tech.

Tom F. Noble
Sperry-Piedmont

P. A. Pepper
Edo Corp.

D. M. Petrie
Boeing Co.

David Price
Sperry Gyroscope

Kenneth C. Ripley
Consultant

J. Rethorst
Vehicle Research Corp.

Frank H. Sellars
Newport News Shipbuilding

David Shefrin
Hamilton Standard

Richard S. Stevens
Office of Naval Research

Jerzy S.C. Straszak
Natl Res Council, Canada

Adorjan J. Szeless
Virginia Polytechnic Inst.

Donald J. Szostak

Ryo Tasoki
University of Michigan

Robert J. Taylor
U.S. Dept. of Comm.

Theodore L. Thorsen
Hydronautics

Dr. Paul Kaplan
Oceanics

Lennert O. Thunberg
U.S. Coast Guard

John Thomas Tothill
Natl Research Council, Canada

Z. George Wachnik
David Taylor Model Basin

Shen Wang
Massachusetts Inst. of Tech.

Nels C. Youngstrom
Bell Telephone

Neal A. Brown
Massachusetts Inst. of Tech.

Justin E. Kerwin
Massachusetts Inst. of Tech.

Rudolph Giffke

Mr. Yeh
David Taylor Model Basin

Mr. Beal
David Taylor Model Basin

Mr. Foster
David Taylor Model Basin

Mr. Frank
David Taylor Model Basin

Mr. Carnich
David Taylor Model Basin

Mr. Imlay
David Taylor Model Basin

Mr. Wolff
David Taylor Model Basin

Mr. Stevens
Office of Naval Research

Mr. Schwartz
David Taylor Model Basin

Davidson Laboratory
Technical Memorandum No. 136

Unclassified
January 1963

NOTES OF 4th BI-ANNUAL SEMINAR
SHIP BEHAVIOR AT SEA

The Fourth Bi-annual Symposium on Ship Behavior at Sea was held on June 11-15, 1962, as a means of disseminating research results obtained at Davidson Laboratory and at other laboratories, both in the United States and abroad. The subject of ship behavior at sea is surveyed, with emphasis on new developments since the Third Bi-Annual Symposium of 1960. The seminar was sponsored by the Office of Naval Research and Stevens Institute of Technology, with the cooperation of Webb Institute of Naval Architecture.

Davidson Laboratory
Technical Memorandum No. 136

Unclassified
January 1963

NOTES OF 4th BI-ANNUAL SEMINAR
SHIP BEHAVIOR AT SEA

The Fourth Bi-annual Symposium on Ship Behavior at Sea was held on June 11-15, 1962, as a means of disseminating research results obtained at Davidson Laboratory and at other laboratories, both in the United States and abroad. The subject of ship behavior at sea is surveyed, with emphasis on new developments since the Third Bi-annual Symposium of 1960. The seminar was sponsored by the Office of Naval Research and Stevens Institute of Technology, with the cooperation of Webb Institute of Naval Architecture.

Davidson Laboratory
Technical Memorandum No. 136

Unclassified
January 1963

NOTES OF 4th BI-ANNUAL SEMINAR
SHIP BEHAVIOR AT SEA

The Fourth Bi-annual Symposium on Ship Behavior at Sea was held on June 11-15, 1962, as a means of disseminating research results obtained at Davidson Laboratory and at other laboratories, both in the United States and abroad. The subject of ship behavior at sea is surveyed, with emphasis on new developments since the Third Bi-Annual Symposium of 1960. The seminar was sponsored by the Office of Naval Research and Stevens Institute of Technology, with the cooperation of Webb Institute of Naval Architecture.

Davidson Laboratory
Technical Memorandum No. 136

Unclassified
January 1963

NOTES OF 4th BI-ANNUAL SEMINAR
SHIP BEHAVIOR AT SEA

The Fourth Bi-annual Symposium on Ship Behavior at Sea was held on June 11-15, 1962, as a means of disseminating research results obtained at Davidson Laboratory and at other laboratories, both in the United States and abroad. The subject of ship behavior at sea is surveyed, with emphasis on new developments since the Third Bi-annual Symposium of 1960. The seminar was sponsored by the Office of Naval Research and Stevens Institute of Technology, with the cooperation of Webb Institute of Naval Architecture.